Forschungszentrum Karlsruhe
in der Helmholtz-Gemeinschaft

Wissenschaftliche Berichte
FZKA 7426

Wechselwirkung von dreiwertigen Actiniden und Lanthaniden mit der Wasser/Mineralphasen Grenzfläche

T. Stumpf

Institut für Nukleare Entsorgung

Juli 2008

Forschungszentrum Karlsruhe

in der Helmholtz-Gemeinschaft

Wissenschaftliche Berichte

FZKA 7426

Wechselwirkung von dreiwertigen Actiniden und Lanthaniden mit der Wasser/Mineralphasen Grenzfläche

Thorsten Stumpf

Institut für Nukleare Entsorgung

von der Fakultät für Chemie und Geowissenschaften
der Ruprecht-Karls-Universität Heidelberg
genehmigte Habilitation

Forschungszentrum Karlsruhe GmbH, Karlsruhe
2008

Für diesen Bericht behalten wir uns alle Rechte vor

Forschungszentrum Karlsruhe GmbH
Postfach 3640, 76021 Karlsruhe

Mitglied der Hermann von Helmholtz-Gemeinschaft
Deutscher Forschungszentren (HGF)

ISSN 0947-8620

urn:nbn:de:0005-074261

Zusammenfassung

Das Migrationsverhalten von Radionukliden in der Umwelt (Geo-, Hydro- und Biosphäre) wird durch Grenzflächenreaktionen (Sorption, Einbau) bestimmt. Natürliche geochemische Systeme sind im Allgemeinen äußerst komplex. Diese Komplexität resultiert aus einer Verknüpfung zahlreicher Einzelreaktionen im molekularen Maßstab. Ein fundiertes Verständnis dieser komplexen Systeme und eine darauf aufbauende Vorhersagbarkeit zum Verhalten von Radionukliden in der Umwelt erfordert die Aufklärung individueller Reaktionsmechanismen an der Wasser/Festphasen-Grenzfläche. Dies setzt den Einsatz moderner spektroskopischer und mikroskopischer Methoden voraus.

Bei den in dieser Habilitationsschrift zusammengefassten Arbeiten zur Wechselwirkung von Lanthaniden und dreiwertigen Actiniden mit Mineraloberflächen konnten verschiedene Einzelreaktionen aufgeklärt werden. Insbesondere die Kombination von zeitaufgelöster Laserfluoreszenzspektroskopie (TRLFS) mit der Röntgenabsorptionsspektroskopie (XAS) hat sich dabei als besonders erfolgreich erwiesen, um komplexe geochemische Reaktionen an der Wasser/Mineralphasen Grenzfläche aufzuklären.

Abstract

Interaction of trivalent actinides and lanthanides with the water/mineral interface.

The behavior of radionuclides in the natural environment (geo-, hydro- and biosphere) is determined by interface reactions like sorption and incorporation processes. In general natural geochemical systems are very complex. This complexity is a result of a combination of several single reactions on the molecular scale. For the understanding of complex systems and for the prediction of radionuclide behavior in the natural environment it is of cardinal importance to clarify the individual reaction mechanisms at the solid/solution interface. The establishment of clarification requires the application of modern spectroscopic and microscopic methods.

The presented studies, which are summarized in this professional dissertation, deal with investigations concerning the interaction of lanthanides and trivalent actinides with mineral surfaces. Several single reactions were deduced from these investigations. In particular the combination of time resolved laser fluorescence spectroscopy (TRLFS) with x-ray absorption spectroscopy (XAS) was proven to be very effective for the elucidation of complex geochemical reactions at the water/mineral interface.

Meinem Mentor Herrn Prof. Dr. Thomas Fanghänel danke ich sehr für seine intensive und freundschaftliche Unterstützung sowie die stete Diskussionsbereitschaft.

Des weiteren bedanke ich mich bei den Mitgliedern der Helmholtz-Hochschul-Nachwuchsgruppe „Aufklärung geochemischer Reaktionsmechanismen an der Wasser/Mineralphasen Grenzfläche“ Frau Dr. Maria Marques-Ferndandes, Herrn Moritz Schmidt und Herrn Markus Freyer sowie bei Herrn Dr. Clemens Walther und Herrn Sebastian Büchner für die enge und ausgesprochen gute Zusammenarbeit.

Ferner gilt mein Dank den Koautoren der den präsentierten Ergebnissen zugrunde liegenden Publikationen:
Herrn Dr. Andreas Bauer, Herrn Dr. Dirk Bosbach, Herrn Dr. Frédéric Coppin, Frau Dr. Hilde Curtius, Frau Dr. Kathy Dardenne, Frau Dr. Melissa A. Denecke, Herrn Prof. Dr. Thomas Fanghänel, Herrn Dr. Horst Geckeis, Herrn Prof. Dr. Ingmar Grenthe, Herrn Dr. Christoph Hennig, Herrn Prof. Dr. Jae Il Kim, Herrn Dr. Reinhardt Klenze, Herrn Dr. Thomas Rabung, Frau Dr. Silvia Stumpf, Herrn Dr. Jan Tits, Herrn Dr. Karsten Ufer, Herrn Dr. Clemens Walther und Herrn Dr. Erich Wieland.

Da ich in der glücklichen Situation bin, dass meine Frau nicht nur meine Partnerin im privaten Bereich ist sondern auch Kollegin, danke ich ihr für die wissenschaftliche Unterstützung und die gemeinsame glückliche Zeit innerhalb und außerhalb des Labors.

Meinen Eltern danke ich für ein harmonisches Umfeld, das nicht nur die Basis für ein glückliches Leben ist, sondern auch das Fundament für eine erfolgreiche Arbeit darstellt.

Inhaltsverzeichnis

"Sorption of Am(III) onto 6-line-Ferrihydrite and its Alteration Products: Investigations by EXAFS"; Silvia Stumpf, Thorsten Stumpf, Kathy Dardenne, Christoph Hennig, Harald Foerstendorf, Reinhardt Klenze, Thomas Fanghänel; Environ. Sci. Technol., 2006, 40, 3522-3528.

4. Kristallchemischer Einbau von Lanthaniden und dreiwertigen Actiniden in Mineralphasen **70**

"A Time-Resolved Laser Fluorescence Spectroscopy (TRLFS) Study of the Interaction of Trivalent Actinides (Cm(III)) with Calcite"; Thorsten Stumpf, Thomas Fanghänel; J. Colloid Interface Sci., 2002, 249, 119-122.

“Structural characterization of Am incorporated into calcite: A TRLFS and EXAFS study”; Thorsten Stumpf, Maria Marques Fernandes, Clemens Walther, Kathy Dardenne, Thomas Fanghänel; J. Colloid Interface Sci., 2006, 302, 240-245.

"Uptake of Cm(III) and Eu(III) by Calcium Silicate Hydrates: A Solution Chemistry and Time-Resolved Laser Fluorescence Spectroscopy (TRLFS) Study"; Jan Tits, Thorsten Stumpf, Thomas Rabung, Erich Wieland, Thomas Fanghänel; Environ. Sci. Technol., 2003, 37, 3568-3573.

"Uptake of Trivalent Actinides (Cm(III)) by Hardened Cement Paste: A Time-Resolved Laser Fluorescence Spectroscopy (TRLFS) Study"; Thorsten Stumpf, Jan Tits, Clemens Walther, Erich Wieland, Thomas Fanghänel; J. Colloid Interface Sci., 2004, 276, 118-124.

“Site-selective time resolved Laser fluorescence spectroscopy study of Eu(III) doped calcite”; Maria Marques Fernandes , Moritz Schmidt, Thorsten Stumpf, Clemens Walther, Dirk Bosbach, Thomas Fanghänel; Geochim. Cosmochim. Acta, 2007 submitted.

“Incorporation of Eu(III) into hydrotalcite: a TRLFS and EXAFS study”; Thorsten Stumpf, Hilde Curtius, Clemens Walther, Kathy Dardenne, Karsten Ufer, Thomas Fanghänel; Environ. Sci. Technol. 2007, 41, 3186-3191.

1. Einleitung

Bei der Erzeugung von Energie durch Kernspaltung fallen abgebrannte Brennelemente an, die neben Plutonium und Uran noch Spaltprodukte und die Transuranelemente Neptunium, Americium und Curium enthalten. Die sichere Entsorgung dieses hochradioaktiven Abfalls erfordert seine Isolierung von der Biosphäre über einen Zeitraum von mehreren hunderttausend Jahren. Abbildung 1 stellt den zeitlichen Verlauf der Radiotoxizität dar. Während die Spaltprodukte die Radiotoxizität in den ersten dreihundert Jahren dominieren, wird die Toxizität für längere Zeiträume von den Transuranelementen bestimmt. Folglich konzentrieren sich Untersuchungen zur Langzeitsicherheit eines Endlagers auf die Actiniden und langlebigen Spaltprodukte.

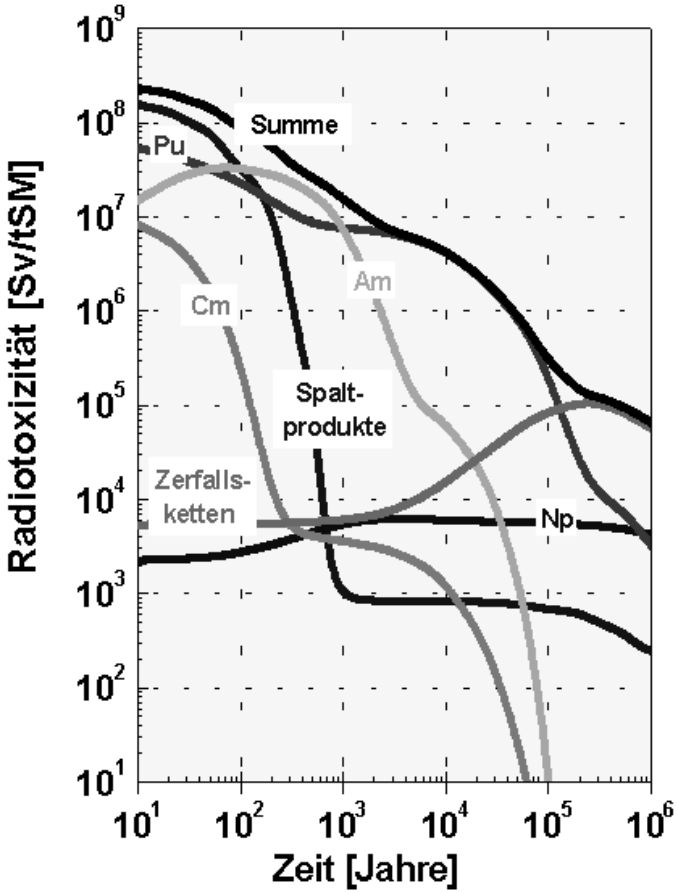

Abbildung 1 Beitrag der Brennelementkomponenten zur Gesamttoxizität

Für die Entsorgung radioaktiver Abfälle werden international zwei Wege beschritten. Eine Möglichkeit der Entsorgung ist die direkte Endlagerung radioaktiver Abfälle in tiefen geologischen Formationen. Eine andere Möglichkeit besteht in der Wiederaufarbeitung der Abfälle. Dazu werden Plutonium und Uran aus den

abgebrannten Brennstäben gewonnen und dem Brennstoffkreislauf erneut zugeführt. Auch bei der Wiederaufarbeitung fällt hochradioaktiver Abfall an (Spaltprodukte und Actiniden), der endgelagert werden muss. Zur Zeit steht in Deutschland noch kein Endlager für hochradioaktive Abfälle zur Verfügung, jedoch finden Untersuchungen zur Standortauswahl und zur Beurteilung der Langzeitsicherheit möglicher Standorte statt. Die Konzepte, die für eine Endlagerung international zur Diskussion stehen, sind die Endlagerung in Granit, Tuffgestein, Tonformationen oder Salz. Das Ziel, welches durch eine Endlagerung erreicht werden soll, besteht darin, die radioaktiven Gefahrstoffe aus der Biosphäre zu entfernen und zu verhindern, dass sie durch den Transport über den Wasserpfad wieder in die Biosphäre gelangen. Der sichere Einschluss radioaktiver Stoffe und die Isolation der Abfälle vor Wasserzutritt in einem Endlager beruht auf einer Reihe von Barrieren, die eine Migration der Radionuklide mit dem Grundwasser durch Rückhaltemechanismen verhindern sollen (Abbildung 2). Die technische Barriere besteht aus dem eigentlichen Abfallprodukt (HAW-Glas; abgebrannter Brennstoff) und aus dem Behälter, der z.B. aus dickwandigem Stahlguss hergestellt ist. Zum Abdichten verbleibender Hohlräume in einem Stollen wird auf Verfüllmaterial als geotechnische Barriere zurückgegriffen. Das Verfüllmaterial soll den Nahbereich des Endlagers gegen Wasserzutritt abdichten. Der Versatz kann im Falle der Einlagerung in eine Steinsalzformation aus Salzgrus, im Falle anderer Endlagerkonzepte aus z.B. quellfähigem Bentonit bestehen. Unter geologischer Barriere versteht man das umgebende Wirtgestein wie z.B. Granit oder Steinsalz.

Die Barrieren im Nah- und Fernfeld eines nuklearen Endlagers sollen zur Immobilisierung von radioaktivem Material führen. Dabei spielen bei der Langzeitsicherheit eines Endlagers die Wechselwirkungen der Actiniden mit der Wasser/Mineralphasen Grenzfläche eine entscheidende Rolle (Abbildung 3). Sorption und kristallchemischer Einbau sollen die Migration von Actiniden in die Ökosphäre nachhaltig verhindern. Aus diesem Grund ist es notwendig, die Reaktionen von Actiniden mit Mineraloberflächen detailliert zu untersuchen und die zugrundeliegenden Reaktionsmechanismen aufzuklären.

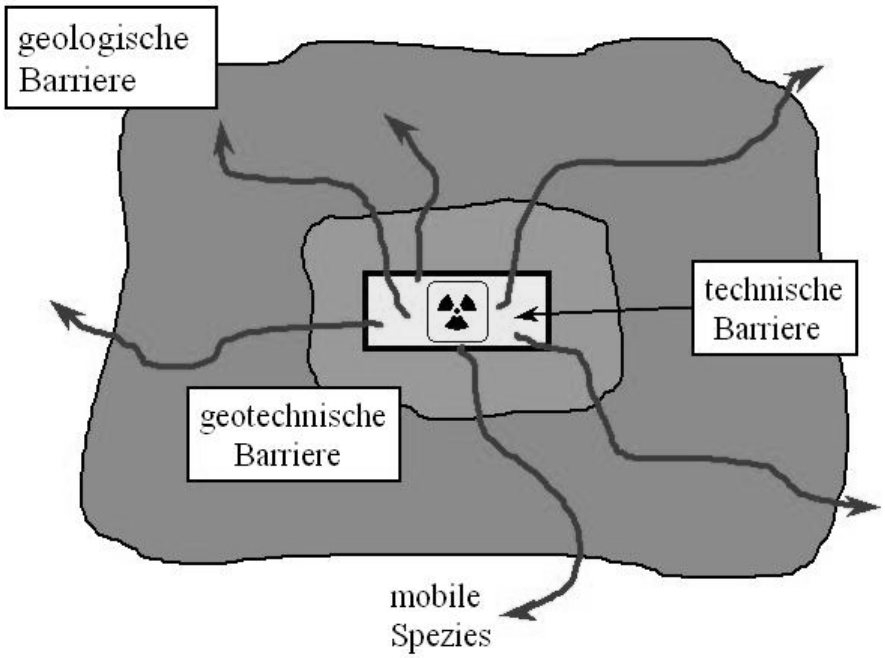

Abbildung 2 Multibarrierenkonzept eines Endlagers

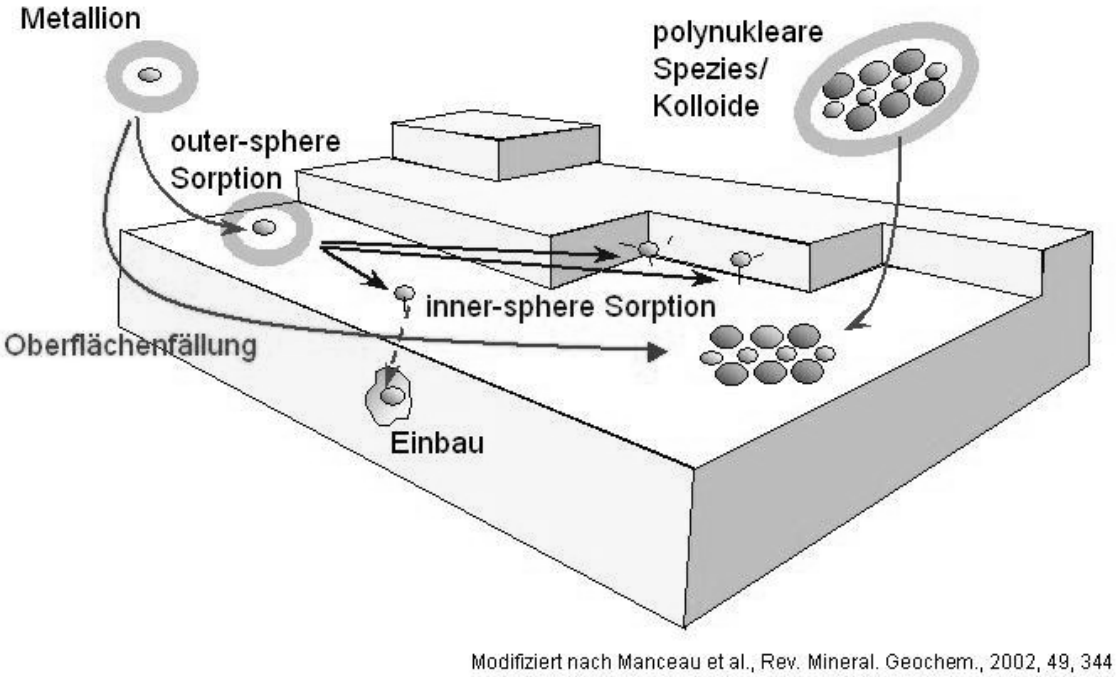

Abbildung 3 Mechanismen der Radionuklidrückhaltung

An der Mineraloberfläche kann es über van der Waals Wechselwirkungen, Dipol-Dipol Wechselwirkungen, Ion-Dipol Wechselwirkungen etc. oder Ionenpaarbildung zur Bildung sog. outer-sphere Komplexen kommen. Bei dieser Art der Wechselwirkung behält das Metallion seine Hydrathülle und sein Ligandenfeld bleibt auch nach der Sorption nahezu unverändert. Die inner-sphere Sorption unter Verlust eines Teils der Metallionhydrathülle und die Bildung von Oberflächenkomplexen (koordinative Bindung über elektrostatische Wechselwirkungen z.T. mit kovalentem Bindungsanteil) stellt ebenfalls eine Reaktion an der Wasser/Mineralphasen Grenzfläche dar. Die dritte Möglichkeit der Radionuklidrückhaltung besteht in Mineralisierungsprozessen, d.h. der Bildung thermodynamisch stabiler Sekundärphasen, festen Lösungen (solid solutions) oder dem metastabilen, kinetisch kontrolliertem Einbau z.B. durch Einschluss bei Mitfällung oder Umlösevorgängen.
Alle genannten Oberflächenprozesse (Sorption/Einbau; Abbildung 3) und die damit verbundene Rückhaltung von Radionukliden sowie weiterer Schwermetalle sind von den Eigenschaften der Mineraloberflächen abhängig. Um allgemeingültige und somit für Endlagersicherheitsprognosen nutzbare/belastbare Aussagen zu erhalten, ist es nötig, die molekularen Mechanismen aufzuklären, die die Stärke und Art der Sorption bestimmen.
Untersuchungen zur Quantifizierung der Sorption erfolgten bislang meist phänomenologisch durch Bestimmung des Verteilungsgleichgewichts zwischen fester und flüssiger Phase (z.B. Kd-Ansatz) ohne Berücksichtigung der in Lösung und an der Oberfläche vorliegenden Radionuklidspezies. Da die untersuchten natürlichen Oberflächen extrem heterogen sind, schwanken die in batch Experimenten erhaltenen Radionuklid Verteilungskoeffizienten, die an ein und dem selben Mineral ermittelt wurden, um Größenordnungen. Scheinbar geringe Variationen der Oberfläche (z.B. durch Einschlüsse von Eisenoxiden oder Tonmineralen) führen zu völlig anderen Kd Werten für die Sorption von Schwermetallen im Spurenkonzentrationsbereich. Belastbare, extrapolierbare Aussagen lassen sich nur durch die Aufklärung der ablaufenden Prozesse und eine thermodynamisch fundierte Quantifizierung der Reaktionen an der Grenzphase erhalten. In den letzten Jahren sind verstärkt Ansätze gemacht worden, Sorptionsvorgänge mit thermodynamischen Modellen, wie etwa dem Oberflächenkomplexierungsmodell, zu parametrisieren. Die Ableitung von Oberflächenkomplexierungskonstanten erfolgt dabei meist durch Anpassung von Sorptionsverteilungsgleichgewichten als Funktion von

Radionuklidkonzentration, pH und Ionenstärke, ohne Möglichkeit, die postulierten Oberflächenkomplexe direkt verifizieren zu können. Um die Spezies, die bei der Wechselwirkung von Actiniden mit Mineraloberflächen auftreten, zu charakterisieren und zu quantifizieren, sind spektroskopische Speziationsverfahren nötig. Als Methoden eignen sich dabei neben anderen besonders die zeitaufgelöste Laserfluoreszenzspektroskopie (TRLFS) sowie die Röntgenabsorptionsspektroskopie (XAS), die auch bei den Untersuchungen, die in dieser Arbeit vorgestellt werden, eine herausragende Rolle spielten. Aufbauend auf den spektroskopischen Daten können die Sorptionsmechanismen auf molekularer Ebene aufgeklärt werden und fest/flüssig-Grenzphasenreaktionen auf Basis eines Oberflächenkomplexierungsmodell thermodynamisch beschrieben werden. Dieses Prozessverständnis auf molekularer Ebene macht das Extrapolieren der Radionuklidausbreitung über lange Zeiträume wesentlich sicherer, als wenn dies nur auf Basis der Ergebnisse aus batch Untersuchungen geschehen würde. Somit liefert die Grundlagenforschung zu den fundamentalen Prozessen, die an den Wasser/Mineralphasen Grenzflächen ablaufen, einen wichtigen Beitrag zur Sicherheit eines nuklearen Endlagers.

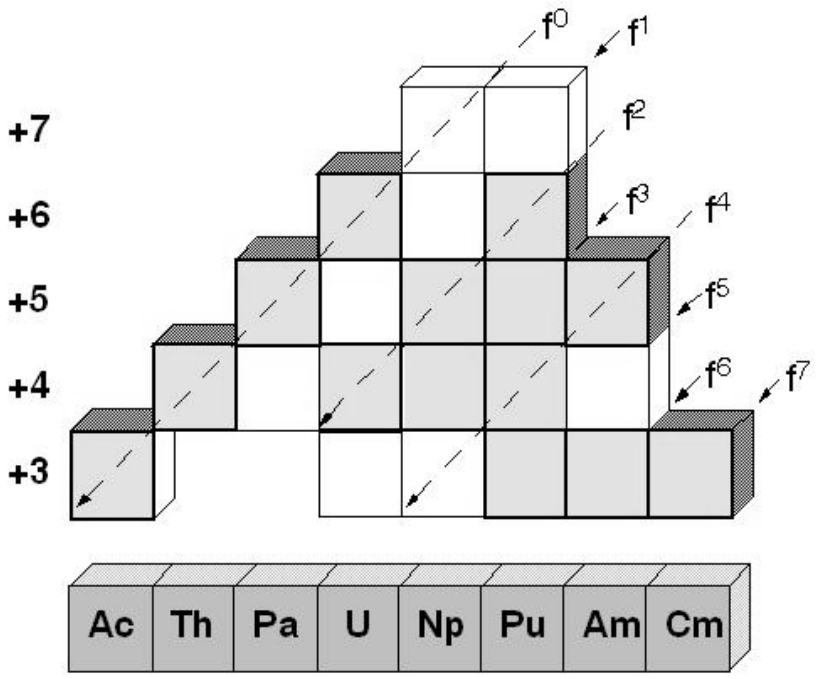

Abbildung 4 f-Elektronenkonfiguration und Oxidationsstufen einiger Actiniden

Abbildung 4 zeigt, dass bei einigen Actiniden eine Vielzahl von Oxidationsstufen auftreten können. Erst ab Americium dominiert in wässriger Umgebung die Wertigkeitsstufe drei. Aufgrund der reduzierenden Bedingungen in der Umgebung eines Tiefenendlagers ist es sinnvoll, besonders die wässrige Chemie der niederwertigen Actinidionen zu untersuchen. Thermodynamische Rechnungen zeigen, dass selbst Plutonium in tiefen geologischen Formationen dreiwertig vorliegen kann. Zudem treten die zur Radiotoxizität in hohem Maße beitragenden Radionuklide Am und Cm unter Endlagerbedingengen ausschließlich dreiwertig auf. Stellvertretend für die dreiwertigen Actiniden wurde in den hier zusammengefassten Arbeiten Curium als Sonde zur Aufklärung der Reaktionen an der Wasser/Mineral Grenzfläche eingesetzt, da die Fluoreszenzeigenschaften dieses Actinids Untersuchungen im nanomolaren Konzentrationsbereich erlauben. Die zeitaufgelöste Laserfluoreszenzspektroskopie (TRLFS) mit Curium hat sich als erfolgreiche Speziationsmethode sowohl in Lösung (z.B. Wimmer et al., 1992; Moulin et al., 1992; Fanghänel et al., 1994, 1998) als auch bei Sorptionsstudien an Oberflächen (Chung et al., 1998; Rabung et al., 2000; Stumpf et al., 2001, 2002, 2004; Pointeau et al., 2001; Tits et al., 2003) erwiesen. Neben der Identifizierung und Quantifizierung der auftretenden Spezies werden Informationen zur Hydratationssphäre der jeweiligen Komponente erhalten (Horrocks und Sudnick, 1979; Kimura und Choppin, 1994). Dies erlaubt es, zwischen outer-sphere Komplexen, inner-sphere Komplexen sowie in das Kristallgitter von Fremdphasen eingebauten Actiniden zu unterscheiden. Im Rahmen der vorliegenden Arbeit sind die Wechselwirkungen von Cm(III) mit γ-Al_2O_3, den Tonmineralen Smectit und Kaolinit, den Feldspäten Albit und Orthoklas, Quarz sowie Calcit, CSH Phasen und Zement untersucht worden. TRLFS Untersuchungen mit den ebenfalls fluoreszierenden f-Elementen Eu(III) und Am(III) wurden im Rahmen der eigenen Arbeiten zur Wechselwirkung von dreiwertigen Lanthaniden und Actiniden mit Mineraloberflächen an folgenden Systemen durchgeführt: Eu(III)/ γ-Al_2O_3, Eu(III)/Tonminerale, Eu(III)/Calcit, Eu(III)/Hydrotalcit und Am(III)/Calcit. Um Strukturparameter (atomare Abstände; Koordinationszahlen) der sorbierten bzw. in ein Wirtsgitter eingebauten Lanthaniden/Actiniden Spezies zu erhalten, wurden röntgenabsorptionsspektroskopische Messungen (XAS) an ausgewählten Systemen durchgeführt. XAS Spektroskopie hat sich als herausragend gute, die TRLFS ergänzende Methode herausgestellt, um Prozesse an der Wasser/Mineralphasen

Grenzfläche zu untersuchen. Diverse Veröffentlichungen zeigen, dass mit Hilfe von EXAFS ein Prozessverständnis zur Reaktion an Oberflächen erreicht werden kann, da im Gegensatz zur Röntgenstrukturanalyse die Strukturparameter der Oberflächenspezies ohne eine vorhandene Fernordnung erhalten werden können (z.B. Reeder et al. 2000, Denecke et al. 2003, 2005, Scheinost et al. 2000, Reich et al. 1998). Die Röntgenabsorptionsspektroskopie wurde in dieser Arbeit bei den Untersuchungen der Systeme Am(III)/Tonminerale, Am(III)/Calcit, Am(III)/Ferrihydrit und Eu(III)/Hydrotalcit eingesetzt.

Zeitaufgelöste Laserfluoreszenzspektroskopie

Die Fluoreszenzspektroskopie an Lanthaniden hat sich in den letzten zehn Jahren in großem Umfang weiterentwickelt und diverse Anwendungen in den Bereichen Lasertechnologie, Materialwissenschaften und in der analytischen Chemie gefunden (insbesondere beim Markieren organischer Moleküle, Immuno Assays, Imaging und beim Messen interatomarer Abstände). Auch die Wechselwirkung von dreiwertigen Metallionen mit der Wasser/Mineralphasen Grenzfläche lässt sich insbesondere mit Hilfe der TRLFS an Eu(III) und Cm(III) untersuchen. In Abbildung 5 ist eine Darstellung des Eu^{3+} Termschemas zu sehen. Eu(III) zeigt ein ^7F-Grundmultiplett sowie ein darüber liegendes, anregbares ^5D-Multiplett. Zur Excitation der Fluoreszenzemission dient häufig der Übergang vom $^7F_0$ Grundzustand in den $^5L_6$ Zustand. Zum Einstrahlen in diese intensivste Absorptionsbande des optischen Spektrums ist eine Excitationswellenlänge von 394.0 nm nötig. Nach strahlungsloser Relaxation wird hauptsächlich der $^5D_0$ Zustand besetzt. Die Eu(III) Emission erfolgt aus diesem Niveau in die ^7F_J-Multiplett Zustände.

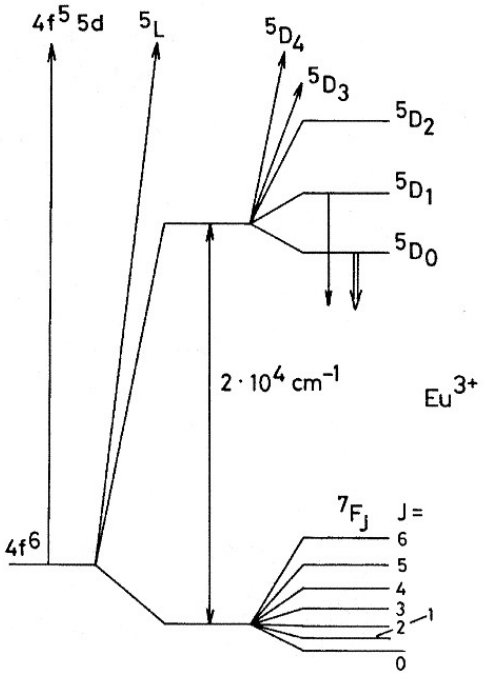

Abbildung 5 Schematische Darstellung des Eu(III) Fluoreszenzprozesses (aus Bünzli und Choppin 1989)

Entsprechend den Auswahlregeln für elektronische (ED) und magnetische (MD) Dipolübergänge gilt neben dem „Laport-Verbot“ ($\Delta\ell$ = +/- 1) für ED ΔJ = 2, 4, 6 und für

MD ΔJ = +/- 1. Die sich daraus ableitenden Eigenschaften der Eu(III) Emissionsspektren sind in Tabelle 1 zusammengestellt.

Tabelle 1 Wellenlängenbereich und charakteristische Eigenschaften der $^5D_0 \rightarrow {}^7F_J$ Übergänge von Eu(III) nach Bünzli und Choppin 1989.

J	Übergänge	λ (nm)	Intensität	Eigenschaften
$^5D_0 \rightarrow {}^7F_J$				
0	ED	575-583	vw	verbotener Übergang, durch „J-Beimischungen“ sichtbar; bei vorhandenem Inversionszentrum verboten
1	MD	585-600	s	Erlaubter Übergang (ΔJ=1); Intensität unabhängig von chemischen Umgebung
2	ED	610-625	s-vs	hypersensitiver Übergang (ΔJ=2); abwesend bei hoher Punkt-Symmetrie
3	ED	640-655	vw	verboten; immer schwach; „J-Beimischungen“ erlauben einen MD Charakter
4	ED	680-710	m-s	empfindlich gegenüber der chemischen Umgebung
5	ED	740-770	v-w	verboten, selten beobachtet
6	ED	810-840	vw	selten gemessen

vw: sehr schwach; m: mittel; s: stark; vs: sehr stark; ED: elektrischer Dipolübergang; MD: magnetischer Dipolübergang

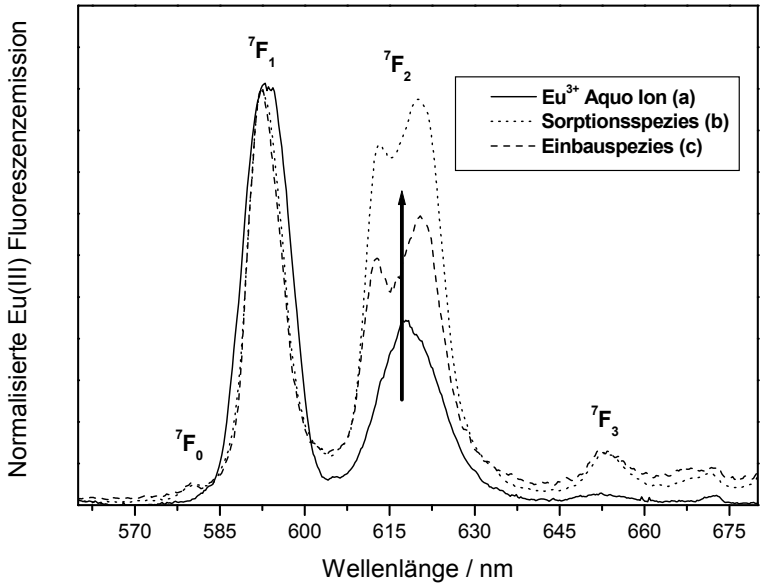

Abbildung 6 Fluoreszenzemissionsspektren des Eu^{3+} Aquo Ions ((a) $3x10^{-6}$ mol/L; pH 2), der Eu(III)/Calcit Sorptionsspezies (b) und der Eu(III)/Calcit Einbauspezies (c).

Abbildung 6 zeigt das Fluoreszenzemissionsspektrum von Eu^{3+} in Wasser ((a) durchgezogene Linie; $3x10^{-6}$ mol/L; pH 2), von einer Eu(III)/Calcit Sorptionsspezies ((b) gepunktete Linie) und von einer Eu(III) Spezies, die in den Calcit eingebaut ist ((c) gestrichelte Linie). Gezeigt sind die Übergänge aus dem $^5D_0$ Zustand in die $^7F_{0,1,2,3}$ Zustände. Das Spektrum des Eu^{3+} Aquoions besitzt ein intensives $^7F_1$ Signal, während der spinverbotene $^5D_0 \rightarrow {}^7F_0$ Übergang nicht beobachtet wird. Für die Spektren der Eu(III)/Calcit Spezies zeigt sich neben einer starken Zunahme der Intensität des $^7F_2$ Signals auch die aufgrund der Kristallfeldwechselwirkung schwach erlaubte $^7F_0$ Bande. Obwohl sich das Ligandenfeld der verschiedenen Metallionen Spezies ((a) voll hydratisiertes Ion, (b) oberflächenkomplexiertes teilhydratisiertes sorbiertes Ion und (c) unter Verlust der Hydrathülle in den Calcitkristall eingebautes Ion) sehr stark unterscheidet, ist in den Eu(III) Spektren keine Verschiebung der Emissionsbanden zu beobachten. Lediglich die Intensität des $^5D_0 \rightarrow {}^7F_2$ Übergangs ändert sich als Folge des "hypersensitiven Effekts" (Carnall, 1988; Carnall et al., 1994; Jörgensen und Judd, 1964). Chemische Informationen aus den Europiumspektren können bei Raumtemperatur und unselektiver Anregung des $^5L_6$ Zustandes meist nur aus der Veränderung der Peakformen, des

Intensitätsverhältnisses zwischen den $^5D_0 \rightarrow {}^7F_1$ und $^5D_0 \rightarrow {}^7F_2$ Übergängen und aus der Fluoreszenzemissionslebensdauer erhalten werden (Richardson, 1982; Dobbs et al. 1989; Stumpf et al., 2002).

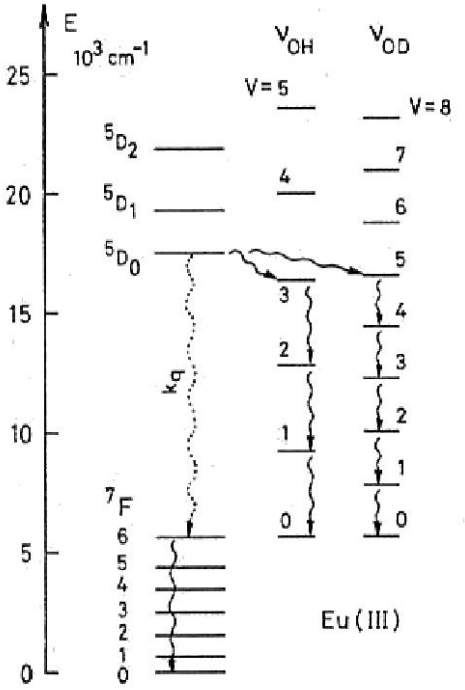

Abbildung 7 Einfluss von O-H und O-D Schwingungen auf die Lebensdauer des angeregten Zustands von Eu(III).

Da für f→f Übergänge das Laport-Verbot gilt, besitzen diese eine geringe Übergangswahrscheinlichkeit. Das hat zur Folge, dass die gemessenen Emissionslebensdauern entsprechend lang sind (bis $>10^{-3}$ s). Im Gegensatz dazu ist im Falle des Eu^{+3} Aquoions in H_2O allerdings eine Zerfallsrate von $k_{obs} \sim 9\ ms^{-1}$ zu detektieren. Dies entspricht einer relativ kurzen Lebensdauer des angeregten Zustandes von 110 µs. Der Grund für die kurze Emissionslebensdauer von Europium im wässrigen System liegt an der Übertragung der elektronischen Energie aus einem angeregten f-Niveau auf Schwingungszustände von H_2O Molekülen in der inneren Koordinationssphäre des Europiums (Fluoreszenzquenchen; Kropp et al., 1965; Stein et al., 1975, Haas et al., 1971). Beim Austausch von H_2O gegen D_2O nimmt die Schwingungsfrequenz der Streckschwingung ab ($\nu_1(OH) = 3405\ cm^{-1}$; $\nu_1(OD) = 2520\ cm^{-1}$) (Heller, 1966). Diese Abnahme in der Schwingungsfrequenz führt zu einer reduzierten Wahrscheinlichkeit der strahlungslosen Relaxation, da zur Überbrückung der Energielücke zwischen Grundzustand und ersten angeregten Zustand des

Europiums (~ 12000 cm^{-1}) eine höhere Oberschwingung erforderlich ist (Abbildung 7). Entsprechend erhöht sich in D_2O die Fluoreszenzemissionslebensdauer auf 2700 µs. Aufgrund der Korrelation zwischen Zerfallskonstante und Anzahl der Wassermoleküle in der ersten Koordinationssphäre ist es möglich, Aussagen zum Hydratationszustand des Eu(III) zu machen und damit strukturelle Informationen über die diversen Eu(III) Spezies zu erhalten. Eine Abnahme der H_2O Moleküle aus der Eu(III) Koordinationssphäre durch die Komplexierung des Metallions führt entsprechend der Gleichung nach Horrocks (Horrocks 1979) zu einer Erhöhung der Lebensdauer.

$$n(H_2O) = 1.07\ k_{obs} - 0.62$$

Diese Abhängigkeit der Emissionslebensdauer vom Hydratationszustand des Metallions wurde in dieser Arbeit zur Charakterisierung von outer-sphere, inner-sphere und ternären Oberflächenkomplexen sowie zum Nachweis von Eu(III) Einbauspezies genutzt.

Weitere chemische Informationen lassen sich aus der direkten Anregung des $D_0 \rightarrow F_0$ Übergangs erhalten (Excitationsspektrum 575-583 nm). Da die $^5D_0$- und $^7F_0$-Zustände nicht entartet sind, gibt es für jede chemisch unterschiedliche Eu(III) Umgebung einen einzigen $^5D_0 \rightarrow {}^7F_0$ Übergang. Durch diese Site-selektive Eu(III) TRLFS ist die Bestimmung der Anzahl an vorhanden Eu(III) Spezies relativ leicht möglich. Diese Form der Spektroskopie ist in der vorliegenden Arbeit an den Systemen Eu(III)/Calcit und Eu(III)/Hydrotalcit angewandt worden und wird in Kapitel 4 ausführlich dargestellt.

Neben den Lanthaniden existiert eine weitere Gruppe von f-Elementen, die Actiniden, die als fluoreszenzzeigende Elemente bisher wenig Beachtung fanden. Aufgrund ihrer Radioaktivität können Experimente mit Transuranelementen nur in entsprechend eingerichteten und überwachten radioaktiven Kontrollbereichen durchgeführt werden. Die Fluoreszenzeigenschaften einiger dieser Elemente, besonders hervorzuheben ist in diesem Zusammenhang das dreiwertige Curium, sind außerordentlich interessant und eröffnen spektroskopische Möglichkeiten, die weit über die bisherige Anwendung der TRLFS mit Lanthaniden hinausgehen. So zeigt Cm(III) im Vergleich Eu(III) und Tb(III) eine zwei bis drei Größenordnungen höhere Fluoreszenzintensität, was den Einsatz von Cm(III) als fluoreszierende atomare Sonde im Ultraspurenkonzentrationsbereich möglich macht. Die TRLFS Nachweisgrenze des Actinids beträgt in Lösung weniger als 10^{-12} mol/L; sorbiert an Oberflächen lassen sind noch aus 10^{-14} mol/cm^2 Cm(III) chemische Informationen erhalten. Diese hohe

Empfindlichkeit der Cm(III) TRLFS ist insbesondere bei Forschungsarbeiten zur Sicherheit eines Endlagers wichtig, da die Freisetzung von Radionukliden aus einem solchen nuklearen Endlager im Spurenkonzentrationsbereich stattfinden wird. Ferner wird auch bei Untersuchungen im neutralen und alkalischem pH Bereich die Löslichkeitsgrenze des Actinids nicht überschritten, so dass die Oberflächenkomplexierung des Actinids aus der wässrigen Lösung ungestört beobachtet werden kann. Zudem können beim Einsatz von Cm(III) die einzelnen Reinkomponenten wesentlich einfacher identifiziert und quantifiziert werden, als dies mit der Europium Spektroskopie möglich ist.

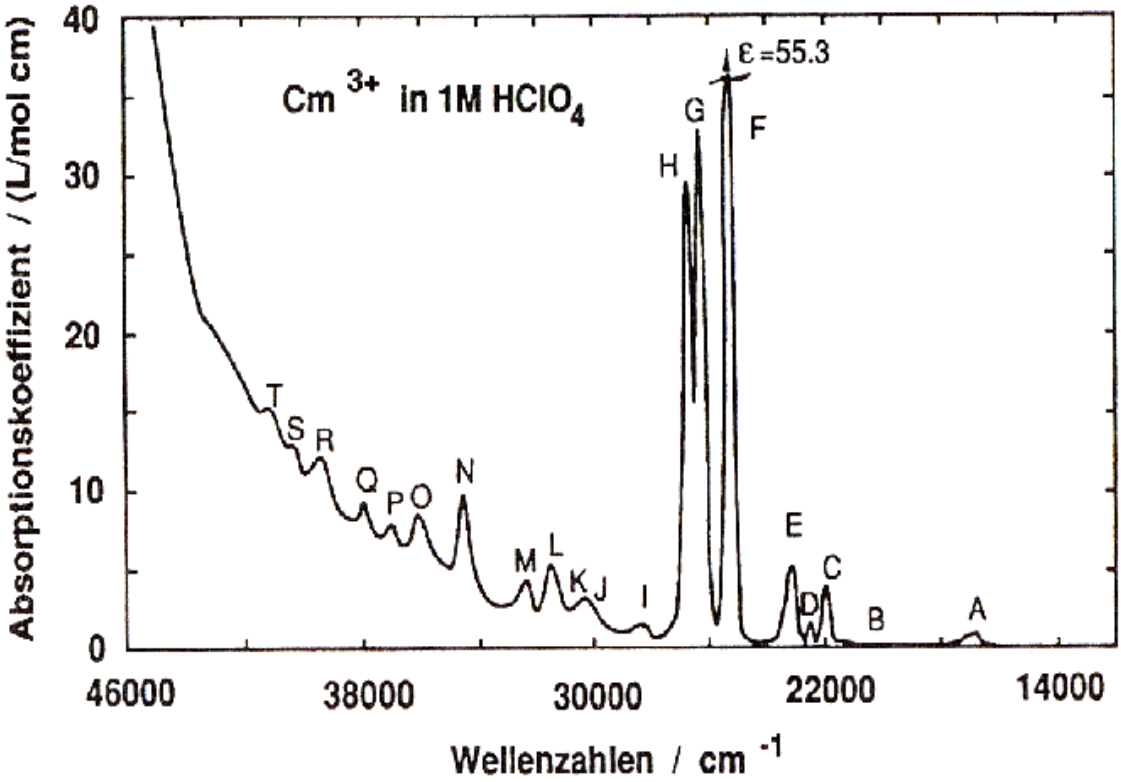

Abbildung 8 Absorptionsspektrum von Cm^{3+} in 1 M Perchlorsäure nach Carnall und Rajnak 1975.

In Abbildung 8 ist das optische Spektrum von Cm^{3+} in 1M $HClO_4$ dargestellt. Eine Vielzahl von f→f Übergängen sind zu beobachten, die mit steigender Energie in alphabetischer Reihenfolge bezeichnet werden. Die Anregung der Cm(III)-Fluoreszenz erfolgt vom Z-Grundzustand ($^8S_{7/2}$) in die angeregten Zustände der drei intensivsten Absorptionsbanden (Carnall, 1989). In Abbildung 9 ist das entsprechende Termschema dargestellt (Beitz, 1991). Die Excitation erfolgt üblicherweise im Maximum der F-Bande bei 396.6 nm. Nach der Anregung relaxieren

die Elektronen strahlungslos in den Zustand A. Die Energielücke zwischen dem angeregten Zustand und dem Grundzustand Z beträgt 16840 cm^{-1}. Die Emission in den entarteten Grundzustand geht von vier Kristallfeldniveaus aus, in die der angeregte Zustand A aufgespaltet ist (304 cm^{-1} in $LaCl_3$ Matrix; Carnall et al., 1988). Somit sollte für die Emissionsbande des Cm(III) Aquoions eine Feinstruktur mit vier Emissionslinien auftreten. Da die Intensität der Emission durch die thermisch bedingte Gleichgewichtsverteilung der Elektronen auf die Kristallfeldzustände bestimmt wird und die Kristallfeldaufspaltung (304 cm^{-1}) mit der thermischen Energie (kT = 210 cm^{-1}) vergleichbar ist, ist bei Raumtemperatur nur das niedrigste Niveau des angeregten Zustandes besetzt und das Spektrum des Cm^{3+} Aquoions weist eine einzige Emissionsbande bei 593.8 nm mit einer Halbwertsbreite von 7.7 nm auf. Bei Komplexierung verschiebt sich das Cm(III) Emissionsmaximum unter Vergrößerung der Halbwertsbreite. Die Verschiebung der Emissionsspektren und die Änderung der Fluoreszenzintensität lässt Rückschlusse auf die chemische Umgebung (Ligandenfeld) und damit den Komplexierungszustand von Curium zu.

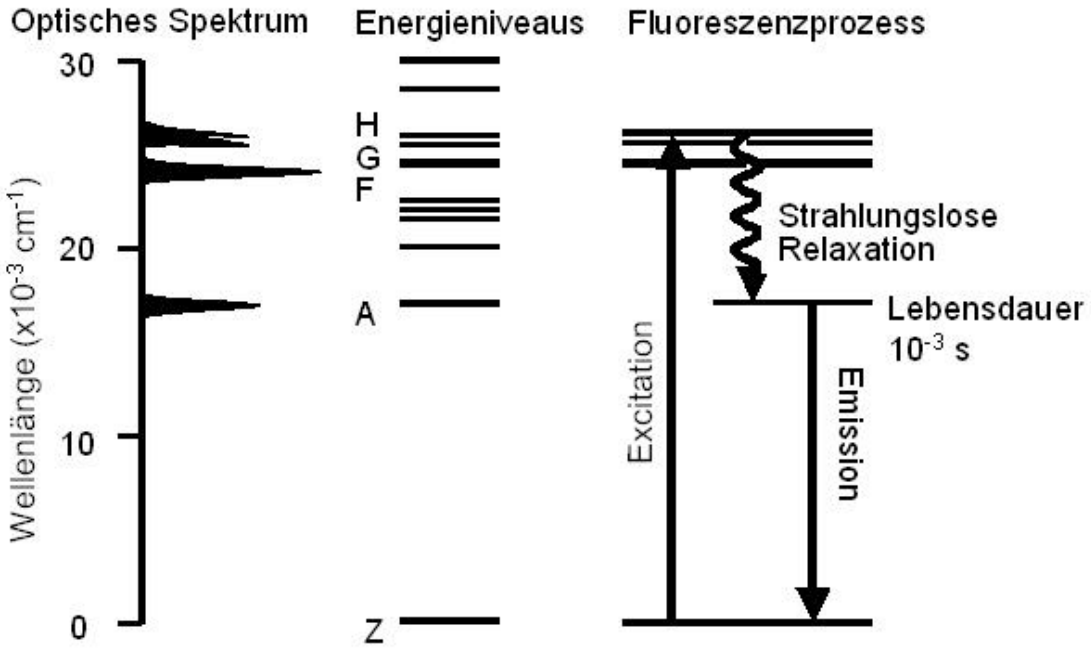

Abbildung 9 Vereinfachtes Termschema; Fluoreszenzprozess von Cm(III) nach Carnall und Crosswhite, 1975.

Abbildung 10 zeigt Spektren der Cm(III) Spezies, die den bereits gezeigten Europiumverbindungen im Calcitsystem entsprechen und im

Spurenkonzentrationsbereich (9x10^{-8} mol/L) aufgenommen wurden. Im Gegensatz zu den multiplen $^5D_0 \rightarrow {}^7F_J$ Übergängen eines Europiumspektrums, ist im Fall von Curium einer Spezies jeweils genau ein gut separiertes Emissionssignal zuzuordnen, das dem $^6D_{7/2} \rightarrow {}^8S_{7/2}$ (Excitationswellenlänge λ = 396.6 nm) Übergang entspricht. Durch Analyse (Peakentfaltung) gemessener Spektrenserien, lässt sich die genaue Anzahl von Reinkomponenten ermitteln und daraus Speziationen errechnen. Somit ist es vergleichsweise einfach, mit Hilfe der Cm(III) TRLFS chemische Reaktionen im Spurenkonzentrationsbereich aufzuklären und zu quantifizieren.

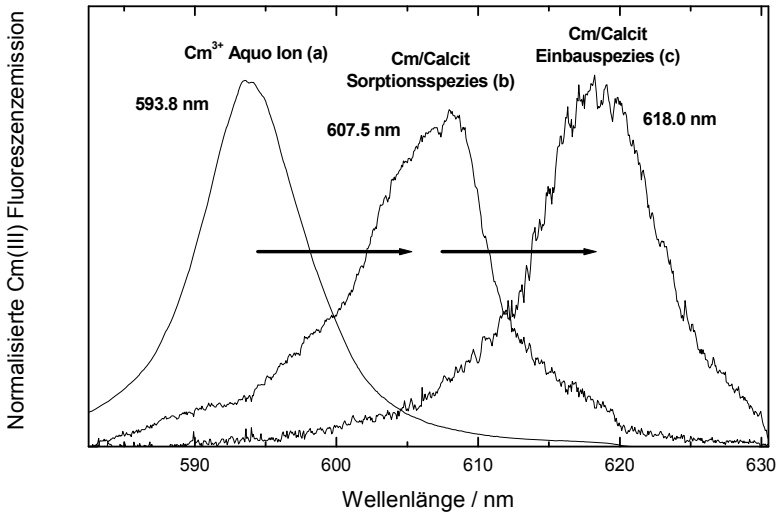

Abbildung 10 Fluoreszenzemissionsspektren des Cm^{3+} Aquoions ((a) 9x10^{-8} mol/L; pH 2), der Cm(III)/Calcit Sorptionsspezies (b) und der Cm(III)/Calcit Einbauspezies (c).

Weitere Information zur Struktur einer Curiumverbindung wird über die Interpretation der Fluoreszenzlebensdauer erhalten. Analog der Eu(III) Spektroskopie erfolgt der Zerfall des angeregten Zustandes in den Grundzustand für eine Cm(III) Spezies nach einem monoexponentiellen Zeitgesetz, das sich additiv aus der Zerfallsrate für den strahlungslosen und strahlenden Übergang zusammensetzt. Nach der Judd Ofelt Theorie wurde eine Lebensdauer des angeregten Zustands von 1.3 ms berechnet (Judd, 1962; Ofeld, 1962; Carnall et al., 1975). Die gemessene Fluoreszenzemissionslebensdauer des angeregten Cm^{3+}_{aq} in H_2O von 68 +/- 3 µs weicht allerdings deutlich von dieser berechneten maximalen Lebensdauer für den angeregten Zustand des Cm(III) ab. Das bedeutet, dass die Quantenausbeute durch strahlungslose Übergänge reduziert ist und hier wie auch im Falle des Eu^{3+} ein sog.

"Fluoreszenzquenchen" vorliegt. Es folgt ein Anstieg der gemessenen Emissionslebensdauer von 68 +/- 3 µs (H_2O) auf 1.3 ms im D_2O System. Messungen der Cm(III) Fluoreszenz in H_2O/D_2O Mischungen zeigen, dass eine lineare Korrelation zwischen der Zerfallskonstanten k_{obs} und der Anzahl Wassermoleküle in der ersten Koordinationssphäre von Cm(III) besteht (Kimura et al., 1994).

$$n(H_2O) = 0.65\ k_{obs} - 0.88$$

k_{obs} entspricht dem reziproken Wert der Lebensdauer des angeregten Zustands. Wenn in wässrigen Systemen der hauptsächliche Quenchbeitrag von O-H Schwingungen herrührt, lassen sich in Analogie zum Eu(III) über die Länge der Emissionslebensdauer des Curiums Informationen zum Hydratationszustand des Actinids erhalten. Sind verschiedene Cm(III) Spezies gleichzeitig vorhanden, so ist die Rate bei einer langsamen Austauschkinetik mehrfach exponentiell. Liegt jedoch eine schnelle Kinetik vor, so ist der Zerfall monoexponentiell und besitzt eine mittlere Lebensdauer.

Ähnlich dem H_2O beeinflussen weitere Verbindungen und Elemente die Lebensdauer der Fluoreszenz. So haben z.B. auch N-H Schwingungen einen quenchenden Einfluss auf die Eu(III) und Cm(III) Emission (Lis 2002, Beeby et al. 1999). Für die Untersuchungen der Wechselwirkung von f-Elementionen mit der Wasser/Mineralphasen Grenzfläche, ist das Quenchen der Emission durch Eisen zu beachten (z. B. Lakowicz 1983, Arakawa et al 2003). In Abhängigkeit von der Eu-Fe bzw. Cm-Fe Entfernung nimmt die Lebensdauer der Fluoreszenz ab, um bei direkter Anbindung des f-Elements an eine Ferrinolgruppe ganz gelöscht zu werden. Aus diesem Grund ist es nicht möglich, strukturelle Informationen zur Sorption oder dem Einbau von Curium an bzw. in Eisenoxidmineralphasen mit Hilfe der TRLFS zu erhalten. In der vorliegenden Arbeit wurde deshalb zur Charakterisierung der Wechselwirkung von dreiwertigen Actiniden mit Eisenoxiden (Hämatit und Goethit) ausschließlich die Röntgenabsorptionsspektroskopie eingesetzt.

In der vorliegenden Arbeit wurde Cm(III) als atomare Sonde eingesetzt, um mit Hilfe der zeitaufgelösten Laserfluoreszenzspektroskopie Reaktionen an der Wasser/Mineralphasen Grenzfläche aufzuklären. Dabei wurden sowohl verschiedene Sorptionsmechanismen an diversen Mineraloberflächen untersucht, als auch der Einbau des Actinids in Sekundärphasen nachgewiesen. Bei allen in dieser Arbeit vorgestellten TRLFS Untersuchungen mit Curium, wurde das Isotop ^{248}Cm

eingesetzt, das sich durch eine lange Halbwertszeit von $\tau_{½}$ = 340000 Jahren auszeichnet. Die Aktivität einer typischen Messprobe lag somit bei wenigen Becquerel. Neben der damit verbundenen vernachlässigbar kleinen Strahlenbelastung für den Experimentator war durch die geringe Zerfallshäufigkeit eine Veränderung des Materials durch Radiolyse auszuschließen.

Röntgenabsorptionsspektroskopie

Neben der Methode TRLFS wurde insbesondere die Röntgenabsorptionsspektroskopie (XAS) bei den Untersuchungen zur Wechselwirkung von dreiwertigen Actiniden mit der Wasser/Mineral Grenzfläche genutzt. XAS und insbesondere EXAFS Messungen bieten die Möglichkeit, die TRLFS Daten mit Hilfe einer anderen spektroskopischen Methode zu untermauern und Strukturparameter wie Atomabstände und Koordinationszahlen für Actinidspezies zu ermitteln (Sorption von Actiniden an Minerale siehe z.B. Allard et al. 1999, Bargar et al. 1999, 2000, Combes et al. 1992, Denecke et al. 2003, 2005, Fuller et al. 2002, Östhols et al. 1997, Rothe et al. 2002, Reich et al. 1996, 1998). Da bei Untersuchungen von Sorptions- bzw. Einbauproben mit Hilfe der Röntgenabsorptionsspektroskopie aufgrund der schlechteren Empfindlichkeit der Methode gegenüber der TRLFS zum einen deutlich höhere Konzentrationen an Actiniden und zum anderen wesentlich größere Mengen an Substrat eingesetzt werden müssen, wurden die EXAFS Messungen an Am(III) durchgeführt. Eingesetzt wurde das langlebige Isotop ^{243}Am ($t_{½}$ = 7370 a), das im Vergleich zu ^{248}Cm leicht verfügbar und um mehrer Größenordnungen preiswerter ist.

Bei der Röntgenabsorptionsspektroskopie wird die zu untersuchende Probe mit monochromatischen Röntgenlicht bestrahlt. Bei Erhöhung der Photonenenergie durchläuft der Strahl die Röntgenabsorptionskanten der Elemente in einer Probe. Das Prinzip der XAS besteht in der Messung der Variation des Absorptionskoeffizienten $\mu(E)$ in Abhängigkeit der Energie der einfallenden Röntgenstrahlung. In Abbildung 9 ist solch ein Absorptionsspektrum dargestellt (L3 Kante von Uran).

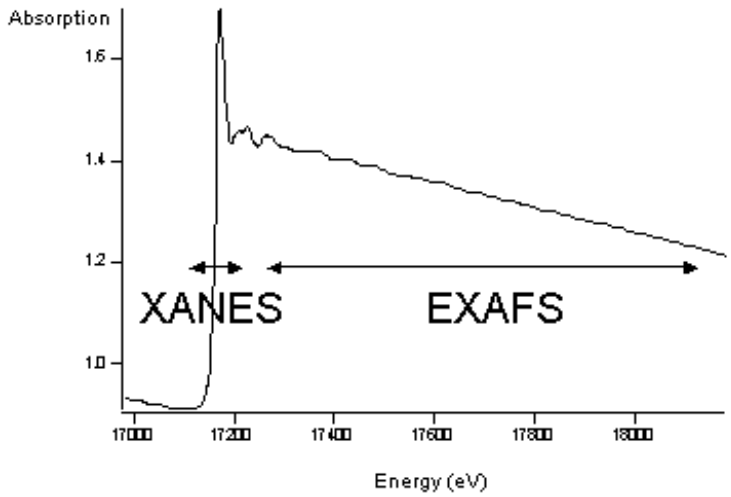

Abbildung 11 Röntgenabsorptionsspektrums der Uran L3 Kante

Das XANES Spektrum (X-ray Absorption Near-Edge Structure) ergibt bei kinetischen Energien mit Wellenlängen im Bereich des ersten interatomaren Bindungsabstands ein physikalisches Bild der unbesetzten Zustände und spiegelt die Dichte der elektronischen Zustände, die die absorbierenden Atome umgibt, wider. Bei höheren kinetischen Energien dominieren intra- und intermolekulare Mehrfachstreuprozesse. Durch Vergleich mit Referenzspektren und mit Hilfe von theoretischen Berechnungen können Informationen über die Valenz und Koordinationsgeometrie absorbierender Atome erhalten werden.

Die Abkürzung EXAFS steht für Extended X-ray Absorption Fine Structure. Das EXAFS Spektrum ergibt das physikalische Bild eines Interferrogramms der atomaren Anordnung, die das absorbierende Atom umgibt.

Aus der Absorption des Röntgenlichts resultieren Photoelektronen mit niedriger kinetischer Energie, die an den umliegenden Atomen rückgestreut werden. Die Emission sowie Rückstreuung können auch als Wellen beschrieben werden. Bei der Interferenz dieser Wellen kommt es zu Effekten wie Auslöschung oder Resonanz, wodurch das Spektrum der Probe eine Feinstruktur erhält. In Abbildung 10 ist das Prinzip der Interferenz schematisch dargestellt.

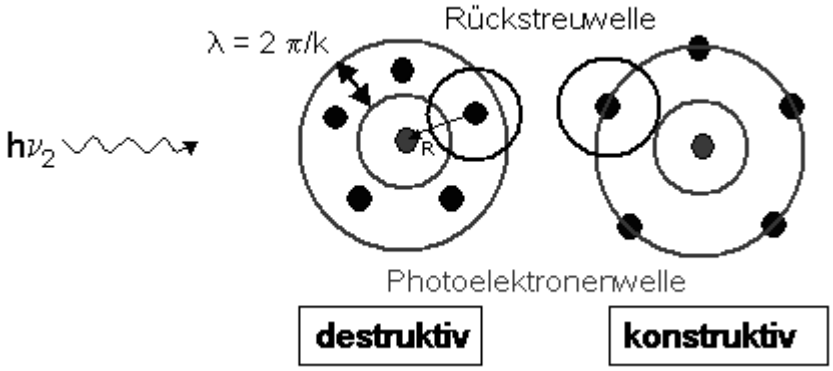

Abbildung 12 Darstellung der Rückstreuung von Photoelektronen des angeregten Atoms an benachbarten Atomen

Aus der Analyse der Feinstruktur lassen sich die Ordnungszahl (Z ± 1), die Bindungslängen (± 0.02 Å) sowie die Anzahl der Atome, die das angeregte Atom umgeben (Präzision ~25 %), bestimmen.

In der vorliegenden Arbeit wurden mit Hilfe der Röntgenabsorptionsspektroskopie die Strukturparameter sowohl für an Mineraloberflächen sorbierte als auch in Sekundärphasen eingebaute Europium- und Americiumionen bestimmt.

2. Sorption von Eu(III), Am(III) und Cm(III) an Oxiden: Das Modellsystem γ-Al_2O_3

γ-Al_2O_3 (γ-Alumina) als käuflicher, wohl definierter Feststoff vereint mehrere interessante Eigenschaften für Untersuchungen an der Wasser/Mineralphasen Grenzfläche in sich, die es zu einem geeigneten Modellsystem für endlagerelevante Minerale macht. Zum einen können die Wechselwirkungen von Metallionen mit den für die Reaktionen an Tonmineraloberflächen wichtigen Aluminolgruppen ohne störende, schwer quantifizierbare Einflüsse von Fremdelementen oder Fremdphasen charakterisiert werden. Da Ton sowohl als endlagerrelevante Gesteinsformation im Gespräch ist, als auch als mögliches Verfüllmaterial zum Verschluss eines Endlagers in Steinsalz oder Granit zum Einsatz kommen wird, sind Untersuchungen zur Aufklärung der Sorptionsmechanismen von Radionukliden an der Tonmineraloberfläche für die Endlagersicherheit wichtig. Zum anderen zeigt die γ-Al_2O_3 Festkörperstruktur große Ähnlichkeit mit der des Ferrihydrits. Ferrihydrit als amorphe Eisenoxidphase findet sich häufig als „Oberflächencoating“ auf anderen Mineralen. Insbesondere durch die Korrosion von eisenhaltigen Behältern ist mit diesem Eisenoxid im Nahbereich eines Endlagers zu rechnen und kann einen großen Teil der zur Sorption zur Verfügung stehenden Oberfläche darstellen. Oberflächenreaktionen der Metallionen Eu(III) und Cm(III) mit Eisenoxidmineralphasen jedoch können aufgrund der bereits beschriebenen Quencheffekte bei der Anbindung der f-Elemente an Ferrinolgruppen nicht mit Hilfe der TRLFS untersucht werden. Somit stellt γ-Alumina ein gut geeignetes Modellsystem dar, um ein Prozessverständnis der Sorption von Actiniden und Lanthaniden an der Wasser/Tonmineral bzw. Wasser/Eisenoxid Grenzfläche zu entwickeln. Die wesentlichen Untersuchungsergebnisse wurden in folgenden Publikationen veröffentlicht:

"Sorption of Am(III) and Eu(III) onto γ-Alumina: Experimental Results and Modelling"; Thomas Rabung, Thorsten Stumpf, Horst Geckeis, Reinhardt Klenze, Jae Il Kim; Radiochim. Acta, 2000, 88, 711-716.

"A spectroscopic study of the Cm(III) sorption onto γ-Alumina"; Thorsten Stumpf, Thomas Rabung, Reinhardt Klenze, Horst Geckeis, Jae Il Kim; J. Colloid Interface Sci., 2001, 238, 219-224.

Um die Wechselwirkung von Eu(III) und Am(III) mit γ-Alumina zu quantifizieren, wurden Sorptionsisothermen im pH Bereich von 4 bis 8 aufgenommen. Die Datensätze ließen sich mit der Annahme zweier Oberflächenplätze bzw. zweier Oberflächenkomplexe beschreiben. Zudem wurde die Ähnlichkeit der γ-Alumina Oberfläche mit einer Eisenoxidoberfläche (Hämatit) bezüglich der Wechselwirkung mit dreiwertigen Actiniden/Lanthaniden bestätigt. Die Sorptionsisothermen in Gegenwart von sowohl γ-Alumina als auch Hämatit konnten mit Hilfe des gleichen "two site surface complexation model" und den selben Komplexierungskonstanten angepasst werden.

Durch das Detektieren des Intensitätsverhältnisses zwischen den $^5D_0 \rightarrow {}^7F_1$ (λ = 593 nm) und $^5D_0 \rightarrow {}^7F_2$ (λ = 618 nm) Übergängen ließ sich mit Hilfe der zeitaufgelösten Laserfluoreszenzspektroskopie an Eu(III) der Sorptionsverlauf verfolgen. Es zeigte sich, dass sich pH Wert abhängig mindestens ein Eu(III)/γ-Alumina inner-sphere Komplex bildet. Die Emissionslebensdauern steigen bei der Anbindung des Lanthanids an die Oberfläche von 114 µs (Eu^{3+} Aquoion) auf bis zu 239 µs an. Diese Zunahme der Lebensdauer deutet auf den Verlust der halben Hydrathülle des Metalls bei der Sorption hin. Um detailliertere Informationen zum Sorptionsmechanismus auf molekularer Ebene zu erhalten, wurden Cm TRLFS Untersuchungen durchgeführt.

Mit den Untersuchungen zur Wechselwirkung von Curium mit γ-Alumina konnte gezeigt werden, dass die zeitaufgelöste Laserfluoreszenzspektroskopie eine geeignete Methode ist, um die Sorption von Cm(III) an einer Mineraloberfläche im Spurenkonzentrationsbereich im Detail aufzuklären. Die Verschiebung des Cm(III) Signals mit der Änderung des pH Wertes lässt das Voranschreiten des Sorptionsprozesses quantifizieren und auf zwei verschiedene gebildete Cm/Alumina Oberflächenkomplexe schließen. Durch eine Analyse der Emissionslebensdauern der jeweiligen Cm Spezies konnte eine Reduktion der Metallhydrathülle bei der Anbindung an die Mineraloberfläche um vier Wassermoleküle nachgewiesen werden. Bei den identifizierten Spezies handelt es sich um das hydratisierte Metallion $Cm(H_2O)_9$, um den Oberflächenkomplex 1 Al-O-$Cm(H_2O)_5$ und um den weiteren Oberflächenkomplex 2 der entweder die hydrolisierte Version des Komplexes 1 Al-O-$Cm(OH)(H_2O)_4$ darstellt oder bei dem es sich um einen Oberflächenkomplex handelt, bei dem das Cm Ion bidentat über Aluminolgruppen an die Mineralfläche angebunden ist. Ein weiteres wichtiges Ergebnis dieser Untersuchung ist, dass

unabhängig von der Actinid/Lanthanid Konzentration immer und ausschließlich die selben Cm Emissionsmaxima der Komplexe 1 und 2 auftreten. Bei Variation der Metallionen Konzentration zwischen 2.7 x 10^{-8} mol/L und 4.5 x 10^{-5} mol/L verschiebt sich zwar wie zu erwarten die pH-edge, da die Mineraloberfläche unterschiedlich stark deprotoniert werden muss, um alle Metallionen zu sorbieren. Die durch ihre Emissionsspektren identifizierten Cm(III)/γ-Alumina Spezies ändern sich jedoch nicht. Dies lässt an dem immer wieder bei Modellrechnungen zur Sorption von Metallionen an Oberflächen postulierten Vorhandensein von "weak" und "strong sites" (also zweier Sorptionsplätze auf der gleichen Oberfläche mit unterschiedlicher Affinität zu den sorbierenden Ionen) im Falle von γ-Alumina zweifeln. Bei einer M(III) Konzentration im Spurenkonzentrationsbereich sollten zuerst die „strong sites“ belegt werden und die entsprechende Sorptionsspezies durch die starke Wechselwirkung mit der Oberfläche ein signifikantes Cm(III) Emissionssignal zeigen. Eine Erhöhung der M(III) Ionenkonzentration sollte zur Absättigung der „strong sites“ führen und die weitere Belegung der Oberfläche an Stellen mit „weak sites“ erfolgen. In einem solchen Fall ist mit einer deutlichen Blauverschiebung (entsprechend der schwächeren Wechselwirkung von Cm(III) mit der/den funktionellen Gruppen an der Mineraloberfläche im Vergleich zur Anbindung an „strong sites“) zu rechnen. Wie bereits erwähnt, konnte diese Veränderungen des Emissionssignals in Abhängigkeit von der M(III) Konzentration nicht beobachtet werden.

Radiochim. Acta **88**, 711–716 (2000)
© by Oldenbourg Wissenschaftsverlag, München

Sorption of Am(III) and Eu(III) onto γ-alumina: experiment and modelling

By Th. Rabung*, Th. Stumpf, H. Geckeis, R. Klenze and J. I. Kim

Forschungszentrum Karlsruhe, Institut für Nukleare Entsorgungstechnik, P.O. Box 3640, D-76021 Karlsruhe, Germany

(Received November 18, 1999; accepted April 4, 2000)

Europium / Americium / γ-Alumina / Sorption isotherms / Surface complexation modelling / Laser fluorescence spectroscopy

Summary. The present paper describes the surface complexation behaviour of trivalent metal ions, Am(III) and Eu(III), on well characterised γ-alumina. Experiments are conducted at different pH (4–8) and ionic strength (0.001–0.1 M $NaClO_4$) either in the presence or absence of CO_2. By varying the metal ion concentration from 10^{-9} to 10^{-4} mol/L, the sorption isotherm is established under each given experimental condition. Different surface complexation models are applied to the experimental results to interpret and appraise the surface sorption processes under different experimental conditions. A comparison of the present results is made with the Eu(III) sorption onto the hematite mineral surface investigated previously. It has been shown that sorption properties of hematite and γ-alumina seem to be quite similar. For both systems, a good agreement is found between experimental data and modelling, once using the two site surface complexation model and the same complexation constants for the respective monodentate surface complex. The Eu(III) sorption reaction is additionally studied *in-situ* by time resolved laser fluorescence spectroscopy (TRLFS). Formation of inner-sphere complexes can be deduced from the emission spectra. The continuous increase of the fluorescence life time with increasing pH starting from pH = 5.0 indicates that surface complexation is accompanied by a decreasing number of hydration water in the first coordination sphere.

Introduction

The reactions of long-lived radionuclides, especially those of actinide ions, at the solid/water interface are important for the long-term performance assessment of nuclear waste repositories [1]. In order to appraise the significance of these reactions on the actinide migration in a natural system characterized by considerable heterogeneities and long reaction time, (1) thermodynamic data of the reactions involved are required for a number of important mineral phases under defined geochemical conditions; (2) mechanistic understanding is necessary for thermodynamic modelling including the knowledge of solid actinide speciation; and (3) kinetics of solid/water reactions have to be known for the respective sorption process e.g. ion exchange, surface complexation, surface precipitation, incorporation into the solid. Some reactions may appear to be irreversible depending on the considered time scale. Surface complexation modelling based on systematic sorption investigations are scarce for metal ions with ionic charges ≥ 3+, especially for actinide ions [2–4]. The application of appropriate spectroscopic methods including X-ray absorption spectroscopy (EXAFS) and laser fluorescence spectroscopy (TRLFS) have been used for the identification of sorbed metal species and thus for the elucidation of sorption mechanisms [5–7].

The aim of the present study is to investigate the Eu(III) sorption on γ-Al_2O_3 as a function of pH. The behaviour of Am(III) is compared with that of Eu(III), often taken as a chemical homologue. The sorbent properties of γ-Al_2O_3 are compared with those of hematite and goethite investigated in previous studies [8, 9]. Hydrous iron oxides are sorbents of high relevance for metal ions in natural aquifers. Even though Al_2O_3 does not occur frequently as a pure mineral in natural systems, its surface characteristics are known to be similar to those of iron oxides with respect to metal ion sorption. In contrast to iron oxides [6, 7] it is transparent for the exciting laser light and γ-Al_2O_3 is therefore an appropriate model sorbent for the time resolved laser fluorescence spectroscopic (TRLFS) studies. The TRLFS investigations are correlated to the sorption reaction mechanism, derived from the isotherm experiments.

Experimental

The hydrous γ-Al_2O_3 particles used in this work (Degussa, Aluminium Oxide C) have already been applied for sorption experiments by other authors [4, 10–12]. Prior to its use γ-alumina was purified based on the reported procedures [10, 12, 13]: first washing with 0.1 M HNO_3, then with 0.1 M NaOH up to pH 10 and finally rinsing with Milli-Q water until the conductivity of the washing solution reached that of pure water. The purified alumina was then stored as a suspension (50 g/L) in Milli-Q water. Using the N_2-BET method the specific surface area of a freeze dried sample was found to be 119 m^2/g and the average particle radius measured by dynamic light scattering (Zeta plus, Brookhaven Inc.) to be about 90 nm. The protonation constants of surface hydroxyl groups and the number of available surface sites

*Author for correspondence (E-mail: rabung@ine.fzk.de).

were determined by acid-base titration of 7.5 g/L γ-Al_2O_3 under Ar atmosphere, as described elsewhere [8], at ionic strengths of 0.1, 0.01 and 0.001 M $NaClO_4$.

The sorption behaviour was investigated by batch experiments for the varying Eu(III) concentration (10^{-9}–10^{-4} mol/L) at different pH (4.0, 5.0, 5.5, 6.0, 7.0 and 8.0) and ionic strengths (0.1, 0.01 and 0.001 M $NaClO_4$). Buffer solutions used for fixing each given pH are: 1 mM β-(4-pyridyl)ethanesulfonic acid (PES), 2-(N-morpholino)ethanesulfonic acid (MES), piperazine-N,N′-bis[2-ethanesulfonic acid] (PIPES) and tris(hydroxymethyl)-aminomethane (Tris). At these concentrations the buffers did not show any competitive complexation with metal ions [9]. Preliminary results indicated that the sorption equilibrium is reached within 2 days. For each batch experiment, 1 mL of the γ-Al_2O_3 stock solution was suspended in 15 mL electrolyte solution and equilibrated for 1 day before adding Eu(III) or Am(III). pH was adjusted by addition of 0.1 M $HClO_4$ or 0.1 M NaOH. The Eu(III) concentration was determined by ICP-AES or ICP-MS and when Am-241 and Eu-152 were used, a radiometric assay was made by γ-spectrometry, after centrifugation at 18.000 rpm for 30 min. Experiments carried out at pH = 7 under argon atmosphere and under air did not differ significantly. Therefore, the atmospheric CO_2 did not noticeably influence the reaction under given experimental conditions (pH $\leq$ 7). However, the CO_2 effect must be taken into account at pH > 7.

TRLFS measurements were performed using a pulsed Nd:YAG pumped dye laser system (Continuum, Powerlite 9030, ND 6000). Laser pulse energy was adjusted to 4 mJ and controlled by a photodiode. The fluorescence emission was detected by an optical multichannel analyzer consisting of a polychromator (Chromex 250 is) with a 300 lines/mm grating. This arrangement allows simultaneous detection of the whole Eu(III) emission spectrum. The emission spectrum was recorded in the range 500–700 nm within a constant time window of 1 ms at the constant excitation wavelength of 393.6 nm (laser dye: Exalite 398). For measuring the time dependent emission decay, the delay time between laser pulse and camera gating was scanned with time intervals between 10 and 15 µs. For the spectroscopic study, the Eu(III) and γ-Al_2O_3 concentrations were fixed to 3.2×10^{-6} mol/L and 0.57 g/L, respectively. Samples were taken from the batch experiment.

Results and discussion

Acid base properties of γ-Al_2O_3

Results of the potentiometric titration for γ-Al_2O_3 are shown for three different ionic strengths in Fig. 1 together with a blank titration of the pure electrolyte solution ($I = 0.1$ $NaClO_4$). The common intersection point for all titration curves appears at pH = 8.6 at the point of zero charge (PZC). The solid lines in Fig. 1 are obtained from the constant capacitance model (CCM) using the computer code FITEQL [8, 17]. A summary of the fit parameters K_{a1}^{int}, K_{a2}^{int}, total concentration of surface hydroxyl groups $[\equiv SOH]_{tot}$ and capacitance C is given in Table 1. All data fall within the range of the published data in the literature [10, 12, 14–16].

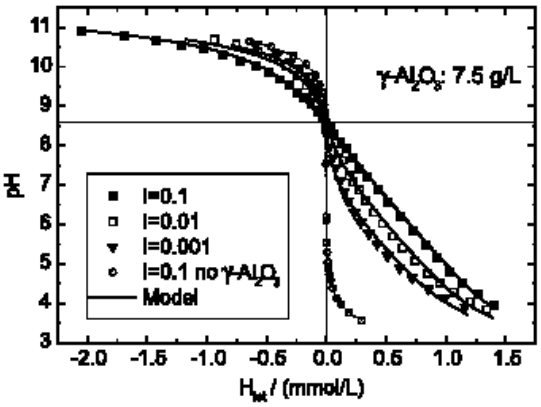

Fig. 1. Titration curves for γ-Al_2O_3 suspensions at $I = 0.1$, 0.01 and 0.001 M $NaClO_4$ including a blank titration of pure electrolyte solution at $I = 0.1$ M; straight lines are calculated using CCM and data from Table 1.

Table 1. Surface protonation and deprotonation constants, surface site concentration/density and capacitance as calculated for γ-Al_2O_3 titration using FITEQL and Constant Capacitance Model. A comparison with literature data for $I = 0.1$ M is also included.

	$NaClO_4$ 0.1 mol/L	$NaClO_4$ 0.01 mol/L	$NaClO_4$ 0.001 mol/L
$\log K_{a1}^{int}$	7.59 ± 0.02	6.87 ± 0.01	6.10 ± 0.03
$\log K_{a2}^{int}$	9.54 ± 0.02	10.40 ± 0.02	10.98 ± 0.03
C (F/m²)	0.8	0.8	0.8
site concentration (mol/g)	1.96×10^{-4}	1.99×10^{-4}	2.38×10^{-4}
site density (nm^{-2})	1.0	1.0	1.2
WSOS/DF	7.06	29.9	49.7

Comparison of γ-Al_2O_3 titration data for $I = 0.1$

$\log K_{a1}^{int}$	$\log K_{a2}^{int}$	site density (nm^{-2})	pH_{pzc}	Reference
7.6	9.5	1.0	8.6	this work
7.9	9.1	0.5	8.5	[10]
7.4	10.0	1.3	8.7	[15]
7.2	9.5	1.3	8.3	[12]
7.5	10.5	1.9	9.2	[16]
7.2	10.3	10	8.9	[14]

With decreasing ionic strength, one observes a decrease of the protonation constant (K_{a1}^{int}) and an increase of the deprotonation constant (K_{a2}^{int}) as noted in the literature [14], while the number of surface sites remains virtually constant. Values for WSOS/DF obtained by using the default error estimates of the FITEQL-code [17] are also given in Table 1. The WSOS/DF-values, which represent a measure for the goodness of fit [17], indicate a better agreement between model and experiment with increasing ionic strength. This finding is consistent with the fact that the CCM is more appropriate to describe the charge distribution at the solid/liquid interface at higher ionic strengths. As most sorption experiments in this work were conducted at $I = 0.1$ mol/L, the data obtained by CCM at this ionic strength are used for further modelling of the Eu(III) sorption onto γ-Al_2O_3.

Sorption isotherms for Eu(III) and Am(III)

Most of the investigations of metal ion sorption onto mineral surfaces published so far in the literature have been confined to the pH-dependent sorption (so called pH-edges) for one or two sorbate concentrations [2, 3, 6, 11, 12]. A direct comparison of these experimental results with one another is difficult as the pH-edge can be very different even if ideal sorption behaviour (Nernst-isotherm: $c_{\text{sorbed}} = k \cdot c_{\text{solution}}$) occurs and the same sorbate to sorbent ratio is maintained at varying volume to sorbent mass ratio [9]. Fig. 2 shows the Eu(III) sorption onto γ-Al_2O_3 as a function of pH for five different Eu(III) concentrations at a constant amount of solid and $I = 0.1$. As expected, the pH-edge shifts to higher pH values with higher Eu(III) concentration [18]. Variation of the metal ion concentration at constant pH provides further information. Fig. 3 illustrates the results for the Eu(III) and Am(III) sorption onto γ-Al_2O_3 over a broad concentration range at different pH in a double logarithmic plot. As expected, a strong increase of sorption is noticed with increasing pH. At lower Eu(III) or Am(III) concentrations, a slope of 1 is observed, typical for an ideal Nernst type adsorption (ideal sorption range). At higher surface coverages, the slope of the isotherm decreases. From Fig. 3 it is apparent that the sorption behaviour of Eu(III) is the same as that of Am(III). Therefore, the sorption of trivalent actinides can be simulated by using Eu(III), especially for the higher metal ion concentrations, where the resulting α-activity of Am(III) may create problems related to experimental handling and radiolysis effects. The error bars in Fig. 3 are calculated by estimating an analytical uncertainty of 5% for the determination of the Eu(III)/Am(III) concentrations. At low pH the sorption is low (e.g. pH 4) and the uncertainty in the determination of the sorbed Eu(III)/Am(III) concentrations therefore becomes quite high. On the other hand, at high pH, when nearly all Eu(III)/Am(III) is sorbed onto the surface, the analytical error for the non-sorbed metal ion concentration increases as the limit of detection is approached. This explains the larger scattering of data obtained at pH 8.

The influence of ionic strength on the sorption reaction at pH 6.0 and 7.0 is plotted in Fig. 4. Within the experimental uncertainties, the sorption seems to be independent of ionic strength in the range studied. This suggests the formation of strong inner sphere complexes even under conditions where the net surface charge of γ-Al_2O_3 is positive (pH < 8.6). This finding indicates that the influence of surface potential on the sorption reaction is of minor importance for the metal ions of higher charge ($z \geq 3+$) and confirms earlier conclusions drawn from the study of the Eu(III)/hematite system [8].

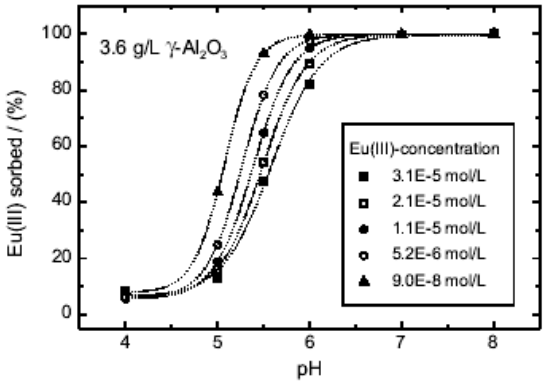

Fig. 2. pH dependence of the Eu(III) sorption onto γ-Al_2O_3 at a constant solid concentration (3.6 g/L) and varying the Eu(III) concentration at $I = 0.1$ M $NaClO_4$.

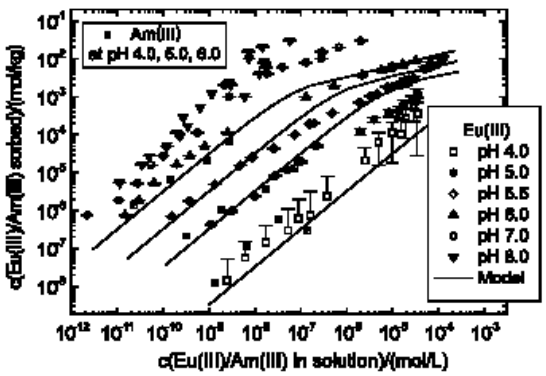

Fig. 3. Sorption isotherms for the Eu(III) sorption onto γ-Al_2O_3 at pH 4.0, 5.0, 5.5, 6.0, 7.0 and 8.0 ($I = 0.1$ M $NaClO_4$); corresponding data for Am(III) at pH 4.0, 5.0 and 6.0. Straight lines are calculated for pH ≤ 6 using $\log K_s^{\text{int}} = 2.50$ and $\log K_\gamma^{\text{int}} = -0.82$ and assuming a "strong" site concentration of 2% of total site density.

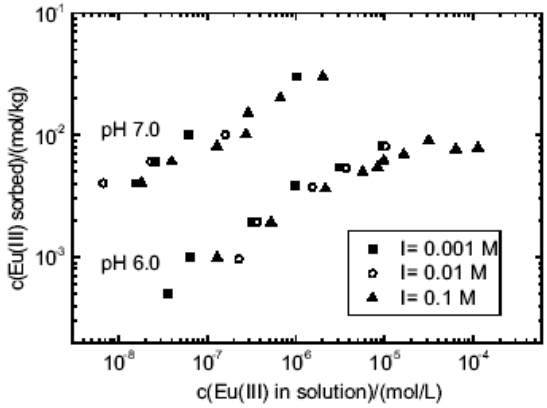

Fig. 4. Influence of ionic strength on the Eu(III) sorption onto γ-Al_2O_3: sorption isotherms for $I = 0.1$, 0.01 and 0.001 M $NaClO_4$ at pH 6 and 7.

Surface complexation modelling

For the modelling of the Eu(III)/Am(III) sorption onto γ-alumina, the same approach is used as in the previous study of Eu(III) sorption onto natural hematite and goethite [8, 9]. In both cases, two different types of surface hydroxyl groups are assumed to participate in the surface complexation reaction: one of relatively high complexation strength but of low concentration, so-called "strong" sites (≡XOH) and the other with higher concentration but lower complexation strength, so-called "weak" sites (≡YOH). The "strong" site complexation prevails at low surface coverage and is responsible for the Nernst shape of the isotherm. The "weak" site complexation is important at higher Eu(III)/Am(III) concentrations. Two- or multiple

site SCM's are frequently used in order to describe sorption isotherms like those obtained in the present work [18]. The presence of different sites with strong and weak complexing properties has been confirmed by an EXAFS study [19] of Pb(II) and Co(II) sorption to γ-Al_2O_3 single crystals. The authors attribute the "strong" and "weak" sites to surface hydroxyl groups at different crystal planes. The surface precipitation or polynucleation at the mineral surface has also been reported to create isotherm shapes as those observed in this work [20, 21]. As the contact time with air during sample preparation is insufficient to reach equilibrium with CO_2, the Eu(III)/Am(III) solubility is estimated using only solubility data for $Eu(OH)_3$/$Am(OH)_3$ and not for $Eu(OHCO_3)$/$Am(OHCO_3)$ [22]. Under the present experimental conditions, surface precipitation is highly improbable at pH ≤ 6, as has been discussed previously [8]. However, at pH ≥ 7 and at Eu(III)/Am(III) concentrations $\geq 10^{-7}$ mol/L, the solubility limits for $Eu(OH)_3$/$Am(OH)_3$ are approached or even exceeded and the surface coverage increases to ca. 15% of the total surface sites. According to the criteria given by Dzombak and Morell [18], surface precipitation is likely to occur when the metal ion concentration $\geq 1/10$ of the solubility limit and the surface coverage $\geq 1/3$. The spectroscopic study, however, supports, as will be described below, the presence of inner-sphere surface complexes even at pH = 8, rather than surface precipitation.

The description of the sorption reaction by SCM is restricted to experimental data obtained at pH ≤ 6. In this pH range and within the solubility limit, only the free metal ion is present without carbonate complexation and hydrolysis of Eu(III)/Am(III) [8]. Under these conditions the following complexation reactions of the Eu^{3+}/Am^{3+}-ions with surface hydroxyl groups are assumed:

$$\equiv\mathrm{XOH} + \mathrm{Eu}^{3+} \Leftrightarrow \equiv\mathrm{XOEu}^{2+} + \mathrm{H}^{+}, \quad K_x^{\mathrm{int}} \qquad (1)$$

$$\equiv\mathrm{YOH} + \mathrm{Eu}^{3+} \Leftrightarrow \equiv\mathrm{YOEu}^{2+} + \mathrm{H}^{+}, \quad K_y^{\mathrm{int}} \qquad (2)$$

Adjusting the concentration of "strong" sites to 2.0% of the total number of surface hydroxyl groups is found to be optimal to describe the sorption data. The total number of surface hydroxyl groups was derived from the potentiometric titrations (c(strong sites) = 3.9×10^{-6} mol/g, c(weak sites) = 1.9×10^{-4} mol/g). The value for the fraction of strong sites is close to that observed by Dzombak and Morel for hydrous ferric oxides (2.4%) [18] and also to that obtained for the Eu(III)/hematite system (3.8%) [8]. A striking result of this study is that the sorption isotherms can be described satisfactorily using the same model assumptions and even an identical data set ($\log K_x^{\mathrm{int}} = 2.50$ and $\log K_y^{\mathrm{int}} = -0.82$) as used earlier to describe the Eu(III)/hematite system [8]. In both systems lateral Coulombic interactions at higher surface coverage are included by taking into account only the sorbed Eu(III) species (Fig. 3). The "strong" site complexation constant has been validated by using the graphical method reported earlier [8] for the linear extrapolation of the number of "strong" sites from the sorption isotherms. Data for $\log K_x^{\mathrm{int}}$ derived from this technique, which does not require the fit parameters obtained from the potentiometric titration data, are summarised in Table 2, and are found to be in a good agreement with the corresponding value determined in the Eu(III)/hematite system [8].

Table 2. Result of graphical determination of "strong" site surface complexation constant for pH 5.0, 5.5 and 6.0.

pH	5.0	5.5	6.0
$\log K_x^{\mathrm{int}}$	2.58 ± 0.03	2.63 ± 0.01	2.54 ± 0.01

average $\log K_x^{\mathrm{int}}$ for the hematite system: 2.50 ± 0.19 [8]

The assumed monodentate surface complexation reaction can be supported by looking at the net proton exchange per sorbed Eu(III) ion, which should be equal to 1 [8]. Rearranging Eq. (1) yields the relation:

$$\log \frac{[\equiv\mathrm{XOEu}^{2+}]}{[\mathrm{Eu}^{3+}]} = \log K_x^{\mathrm{int}} + \log \frac{[\equiv\mathrm{XOH}]}{[\mathrm{H}^{+}]} \qquad (3)$$

A plot of this relationship using isotherm data for pH ≤ 7 and low surface coverage, where only "strong" site complexation is considered, is shown in Fig. 5. [≡XOH] is calculated from the protonation constants (K_{a1}^{int}, K_{a2}^{int}), the concentration of sorbed Eu(III), and the total concentration of strong binding sites $[\equiv\mathrm{XOH}]_{\mathrm{tot}}$. For pH ≤ 6, a linear relation with a slope of 0.99 verifies the assumption of monodentate surface complexation. The intersection point with the y axis yields $\log K_x^{\mathrm{int}} = 2.66$ which is in good agreement with the corresponding values given in Table 2. For the data at pH 7 and 8, this linear relationship is no longer valid, even if hydrolysed Eu(III) species in solution are taken into account. This is attributed to the possible existence of hitherto unknown hydrolysed Eu(III) surface species.

As the sorption reaction is independent of the ionic strength, an electrostatic correction term was not necessary at the low surface coverages of hematite, goethite and alumina. Thus, the sorption reaction of Eu(III) and Am(III) onto iron and aluminum oxides in the natural metal ion concentration range can be described for pH ≤ 6 simply by the formation of a monodentate surface complex. For understanding the processes occurring at higher metal ion concentrations and at pH > 6, further investigation of the possibility of ternary surface complex formations is necessary.

TRLFS study

In general, the lanthanide fluorescence emission wavelengths for the transition $^5D_0 \rightarrow {}^7F_j$ are only weakly de-

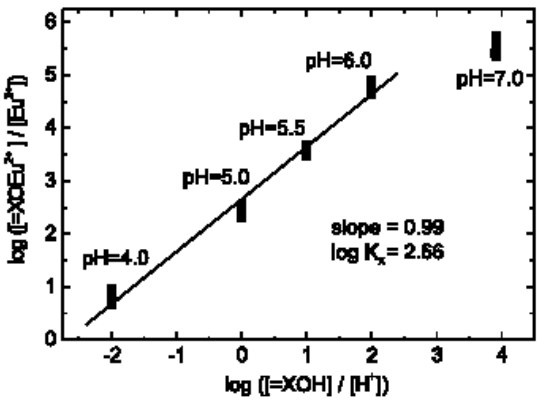

Fig. 5. Function plot of (3) for isotherm data at low surface coverage and pH ≤ 7.

pendent on the chemical environment of the metal ion. The intensity for the $^5D_0 \rightarrow {}^7F_2$ transition, however, changes significantly on variation of the first coordination sphere due to the so-called "hypersensitive effect" [23–25]. The ratio of the emission intensity ratio obtained for the $^5D_0 \rightarrow {}^7F_1$ ($\lambda = 594$ nm) and $^5D_0 \rightarrow {}^7F_2$ (619 nm) transitions together with the fluorescence lifetime provide valuable information on the Eu(III) speciation [26–28]. Fluorescence emisson spectra obtained for Eu(III) in the presence of alumina at different pH are shown in Fig. 6. No clear change of the peak shape and position at $\lambda = 594$ nm and 619 nm are observed. The intensity ratio decreases with increasing pH and simultaneously with the progress of the sorption reaction. The fluorescence lifetime increases from 110 µs at pH 4 and 5 to 235 µs at pH 7–8 (Table 3). According to the Horrocks relation [27], the increase of the fluorescence lifetime is related to a decrease in the hydration number. The number of H_2O molecules in the first coordination sphere, calculated from the fluorescence lifetime, decreases from 9 for the free Eu^{3+} ion to 5 ± 1 at pH = 8 indicating the formation of inner-sphere surface complexes. Polynucleation and surface precipitation reactions imply the close neighborhood of sorbed Eu(III) ions. In that case, the phonon assisted transition process leads to a decrease of the fluorescence lifetime [29]. The opposite is found in this study indicating a disperse Eu(III) distribution rather than cluster formation or precipitation at the surface even though solubility limits of $Eu(OH)_3$ at pH = 8 with respect to the total Eu(III) concentration are exceeded.

Under the given experimental conditions, practically 100% of Eu(III) is sorbed at pH $\geq$ 7.0. Increasing pH from 7.0 to 8.0 does not influence the fluorescence lifetime and thus no change in the surface speciation of Eu(III) can be observed in the fluorescence spectra in this pH range. However, more detailed spectroscopic work is necessary to clearly identify the nature of sorbed species. Formation of hydrated Eu(III) species at the alumina surface can be assumed as deduced earlier from a spectroscopic study of Cm(III) sorption onto silica at pH < 7 [6]. However, different from the present results for the Eu(III)/alumina system, a further increase of the fluorescence lifetime at pH > 7 has been observed in the case of the Cm(III)/silica system [6] and interpreted as a total loss of H_2O in the first coordination sphere, which is understood as an inclusion of Cm(III) into the solid.

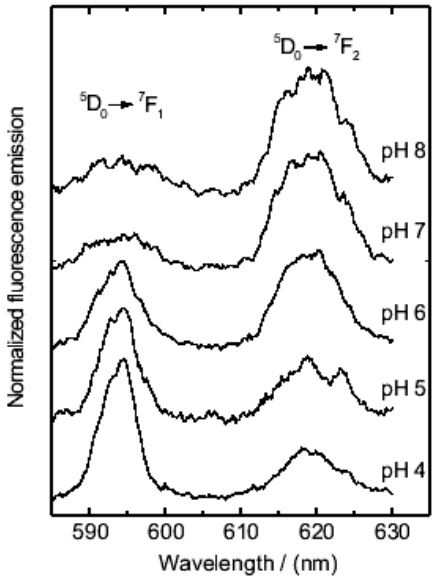

Fig. 6. Laser fluorescence spectra for Eu(III) sorption onto γ-Al_2O_3 at different pH, c(Eu(III)) = 3.2×10^{-6} mol/L, $c(\gamma\text{-}Al_2O_3) = 0.57$ g/L, $I = 0.1$ M $NaClO_4$.

Table 3. Results from fluorescence spectra for Eu(III) sorption onto γ-Al_2O_3: lifetime and $^5D_0 \rightarrow {}^7F_1/{}^5D_0 \rightarrow {}^7F_2$ intensity ratio.

pH	4.0	5.0	6.0	7.0	8.0
Lifetime	114 µs	105 µs	183 µs	239 µs	235 µs
$^5D_0 \rightarrow {}^7F_1/{}^5D_0 \rightarrow {}^7F_2$	2.4	1.6	0.9	0.4	0.3

Conclusions

The Eu(III)/Am(III) sorption onto γ-Al_2O_3 can be described using a two site complexation model and assuming the presence of a monodentate surface complex (pH $\leq$ 6). The results are consistent with those found for the Eu(III) sorption onto natural hematite. The SCM constants are found to be identical for iron oxides and alumina, indicating the very close similarity for the sorption properties of both types of minerals. Consequently, it is assumed that spectroscopic findings on the sorption mechanism on alumina can also be applied to iron oxides.

In the low metal ion concentration range, the surface complexation modelling is applied successfully to describe the sorption behaviour of trivalent actinides. Understanding of the actinide ion sorption at higher metal ion concentrations and at pH > 6 however, demands a further understanding of the sorption mechanism. A first TRLFS study shows the suitability of this technique for the speciation of sorbed metal ions on colloid surfaces and supports the formation of inner-sphere surface complex species rather than polynucleation at the surface. More detailed work is necessary however, to attain further information on number and nature of surface sorbed species.

References

1. Degueldre, C., Ulrich, H. J., Silby, H.: Sorption of ^{241}Am onto Montmorillonite, Illite and Hematite Colloids. Radiochim. Acta **65**, 173 (1994).
2. Kosmulski, M.: Standard Enthalpies of Adsorption of Di- and Trivalent Cations on Alumina. J. Colloid Interface Sci. **192**, 215 (1997).
3. Nordén, M., Ephraim, J. H., Allard, B.: The Influence of a Fulvic Acid on the Adsorption of Europium and Strontium by Alumina and Quartz: Effect of pH and Ionic Strength. Radiochim. Acta **65**, 265 (1994).
4. Csobán, K., Joó, P.: Sorption of Cr(III) on Silica and Aluminium Oxide: Experiments and Modelling. Colloids Surfaces **151**, 97 (1999).
5. Sposito, G.: In: *Geochemical Processes at Mineral Surfaces* (Davis, J.A., Hayes, K.F. eds.) ACS Symposium Series 323, American Chemical Society, Washington, DC, 1986, pp. 217–230.

6. Chung, K.H., Klenze, R., Park, K.K., Paviet-Hartmann, P., Kim, J.I.: A Study of the Surface Sorption Process of Cm(III) on Silica by Time-Resolved Laser Fluorescence Spectroscopy (I). Radiochim. Acta **82**, 215 (1998).
7. Geckeis, H., Klenze, R., Kim, J.I.: Solid-Water Interface Reaction of Actinides and Homologues: Sorption onto Mineral Surfaces. Radiochim. Acta **87**, 13 (1999).
8. Rabung, Th., Geckeis, H., Kim, J.I., Beck, H.P.: Sorption of Eu(III) on a Natural Hematite: Application of a Surface Complexation Model. J. Colloid Interface Sci. **208**, 153 (1998).
9. Rabung, Th.: Der Einfluß von Huminsäure auf die Sorption von Eu(III) auf Hämatit, Dissertation, Anorganische und Analytische Chemie und Radiochemie, Universität des Saarlandes 1998.
10. Huang, C.-P., Stumm, W.: Specific Adsorption of Cations on Hydrous γ-Al_2O_3. J. Colloid Interface Sci. **43**, 409 (1973).
11. Baumgarten, E., Kirchhausen-Düsing, U.: Sorption of Metal Ions on Alumina. J. Colloid Interface Sci. **194**, 1 (1997).
12. Hohl, H., Stumm, W.: Interaction of Pb^{2+} with Hydrous γ-Al_2O_3, J. Colloid Interface Sci. **55**, 281 (1976).
13. Horst, J., Höll, W. H.: Application of the Surface Complex Formation Model to Ion Exchange Equilibria, Part IV: Amphoteric Sorption onto γ-Aluminium Oxide. J. Colloid Interface Sci. **195**, 250 (1997).
14. Hayes, K.F., Redden, G., Ela, W., Leckie, J.O.: Surface Complexation Models: An Evaluation of Model Parameter Estimation Using FITEQL and Oxide Mineral Titration Data. J. Colloid Interface Sci. **142**, 448 (1991).
15. Kummert, R., Stumm, W.: The Surface Complexation of Organic Acids on γ-Al_2O_3. J. Colloid Interface Sci. **75**, 373 (1980).
16. Girvin, D.C., Gassman, P.L., Bolton, H.: Adsorption of Aqueous Cobalt Ethylenediamine-tetraacetate by γ-Al_2O_3. Soil Sci. Soc. Am. J. **57**, 47 (1993).
17. Westall, J.C., Morel, F.M.M.: FITEQL: A General Algorithm for the Determination of Metal-Ligand Complex Stability Constants from Experimental Data, Technical Note 18, Ralph M. Parsons Laboratory, Department of Civil Engineering, Massachusetts Institute of Technology, Cambridge, Mass 1977.
18. Dzombak, D.A., Morel, F.M.: Surface Complexation Modelling: Hydrous Ferric Oxide, Wiley-Intersience, New York, 1990.
19. Bargar, J.R., Towle, S.N., Brown, G.E., Parks, G.A.: XAFS and Bond-Valence Determination of the Structures and Compositions of Surface Functional Groups and Pb(II) and Co(II) Sorption Products on Single- Crystal γ-Al_2O_3, J. Colloid Interface Sci. **185**, 473 (1997).
20. Farley, K.J., Dzombak, D.A., Morel, F.M.M.: A Surface Precipitation Model for the Sorption of Cations on Metal Oxides, J. Colloid Interface Sci. **106**, 226 (1985).
21. Katz, L.E., Hayes, K.F.: Surface Complexation Modeling, I. Strategy for Modeling Monomer Complex Formation at Moderate Surface Coverage, J. Colloid Interface Sci. **170**, 477 (1995).
22. Bernkopf, M.F., Kim, J.I.: Hydrolysereaktionen und Karbonatkomplexierung von dreiwertigem Americium in natürlichen aquatischen Systemen, Report RCM 02884, Inst. für Radiochemie, Techn. Univ. München 1984.
23. Carnall, W.T., Goodman, G.L., Rajnak, K., Rana, R.S.: A Systematic Analysis of the Spectra of the Lanthanides Doped into Single Crystal LaF_3, Report ANL-88-8, Argonne National Laboratory, Argonne 1988.
24. Carnall, W.T.: The Absorption and Fluorescence Spectra of Rare Earth Ions in Solution, In: *Handbook on the Physics and Chemistry of Rare Earth*, North Holland Publishing, Amsterdam 1976.
25. Jörgensen, C.K., Judd, B.R.: Hypersensitive Pseudoquadrupole Transitions in Lanthanides. Mol. Phys. **8**, 281 (1964).
26. Dobbs, J.C., Susetyo, W., Knight, F.E., Castles, M.A., Carreira, L. A., Azarraga, L. V.: Characterization of Metal Binding Sites in Fulvic Acids by Lanthanide Ion Probe Spectroscopy: Anal. Chem. **61**, 483 (1989).
27. Horrocks, W. DeW., Sudnick, D.R.: Lanthanide Ion Probes of Structure in Biology. Laser Induced Luminescence Decay Constants Provide a Direkt Measure of the Number of Metal-Coordinated Water Molecules. J. Am. Chem. Soc. **101**, 334 (1979).
28. Richardson, F.S.: Terbium(III) and Europium(III) Ions as Luminescent Probes and Stains for Biomolecular Systems: Chem. Rev. **82**, 541 (1982).
29. Takahashi, Y., Kimura, T., Kato, Y., Minai, Y., Tominaga, T.: Characterization of Eu(III) Species Sorbed on Silica and Montmorillonite by Laser-Induced Fluorescence Spectroscopy. Radiochim. Acta **82**, 227 (1998).

Journal of Colloid and Interface Science **238,** 219–224 (2001)
doi:10.1006/jcis.2001.7490, available online at http://www.idealibrary.com on IDEAL®

Spectroscopic Study of Cm(III) Sorption onto γ-Alumina

Th. Stumpf,[1,2] Th. Rabung, R. Klenze, H. Geckeis, and J. I. Kim

Institut für Nukleare Entsorgung, Forschungszentrum Karlsruhe, P.O. Box 3640, D-76021 Karlsruhe, Germany

Received December 21, 2000; accepted February 22, 2001

The surface sorption of Cm(III) onto aqueous suspensions of alumina is investigated by time-resolved laser fluorescence spectroscopy (TRLFS). The experiment is performed under an Ar atmosphere at an ionic strength of 0.1 M $NaClO_4$. The pH is varied between 2 and 10 and the metal ion concentration between 2.7×10^{-8} and 4.5×10^{-5} mol/L. With increasing pH, two Cm(III)–alumina surface species are identified which are attributed to $\equiv Al-O-Cm^{2+}(H_2O)_5$ and $\equiv Al-O-Cm^{+}(OH)(H_2O)_4$. The two curium–alumina surface complexes are characterized by their emission spectra (peak maxima at 601.2 nm and 603.3 nm, respectively) and fluorescence emission lifetime (both 110 μs). In the concentration range investigated, the surface complex formation is not dependent on the metal ion concentration but only on the pH. Additionally, the concentration ratio of the two surface species is found to be independent of the metal ion concentration. No spectroscopic evidence for the presence of "strong" and "weak" sites can be found at different surface coverages. © 2001 Academic Press

Key Words: curium; alumina; surface complexation; TRLFS.

INTRODUCTION

For the long-term performance assessment of nuclear waste repositories, knowledge on the interactions of actinide ions with mineral surfaces is imperative. The mobility of released radionuclides is strongly dependent on the sorption and desorption processes at mineral surfaces. Therefore, it is necessary to characterize the surface species formed and to elucidate the reaction mechanisms involved. An insight into the sorption mechanisms as given by identification of surface species is of cardinal importance for a predictive modeling of the radionuclide migration.

Some studies of the interactions of americium and curium and their homologues, europium and gadolinium, with different mineral surfaces have appeared in the literature (1–9). These studies have revealed the strong sorption of trivalent elements onto oxides, increasing with increasing pH. The sorption reaction has been described by surface complexation modelling (1, 4, 6–8). When different models are applied, the derived complexation constants are not directly comparable with one another. Recent studies with time-resolved laser fluorescence spectroscopy (TRLFS) elucidate the sorption mechanism in terms of the speciation of surface sorbed metal ions (8, 9). Due to the high fluorescence yield of Cm(III), TRLFS makes it possible to investigate its speciation in the nanomolar concentration range. The surface complexation study of Rabung *et al.* (8) shows that the sorption behavior is very similar for Eu(III) and Am(III), and the derived surface complexation constants for γ-Al_2O_3 are almost identical to those found when hematite was used as sorbent (1). The preliminary TRLFS study of Eu(III) as a fluorescence probe indicates that the Eu(III) sorption takes place as a surface complexation rather than as an inclusion into the sorbent structure. The sorption study of Cm(III) on silica with TRLFS by Chung *et al.* (9) shows two different inner-sphere complexes and concludes that the second complex is an unhydrated Cm^{3+} ion embedded in the bulk silica structure. The present paper deals with the spectroscopic identification of surface-sorbed species of trivalent actinides. Using Cm(III) with spectroscopic characteristics superior to those of Eu(III), a better insight into the surface complexation is anticipated.

EXPERIMENTAL

The type of hydrous γ-Al_2O_3 particles used in this work (Degussa, aluminum oxide C) has already been studied in sorption experiments by other authors (8, 10–12). Prior to its use, γ-Al_2O_3 was purified according to the reported procedures (10–12): initial washing with 0.1 M HNO_3, followed by addition of 0.1 M NaOH, until the pH reached 10, and finally rinsing with Milli-Q water until the conductivity of the washing solution reached the value of pure Milli-Q water. Alumina was then stored in suspension in Milli-Q water at the concentration of 57.2 g/L. The BET surface (N_2) of the dried γ-Al_2O_3 particles was found to be 119 m^2/g. Data on the potentiometrically determined acid–base properties and the concentration of surface hydroxyl groups are available from the previous work (8). The site concentration calculated from the titration data in 0.1 mol/L $NaClO_4$ amounts to 1.96×10^{-4} equiv/g of alumina corresponding to a site density of 1 site/nm^2. The protonation and deprotonation constants determined according to the constant capacitance model (1, 10) are $\log Ka_1^{int} = 7.59 \pm 0.02$ and $\log Ka_2^{int} = 9.54 \pm 0.02$ (capacitance = 0.8 F/m^2). For the complexation study, a ^{248}Cm ($t_{1/2} = 3.40 \times 10^5$ years) stock solution in concentrated HCl was used (97.2% Cm-248, 2.8% Cm-246, and

[1] Present address: Institut für Radiochemie, Forschungszentrum Rossendorf, P.O. Box 510119, D-01324 Dresden, Germany.

[2] To whom correspondence should be addressed.

0021-9797/01 $35.00
Copyright © 2001 by Academic Press
All rights of reproduction in any form reserved.

less than 0.01% Cm-244). The curium mass concentration in all solutions was determined by ICP mass spectroscopy and liquid scintillation counting (LSC). All measurements were performed at 25 ± 1°C, in a glove box under argon atmosphere.

TRLFS measurements were performed using a pulsed Nd:YAG pumped dye laser system (Continuum, Powerlite 9030, ND 6000). A laser pulse energy of at most 4 mJ was controlled by a photodiode. The fluorescence emission was detected by an optical multichannel analyzer consisting of a polychromator (Chromex 250 is) with a 1200 lines/mm grating, which allowed simultaneous detection of an entire Cm(III) emission spectrum in the range 580–620 nm within a constant time window of 1 ms width exciting at 396.6 nm (laser dye, Exalite 398). For measuring the emission decay, the delay time between laser pulse and camera gating was scanned with time intervals between 10 and 15 μs.

RESULTS AND DISCUSSION

Fluorescence emission spectra of 2.7×10^{-7} mol/L Cm(III) in 0.6 g/L alumina suspension, recorded at pH ranging from 4.4 to 9.6, are shown in Fig. 1, together with the spectrum of the Cm^{3+} aquo ion at pH 2. The emission band with a peak maximum at 593.8 nm corresponds to the Cm^{3+} aquo ion. With increasing pH, the intensity of this peak decreases and a red-shift of the fluorescence emission starting at pH 4 appears. The red-shifted band can be ascribed to curium species sorbed onto the alumina surface. Taking the solubility and hydrolysis data of Stadler and Kim (13) for Am(III), the solubility limit for the given Cm(III) concentration in the absence of alumina will be exceeded around pH 7.5. Precipitation of $Cm(OH)_3$ is obviated by addition of the Cm(III) stock solution to the alumina suspension at pH < 5 and subsequent pH adjustment by addition of NaOH. Under the present experimental conditions the molar ratio of Cm(III) and alumina hydroxyl groups is 2.3×10^{-3}; i.e., 0.23% of the surface sites are occupied at quantitative uptake of Cm(III) by alumina, if monodentate surface complexation is assumed (8). Therefore, the observed band is attributed to the inner-sphere complex formation of Cm(III) even at pH higher than 7.5, rather than precipitation or surface precipitation.

Peak deconvolution is carried out to distinguish the individual species from the composite fluorescence emission spectra. Only the spectrum of the Cm^{3+} aquo ion is found up to pH 4. The spectrum at pH 9.6 is attributed to a single surface-sorbed curium species. Taking into account the two boundary components, all mixed spectra can be deconvoluted. The primary spectra of the species identified by the deconvolution procedure are plotted in Fig. 2. Two different surface-sorbed curium species are characterized by the emission bands at 601.2 nm (appearing at pH > 4) and 603.3 nm (appearing at pH > 5.5).

The intensity of fluorescence emission bands decreases upon Cm(III) sorption onto alumina. The fluorescence intensity factor (FI) for both surface species is calculated to be 0.208 relative to $FI(Cm^{3+}_{aquo}) = 1$. From the peak deconvolution data and the respective FI values the mole fractions of three Cm(III) species involved are determined as a function of pH by a least-squares fit. Figure 3 gives the speciation plot for the Cm(III)/alumina system together with the pH-dependent sorption of Eu(III) onto alumina published earlier (8). The rise of Cm(III)–alumina complexes agrees with the pH-dependent increase of Eu(III) sorption onto alumina, showing the consistent sorption behavior. The fact that the sorption of trivalent metal ions onto γ-alumina and hematite can be described consistently by the same surface complexation model (1, 8) indicates that the speciation made

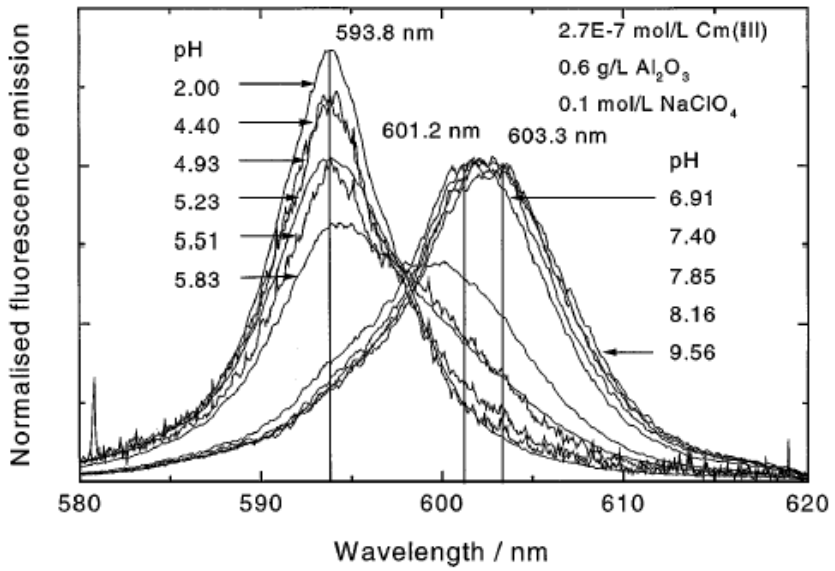

FIG. 1. Fluorescence emission spectra of Cm(III) in aqueous alumina suspension at various pH values; spectra are scaled to the same peak area.

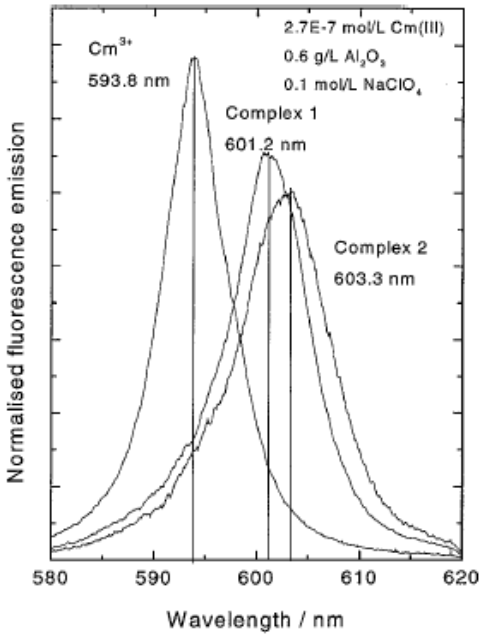

FIG. 2. Fluorescence emission spectra of Cm^{3+} aquo ion, Cm(III)–alumina complex 1, and Cm(III)–alumina complex 2 as derived by peak deconvolution; spectra are scaled to the same peak area.

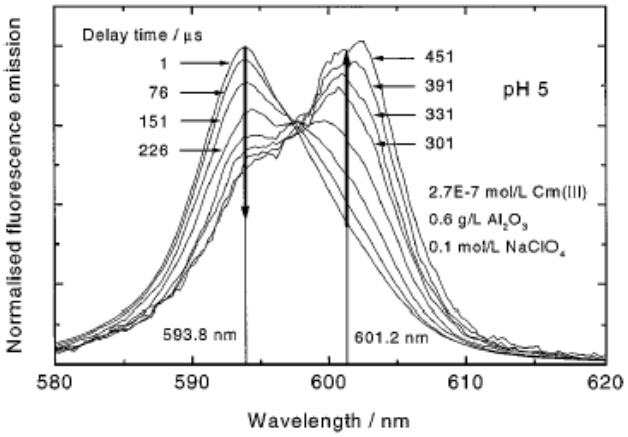

FIG. 4. Fluorescence emission spectra of Cm(III) in aqueous alumina suspension at pH 5 at different delay times; spectra are scaled to the same peak area.

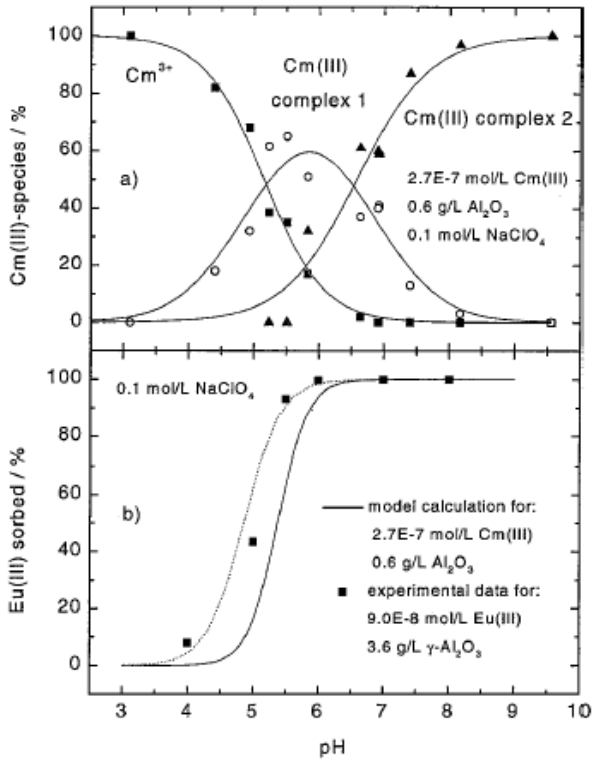

FIG. 3. Speciation plot for the Cm(III)/alumina system (a), together with the pH-dependent sorption of Eu(III) onto γ-alumina (b).

on the Cm(III)/alumina system may also be applicable to the Cm(III)/hematite system. However, this assumption has to be verified by experiment.

The presence of different curium species is further confirmed by the time-dependent emission spectra. In Fig. 4 the normalized emission spectra of Cm(III) in 0.6 g/L alumina suspension at pH 5 are shown; the detection time delay relative to the laser pulse was varied from 1 μs to 451 μs. The fluorescence emission of the Cm^{3+} aquo ion (at 593.8 nm) decays with a fluorescence emission lifetime of 68 μs, while the first Cm–alumina species emitting at 601.2 nm has a lifetime of 110 μs. Increasing the delay time, the emission band of the Cm^{3+} aquo ion disappears and the fluorescence spectrum of the first Cm(III) surface complex (complex 1) becomes dominant. Consequently, the measurement of the fluorescence lifetime at pH 5 (Fig. 5) exhibits biexponential decay. This finding indicates that the lifetime of the excited

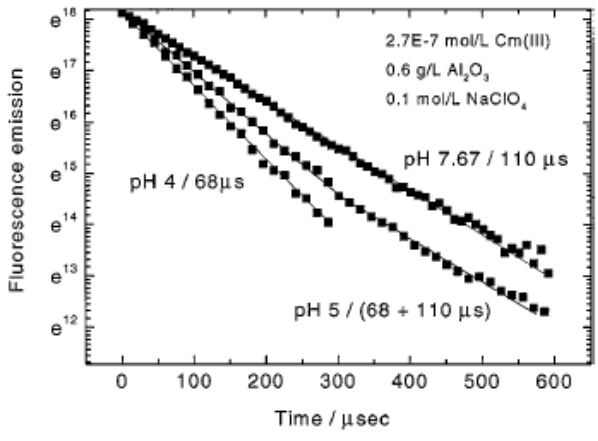

FIG. 5. Time dependency of emission decay of Cm(III) in aqueous alumina suspension at various pH values; mono- and biexponential shapes.

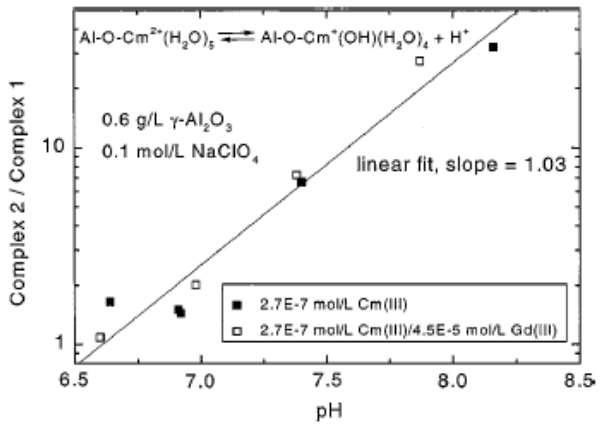

FIG. 6. Correlation of the experimentally determined ratio of log(complex 2/complex 1) with the pH.

state of Cm(III) is short compared to the exchange rate between the Cm^{3+} aquo ion and complex 1 (14). The fluorescence decay at pH 7.7, where the two Cm(III) surface species with emission peak maxima at 601.2 nm and 603.3 nm are present, is monoexponential. At pH 9.6, where the second Cm(III) surface complex (complex 2) predominates, a lifetime of 110 μs is obtained. Within the experimental uncertainty no difference in the emission lifetime is observed for the two surface species.

The increase in lifetime by complexation reflects the exclusion of hydrated water molecules from the first coordination sphere of Cm(III). In the first coordination sphere H_2O acts as a fluorescence quencher and, therefore, causes a decrease of the emission lifetime. Using the method developed by Horrocks *et al.* for Eu(III) (15) and applied later to Cm(III) (14, 16), the number of water molecules in the first coordination shell of complexes 1 and 2 is determined to be 5 ± 0.2. The same value is found for the surface complexation of Eu(III) onto alumina under the same conditions (8).

Complexes 1 and 2 are characterized by the same fluorescence intensity and lifetime, implying that the number of quenching ligands in the first Cm(III) coordination sphere remains unchanged. A plausible explanation for this observation is the formation of ternary hydrolyzed surface species at higher pH values. OH^- ions act as quenchers similar to H_2O. The correlation of the ratio log(complex 2/complex 1) with pH gives a slope of 1.03, indicating the exchange of one proton, and hence supports the assumption of ternary hydroxo/alumina complexes being formed (Fig. 6). On the basis of the surface complexation model developed for the description of the sorption of Am(III) and Eu(III) onto alumina (see Ref. (8)),

$$\equiv\text{Al–O–H} + \text{Cm}^{3+}(\text{H}_2\text{O})_9 \leftarrow \equiv\text{Al–O–Cm}^{2+}(\text{H}_2\text{O})_5 + 4\text{H}_2\text{O} + \text{H}^+$$

the hydrolysis of complex 1 can be formulated according to the reaction,

$$\equiv\text{Al–O–Cm}^{2+}(\text{H}_2\text{O})_5 \leftarrow \equiv\text{Al–O–Cm}^{+}(\text{OH})(\text{H}_2\text{O})_4 + \text{H}^+.$$

The exchange of 4 H_2O from the first coordination sphere upon formation of $\equiv$ Al–O–$Cm^{2+}(H_2O)_5$ can be explained by the

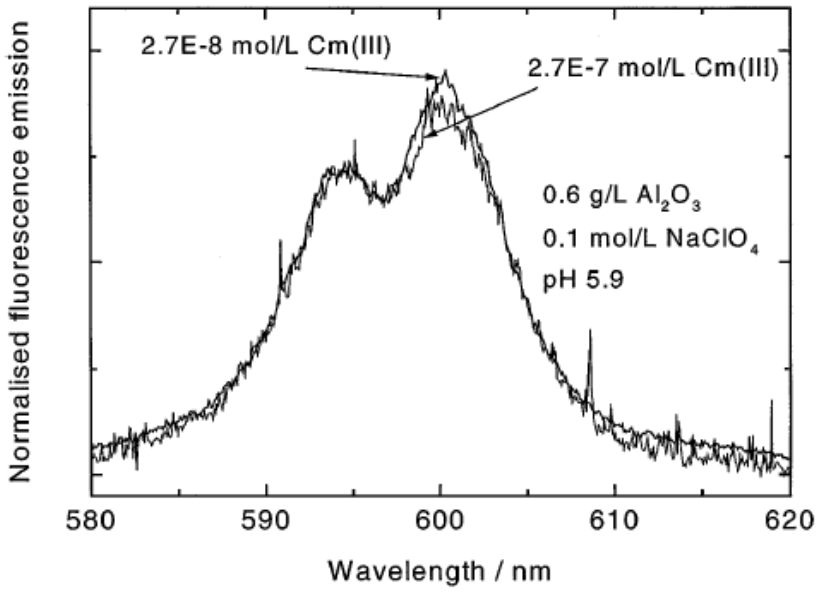

FIG. 7. Fluorescence emission spectra of 2.7×10^{-7} and 2.7×10^{-8} mol/L Cm(III) in aqueous alumina suspension (0.6 g/L γ-alumina) at pH 5.9; spectra are scaled to the same peak area.

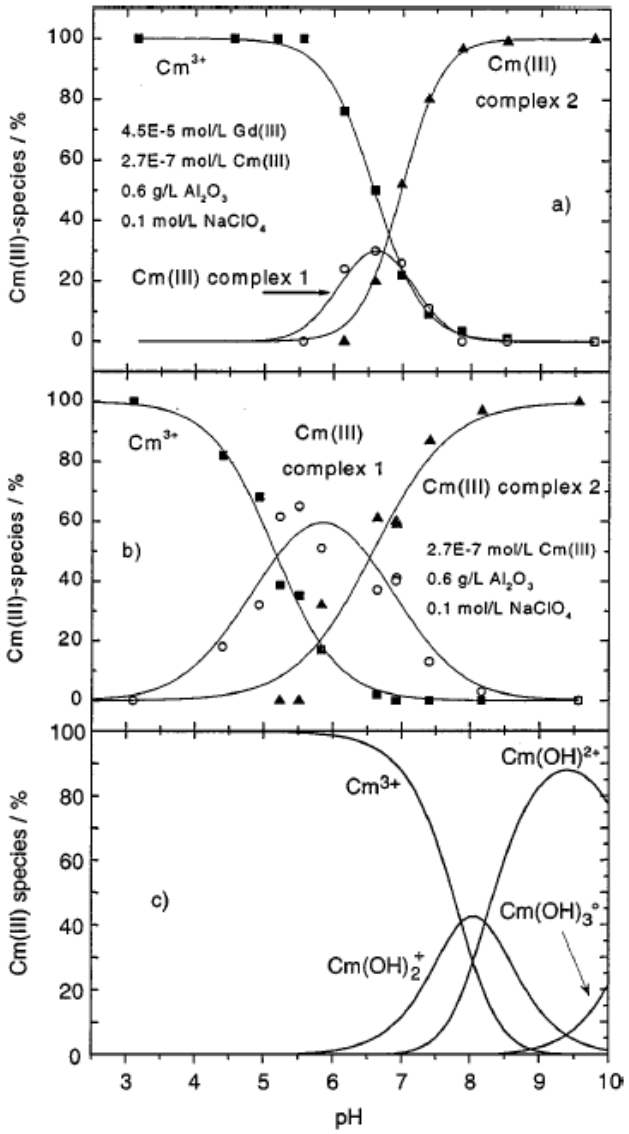

FIG. 8. Calculated speciation of Cm(III) in solution in the absence of CO_2 (c), together with the measured species distributions in the Cm(III)/alumina system (b) and the Cm(III)/Gd(III)/alumina system (a).

steric situation at the alumina surface prohibiting more H_2O molecules from approaching the surface-sorbed Cm(III) ion.

Surface complexation of Am(III) and Eu(III) onto hematite and γ-alumina has been modeled by a two-site approach, postulating "strong" and "weak" binding surface hydroxyl groups (1, 8). Two- or multiple-site surface complexation models are frequently used to describe the shape of the isotherm obtained for the metal ion sorption onto mineral surfaces (18). In order to appraise the existence of spectroscopically different Cm(III) complexes with "strong" and "weak" sites, the pH was kept at 5.9 for a suspension consisting of 2.7×10^{-7} mol/L Cm(III)/0.6 g/L alumina and the metal ion concentration was varied by the subsequent addition of Gd(III) up to a total metal ion concentration of 4.5×10^{-5} mol/L. On the basis of previous experience (see Ref. (8)), it is assumed that the sorption behaviors of Cm(III) and Gd(III) should be more or less identical. With increasing Gd(III) concentration, the surface-sorbed Cm(III) is displaced from the alumina surface into the solution. Therefore, the corresponding emission peak for the complex 1 decreases and the peak for the Cm(III) aquo ion increases. The displacement of Cm(III) from the surface within 24 h after addition of Gd(III) reveals the reversibility of the sorption reaction. However, no shift in the peak maximum of the sorbed species is observed with increasing metal ion concentration. A further decrease of the Cm(III) concentration to 2.7×10^{-8} mol/L also does not effect any significant difference in the spectrum (Fig. 7). This is interpreted to mean that over the entire metal ion concentration range studied only one surface species exists at pH 5.9 on the basis of spectroscopic evidence. As the metal ion concentration is varied over a range of 3 orders of magnitude this might be an indication that under the given experimental conditions Cm(III) complexes with "strong" and "weak" sites of the alumina surface do not exist or at least are not distinguishable by TRLFS.

Increasing the metal ion concentration to 4.5×10^{-5} mol/L by addition of Gd(III) increases the concentration of the Cm^{3+} aquo ion due to displacement of sorbed Cm(III) but does not change the relative concentration of both sorbed Cm(III) species at constant pH (see Fig. 6). This is taken as further proof that complex 2 exists as a hydrolyzed ternary surface complex, because the concentration ratio of complexes 1 and 2 depends only on pH. The formation of the ternary complex 2 follows the hydrolyzed trivalent actinide ions in aqueous solution (17). Figure 8 shows the calculated speciation of Cm(III) together with the measured species distribution in the Cm(III)/Gd(III)/alumina systems.

CONCLUSIONS

The present study shows the potential of TRLFS for the identification of sorption mechanisms and identification of surface-sorbed Cm(III) species. This information is considered as an important prerequisite for the development of a straightforward surface complexation model. The spectroscopic identification and quantification of hydrolyzed surface complexes of Cm(III) at the alumina surface in the trace metal ion concentration range reveals the importance of such ternary complexes which even may dominate the speciation of polyvalent metal ions under natural conditions. A similar conclusion has been drawn by Waite *et al.* in the case of U(VI) sorption to ferrihydrite (19). On the basis of a surface complexation study they suggested the existence of a ternary surface complex with UO_2CO_3 binding to a bidentate surface site. In contrast to the results obtained for the investigation of Cm(III) sorption onto silica (9), Cm(III)–alumina surface species are not embedded in the bulk alumina structure. Apparently, the fundamental difference in the

mechanisms of metal ion reactions at the solid/water interface may be true for different minerals. The present study demonstrates the necessity of studying the sorption reactions on a molecular level. Results of modeling the experimental observations will be published separately.

REFERENCES

1. Rabung, Th., Geckeis, H., Kim, J. I., and Beck, H. P., *J. Colloid Interface Sci.* **208,** 153–161 (1998).
2. Geckeis, H., Klenze, R., and Kim, J. I., *Radiochim. Acta* **87,** 13 (1999).
3. Nordén, M., Ephraim, J. H., and Allard, B., *Radiochim. Acta* **65,** 265–270 (1994).
4. Kosmulski, M., *J. Colloid Interface Sci.* **192,** 215–227 (1997).
5. Csobán, K., and Joó, P., *Colloids Surf.* **151,** 97–112 (1999).
6. Sposito, G., *in* "Geochemical Processes at Mineral Surfaces" (J. A. Davis and K. F. Hayes, Eds.), ACS Symposium Series 323, pp. 217–230, Am. Chem. Soc. Washington, DC, 1986.
7. Degueldre, C., Ulrich, H. J., and Silby, H., *Radiochim. Acta* **65,** 173–179 (1994).
8. Rabung, Th., Stumpf, Th., Geckeis, H., Klenze, R., and Kim, J. I., *Radiochim. Acta* **88,** 711 (2000).
9. Chung, K. H., Klenze, R., Park, K. K., Paviet-Hartmann, P., and Kim, J. I., *Radiochim. Acta* **82,** 215–219 (1998).
10. Huang, C.-P., and Stumm, W., *J. Colloid Interface Sci.* **43,** 409–420 (1973).
11. Hohl, H., and Stumm, W., *J. Colloid Interface Sci.* **55,** 281–286 (1976).
12. Horst, J., and Höll, W. H., *J. Colloid Interface Sci.* **195,** 250–260 (1997).
13. Stadler, S., and Kim, J. I., *Radiochim. Acta* **44/45,** 39 (1988).
14. Fanghänel, Th., and Kim, J. I., *J. Alloys Compd.* **271–273,** 728–737 (1998).
15. Horrocks, W. DeW., and Sudnick, D. R., *J. Am. Chem. Soc.* **101,** 334–340 (1979).
16. Kimura, T., and Choppin, G. R., *J. Alloys Compd.* **213/214,** 313–317 (1994).
17. Neck, V., Fanghänel, Th., and Kim, J. I., Aquatische Chemie und thermodynamische Modellierung von trivalenten Actiniden, Wissenschaftliche Berichte, FZKA 6110, Forschungszentrum Karlsruhe.
18. Dzombak, D. A., and Morel, F. M. M., "Surface Complexation Modeling; Hydrous Ferric Oxide," Wiley, New York, 1990.
19. Waite, T. D., Davis, J. A., Payne, T. E., Waychunas, G. A., and Xu, N., *Geochim. Cosmochim. Acta* **58**(24), 5465–5478 (1994).

3. Wechselwirkung von Eu(III), Am(III) und Cm(III) mit natürlichen, endlagerrelevanten Mineralen

Aufbauend auf den Untersuchungen zur Wechselwirkung von Eu(III) und Cm(III) mit der Wasser/γ-Al_2O_3 Grenzfläche schlossen sich weitere Studien mit natürlichen, endlagerrelevanten Mineralen (Kaolinit, Smectit, Albit, Orthoklas und Ferrihydrit) an. Aufgrund ihrer Verbreitung und der angedachten Rolle als Wirtsgestein und/oder Verfüllmaterial beim Bau eines nuklearen Endlagers wurde in dieser Arbeit besonderes Augenmerk auf die Tonminerale Smectit und Kaolinit gelegt.

Bei dem in Kontakt mit Wasser quellfähigem Smectit, handelt es sich um ein „drei Schicht-Tonmineral“, das aus Siliciumtetraeder-Aluminiumoktaeder-Siliciumtetraeder (TOT) Schichten aufgebaut ist. Diese TOT Formationen können durch den Austausch von Al(III) gegen zweiwertige Ionen oder den Ersatz von Si(IV) gegen M(III) eine negative Ladung besitzen. Diese wird durch Anlagerung von Kationen in TOT-TOT Zwischenschichten kompensiert. Die angelagerten Kationen (z.B. Na(I), K(I) oder Ca(II)) können durch Actiniden und Lanthaniden verdrängt werden. Bei dieser auf elektrostatische Wechselwirkungen basierenden Sorption behalten die Ionen ihre Hydrathülle und man spricht von „outer-sphere“ Komplexen (im Gegensatz zu „inner-sphere“ Komplexen, die einen kovalenten Bindungsanteil aufweisen und bei denen ein Teil der Hydrathülle des Kations bei der Sorption verloren geht). Mit den Hydrathüllen der Gegenionen nehmen die Zwischenschichten Wasser auf und lassen einen Smectit bei Kontakt mit H_2O aufquellen. Zudem besitzt ein solches drei Schicht-Tonmineral durch die TOT-TOT Zwischenschichten eine große „innere“ Oberfläche. Im Gegensatz dazu besteht ein Kaolinit nur aus zwei Schichten (TO), bildet keine Zwischenschichten aus und ist nicht quellfähig.

Den Tonmineralen verwandt sind Feldspäte, die neben Quarz und Glimmer den Hauptbestandteil des ebenfalls als Wirtsgestein zur Diskussion stehenden Granit darstellen. Bei den in dieser Arbeit untersuchten Kalifeldspäten Orthoklas $K[AlSi_3O_8]$ und Albit $Na[AlSi_3O_8]$ handelt es sich um Gerüstsilicate, die aus AlO_4 und SiO_4 Tetraedern aufgebaut sind. Albit geht bei Verwitterung direkt in das Tonmineral Kaolinit über. Die zu dem Themenkomplex Wechselwirkung von dreiwertigen Actiniden und Lanthaniden mit Tonmineralen und Feldspäten erarbeiteten Ergebnisse wurden in den folgenden Artikeln veröffentlicht:

"Time-Resolved Laser Fluorescence Spectroscopy (TRLFS) Study of the Sorption of Cm(III) onto Smectite and Kaolinite"; Thorsten Stumpf, Andreas Bauer, Frederic Coppin, Jae Il Kim; Environ. Sci. Technol., 2001, 35, 3691-3694.

"Sorption of Cm(III) onto different Feldspar surfaces: a TRLFS Study"; Silvia Stumpf, Thorsten Stumpf, Clemens Walther, Dirk Bosbach, Thomas Fanghänel; Radiochim. Acta, 2006, 94, 243-248.

"An EXAFS and TRLFS Study of the Sorption of Trivalent Actinides onto Smectite and Kaolinite"; Thorsten Stumpf, Christoph Hennig, Andreas Bauer, Melissa A. Dennecke, Thomas Fanghänel; Radiochim. Acta, 2004, 92, 133-138.

"Inner-sphere, outer-sphere and ternary surface complexes: a TRLFS study of the sorption process of Eu(III) onto smectite and kaolinite"; Thorsten Stumpf, Andreas Bauer, Frederic Coppin, Thomas Fanghänel, Jae Il Kim; Radiochim. Acta, 2002, 90, 345-349.

Die TRLFS Untersuchungen zur Wechselwirkung von Curium mit den Tonmineralen Smectit und Kaolinit zeigen, dass in beiden Fällen die selben zwei Reinspektren für Oberflächenkomplexe zu detektieren sind. Dies bedeutet, dass, unabhängig davon ob ein zwei Schicht- oder drei Schicht-Tonmineral vorliegt, die selben Actinid inner-sphere Komplexe an der Mineraloberfläche gebildet werden. Mit den Spektren der drei Reinkomponenten Cm Aquoion (Peakmaximum 593.8 nm), Cm/Ton Sorptionsspezies 1 (Peakmaximum 598.8 nm) und Cm/Ton Sorptionsspezies 2 (Peakmaximum 603.3 nm) war es möglich, alle gemessenen Emissionsspektren anzupassen und davon ausgehend, eine Speziation zu berechnen. Der Verlauf der Speziation für beide Systeme (Kaolinit und Smectit) ist sehr ähnlich. Die Fluoreszenzemissionslebensdauern von 110 +/- 7 µs für beide Cm/Ton Spezies lassen auf den Verlust von vier Wassermolekülen in der ersten Koordinationssphäre des Actinidions bei Anbindung an die Mineraloberfläche schließen.
Bei der Untersuchung der Curiumwechselwirkung mit den Kalifeldspäten Albit und Orthoklas zeigte sich ebenfalls, dass die an der Oberfläche der beiden Minerale gebildeten Sorptionsspezies spektroskopisch nicht unterscheidbar sind. Die Cm/Feldspat Peakmaxima unterscheiden sich zwar von denen, die für die Cm/Tonspezies detektiert wurden, für die Systeme Cm/Albit und Cm/Orthoklas

allerdings finden sich die selben zwei Emissionsspektren (Peakmaxima 601.4 nm und 603.6 nm). Die Fluoreszenzemissionslebensdauer beträgt bei diesen inner-sphere Komplexen 107 +/-3 µs, was auf den Verlust von ca. der halben Cm(III) Hydrathülle bei der Sorption hindeutet. Der Vergleich zwischen den Cm(III) Oberflächenspezies, die sich an Tonoberflächen und Feldspatoberflächen bilden, zeigt, dass zwar eine Ähnlichkeit hinsichtlich der Rotverschiebung der Emissionsmaxima und eine Deckungsgleichheit bei den Fluoreszenzemissionslebensdauern existiert, aber die spektralen Unterschiede der jeweiligen Reinkomponenten dennoch signifikant sind. Dies bedeutet, dass die Sorptionsspezies die sich an einer Oberfläche einer Mineralklasse (Tone bzw. Feldspäte) bilden, spektroskopisch identisch sind, während von Mineralklasse zu Mineralklasse kleine aber deutliche Unterschiede existieren.

Um weitere Strukturinformationen zu den Actinid/Tonmineral Sorptionsspezies zu erhalten, wurden EXAFS Untersuchungen an Americium in Gegenwart von Smectit und Kaolinit durchgeführt.

Sowohl die mit Hilfe der Cm TRLFS als auch mit Am EXAFS erhaltenen Ergebnisse zur Sorption von dreiwertigen Actiniden an Tonmineralen zeigen, dass bei niedrigen pH Werten (< 5) ausschließlich das Aquoion vorliegt. Da parallel durchgeführte batch Experimente die Sorption an der Oberfläche des permanent geladenen Smectits bei diesen niedrigen pH Werten belegen, muss es sich bei der Sorptionsspezies um einen outer-sphere Komplex handeln. Mit Hilfe der Röntgenabsorptionsspektroskopie wurde für das vollständig hydratisierte Am^{3+} Ion ein mittlerer Am-O Abstand von 2.47 Å – 2.49 Å und eine Koordinationszahl von acht bis neun ermittelt. Mit zunehmender inner-sphere Sorption des Actinids an der Tonoberfläche durch die Erhöhung des pH Werts, ist eine geringe Verkürzung des mittleren Am-O Abstands zu beobachten, während die Am Koordinationszahl bei pH 6 im Vergleich zum Am^{3+} Aquoion konstant bleibt. Da die Cm(III) TRLFS Untersuchungen bei inner-sphere Komplexierung eine Halbierung der Actinid Hydrathülle zeigen, sprechen die EXAFS Daten dafür, dass das dreiwertige Metallion bei der Sorption den Verlust von vier Wassermolekülen durch Kontakte zu einer entsprechenden Anzahl von Sauerstoffatomen der Oberfläche kompensiert. Die Auswertung weiterer Am(III) EXAFS Spektren zeigt eine Reduktion der Koordinationszahl des Actinids in Gegenwart von Kaolinit oder Smectit mit der Erhöhung des pH Werts auf pH 8. Bei pH 8 finden sich im Gegensatz zu pH 6 nur noch sechs bis sieben Sauerstoffatome

in der ersten Koordinationssphäre des Am(III). Diese scheinbare Abnahme der Koordinationszahl deutet auf die Bildung eines Ton/Am/Hydrolyse Komplexes hin.
Neben der inner-sphere Sorption der dreiwertigen Actiniden an γ-Al_2O_3, an die Tonminerale Smectit und Kaolinit sowie an die Feldspäte Albit und Orthoklas unter Verlust von koordinierten Wassermolekülen ließ sich bei jedem untersuchten System eine weitere Sorptionsspezies finden, die bei höherem pH (> pH 8) die Speziation dominiert. Diese Sorptionsspezies konnte als "ternärer" inner-sphere Hydrolysekomplex $(X\text{-}O\text{-}An(OH)^-(H_2O)_4$ identifiziert werden. Als weiterer stark Actiniden komplexierender Ligand in natürlichen wässrigen Systemen kommt neben OH^- Carbonat in Frage. Um die Frage zu beantworten, ob "ternäre" Carbonatsorptionsspezies bei Anwesenheit von CO_2 spektroskopisch nachgewiesen werden können, wurden mit Hilfe der TRLFS Eu(III)/Tonmineral (Kaolinit und Smectit) Systeme in An- und Abwesenheit von Carbonat untersucht.
Spektroskopisch lässt sich die inner-sphere Sorption des Eu(III) an die Tonmineraloberflächen durch das Detektieren der Veränderungen der Intensitätsverhältnisses zwischen den Übergängen $^5D_0 \rightarrow {}^7F_1$ und $^5D_0 \rightarrow {}^7F_2$ mit der Änderung des pH Wertes verfolgen. Dabei zeigt sich, dass ab einem pH von 6.65 unter atmosphärischen Bedingungen andere Intensitätsverhältnisse auftreten als für Messungen in Abwesenheit von CO_2. Ferner zeigt die Peakform des $^5D_0 \rightarrow {}^7F_2$ Übergangs in Gegenwart von Carbonat eine Feinstruktur, die unter reiner Stickstoffatmosphäre in Abwesenheit von CO_2 nicht zu beobachten ist. Um Informationen zu der ersten Koordinationssphäre der Eu(III) Spezies zu erhalten, wurde besonderes Augenmerk auf die Fluoreszenzemissionslebensdauern der Europium/Tonmineral Sorptionsspezies gelegt. Bei pH 7.15 +/- 0.05 finden sich für beide Systeme deutlich unterschiedliche Eu(III) Emissionslebensdauern. In Abwesenheit von Carbonat wird für den Eu/Smectit inner-sphere Komplex eine Lebensdauer von 188 +/- 20 µs gemessen, was einer Anzahl von 5.1 +/- 0.6 in der ersten Eu(III) Koordinationsschale verbliebenen Wassermolekülen entspricht. Unter atmosphärischen Bedingungen werden dagegen bei einem vergleichbaren pH Wert 333 +/- 20 µs detektiert. Ein solcher Wert korreliert mit nur noch 2.6 +/- 0.3 H_2O in der ersten Hydrathülle des Lanthanidions. Der Unterschied von zwei bis drei koordinierten Wassermolekülen kann mit einem Verdrängen dieser Moleküle durch die Komplexierung des Europiumoberflächenkomplexes mit die Fluoreszenzlebensdauer nicht quenchendem Carbonat erklärt werden - eine

"ternäre" Tonmineral/Eu/Carbonat Spezies hat sich in Gegenwart von atmosphärischem CO_2 gebildet.
Interessant hinsichtlich der Endlagersicherheit dabei ist, dass bei Anwesenheit von geringen Mengen an CO_2 sorbierte Lanthanide/Actinide durch die Bildung löslicher Carbonatkomplexe nicht desorbiert werden, sondern sich ternäre Carbonat/M(III)/Tonmineraloberlächenkomplexe bilden. Die retardierenden Eigenschaften der Tonmineraloberflächen bezüglich der Ausbreitung von Radionukliden bleibt also auch in Gegenwart von geringen Mengen an CO_2 erhalten.

Eisenoxide können im Nah- und Fernfeld eines Endlagers retardierend auf freigesetzte Schwermetalle wirken. Dabei spielen sowohl die Fe-O Minerale als auch Eisenoxid Coatings eine große Rolle. Insbesondere die amorphen Ferrihydrit Phasen mit ihren großen Oberflächen (~150 m^2/g) können als effektive Sorptionsflächen wirken. Wie bereits erwähnt, sind aufgrund der Auslöschung der Cm(III) und Eu(III) Emission bei Kontakt mit Eisen, TRLFS Untersuchungen zur Wechselwirkung dieser f-Elemente mit Eisenoxidoberflächen nicht möglich. Eine Methode diese Wechselwirkungen dennoch zu studieren und Strukturinformationen zu erhalten, bietet die Röntgenabsorptionsspektroskopie (XAS). Die Sorption von Am(III) an Ferrihydrit und der Einbau des Actinids bei der Kristallisation des amorphen Materials unter Bildung von Hämatit und Goethit wurden mit Hilfe von XAS untersucht. Die Ergebnisse dieser Untersuchung sind in der folgenden Publikation veröffentlicht.

"Sorption of Am(III) onto 6-line-Ferrihydrite and its Alteration Products: Investigations by EXAFS"; Silvia Stumpf, Thorsten Stumpf, Kathy Dardenne, Christoph Hennig, Harald Foerstendorf, Reinhardt Klenze, Thomas Fanghänel; Environ. Sci. Technol., 2006, 40, 3522-3528.

XAS Messungen am System Am(III)/6-Linien Ferrihydrit zeigen, dass das dreiwertige Actinid bei pH 5.5 und pH 8 an die Eisenoxidoberfläche sorbiert. Für die Americium-Sauerstoffabstände wurde ein gemittelten Wert von 2.48 Å gefunden. Um die Struktur des Oberflächenkomplexes aufzuklären, ist allerdings die Bestimmung des Am-Fe Abstands nötig. Dieser beträgt 3.70 Å und lässt sich nur mit einer bidentaten Anbindung des Actinids an die Mineraloberfläche erklären. Da Ferrihydrit ein metastabiles Zwischenprodukt darstellt und sich in die über lange Zeiträume

beständigen Eisenoxide Goethit und Hämatit umwandelt, wurde untersucht, wie sich das sorbierte Actinid bei bzw. nach der Umwandlung in die kristallinen Eisenphasen verhält. Das Tempern der Ferrihydrit Suspension in Gegenwart von Am(III) über einen Zeitraum von 67 Tagen bei 85°C führte zu der erwarteten Kristallisation des vormals amorphen Materials. XANES und EXAFS Spektren zeigen, dass das Americium bei der Umwandlung des Ferrihydrits teilweise in die Struktur des Eisenoxids eingebaut wurde. Belegt werden konnte dies durch eine Verkürzung sowohl der Am-O (2.46 Å) als auch der Am-Fe (3.32 Å und 3.59 Å) Abstände im Vergleich zur Am/Ferrihydrit Sorptionsspezies.

Diese Ergebnisse zeigen, dass die Sorption von Radionukliden an der metastabilen Mineralphase Ferrihydrit zu einer nachhaltigen, wirkungsvollen Immobilisierung der Actiniden führen kann, da bei der Kristallisation der amorphen Festphase die angelagerten Radionuklide in die Kristallstruktur der Eisenoxide eingebaut werden. Die Korrosion von eisenhaltigem Material in einem Endlager führt also nicht zwangsläufig zur Freisetzung des radioaktiven Abfalls, sondern kann in Form der gebildeten Sekundärphasen durchaus retardierend auf die Migration von Actiniden wirken.

Environ. Sci. Technol. **2001**, *35*, 3691−3694

Time-Resolved Laser Fluorescence Spectroscopy Study of the Sorption of Cm(III) onto Smectite and Kaolinite

THORSTEN STUMPF*

Forschungszentrum Rossendorf, Institut für Radiochemie, P.O. Box 510119, D-01324 Dresden, Germany

ANDREAS BAUER

Forschungszentrum Karlsruhe, Institut für Nukleare Entsorgung, P.O. Box 3640, 76021 Karlsruhe, Germany

FREDERIC COPPIN

University Paul Sabatier, UMR 5563 - LMTG, 38 rue des 36-Ponts, 31400 Toulouse, France

JAE IL KIM

Forschungszentrum Karlsruhe, Institut für Nukleare Entsorgung, P.O. Box 3640, 76021 Karlsruhe, Germany

For long-term performance assessment of nuclear waste repositories knowledge concerning interactions of actinides with mineral surfaces is imperative. The mobility and bioavailability of released radionuclides is strongly dependent on sorption/desorption processes onto mineral surfaces. Therefore it is necessary to characterize the surface species formed and to elucidate the reaction mechanisms involved. The high fluorescence spectroscopic sensitivity of Cm(III) has attracted our interest regarding the complexation process of Cm(III) onto smectite and kaolinite as a model system for the sorption of trivalent actinides in the trace concentration range. We conclude that at low pH Cm(III) is sorbed onto kaolinite and smectite as an outer-sphere complex and retains its complete primary hydration sphere. With increasing pH inner-sphere adsorption onto kaolinite and smectite occurs via the aluminol edge sites. The same evolution of the Cm(III)-clay surface species as a function of pH was observed for both minerals. Starting at a pH ≥ 5 we observe the formation of a $\equiv Al-O-Cm^{2+}(H_2O)_5$ surface complex, which is replaced by a second species at higher pH. The second surface complex may be a monodentate $\equiv Al-O-Cm^{+}(OH)(H_2O)_4$ species or bidentate $\equiv(Al-O)_2-Cm^{+}(H_2O)_5$ species. The Cm(III)/clay surface complexes are characterized by their emission spectra (peak maxima at 598.8 and 603.3 nm) and their fluorescence lifetime (both 110 ± 7 μs). An important result in view of the mobility and bioavailability of radionuclides is that no incorporation of Cm(III) into the bulk clay structure was observed.

Introduction

Sorption to mineral surfaces is a major process controlling the concentration, mobility, and bioavailability of radionuclides in nature. Oxide and clay minerals are the main constituents in groundwater and soil systems responsible for metal ion sorption. In most cases, experimental sorption data have been macroscopically interpreted through empirical means, such as partition coefficients and adsorption isotherms (e. g., ref *1* and references therein). The results from surface sorption models are increasingly employed to describe the sorption process. Despite their usefulness in appraising sorption mechanisms their application has been applied mostly to simple oxide or hydroxide minerals. This mainly results from the lack of information on the chemical composition of mineral surfaces and mineral water interfaces (*2*). As clay minerals have a complex surface structure, they show complicated sorption characteristics, especially at low ionic strength (*3*). An application of surface complexation models (SCM) for clays is not as successful as for oxides or hydroxides. Therefore molecular level spectroscopic information is needed to identify the sorption mechanisms including the structure of the species involved in the sorption process and to validate the applicability of SCM.

Kaolinite is a 1:1 layer type clay mineral in which each Si-, Al-hydro(oxide) component exists in two distinct structural environments at the surface. There is only minimal substitution of variable valence cations in the structure and hence only minor permanent structural charge. In contrast to kaolinite in smectite each aluminous octahedral layer is bound to two silica rich tetrahedral layers. Smectite is an expandable 2:1 layer type clay mineral that has both interlayer sites and ionizable hydroxyl sites on its external surface for the metal cation sorption. Substitution of Mg^{2+} and Fe^{2+} atoms for Al^{3+} in the octahedral layer creates a positive charge deficit giving the overall structure a net negative charge. The O and OH atoms at the edges of kaolinite and smectite, or at the gibbsite basal plane of kaolinite, become hydrolyzed and form Lewis base or Lewis acid functional groups, which are the source of the pH dependent charge (*4*). Binding to these hydroxyl sites on the external surface is thought to be a complexation reaction similar to that occurring at the oxide mineral surface. The aim of this study is to verify this assumption and to investigate the sorption mechanism of metal cations onto kaolinite and smectite. As representative for trivalent actinides curium was chosen, because its fluorescence spectroscopic sensivity enables speciation studies at very low concentrations. The limit of detection for Cm^{3+}(aq) by **t**ime-**r**esolved **l**aser **f**luorescence **s**pectroscopy (**TRLFS**) is 5×10^{-12} mol/L (*5*), and thus speciation may be performed in the subnanomole concentration range. TRLFS has been proven as a versatile tool to study both solution chemistry of curium (*6*−*11*) and surface complexation of Cm(III) onto silica (*12*) and γ-alumina (*13*). A review of the spectroscopic properties of Cm(III) is given elsewhere (*5*). In this paper the speciation of surface sorbed metal ions was studied by TRLFS in the nanomolar concentration range, as a function of pH at low ionic strength.

Experimental Section

Materials and Methods. Well crystallized, fine grained kaolinite (≤ 2 μm) from St. Austell (UK) was used. The smectite used was < 0.1 μm fraction of the Ceca bentonite separated by sedimentation technique. The cation exchange capacity (CEC) of the initial and the reacted products was determined according to Meier and Kahr (*14*) and was found to be 3.7 mequiv/100 g for kaolinite and 75 mequiv/100 g for smectite. A detailed description of the clay samples is given elsewhere (*15*).

* Corresponding author phone: (0049)351-260 2432; fax: (0049)-351-260 3553; e-mail: T.stumpf@fz-rossendorf.de.

10.1021/es001995o CCC: $20.00 © 2001 American Chemical Society
Published on Web 08/16/2001

Solutions were prepared from analytical grade chemicals. For the experiment Cm-248 ($t_{1/2} = 3.4 \times 10^5$ years) was used. The stock solution consists of 97.2% Cm-248, 2.8% Cm-246, and less than 0.01% Cm-244 in concentrated HCl. The initial curium concentration was adjusted to 3.0×10^{-7} mol/L and controlled in the starting solution by ICP-mass spectroscopy.

Experimental Setup. As reaction vessels 20 mL polypropylene bottles were used. Batch experiments were performed in a glovebox under argon atmosphere at 25 °C to avoid contamination with atmospheric CO_2, which can lead to the formation of Cm(III) carbonate complexes. To prevent precipitation we started at pH 3.5 and increased the pH up to nine in small steps. As background electrolyte we used $NaClO_4$ solutions ($I = 0.025$ M). Clay samples (S:L 0.25 g L^{-1}) were equilibrated at pH 6.7 for 1 week in the dark. Kinetic tests were performed at different Eu(III) trace concentrations (Eu(III) serves as a Cm(III) homologue) as a function of pH for times between 1 and 30 days. No kinetic effects were observed, i.e., a steady state was reached within 1 day. Nevertheless, batch samples were stored for at least 2 days and shaken periodically. The pH was adjusted by adding analytical grade NaOH or $HClO_4$.

TRLFS measurements were performed using a pulsed Nd:YAG pumped dye laser system (Continuum, Powerlite 9030, ND 6000). Details on the experimental setup are given elsewhere (*16*–*18*). The system consists of a polychromator (Chromex 250) with a 1200 lines/mm grating. The emission spectrum of Cm(III) in aqueous kaolinite and smectite suspensions was recorded at room temperature in the 580–620 nm range, within a constant time window of 1 ms exciting at 396.6 nm (laser dye: Exalite 398). The emission spectrum was recorded 1 μs after the laser pulse to fade out any background fluorescence. For measuring the emission decay, the delay time between laser pulse and camera gating was scanned with time intervals between 10 and 20 μs.

Results and Discussion

The fluorescence emission band of the Cm(III) aquo ion has a peak maximum at 593.8 nm at pH ≤ 6. The evolution of the fluorescence emission spectra of Cm(III) with kaolinite in aqueous suspension at various pH is shown in Figure 1a. At pH ≤ 4 only the signal of the Cm(III) aquo ion is detected. At pH ≥ 5, the intensity of the 593.8 nm peak decreases and two other peaks appear with maxima at 598.8 nm (pH ≥ 5) and 603.3 nm (pH ≥ 7.22). Comparable evolution is observed for the smectite suspension (Figure 1b). With increasing pH, the intensity of the 593.8 nm peak decreases and the same red shifted peak maxima appear at 598.8 nm (≥ pH 5.40) and 603.3 nm (pH ≥ 7.15).

It is remarkable that, in case of smectite and kaolinite, the spectra of the sorbed Cm(III) species at low pH (≤ 5) show no difference to spectra of the Cm(III) aquo ion. This observation indicates that at pH values ≤ 5 the sorbed Cm(III) ion retains its hydration sphere. Such a sorption process suggests outer-sphere complex formation on the interlayer sites.

The red shift of the fluorescence emission of Cm(III) at higher pH (> 5) in the kaolinite and smectite suspensions is caused by a change in the ligand field of the Cm(III) ion and indicates inner-sphere complex formation. A peak deconvolution was carried out to resolve the individual species from the composite fluorescence emission spectra at pH ≥ 5. Three different species have been identified. In addition to the Cm(III) aquo ion, two different inner-sphere Cm(III) surface complexes are formed. All measured spectra have been deconvoluted using pure component spectra with peak maxima at 598.8 and 603.3 nm.

In Figure 2 Cm(III) species distribution in the presence and absence of clay minerals are shown. Previous studies confirm that in the absence of kaolinite and smectite the

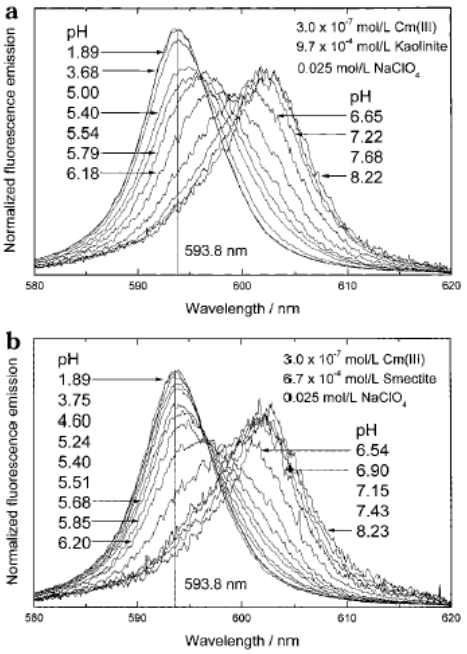

FIGURE 1. Fluorescence emission spectra of 3.0×10^{-7} mol/L Cm-(III) in aqueous kaolinite (a) and smectite (b) suspensions at various pH; spectra are scaled to the same peak area.

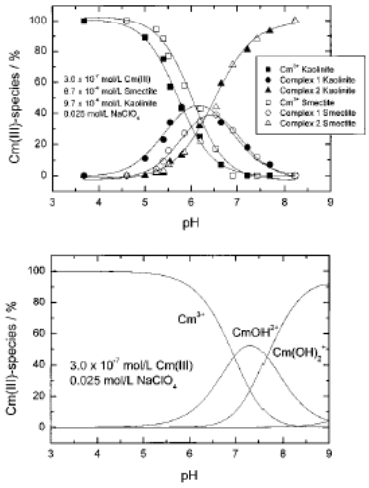

FIGURE 2. Species distribution of Cm(III) as a function of pH in the presence and absence of kaolinite and smectite.

shift of the Cm(III) emission spectrum starts with reaching pH 5 by forming the first hydrolysis complex $Cm(OH)^{2+}$. The Cm^{3+} hydrolysis process stops not until reaching pH 8. Even at pH 7.5 more than 15% of the Cm^{3+} aquo ion is detectable in a carbonate free curium solution as it was shown by Fanghänel and Neck (*6*, *19*). By comparing the species distribution of the hydrolysis of curium and the sorption of Cm(III) onto kaolinite and smectite one can see that the hydrolysis of the actinide plays no role in the sorption process. When hydrolysis occurs all of the Cm(III) is already sorbed.

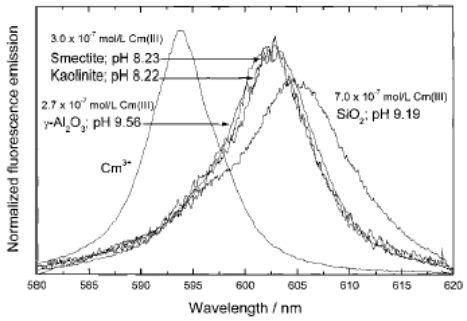

FIGURE 3. Fluorescence emission spectra of Cm(III) in aqueous kaolinite, smectite, γ-alumina, and silica suspensions in the pH range between 8.22 and 9.56; spectra are scaled to the same peak area.

That is furthermore a proof that precipitation can be neglected. The pH dependence of the spectroscopic data decay indicates that one proton is involved in the formation of the second Cm(III) surface complex from the first inner-sphere complex according to the reaction

$$\text{complex 1} \rightarrow \text{complex 2} + H^+$$

This is verified by a slope analysis. The concentration ratio, log(complex 2/complex 1), as a function of pH is linear with a slope of one. There are two plausible different reactions, which would involve the release of one proton. One reaction is the hydroxo complex formation according to

$$\equiv X{-}O{-}Cm^{2+} \bullet nH_2O \rightarrow \equiv X{-}O{-}Cm^{+}(OH) \bullet (H_2O)_{n-1} + H^+$$

the second reaction is the transformation of a monodentate to a bidentate Cm complex according to

$$\equiv X{-}O{-}Cm^{2+} \bullet nH_2O + \equiv X{-}O{-}H \rightarrow (\equiv X{-}O)_2{-}Cm^{+} \bullet nH_2O + H^+$$

The peak maximum at 603.3 nm in the kaolinite and smectite spectrum at pH 8.22 corresponds to the second Cm(III) surface complex, which was also found in the alumina system (*13*). Fluorescence emission spectra of Cm(III) in kaolinite, smectite, γ-alumina (*13*), and silica (*12*) suspensions between pH 8.22 and 9.56 are shown in Figure 3 together with the spectrum of Cm(III) aquo ion at pH 1.89. The similarity of spectra of sorbed curium measured in γ-Al_2O_3 and clay suspensions and their difference compare to the spectrum of sorbed Cm(III) in silica suspension suggest that inner-sphere complexation occurs via the aluminol sites.

Fluorescence decay rates are caused by radiative and nonradiative processes. For the $^6D_{7/2} \rightarrow {}^8S_{7/2}$ transition of Cm(III) in 1 M $HClO_4$, the decay rate is calculated to be 770 s^{-1} (*20*). This corresponds to a radiative lifetime (reciprocal decay rate) of 1.3 ms. Nonradiative decay is mainly due to energy transfer from the excited state to ligand vibronics, e.g., OH vibration of coordinated H_2O or OH^- molecules. A lifetime of 68 ± 3 μs is determined for the Cm(III) aquo ion (*21–23*). The increase in lifetime by complexation reflects the exclusion of water molecules of the first coordination sphere of the Cm(III). Using the method developed by Kimura and Choppin a lifetime of 68 μs, determined for the Cm(III) aquo ion, corresponds to nine water molecules, and a value of 1.3 ms corresponds to zero H_2O molecules in the first coordination shell of Cm(III) (*16*).

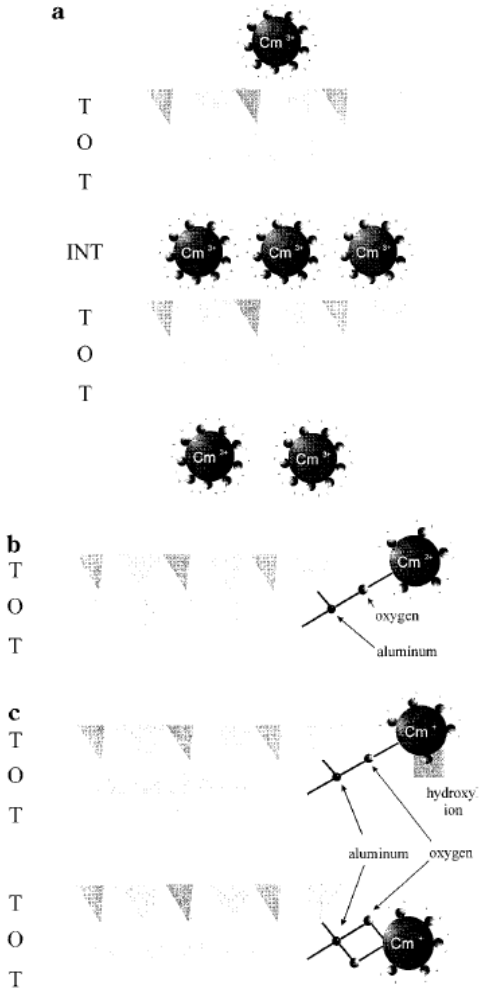

FIGURE 4. Schematic representation of Cm(III) sorption onto smectite. TOT refers to tetrahedral/octahedral/tetrahedral sheets. INT is the abbreviation for the interlayer sites. (A) At low pH Cm(III) is sorbed as an outer-sphere complex onto smectite and retains its complete primary hydration sphere. (B) Starting at a pH ≥ 5 a ≡ Al−O−$Cm^{2+}(H_2O)_5$ surface complex is formed. (C) The first inner-sphere complex is replaced by a second species at higher pH. The second surface complex may be a monodentate ≡Al−O−Cm^{+}-$(OH)(H_2O)_4$ species or a bidentate ≡$(Al-O)_2-Cm^{+}(H_2O)_5$ species.

The fluorescence emission lifetime of Cm(III) in the kaolitite and smectite suspensions at various pH was determined. In both cases at pH ≤ 5, the number of water molecules in the first coordination shell of the Cm(III) was found to be 9. This proves that the outer-sphere complex has not only the same fluorescence emission spectrum like the Cm(III) aquo ion with the peak maximum at 593.8 nm but also the same number of water molecules in the first coordination shell of curium. As the pH increases, inner-sphere adsorption becomes more important. The fluorescence emission lifetime increases from 68 ± 3 μs to 110 ± 7 μs corresponding to a decrease in the number of water molecules in the first coordination shell of about 5.0 ± 0.4

at pH ≥ 7. As a conclusion the Cm(III) species adsorbed onto smectite and kaolinite are illustrated schematically in Figure 4.

The fluorescence lifetimes of Cm(III) sorbed onto kaolinite, smectite, and γ-alumina are very similar. The lifetime of 110 ± 7 μs was observed for Cm(III) sorbed onto these minerals corresponding to five water molecules in the first coordination shell of the sorbed Cm(III) and differs from the lifetime found for a Cm(III) silica suspension at pH ≥ 8.7 (*12*). The long Cm(III) fluorescence lifetime observed in the silica system at high pH indicates that curium has lost its primary hydration sphere during the sorption process and is imbedded into the silica structure. By comparison, this also suggests that Cm-(III) is not incorporated into the clay structure.

Our results give a detailed description of the sorption mechanisms of Cm(III) onto kaolinite and smectite in the trace concentration range as a function of pH. This insight into the sorption mechanisms of a trivalent radionuclide onto a clay mineral surface will be of importance for the predictive modeling of radionuclide migration.

Literature Cited

(1) Bradbury, M. H.; Baeyens, B. *Geochim. Cosmochim. Acta* **1999**, *63*, 325.
(2) Hyun, S. P.; Cho, Y. H.; Kim, S. J.; Hahn, P. S. *J. Colloid Interface Sci.* **2000**, *222*, 254.
(3) Bayens, B.; Bradbury, M. H. *J. Contam. Hydrol.* **1997**, *27*, 199.
(4) Strawn, D. G.; Sparks, D. L. *J. Colloid Interface Sci.* **1999**, *216*, 257.
(5) Kim, J. I.; Klenze, R.; Wimmer, H. *Eur. J. Solid State Inorg. Chem.* **1991**, *28*, 347.
(6) Fanghänel, T.; Kim, J. I.; Paviet, P.; Klenze, R.; Hauser, W. *Radiochim. Acta* **1994**, *66/67*, 81.
(7) Paviet, P.; Fanghänel, T.; Klenze, R.; Kim, J. I. *Radiochim. Acta* **1996**, *74*, 99.
(8) Könnecke, Th.; Fanghänel, Th.; Kim, J. I. *Radiochim. Acta* **1997**, *76*, 131.
(9) Fanghänel, T.; Weger, H. T.; Schubert, G.; Kim, J. I. *Radiochim. Acta* **1998**, *82*, 55.
(10) Aas, W.; Steinle, E.; Fanghänel, Th.; Kim, J. I. *Radiochim. Acta* **1999**, *84*, 85.
(11) Fanghänel, Th.; Könnecke, Th.; Weger, H.; Paviet-Hartmann, P.; Neck, V.; Kim, J. I. *J. Solution Chem.* **1999**, *4*, 447.
(12) Chung, K. H.; Klenze, R.; Park, K. K.; Paviet-Hartmann, P.; Kim, J. I. *Radiochim. Acta* **1998**, *82*, 215.
(13) Stumpf, Th.; Rabung, Th.; Klenze, R.; Geckeis, H.; Kim, J. I. *J. Colloid Interface Sci.* **2001**, *238*, 219.
(14) Meier, L.; Kahr, G. *Clays Clay Miner.* **1999**, *47*, 386.
(15) Bauer, A.; Berger, G. A. *Applied Geochem.* **1998**, *13*, 905.
(16) Kimura, T.; Choppin, G. R. *J. Alloys Comp.* **1994**, *213/214*, 313.
(17) Wimmer, H.; Klenze, R.; Kim, J. I. *Radiochim. Acta* **1992**, *56*, 79.
(18) Klenze, R.; Kim, J. I.; Wimmer, H. *Radiochim. Acta* **1991**, *52/53*, 97.
(19) Neck, V.; Fanghänel, Th.; Kim, J. I. *Bericht FZKA 6110* **1998**.
(20) Carnall, W. T.; Crosswhite, H. M. *Report ANL-84-90* **1995**.
(21) Beitz, J. V.; Hessler, J. P. *Nucl. Techn.* **1980**, *51*, 169.
(22) Beitz, J. V.; Bowers, D. L.; Doxtader, M. M.; Maroni, V. A.; Reed, D. T. *Radiochim. Acta* **1988**, *44–45*, 87.
(23) Fanghänel, T.; Kim, J. I.; Klenze, R.; Kato, J. *J. Alloys Comp.* **1995**, *225*, 308.

Received for review December 20, 2000. Revised manuscript received June 25, 2001. Accepted June 27, 2001.

ES001995O

Radiochim. Acta **94**, 243–248 (2006) / **DOI** 10.1524/ract.2006.94.5.243
© by Oldenbourg Wissenschaftsverlag, München

Sorption of Cm(III) onto different Feldspar surfaces: a TRLFS study

By S. Stumpf[1,*], Th. Stumpf[2], C. Walther[3], D. Bosbach[3] and Th. Fanghänel[2,3]

[1] Institut de Recherches Subatomiques, 23 Rue de Loess, P.O. Box 28, 67037 Strasbourg, France
[2] Ruprecht-Karls-Universität Heidelberg, Physikalisch-Chemisches Institut, Im Neuenheimer Feld 253, 69120 Heidelberg, Germany
[3] Forschungszentrum Karlsruhe, Institut für Nukleare Entsorgung, P.O. Box 3640, 76021 Karlsruhe, Germany

(Received September 26, 2005; accepted in revised form December 22, 2005)

Curium / Feldspars / Alteration / Surface complexation / Sorption / TRLFS

Summary. The pH dependent sorption of Cm(III) onto alkali Feldspars (albite and orthoclase) is investigated by time resolved laser fluorescence spectroscopy (TRLFS) in the pH range from 3.4 to 9.4. Three single components are calculated from the raw spectra for both feldspar systems. The first component which corresponds to the Cm(III) aquo ion has a peak maximum at 593.8 nm and a fluorescence emission lifetime of 68 ± 4 µs. This lifetime corresponds to a Cm(III) coordination of nine water molecules in the first coordination sphere of the actinide ion. The second component with a peak maximum at 601.4 nm corresponds to an adsorbed species. Its lifetime of 107 ± 3 µs indicates a reduction of coordinating H_2O/OH^- ligands from nine to five caused by inner-sphere complex formation. The third component (603.6 nm) can be attributed to another sorption species. The corresponding lifetime is again 107 ± 3 µs. Hence the number of coordinating ligands remains constant while the ligand field changes caused by the hydrolysis of the sorbed Cm(III).

In a further set of experiments the Cm(III) sorption onto albite which is altered at pH 6.0 and pH 9.0 is also investigated by TRLFS. Independent of the dissolution and different surface morphologies caused by the alteration process the same Cm(III) species are formed as found for the sorption onto the untreated albite surface. With regard to the clarification of a feldspar dissolution mechanism the TRLFS results of the Cm(III) sorption onto altered feldspar surfaces give no evidence for a dissolution-reprecipitation based alteration mechanism.

1. Introduction

Radionuclide migration in natural aqueous systems is an ongoing concern in environmental research and for the long term performance of nuclear waste repositories. The transport of actinides is strongly influenced by adsorption onto mineral surfaces. The process at the solid-solution interface determines the migration behaviour of the actinides. Insight into the sorption mechanisms and identification of surface species is of cardinal importance for a reliable predictive modelling of sorption reactions. Therefore it is necessary to characterize the surface species formed and to elucidate the reaction mechanisms involved.

*Author for correspondence (E-mail: silvia.stumpf@ires.in2p3.fr).

In this study time resolved laser fluorescence spectroscopy (TRLFS) was used for the characterization and speciation of actinides interacting with feldspar surfaces. Cm(III) was selected as a representative of a trivalent actinide ion. Due to the high fluorescence yield of Cm(III) TRLFS allows speciation studies in the nanomolar concentration range corresponding to a surface loading far below a monolayer. The different Cm(III) species are characterized by their emission spectra and fluorescence emission lifetimes. The quenching behaviour of the Cm(III) fluorescence is influenced by H_2O and OH^- ligands which cause vibration transfer processes. The resulting correlation between emission lifetime and the number of quenchers in the first coordination sphere of curium allows a further characterization of different Cm(III) species [1].

Up to now the sorption of Cm(III) onto mineral surfaces like quartz [2], amorphous silica [3], γ-Al_2O_3 [4], clay minerals [5], calcite [6] and CSH phases [7, 8] has been studied. Feldspars are the most abundant minerals and represent beside quartz and mica one component of granite which is considered as potential repository hostrock. To establish a comprehensive understanding of actinide behavior in a granitic environment it is important to elucidate the actinide interaction with each of the system components, alteration products and impurities like iron mineral phases. Therefore in this study the interaction of Cm(III) with untreated and altered alkali feldspars albite ($Na[AlSi_3O_8]$) and orthoclase ($K[AlSi_3O_8]$) was investigated. From literature it is known that feldspars have a great tendency to alterate in solution [9–11]. The overall feldspar weathering process can be simplified as the alteration of feldspar (here albite) to clay (here kaolinite):

$$NaAlSi_3O_8 + 2\,H^+ + 9\,H_2O \leftrightarrow Al_2Si_2O_5(OH)_4 + 4\,H_4SiO_4 + 2\,Na^+ \qquad (1)$$

The equation for the dissolution of the feldspar surface Eq. (1) implies the stoichiometric release of feldspar components. However, feldspar dissolution is usually non stoichiometric in the initial phase of dissolution [12]. This is a result of exchange and adsorption/desorption reactions in the first few minutes when the fresh feldspar surface is placed in solution. The non stoichiometric dissolution over long periods can be attributed to the preferential removal of one component of the structure, the precipitation of a secondary phase

or the preferential dissolution of distinct regions [12]. The dissolution process therefore results in a change of the surface composition and morphology. Up to now the underlying mechanism of dissolution is not clarified. The intension of this study is to clarify whether the change in composition and morphology has any effect on the actinide speciation. Flow-through reactor experiments can be used as a tool to quantify surface reaction controlled dissolution. Therefore such experiments were performed with albite at pH 6.0 and pH 9.0. The sorption of Cm(III) onto these altered feldspar surfaces was studied by TRLFS measurements and the results were compared with the investigations of the non altered feldspar system.

2. Experimental

2.1 Materials

A stock solution of the long-lived curium isotope Cm-248 ($t_{1/2} = 3.4 \times 10^5$ years) with the isotopic composition 97.3% Cm-248, 2.6% Cm-246, 0.04% Cm-245, 0.02% Cm-247 and 0.009% Cm-244 in 1.0 M $HClO_4$ was used for the experiments. The initial curium concentration determined by ICP-mass spectrometry was adjusted to 1.0×10^{-7} mol/l.

The orthoclase sample used in this study was obtained from La Cabrerra/Guadarrama, Spain. The albite sample was from Iveland, Norway. Both feldspar powders were crushed in a mortar and sieved to get fractions < 20 µm (surface 2 ± 1 m^2/g). A < 5 µm fraction (surface 12 ± 3 m^2/g) used for the TRLFS experiments was selectively obtained *via* centrifugation (Centrikon T124; 20 × 60 min; 100 g). The albite fraction < 20 µm was used for flow-through experiments. The point of zero charge was determined for both feldspars (PZC_{albite} pH 5.25; $PZC_{orthoclase}$ pH 5.6) by acid base titration at three different ionic strengths (0.1 M $NaClO_4$, 0.01 M $NaClO_4$, 0.001 M $NaClO_4$). As the fluorescence emission behavior of Cm(III) is influenced by iron, the metal contamination of both feldspars was determined by ICP-MS. The iron content was 494 ppm for the albite and 616 ppm for the orthoclase. The consequence of this contamination on the realization of TRLFS experiments will be discussed in the next section.

All sorption experiments were made at 25 ± 1 °C in a glovebox under argon atmosphere. The electrolytic background of each sample ($I = 0.1$ mol/l) was set by the use of $NaClO_4$ solutions from analytical grade. For the investigation of the Cm(III) sorption onto the feldspar surfaces the pH of each sample was raised by adding analytical grade NaOH (and $HClO_4$ for adjustment) within two weeks from pH 3.4 up to pH 9.4 in steps of almost 0.3 pH unit. Before measuring and adjusting the pH of each sample the electrode (Type: Blue Line 16 pH Schott) was calibrated in a standard procedure in H^+ concentration units. According to former studies [5] the steady state was bided for 24 h. That is to say, the cited pH values were determined one day after adjustment. During this curium/feldspar contact time the samples were shaken periodically.

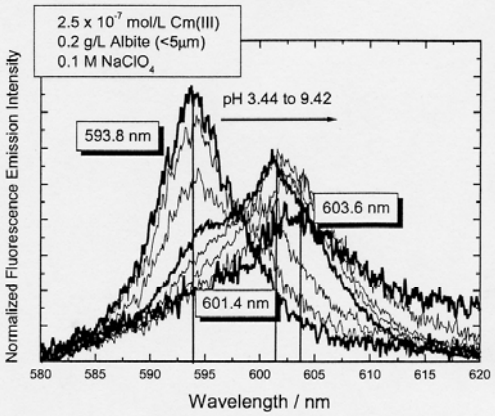

Fig. 1. Fluorescence emission spectra of 2.5×10^{-7} mol/l Cm(III) in a suspension of 0.2 g/l albite at different pH values.

2.2 Method

2.2.1 TRLFS (Time Resolved Laser Fluorescence Spectroscopy)

TRLFS measurements were performed using a dye laser (Lambda Physics, scanmate) pumped by a XeCl-excimer laser (Lambda Physics, EMG , 308 nm, 24 ns) for excitation. The fluorescence emission was detected by an optical multichannel analyzer consisting of a polychromator (Jobin Yvon, HR 320) with a 300/600/1200 lines/mm grating

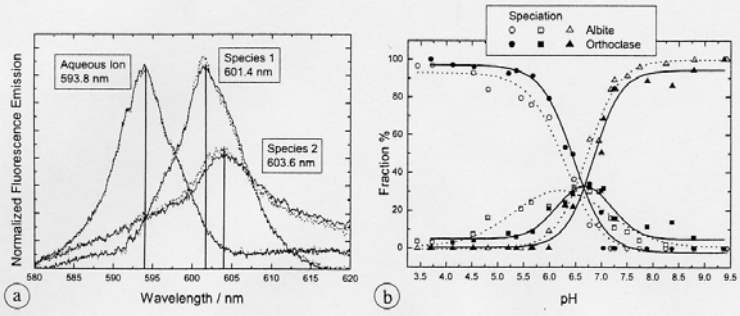

Fig. 2. (**a**) Calculated single components and (**b**) speciation plot for the sorption of Cm(III) onto feldspars.

and a photodiode array (Spectroscopy instruments, ST 180, IRY 700G). The spectral resolution of the monochromator is 0.2 nm for the 1200 lines/mm grating and 0.9 nm for the 300 lines/mm grating. The Cm(III) was excited at 396.6 nm. The emission spectra of Cm(III) were recorded in the 580–620 nm range (1200 lines/mm grating). For measuring the time dependent emission decay (300 lines/mm grating), the delay time between laser pulse and camera gating was scanned with time intervals between 5 and 10 µs using a constant time window of 1 ms. All sorption samples were agitated during the measurement.

2.2.2 Flow-through experiment

Alteration experiments at pH 6.0 and pH 9.0 were conducted in continuously stirred flow-through reactors of ~ 45 ml [13]. The reactor for the experiment at pH 9.0 was placed in a glovebox with argon atmosphere to inhibit the contact with CO_2. Both reactors were put into a water bath to keep the reaction temperature at 25 ± 0.5 °C. Each reactor was filled with 1 g of albite powder (< 20 µm). The dissolution experiments were carried out in solutions comprised of Milli-Q water (18.2 MΩ), HCl (Ultrapure, Merck) and high purity $NaClO_4$ (99.9%, Merck) as background electrolyte. No additional additives or buffers were used. Solutions with an ionic background of 0.1 M $NaClO_4$ were pumped through the reactors with a rate of 0.1 ml/min. The inlet and outlet solutions passed through a 0.45 µm filter. The outlet solutions were continuously collected, analyzed for pH, acidified with HNO_3 and analyzed for monomeric Si (Carry 5G UV-VIS-NIR Spectrophotometer; Spectroquant; Merck) to determine the steady state of the dissolution reaction.

TRLFS measurements of the Cm(III) sorption onto the altered feldspar surfaces were performed just after equilibration of pH (24 h) to avoid the influence of further surface alteration.

3. Results and discussion

3.1 Sorption of Cm(III) onto albite and orthoclase (< 5 µm)

2.5×10^{-7} mol/l Cm(III) were added to an albite and orthoclase suspension with a mineral concentration of 0.2 g/l and an ionic background of 0.1 M $NaClO_4$. The pH of each sample was raised as described above. For each pH value a fluorescence emission spectrum was measured. The according series of emission spectra are exemplarily shown for the albite system in Fig. 1. The peak maximum of the Cm(III) fluorescence emission varies with pH from 593.8 nm up to 603.6 nm. Analogue spectra were obtained for the pH dependent interaction of Cm(III) with the potassium feldspar orthoclase. The raw emission spectra were deconvoluted and the Cm(III) speciation was calculated for both alkali feldspars taking the fluorescence intensity factors (FIs) into account (Fig. 2). The deconvolution was performed using a factor analysis programme that determines the eigenvalues of the system. Details of this procedure are described elsewhere [14]. Independent on the alkali ion (Na^+ for albite and K^+ for orthoclase) identical single component spectra with peak maxima at 593.8 nm (FI: 1), 601.4 nm (FI: 3.5) and 603.6 nm (FI: 1) were calculated for both feldspar systems. The speciation plot in Fig. 2 shows that up to a pH of ~ 5 the first Cm(III) species dominates the system. With increasing pH the second species is formed with a maximal ratio of 30% at pH 6.2 and a third species is formed when the pH is further increased. A similar speciation is found for the Cm(III) interaction with orthoclase. In this case the sorption process is shifted to higher pH values (0.5 pH unit). This shift for the orthoclase system can be explained by the higher point of zero charge of

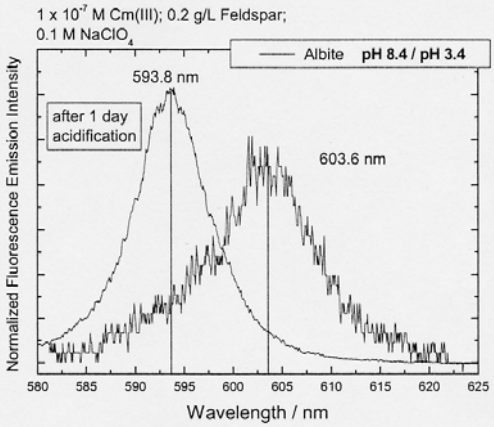

Fig. 3. Fluorescence emission spectra of the sorption of Cm(III) onto feldspars at pH 9.8 and 8.4 compared to spectra after 1 day of acidification to pH 3.4 and 3.5, respectively.

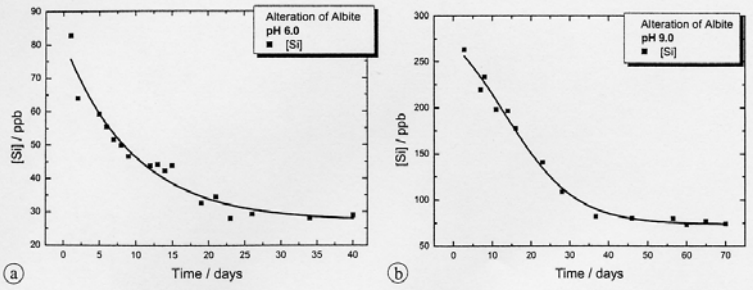

Fig. 4. Flow-Through Experiment: The change of Si concentration with time at (**a**) pH 6.0 and (**b**) pH 9.0.

the orthoclase in comparison to the one of albite (PZC_{albite} pH 5.25; $PZC_{orthoclase}$ pH 5.6).

The first component (593.8 nm) has a fluorescence lifetime of 68 ± 4 µs and corresponds to the Cm(III) aquo ion with 9 H_2O molecules in the first coordination sphere [1]. A lifetime of 107 ± 3 µs can be attributed to the second Cm(III) component in the albite as well as in the orthoclase system. The number of water molecules (quenchers) is reduced from nine to five. This reduction can be interpreted by the sorption of Cm(III) onto the feldspar surfaces and the formation of inner-sphere complexes. The lifetime of the third Cm(III) component again has a value of 107 ± 3 µs. The difference in the spectral positions of the second and third component indicate different ligand fields for both sorbed species. As it is demonstrated by the invariant lifetime this change cannot be attributed to a further reduction of the first hydration sphere. Hence, the number of quenching ligands keeps constant. Moreover, the spectral shift can be explained by the hydrolyses of the sorbed Cm(III) species as it is already described in literature [2, 4, 5]

The reversibility of the sorption process was examined by acidifying the alkaline samples (Fig. 3). Within one day the Cm(III) aquo ion is reobtained.

3.2 Sorption of Cm(III) onto altered albite (< 20 µm)

The dissolution of feldspars in closed systems (batch experiments) results in a change of solution composition with time. As a result the morphology of the surface is not defined. This is the case for the sorption experiments performed and described above. Therefore in a next step the alteration of albite at pH 6.0 and pH 9.0 was performed as a flow-through experiment where solution is continuously added and removed from a reactor. This allows the system to remain undersaturated with regard to the feldspar components and offers the possibility to study alteration under controlled conditions. From literature it is known that the feldspar dissolution rate is high at the beginning of the process and decreases with time until a nearly constant value is reached [15]. This so called steady state was determined for the alteration of albite at pH 6.0 and pH 9.0 by measuring the Si concentration of the output solution. Because the reactor is well mixed and there is a continuous exchange of solution the composition of the output solution is identical with the one in contact with the albite over time. In both flow-through experiments at pH 6.0 and pH 9.0 the Si concentration of the output solutions followed the trend noted by other flow-through reactor studies [16]. Starting with a high initial Si concentration it gradually decreases for about 40 days to a constant value (Fig. 4). The change of the albite surface structure caused by alteration processes is demonstrated in Fig. 5. The SEM pictures of the untreated feldspar grains show no typical crystal morphology, but as a consequence of a grinding procedure an irregular surface morphology. The soft surface structure can be attributed to the formation of a diffuse surface layer. Light spots in the picture can be assigned to surface precipitates like $NaClO_4$. The surface of the altered albite at pH 6.0 is more structured. The SEM picture clearly shows several layers. Also the altered surface at pH 9.0 has a crystal morphology. Moreover etching cavities can be distinguished. The cavities indicate the dissolution of the mineral frame during the alteration process. Measurements of the BET surface (N_2 gas) confirm the change of morphology. The feldspar surface enlarges from 1 m^2/g to 1.8 m^2/g at pH 6.0 and to 3.2 m^2/g at pH 9.0.

The sorption of 1×10^{-7} mol/l Cm(III) onto the different albite surfaces was performed in two steps. Firstly, the pH of two Cm(III) solutions (1×10^{-7} mol/l) with an ionic background of 0.1 mol/l $NaClO_4$ was adjusted to a value of 6.0. In a second step 1 g/l albite powder (< 20 µm) altered

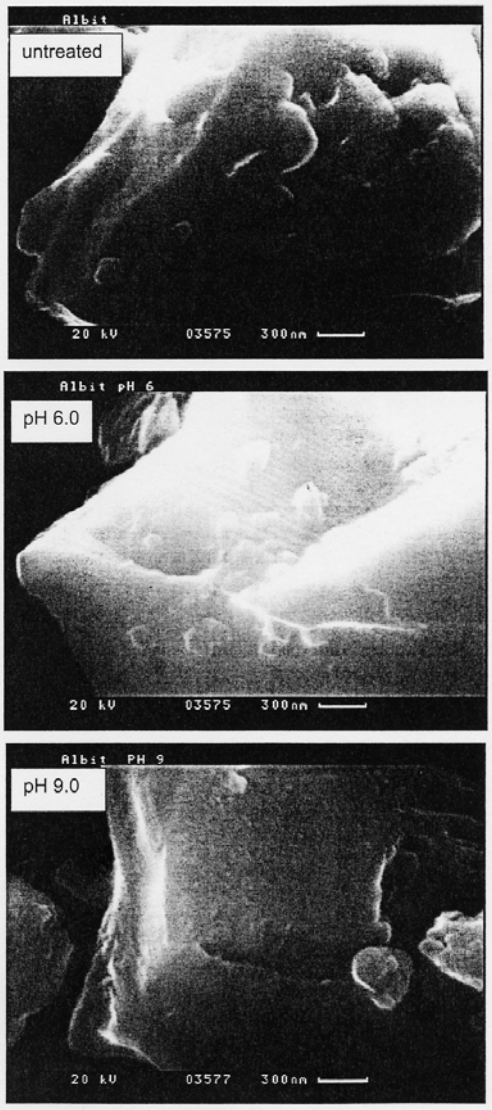

Fig. 5. SEM images of untreated albite and altered albite at pH 6.0 and pH 9.0.

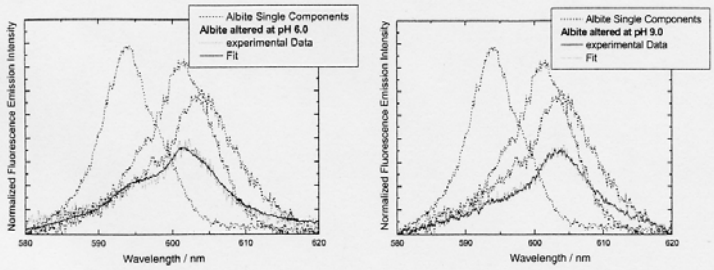

Fig. 6. Fit of the TRLFS spectra of Cm(III) sorbed onto altered albite (pH 6.0 / 9.0); basis of calculation: single components of the Cm(III) sorption onto untreated albite.

at pH 6.0 was added to the first solution. Because the albite has a particle size of $< 20\ \mu m$ and therefore a lower sorption surface, the start of the sorption process should be shifted to higher pH compared to the sorption experiments performed before in batch experiments with albite $< 5\ \mu m$ (see speciation in Fig. 2) [17]. Therefore the pH of this suspension (albite $< 20\ \mu m$) was raised to a value of 6.5. To the second solution 1 g/l albite powder altered at pH 9.0 was added and the pH of the suspension was then raised up to a value of 8.0. At higher pH the Cm(III) fluorescence signal is very low and the calculation of the Cm(III) speciation is not possible. The low fluorescence emission intensity is probably a result of the hydrolysis of Fe (albite contamination) and the formation of iron colloids at higher pH values. As it is reported in literature these colloids tend to form mineral coatings [18]. The low fluorescence emission intensity is due to quenching effects supposably caused by the sorption of Cm(III) onto the iron coating as it is shown in previous studies [19]. Therefore the pH of the suspension was lowered from 9.0 to 8.0 in order to reduce quenching effects.

The TRLFS spectra of the Cm(III) sorption onto altered albite are shown in Fig. 6. Both spectra fit in the calculation of the single components of the Cm(III) sorption onto untreated feldspar. This calculation demonstrates that the surface morphology of the feldspar has no influence on the Cm(III) speciation.

Moreover the results provide an indication of the feldspar dissolution mechanism that is discussed in different ways in literature [20, 21].

3.3 Feldspar dissolution mechanism

During feldspar dissolution an altered surface zone is observed. This zone is depleted in interstitial cations like Ca (plagioclase series), Na and K (alkali feldspars) and certain framework elements like Al whereas it is enriched in H, O and Si. The prevailing dissolution model postulates a preferential leaching of cations and interdiffusion with H^+ [20]. Whereas Hellmann *et al.* postulates an interfacial dissolution-reprecipitation process [21]. If there were a reprecipitation of a silica gel as it is postulated by Hellmann *et al.* sorbed Cm(III) would be incorporated in a gel like structure. Such an incorporation process is reported in literature by Chung *et al.* [3] and Stumpf *et al.* [2]. Both authors find a strong increase of fluorescence emission lifetime ($740 \pm 35\ \mu s$ [3] and $> 500\ \mu s$ [2]) for the incorporated Cm(III) species. These fluorescence lifetimes indicate the complete loss of the Cm(III) hydration sphere by incorporation in a gel like structure. No longer lifetimes are determined for the investigated interaction of Cm(III) with different feldspar surfaces in this study. On the basis of these experiments it can be ruled out that Cm(III) takes part in a precipitation reaction.

4. Conclusion

The sorption of curium onto albite and orthoclase was investigated by TRLFS. Three species could be calculated from the raw data. Additional lifetime measurements indicate a coordination of nine water molecules in the first coordination sphere for the Cm(III) aquo ion and five water molecules for both sorbed species. The results indicate a Cm(III) inner-sphere sorption onto the mineral surface in a first step and the hydrolysis of the surface complex in a second step. Sorption experiments onto altered albite show that the morphology of the surface has no influence on the Cm(III) speciation. Moreover the investigations show that Cm(III) TRLFS is a good tool to clarify dissolution mechanisms of feldspar surfaces.

Acknowledgment. We thank Dr. Thuro Arnold for allocating the albite and orthoclase. Thanks to Dr. Felix Brandt for making the flow-through reactor available. We thank Dr. André Rossberg for providing the factor analysis program code designed for the analysis of EXAFS, UV-VIS and TRLFS spectra.

References

1. Kimura, T., Choppin, G. R.: Luminescence study on determination of the hydration number of Cm(III). J. Alloys Compd. **213/214**, 313 (1994).
2. Stumpf, S., Stumpf, Th., Lützenkirchen, J., Walther, C., Fanghänel, Th.: Speciation of Cm(III) on particles and single crystals of quartz in the presence and absence of excess silicic acid by TRLFS. J. Colloid Interf. Sci., submitted.
3. Chung, K. H., Klenze, R., Park, K. K., Paviet-Hartmann, P., Kim, J. I.: A study of the surface sorption process of Cm(III) on silica by time-resolved laser fluorescence spectroscopy (I). Radiochim. Acta **82**, 215 (1998).
4. Stumpf, Th., Rabung, Th., Klenze, R., Geckeis, H., Kim, J. I.: A spectroscopic study of the Cm(III) sorption onto γ-alumina. J. Colloid Interf. Sci. **238**, 219 (2001).
5. Stumpf, Th., Bauer, A., Coppin, F., Kim, J. I.: Time-resolved laser fluorescence spectroscopy (TRLFS) study of the sorption of Cm(III) onto smectite and kaolinite. Environ. Sci. Technol. **35**, 3691 (2001).
6. Stumpf, Th., Fanghänel, Th.: A Time-resolved laser fluorescence spectroscopy (TRLFS) study of the interaction of trivalent actinides (Cm(III)) with calcite. J. Colloid Interf. Sci. **249**, 119 (2002).

7. Tits, J., Stumpf, T., Rabung, T., Wieland, E., Fanghänel, Th.: Uptake of Cm(III) and Eu(III) by calcium silicate hydrates: A solution chemistry and time-resolved laser fluorescence spectroscopy (TRLFS) study. Environ. Sci. Technol. **37**, 3568 (2003).
8. Stumpf, Th., Tits, J., Walther, C., Fanghänel, Th.: Uptake of trivalent actinides (Cm(III)) by cement: A time-resolved laser fluorescence spectroscopy (TRLFS) study. J. Colloid Interf. Sci. **276**, 118 (2004).
9. Fung, P. C., Bird, G. W., Mc Intyre, N. S., Sanipelli, G. G.: Aspects of feldspar dissolution. Nucl. Technol. **51**, 188 (1980).
10. Chou, L., Wollast, R.: Study of the weathering of albite at room temperature and pressure with a fluidised bed reactor. Geochim. Cosmochim. Acta **48**, 2205 (1984).
11. Holdren, G. R., Berner, R. A.: Mechanism of feldspar weathering. I. Experimental studies. Geochim. Cosmochim. Acta **43**, 1161 (1979).
12. Stillings, L. L, Brantley, S. L.: Feldspar dissolution at 25 °C and pH 3: Reaction stoichiometry and the effect of cations. Geochim. Cosmochim. Acta **59**, 1483 (1995).
13. Brandt, F., Bosbach, D., Krawczyk-Baersch, E., Arnold, T., Bernhard, G.: Chlorite dissolution in the acid pH range: A combined microscopic and macroscopic approach. Geochim. Cosmochim. Acta **67**, 1451 (2003).
14. Rossberg, A., Reich, T., Bernhard, G.: Complexation of uranium(VI) with protocatechuic acid – application of iterative transformation factor analysis to EXAFS spectroscopy. Anal. Bioanal. Chem. **376**, 631 (2003).
15. Blum, A. E., Stillings, L. L.: Feldspar Dissolution Kinetics in: Rev. Mineral. Vol. 31; Chemical Weathering Rates of Silicate Minerals. (White, A. F., Brantley, S. L., eds.) Mineralogical Society of America (1995).
16. Chou, L., Wollast, R.: Study of the weathering of albite at room temperature and pressure with a fluidized bed reactor. Geochim. Cosmochim. Acta **48**, 2205 (1984).
17. Kosmulski, M.: Adsorption of trivalent cations on silica. J. Colloid Interf. Sci. **195**, 395 (1997).
18. Stumpf, S., Stumpf, Th., Dardenne, K., Hennig, C., Foerstendorf, H., Klenze, R., Fanghänel, Th.: Sorption of Am(III) onto 6-line-ferrihydrite and its alteration products: Investigations by EXAFS. Environ. Sci. Technol., accepted for publication.
19. Stumpf, S., Stumpf, Th., Fanghänel, Th., Klenze, R., Bernhard, G., Kim, J. I.: The effect of Fe on the Cm(III) fluorescence emission: Investigations of quenching processes by TRLFS. In preparation
20. Chou, L., Wollast, R.: Steady-state kinetics and dissolution mechanisms of albite. Am. J. Sci. **285**, 963 (1985).
21. Hellmann, R., Penisson, J. M., Hervig, R. L., Thomassin, J. H., Abrioux, M. F.: An EFTEM/HRTM high-resolution study of the near surface of labradorite feldspar altered at acid pH: Evidence for interfacial dissolution-reprecipitation. Phys. Chem. Minerals **30**, 192 (2003).

Radiochim. Acta **92**, 133–138 (2004)
© by Oldenbourg Wissenschaftsverlag, München

An EXAFS and TRLFS study of the sorption of trivalent actinides onto smectite and kaolinite

By Th. Stumpf[1,2,*], C. Hennig[1], A. Bauer[2], M. A. Denecke[2] and Th. Fanghänel[2]

[1] Forschungszentrum Rossendorf, Institut für Radiochemie, P.O. Box 510119, D-01314 Dresden, Germany
[2] Forschungszentrum Karlsruhe, Institut für Nukleare Entsorgung, P.O. Box 3640, D-76021 Karlsruhe, Germany

(Received November 24, 2003; accepted in revised form December 16, 2003)

Actinides / Clay minerals / EXAFS / Surface complexation / TRLFS

Summary. The structure parameters of the Am^{3+} aquo ion and of Am(III) sorbed onto smectite and kaolinite at varying pH are analyzed using EXAFS. An Am–O distance of 2.47–2.49 Å is found and a coordination number of 8–9 oxygen atoms is observed for the Am^{3+} and its hydration sphere. Combined TRLFS (Cm(III)) and EXAFS (Am(III)) results show that An(III) sorbs onto smectite at pH 4, forming an outer-sphere complex and retains its complete primary hydration sphere. With increasing pH, inner-sphere sorption onto smectite and kaolinite occurs. The overall number of oxygen atoms coordinating the actinide ion remains about the same at pH 6, with four water molecules being replaced by oxygen atoms from the mineral surface during inner-sphere complex formation. The coordination number of sorbed Am(III) at pH 8 exhibits an apparent decrease, which may be affected by the formation of ternary OH^-/Am/clay mineral surface species.

Introduction

Long term storage of high-level nuclear waste canisters within engineered clay barriers in deep geological clay-rich host formations has been proposed (Opalinus shale (Switzerland), Haute Marne/Meuse Site (France)). The principal concern with nuclear waste disposal is the potential for leaching of radionuclides into the surrounding groundwater and the associated risk of ecological and human exposure. Therefore, knowledge of radionuclide sorption behaviour onto clay mineral surfaces, as a possible process controlling released radionuclide concentration, mobility, and bioavailability, is imperative.

Kaolinite is one of the main mineral components of clay-rich host formations (*e.g.*, 20% of the Opalinus Shale [1]), whereas smectites have been proposed as waste disposal site backfill material. Kaolinite is a 1 : 1 layer type clay mineral, in which each Si–, Al–OH, (O) component exists in two distinct structural environments at the surface. There is only minimal substitution of cations with variable valence in the structure and hence only minor permanent structural charge. In contrast to kaolinite, each aluminium octahedral layer in smectite is bound to two silica rich tetrahedral layers; smectite is an expandable 2 : 1 layer type clay mineral. It has both interlayer sites and ionizable hydroxide sites on its external surface available for metal cation sorption. Substitution of Al^{3+} by Mg^{2+} and Fe^{2+} atoms in the octahedral layer creates a positive charge deficit, giving the overall structure a net negative charge. The O atoms and OH groups at the edges of both kaolinite and smectite, or at the gibbsite basal plane of kaolinite, are Lewis base or Lewis acid functional groups, which are the source of the pH dependent charge [2]. Time-resolved fluorescence spectroscopy (TRLFS) studies with Cm(III) indicate that binding to these sites on the external surface may be viewed as a complexation reaction similar to that occurring at oxide mineral surfaces. At pH values ≤ 5, Cm(III) is sorbed onto smectite as an outer-sphere complex [3]. At higher pH (> 5), Cm(III) inner-sphere surface complexation onto smectite, kaolinite and γ-alumina [4] occurs at the aluminol sites. The inner-sphere complex formation leads to a red-shift of the fluorescence emission and to an increase in the fluorescence emission lifetime.

TRLFS measurements were performed in D_2O to evaluate whether the linear correlation between decay rate (reciprocal lifetime) and hydration number can be used directly to determine the Cm(III) hydration number for Cm/clay inner-sphere sorption species. To identify and characterize the surface species observed to form during the sorption process with TRLFS studies, the sorption process of Am(III) onto smectite and kaolinite as a function of pH is studied by extended X-ray absorption fine structure (EXAFS) spectroscopy.

Experimental

Starting materials

Hydrous γ-alumina (Degussa, aluminium oxide C) with a particle size of around 90 nm and a BET (method developed by Brunauer, Emmett, and Teller) surface (N_2) of 119 m^2/g is used for Cm(III) TRLFS measurements in D_2O. For Cm(III) and Am(III) sorption experiments in aqueous milieu, well crystallized, fine grained kaolinite (≤ 2 µm) from St. Austell (UK) and smectite (< 0.1 µm fraction of

*Author for correspondence
(E-mail: Thorsten.Stumpf@ine.fzk.de).

the Ceca bentonite separated by sedimentation technique) are used. The cation exchange capacity (CEC) of the initial samples is found to be 3.7 meq/100 g for kaolinite and 75 meq/100 g for smectite.

For the TRLFS study, a Cm-248 ($t_{1/2} = 3.4 \times 10^5$ years) stock solution in concentrated HCl is used (97.2% ^{248}Cm, 2.8% ^{246}Cm, and less than 0.01% ^{244}Cm). The curium mass concentration in solution is determined by ICP mass spectroscopy and liquid scintillation counting (LSC). The fluorescence measurements are performed at 25 ± 1 °C, in a glove box, under argon atmosphere. The Cm/smectite sample consists of 3×10^{-7} mol/L Cm(III) in 0.25 g/L clay suspension. As background electrolyte, we use a $NaClO_4$ solution ($I = 0.025$ M).

For the EXAFS study, each sample contains 0.1 g clay, which was equilibrated at pH 6.7 for one week in the dark. As background electrolyte, we use 0.025 M $NaClO_4$ solutions. The long-lived americium isotope Am-243 ($t_{1/2} =$ 7370 years) is provided by the Oak Ridge National Laboratory. The initial americium concentration is adjusted to 1×10^{-3} mol/L. EXAFS samples are prepared at room temperature in a glove box under nitrogen atmosphere. To avoid Am(III) precipitation, the actinide is initially added to 40 mL clay suspensions in the acidic range (pH 3.5), followed by increasing the pH in small steps to reach the final value in each sorption sample after 2–4 weeks (*i.e.*, S/4 smectite pH 4; S/6 smectite pH 6 and S/8 smectite pH 8; K/6 kaolinite pH 6 and K/8 kaolinite pH 8). The suspensions (40 mL each) are centrifuged (6000 rpm; 10 min) and the wet pastes transferred into polypropylene (pp) vials.

Methods

TRLFS measurements are performed using a pulsed Nd:YAG pumped dye laser system (Continuum, Powerlite9030, ND 6000). A laser pulse energy of at most 4 mJ is controlled by a photodiode. The fluorescence emission is detected by an optical multichannel analyzer consisting of a polychromator (Chromex 250 is) with a 1200 lines/mm grating, which allows simultaneous detection of an entire Cm(III) emission spectrum in the range 580–620 nm, within a constant time window of 1 ms width, exciting at 396.6 nm (laser dye, Exalite 398). For measuring the emission decay, the delay time between laser pulse and camera gating is scanned with time intervals of 50 µs in the D_2O system and of 10 µs in the presence of water.

EXAFS measurements are carried out on the Rossendorf Beamline (ROBL) at the European Synchrotron Radiation Facility (ESRF) [5]. Two Si(III) crystals, the first being water cooled, are used in the double-crystal monochromator in pseudo channel-cut mode. Higher harmonics are rejected by two Pt coated mirrors. The samples, contained in their pp vials, are sealed with polyethylene foil and put into a lead shielding. All measurements are performed at room temperature. Fluorescence data are recorded using a four-pixel Ge detector. The energy is calibrated by assigning the first inflection point at the *K*-edge absorption spectrum of a Zr metal foil to 17 998 eV. EXAFS spectra are analysed according to standard procedures in two independent ways. First, the spectra are fit to the EXAFS equation in *k*-space using the computer program EXAFSPAK [7]. The *ab initio* curved-wave multiple-scattering program FEFF8.0 [8] is used to calculate the backscattering phase and amplitude functions of the neighboring atoms used for fitting the data. These fits are performed in the 3.3–9.9 Å^{-1} range to k^3-weighted spectra. The hydration number of the Am(III) aquo ion is assumed to be 9 and its EXAFS is initially fit while allowing the reduction factor, S_0^2, to vary and holding the coordination number (N) of the Am−O sphere constant at 9. The value for S_0^2 obtained from this fit, 0.72, is then kept constant at this value for the fits to k^3-weighted $\chi(k)$ for the Am(III) sorbed clay samples. The second method of fitting is performed to the Fourier transform (FT) data, in k^2-weighted *R*-space, using the feffit software [9]. For these fits, a hypothetical AmO_8 cluster with dodecahedral symmetry is used to calculate the backscattering phase and amplitude functions with FEFF8.0. A Dirac–Hira exchange potential with a −2 eV edge shift and a 1 eV innerpotential for the americium are used in the calculation.

Results and discussion

TRLFS study of the lifetime of Cm(III) sorbed onto γ-alumina and smectite

The Cm(III) fluorescence emission lifetime provides information on the composition of the first coordination sphere. Fluorescence decay rates are caused by radiative and non-radiative processes. For the $^6D_{7/2} \rightarrow {}^8S_{7/2}$ transition of Cm(III) in 1 M $HClO_4$, the decay rate is calculated to be 770 s^{-1} [10]. This corresponds to a radiative lifetime (reciprocal decay rate) of 1.3 ms. Non-radiative decay is mainly due to energy transfer from the excited state to ligand vibronic states, *e.g.*, OH vibration of coordinating H_2O or OH^- molecules. According to the method developed by Kimura and Choppin [11], there is an empirical linear correlation between the decay rate and the number of H_2O molecules in the first coordination sphere. This linear correlation is given by:

$$n(H_2O/OH^-) = 0.65k_{obs} - 0.88\,, \qquad (1)$$

where k_{obs} is the observed decay rate of the excited state [ms^{-1}] and $n(H_2O/OH^-)$ is the number of coordinated water molecules or hydroxyl ions. Nonahydrated Cm(III), $Cm(H_2O)_9{}^{3+}$, exhibits a 68 ± 3 µs lifetime [12–15]. When no water is coordinated, the lifetime is 1250 ± 80 µs [16].

To evaluate if this correlation can be used directly to determine the Cm(III) hydration number during a sorption process, TRLFS measurements are performed in D_2O in the presence of mineral at various pH values. γ-alumina is chosen as a representative mineral surface. Fig. 1 shows the fluorescence emission spectra of 2×10^{-7} mol/L Cm(III) in D_2O in 2 g/L γ-alumina suspension at pH 3 and pH 10. At pH 3, the emission spectrum of the Cm^{3+} aquo ion with a peak maximum at 593.8 nm is obtained. In the alkaline region a shift of the fluorescence signal from 593.8 nm to 604.3 nm is detected, indicating a change in the Cm(III) coordination. At this pH, Cm(III) is likely sorbed as an inner-sphere complex onto the mineral surface. Lifetime measurements yield 1388 ± 11 µs at pH 3 and 1106 ± 20 µs in the alkaline region. These values are comparable; the marginal

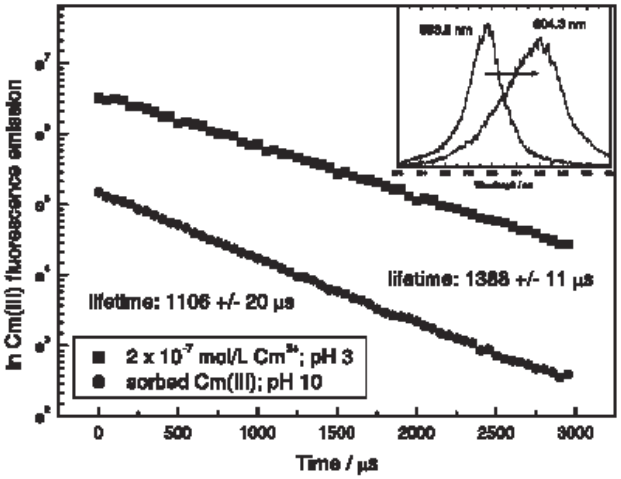

Fig. 1. Time dependence of fluorescence emission decay and fluorescence emission spectra of 2×10^{-7} mol/L Cm(III) in D_2O, in the presence of 2 g/L γ-alumina, at pH 3 and pH 10.

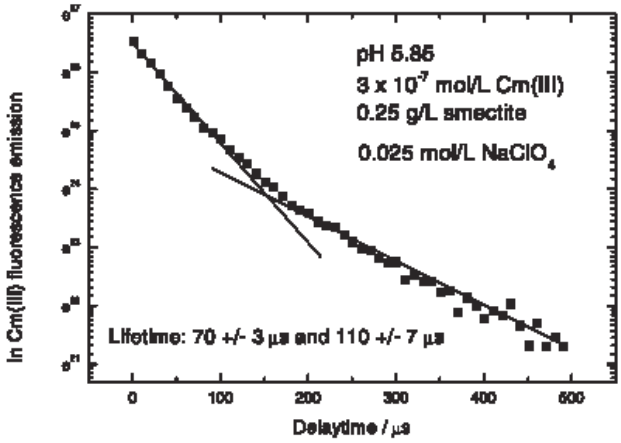

Fig. 3. Time dependence of fluorescence emission decay of 3×10^{-7} mol/L Cm(III) in 0.25 g/L smectite suspension at pH 5.85. Bi-exponential decay behaviour is obtained with lifetimes $t_1 = 70 \pm 3$ µs and $t_2 = 110 \pm 7$ µs.

decrease in the lifetime at high pH can be explained by water impurities in the added NaOD. No substantial increase in fluorescence emission lifetime with Cm(III)/surface complex formation in the absence of water, *i.e.* in D_2O and absence of O–H vibronics, is observed. This suggests that an increase in Cm(III) fluorescence emission lifetime during the sorption process in water is effected only by the reduction of the number of water molecules coordinated to Cm(III) in the first hydration shell.

Fig. 2 shows fluorescence emission spectra of 3×10^{-7} mol/L Cm(III) in 0.25 g/L smectite suspension at pH 5.85 recorded with different delay times. The spectrum measured after 1 µs is dominated by the Cm^{3+} aquo ion signal with its peak maximum at 593.8 nm. Centrifugation of the sample (4000 rpm; 30 min) and analysis of the supernatant and solid phase shows that nearly all Cm(III) is sorbed onto the smectite. Because Cm(III) is largely associated with smectite and exhibits a spectrum with a peak maximum similar that for Cm^{3+} aquo ion, we conclude that most (~ 70%) of the sorbed Cm(III) in this sample does not change its ligand field during the sorption process

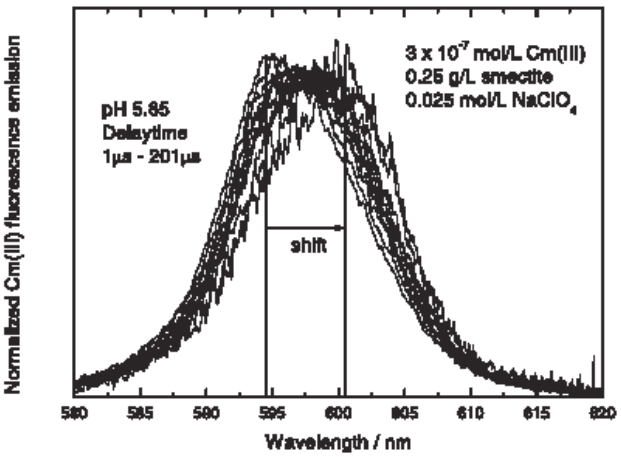

Fig. 2. Fluorescence emission spectra of 3×10^{-7} mol/L Cm(III) in 0.25 g/L smectite suspension, pH 5.85, at different delay times. The spectra are scaled to the same peak area.

and retains its hydration sphere. This suggests outer-sphere complex formation, most probably onto the interlayer sites. With increasing delay time, a red shift of the peak maximum is obtained, indicating the existence of two Cm(III) species with different fluorescence emission lifetimes. The shorter lifetime is attributed to the Cm^{3+} outer-sphere complex showing a peak maximum at 593.8 nm, while the longer lifetime is attributed to a Cm/smectite inner-sphere surface species.

A plot of the Cm(III) fluorescence emission intensity (on a logarithmic scale) with increasing delay time is shown in Fig. 3. The decay of the fluorescence signal follows a bi-exponential decay law, indicating the existence of two different sorbed species with two different lifetimes. A fit of the decay curve gives lifetimes of 70 ± 3 µs for the Cm^{3+} outer-sphere complex and a lifetime of 110 ± 7 µs for the inner-sphere sorbed Cm(III) species. According to Eq. (1), a lifetime of 70 ± 3 µs corresponds to 8.4 water/OH^- molecules in the first coordination sphere of Cm(III), whereas a lifetime of 110 ± 7 µs corresponds to five water molecules in the first hydration shell of the Cm(III)/clay sorption species. A value of five water molecules in the first coordination sphere of Cm(III)/mineral sorption species is also found for curium sorbed onto kaolinite [3] and γ-alumina [4]. Structural information about surface bound Cm(III) species such as metal-oxygen and metal-Al/Si binding type (*e.g.*, mono- or bidentate), bond lengths and coordination numbers cannot be derived from TRLFS measurements. Therefore, an EXAFS study of Am(III) sorbed onto clay mineral surfaces is carried out.

EXAFS study of the Am^{3+} aquo ion

The k^3 weighted fluorescence Am L_{III} edge EXAFS spectra and corresponding FT of the Am^{3+} aquo ion is shown in Fig. 4. A single oscillation in the EXAFS and one Am–O coordination shell in the FT is observed. The metrical parameters obtained in the two independent fits to the data are listed in Table 1. The R(Am–O) value obtained from the fits is 2.47–2.49 Å. This distance is in good agreement with the Am/O Am(III)/hydration shell bond length re-

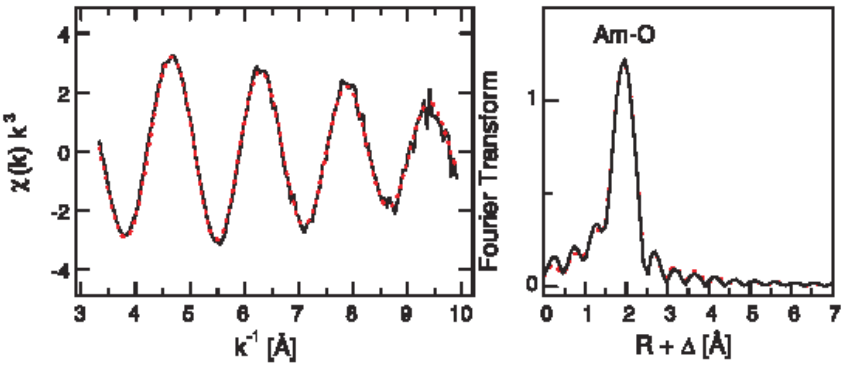

Fig. 4. L_{III}-edge k^3-weighted EXAFS spectra and corresponding Fourier transform for the Am^{3+} aquo ion (solid line – experiment; dotted line – theoretical fit result).

Table 1. Bond distances (R), coordination numbers (N), mean square displacements (σ^2), and relative shifts in ionization potential (ΔE_0) obtained from the two independent fits to the data for the Am(III) aquo ion and Am(III) sorbed onto smectite at pH 4, 6, 8 and onto kaolinite at pH 6 and 8. Results for k-space fits are listed first, those in R-space follow in italics. The standard deviations of the fit results are given in parentheses. The precision of the values determined is assumed to be that generally valid for EXFAS analysis: ±0.01–0.02 Å for relative R and absolute R determinations and ±10%–20% for corresponding N values.

Sample	R [Å]	N	σ^2 [Å^2]	ΔE_0 [eV]
Am(III) aquo	2.494(2)	9[a]	0.0058(3)	−1.8
	2.473(4)	*8.3(4)*	*0.0071(6)*	*−12.2(5)*
S/4	2.486(4)	8.4(5)	0.0047(6)	−2.1
	2.478(9)	*7.9(8)*	*0.006(1)*	*−11(1)*
S/6	2.480(5)	9.4(5)	0.0074(6)	−2.5
	2.474(7)	*8.5(6)*	*0.008(1)*	*−12(1)*
S/8	2.475(7)	7.8(7)	0.008(1)	−2.0
	2.466(9)	*7.2(6)*	*0.009(1)*	*−12(1)*
K/6	2.487(5)	9.7(6)	0.0077(7)	−2.0
	2.481(8)	*8.9(7)*	*0.009(1)*	*−11.4(9)*
K/8	2.479(6)	6.8(5)	0.0095(9)	−1.6
	2.470(2)	*6.2(9)*	*0.010(2)*	*−12(1)*

a: Held constant during the fit. See text for details of fit procedure.

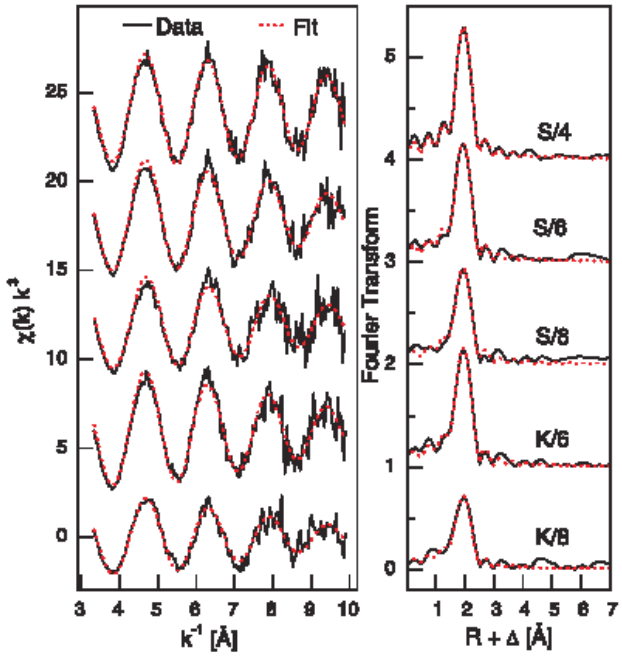

Fig. 5. L_{III}-edge k^3-weighted EXAFS spectra and corresponding FT's of Am(III) sorbed onto smectite (S) and kaolinite (K) at pH 4, 6 and 8. (Solid line – experiment; dotted line – theoretical fit results from fits to $\chi(k)$ as described in the text).

ported for Am^{3+} in 0.25 M HCl solution, 2.48 Å [17]. In the R-space fit, a value for N of 8.3, somewhat smaller than 9, is obtained. It appears tempting to interpret the determined $8 < N < 9$ as an indication of an equilibrium between octa and nonahydrated species, similar to that for the intermediate lanthanide aquo species between Gd(III) and Sm(III) [18]. This difference is, however, within the error of the EXAFS method and cannot be considered significant.

EXAFS study of Am(III) sorbed onto smectite and kaolinite

The Am L_{III} EXAFS spectra and their corresponding FT's for Am(III) sorbed onto smectite and kaolinite at different pH are shown in Fig. 5. In all FT spectra one peak dominates, which can be attributed to an average Am–O coordination shell composed of oxygen atoms from both water molecules and oxygen atoms binding the Am(III) cation to the clay mineral surface. This oxygen shell FT peak is visibly smaller for the S/8 and K/8 samples. No indication of any Am−Am distance, as a consequence of Am precipitation, is observed in any of the spectra. There are also no further distant FT peaks, which might be attributed to an Am−Al or Am−Si distance (Al and Si are $Z+1$ and cannot be distinguished by EXAFS). Observation of an Am−Al/Si peak would be direct evidence for the sorbate-substrate interaction. However, the backscattering amplitude of Al or Si is weak in comparison to, *e.g.*, the Am−Fe backscattering amplitude. A distinct Am-Fe distance is observed in the Am L_{III} EXAFS for Am(III) sorbed onto iron oxides [19]. With no evidence for an Am−Al/Si distance we are not able to distinguish between an outer-sphere and an inner-sphere complex nor can we identify monodentate or bidentate binding to the surface in the case of inner-sphere complexation of the Am(III) species onto the clay mineral. However, a monodentate ligated silanol or aluminol group would be expected to have a relatively long Am−Si/Al distance and

greater variability in the Am−O−Si/Al angle so that we do not anticipate a strong EXAFS oscillation to result from this configuration. For this reason, the lack of a FT peak or coordination shell further distant than the oxygen shell in sorption samples is often interpreted as indicating the presence of a monodentate surface species [20].

The EXAFS parameters obtained by fitting the spectra of Am(III) sorbed onto the clay surfaces are also listed in Table 1. The R(Am−O) values determined for the Am/smectite sorption species generally contracts in the series S/4, S/6 to S/8 and going from K/6 to K/8. However, the contraction is less than the experimental error associated with the EXAFS method. The value of N obtained for the Am(III) sorbed clay samples prepared at pH 4 and pH 6 does not vary significantly. However, N obtained from fits for both the S/8 and K/8 samples is observed to be lower than that observed for the other samples, in accord with the smaller EXAFS amplitude exhibited by these samples.

TRLFS investigations of the sorption process of aqueous Cm(III) [3, 4] and Eu(III) [22, 23] onto smectite, kaolinite and γ-alumina at pH 6 show an increase of the fluorescence emission lifetime with increasing complexation of the mineral with metal ions. The observed increase in emission lifetime indicates a loss of approximately four water molecules in the first coordination sphere of the sorbed Cm(III) and Eu(III) cations. The analysis of the EXAFS spectra for samples S/6 and K/6 yields overall N values comparable to that for the Am(III) aquo species and for the Am(III)/clay outer-sphere complexes, 8–9. This indirectly indicates that the reduction of the metal ion hydration number by four, as indicated by TRLFS results, during the sorption process is not accompanied by a decrease in the overall coordination number of the trivalent actinide. Hence, the water molecules removed in the first coordination sphere of Am(III) upon sorption must be replaced by oxygen atoms from the mineral surface coordinating Am(III). Combining TRLFS and EXAFS results leads to the conclusion that Am(III) is bound to four oxygen atoms at the mineral surface and its remaining first coordination sphere is completed with approximately five water molecules.

EXAFS analysis suggests that samples K/8 and S/8 exhibit N significantly less than 9. This decrease in N in comparison to the other samples may not necessarily result from an actual decrease in the overall coordination number but rather result from the introduction of more asymmetry in the Am−O coordination sphere. A loss in EXAFS oscillatory intensity can be caused by destructive interferences of a number of oscillations having small differences in their frequencies, due to a variation in their bond distances. The length of an Am−OH bond is expected to be shorter than the Am−O distances associated with those of coordinated water molecules and the oxygen atoms of surface binding sites. By comparison to a reported hydroxyl An−O bond length for Np(VI) [24] and scaling to ionic radii [25], we expect R(Am−O) for a hydroxo ligand to be about 2.38 Å. Therefore, we suggest that the apparent decrease in N for Am(III) in the samples prepared at pH 8 might be an indication for the formation of a ternary OH^-/Am/clay surface species. In this species, the Am coordination sphere is expected to be highly asymmetric and a dampening of its EXAFS amplitude is expected. The observed increase in the mean square displacement of oxygen atoms σ^2 for the samples prepared at pH 8 in comparison to that for the pH 6 samples can also be considered as an indication of increased asymmetry in the Am(III) oxygen coordination sphere at the higher pH.

Conclusion

The structure parameters of the Am^{3+} aquo ion are analyzed using EXAFS (Am−O distance 2.47–2.49 Å; coordination number 8–9). TRLFS (Cm(III)) and EXAFS (Am(III)) combined measurements show that An(III)/smectite outer-sphere complexes are formed at pH 4. With increasing pH, inner-sphere sorption onto smectite and kaolinite occurs. Combining TRLFS and EXAFS results leads to the conclusion that at pH 6 An(III) is bound to four oxygen atoms at the mineral surface and its remaining first coordination sphere is completed with approximately five water molecules. The coordination number of sorbed Am(III) at pH 8 exhibits an apparent decrease, which may be affected by the formation of ternary OH^-/Am/clay mineral surface species.

Acknowledgment. We thank Harald Funke, Henry Moll, Tobias Reich, André Roßberg and Silvia Stumpf for their experimental assistance at the European Synchrotron Radiation Facility.

References

1. Taubald, H., Bauer, A., Schäfer, T., Geckeis, H., Satir, M., Kim, J. I.: Experimental investigation of the effect of high pH solutions on the Opalinus shale and the Hammerschmiede clay. Clay Minerals **35**, 515 (2000).
2. Strawn, D. G., Sparks, D. L.: The use of XAFS to distinguish between inner- and outer-sphere lead adsorption complexes on montmorillonite. J. Colloid Interface Sci. **216**, 257 (1999).
3. Stumpf, Th., Bauer, A., Coppin, F., Kim, J. I.: Time-resolved laser fluorescence spectroscopy (TRLFS) study of the sorption of Cm(III) onto smectite and kaolinite. Environ. Sci. Technol. **35**, 3691 (2001).
4. Stumpf, Th., Rabung, Th., Klenze, R., Geckeis, H., Kim, J. I.: A spectroscopic study of the Cm(III) sorption onto γ-Alumina. J. Colloid Interface Sci. **238**, 219 (2001).
5. Matz, W., Schell, N., Bernhard, G., Prokert, F., Reich, T., Claußner, J., Oehme, W., Schlenk, R., Dienel, S., Funke, H., Eichhorn, F., Betzl, M., Pröhl, D. Strauch, U., Hüttig, G., Krug, H., Neumann, W., Brendler, V., Reichel, P., Denecke, M. A., Nitsche, H.: ROBL – a CRG beamline for radiochemistry and materials research at the ESRF. J. Synchrotron Rad. **6**, 1076 (1999).
6. Ankudinov, A. L., Ravel, B., Rehr, J. J., Conradson, S. D.: Real-space multiplescattering calculation and interpretation of X-ray-absorption near-edge structure. Phys. Rev. B **58**, 7565 (1998).
7. George, G. N., Pickering, I. J.: *EXAFSPAK: A suite of computer programs for analysis of X-ray absorption spectra*. Stanford Synchrotron Radiation Laboratory, Stanford (1995).
8. Ankudinov, A. L., Ravel, B., Rehr, J. J., Conradson, S. D.: Real-space multiplescattering calculation and interpretation of X-ray-absorption near-edge structure. Phys. Rev. B **58**, 7565 (1998).
9. Newville, M., Livins, P., Yacoby, Y.,Rehr, J. J., Stern, E. A.: Near-edge X-ray-absorption fine-structure of Pb – a comparison of theorie and experiment. Phys. Rev. B **47**, 14 126 (1993).
10. Carnall, W. T., Crosswhite, H. M.: Optical Spectra and Electronic Structure of Actinide Ions in Compounds and Solutions. Report ANL (1995) p. 84.
11. Kimura, T., Choppin, G. R.: Luminescence study on determination of the hydration number of Cm(III). J. Alloys Compd. **213/214**, 313 (1994).

12. Wimmer, H., Klenze, R., Kim, J. I.: A study of hydrolysis reaction of curium(III) by time resolved laser fluorescence spectroscopy. Radiochim. Acta **56**, 79 (1992).
13. Fanghänel, T., Kim, J. I., Klenze, R., Kato, J.: Formation of Cm(III) chloride complexes in $CaCl_2$ solutions. J. Alloys Compd. **225**, 308 (1995).
14. Beitz, J. V., Hessler, J. P.: Oxidation state specific detection of transuranic ions in solution. Nucl. Technol. **51**, 169 (1980).
15. Beitz, J. V., Bowers, D. L., Doxtader, M. M., Maroni, V. A., Reed, D. T.: Detection and speciation of trans-uranium elements in synthetic groundwater *via* pulsed-laser excitation. Radiochim. Acta **44–45**, 87 (1988).
16. Fanghänel, Th.: unpublished work.
17. Allen, P. G., Bucher, J. J., Shuh, D. K., Edelstein, N. M., Craig, I.: Coordination chemistry of trivalent lanthanide and actinide ions in dilute and concentrated chloride solutions. Inorg. Chem. **39**, 595 (2000).
18. See, *e.g.*, Rizkalla, E. N., Choppin, G. R.: In: *Handbook on the Physics and Chemistry of Rare-Earths.* (Gschneider, K. A., Eyring, L., Choppin, G. R., Lander, G. H., eds.) Elsevier, North-Holland, Amsterdam (1994) Chapt. 18, p. 127.
19. Stumpf, S., Stumpf, Th., Fanghänel, Th.: in preparation.
20. See, *e.g.*, Dardenne, K., Schäfer, T., Denecke, M. A., Rothe, J., Kim, J. I.: Identification and characterization of sorbed lutetium species on 2-line ferrihydrite by sorption data modeling, TRLFS and EXAFS. Radiochim. Acta **89**, 469 (2001).
21. Yaita, T., Tachimori, S., Edelstein, N. M., Bucher, J. J., Rao, L., Shuh, D. K., Allen, P. G.: EXAFS studies of americium(III)–benzimidazole complex in ethanol. J. Synchrotron Rad. **8**, 663 (2001).
22. Stumpf, Th., Bauer, A., Coppin, F., Fanghänel, Th., Kim, J. I.: Inner-sphere, outer-sphere and ternary surface complexes: a TRLFS study of the sorption process of Eu(III) onto smectite and kaolinite. Radiochim. Acta **90**, 345 (2002).
23. Rabung, Th., Stumpf, Th., Geckeis, H., Klenze, R., Kim, J. I.: Sorption of Am(III) and Eu(III) onto gamma-alumina: experiment and modelling. Radiochim. Acta **88**, 711 (2000).
24. Denecke, M. A., Marquardt, C. M., Rothe, J., Dardenne, K., Jensen, M. P.: XAFS studies of actinide coordination structure in Np(IV)-fulvates. J. Nucl. Sci. Technol. **3**(Suppl.), 410 (2002).
25. Shannon, R. D., Prewitt, C. T.: Effective ionic radii in oxides and fluorides acta. Cryst. B **25**, 925 (1969).
26. Allen, P. G., Bucher, J. J., Shuh, D. K., Edelstein, N. M., Reich, T.: Investigation of aquo and chloro complexes of UO_2^{2+}, NpO_2^{+}, Np^{4+}, and Pu^{3+} by X-ray absorption fine structure spectroscopy. Inorg. Chem. **36**, 4682 (1997).
27. Moll, H., Reich, T., Szabó, Z.: Solution coordination chemistry of uranium in the binary UO_2^{2+}-SO_4^{2-} and the ternary UO_2^{2+}-SO_4^{2-}-OH^- system. Radiochim. Acta **88**, 411 (2000).

Radiochim. Acta **90**, 345–349 (2002)
© by Oldenbourg Wissenschaftsverlag, München

Inner-sphere, outer-sphere and ternary surface complexes: a TRLFS study of the sorption process of Eu(III) onto smectite and kaolinite

By Th. Stumpf[1,*], A. Bauer[2], F. Coppin[3], Th. Fanghänel[1] and J. I. Kim[2]

[1] Forschungszentrum Rossendorf, Institut für Radiochemie, P.O. Box 510119, D-01314 Dresden, Germany
[2] Forschungszentrum Karlsruhe, Institut für Nukleare Entsorgung, P.O. Box 3640, D-76021 Karlsruhe, Germany
[3] Univ. Paul Sabatier, UMR 5563 – LMTG, 38 rue des 36-Ponts, F-31400 Toulouse, France

(Received November 21, 2001; accepted in revised form January 16, 2002)

Europium / TRLFS / Clay minerals / Surface complexation / Ternary complexes

Summary. The surface sorption process of Eu(III) onto smectite and kaolinite was investigated by time-resolved laser fluorescence spectroscopy (TRLFS) in the trace concentration range. The experiments were performed in 0.025 M and 0.45 M $NaClO_4$. The sorption process of Eu(III) onto smectite was obtained by TRLFS under atmospheric conditions and in absence of CO_2. The pH was varied between 3.5 and 9 at a fixed metal ion concentration of 3.3×10^{-6} mol/L Eu(III). At low pH (< 4) the metal ion keeps its complete hydration sphere indicating outer-sphere complexation. With increasing pH the formation of an inner-sphere Eu(III) surface complex was observed. The differences in the spectra and the fluorescence emission lifetimes of the surface sorbed Eu(III) in presence and absence of carbonate indicate the formation of ternary clay/Eu(III)/carbonate complexes. The different europium/clay surface complexes were characterized by their fluorescence emission spectra ($^5D_0 \rightarrow {}^7F_1 / {}^5D_0 \rightarrow {}^7F_2$ intensity ratio) and their fluorescence emission lifetime.

Introduction

Clay minerals are known to be highly efficient in radionuclide retention in natural water systems. They are proposed as backfill in future nuclear waste repositories. Prediction of the retention mechanisms of radionuclides is a fundamental concern in evaluating the suitability of proposed sites for the geologic disposal of nuclear waste. In our study, europium (Eu(III)) is used as a chemical anaologue for trivalent actinides (*e.g.*, Am(III) and Cm(III)).

As clay minerals have a complex surface structure, they show complicated sorption characteristics especially at low ionic strength [1]. An application of surface complexation models (SCM) for clays is less successful than for oxides or hydroxides. Therefore spectroscopic information is needed to identify the sorption mechanisms, including the structure of the species involved in the sorption process and to validate the applicability of SCM.

Kaolinite is a 1 : 1 layer type clay mineral in which each Si-, Al-OH, (O) component exists in two distinct structural environments at the surface. There is only minimal substitution of cations with variable valence in the structure and hence only minor permanent structural charge. In contrast to kaolinite, each aluminium octahedral layer in smectite is bound to two silica rich tetrahedral layers. Smectite is an expandable 2:1 layer type clay mineral that has both interlayer sites and ionizable hydroxide sites on its external surface available for the metal cation sorption. Substitution of Mg^{2+} and Fe^{2+} atoms by Al^{3+} in the octahedral layer creates a positive charge deficit giving the overall structure a net negative charge. The O and OH atoms at the edges of kaolinite and smectite, or at the gibbsite basal plane of kaolinite, have Lewis base or Lewis acid functional groups which are the source of the pH dependent charge [2]. Binding to these sites on the external surface maybe looked upon as a complexation reaction similar to that occurring at the oxide mineral surface.

The aim of the **t**ime-**r**esolved **l**aser **f**luorescence **s**pectroscopy (**TRLFS**) study was to investigate the sorption mechanism of Eu(III) on kaolinite and smectite and to study the influence of CO_2 on the sorption mechanism. For this purpose, the speciation of surface sorbed Eu(III) ions was studied by TRLFS in the micromolar concentration range as a function of pH and at different ionic strengths.

The position of the europium fluorescence emission bands is almost independent of the chemical environment of the metal ion. Only the intensity of the $^5D_0 \rightarrow {}^7F_2$ transition changes significantly when Eu(III) is sorbed. This is a consequence of the so-called "hypersensitive effect" which is described elsewhere [3–5]. The ratio of the emission intensity obtained for the $^5D_0 \rightarrow {}^7F_1$ ($\lambda = 594$ nm) and $^5D_0 \rightarrow {}^7F_2$ ($\lambda = 619$ nm) transitions together with the lifetime of the fluorescence emission provide information on the europium(III) speciation [6, 7]. The high fluorescence sensitivity of europium makes it possible to study the complexation process of Eu(III) on kaolinite and smectite as a model ion for the surface sorption behaviour of trivalent actinides.

Experimental

Starting materials

Well crystallized, fine grained kaolinite [$Al_2Si_{1.99}Ca_{0.0025}K_{0.0016}O_5(OH)_4$] ($\leq 2$ µm) from St. Austell (UK) was used.

*Author for correspondence (E-mail: T.stumpf@fz-rossendorf.de).

The smectite $[(Si_{7.98}Al_{0.02})^{IV}(Al_{3.11}Fe_{0.3}{}^{3+}Fe_{0.04}{}^{2+}Mg_{0.5})^{IV}O_{22}(Na_{0.45}{}^{+}K_{0.01}{}^{+}Ca_{0.1}{}^{2+})]$ used was < 0.1 µm fraction of the Ceca bentonite separated by sedimentation technique. The cation exchange capacity (CEC) of the initial and the reacted products was determined according to Meier and Kahr [8] and was found to be 3.7 meq/100 g for kaolinite and 75 meq/100 g for smectite. A detailed description of the clay samples is given elsewhere [9].

Experimental set-up

Batch experiments were performed at 25 °C in 20 ml polypropylene bottles in the pH range from 2 to 9 under atmospheric conditions. Another set of batch samples was prepared in a glove box under N_2 atmosphere. To avoid carbonate complexation of the metal ion CO_2 free water and NaOH solution was used. The europium stock solution we used was a ICP/DCP standard solution (Alfa) containing 1 ppm of Eu. The Eu(III) concentration was fixed to 3.3×10^{-6} mol/L in all TRLFS experiments. As background electrolyte we used $NaClO_4$ solutions ($I = 0.025$ mol/L & 0.45 mol/L). Clay samples (S:L 0.25 g/L) were equilibrated at pH 6.7 for one week in the dark. Kinetic tests were performed during a period between 1 and 30 days at different Eu(III) trace concentrations as a function of pH. No kinetic effects were observed, *i.e.*, a equilibrium was reached within 1 day [10]. Nevertheless batch samples were stored for at least two days and shaken periodically. The pH was adjusted by adding analytical grade NaOH or $HClO_4$.

After the reaction was completed the suspension was divided in two parts. In the first the solid was separated from solution by centrifugation (45 min at 4000 rot/min). The supernatant was diluted, partially acidified (2% HNO_3) and analysed by ICP-MS (Elan 6000). We evaluated the blank of the protocol by reacting clay minerals with background electrolytes during 3 days without any addition of REE. The second part was used for selected samples for time-resolved laser fluorescence spectroscopy (TRLFS) measurements. TRLFS measurements were performed by using a pulsed Nd:YAG pumped dye laser system (Continuum, Powerlite 9030, ND 6000) and by using a flash lamp pumped Ti:sapphire laser (Elight, Titania). Details on the experimental set-up are given elsewhere [11–16]. Laser pulse energy of at most 4 mJ was controlled by a photodiode. The fluorescence emission was detected by an optical multichannel analyzer, which allows simultaneous detection of the whole Eu(III) emission spectrum. One system consists of a polychromator (Chromex 250 is) with a 300 lines/mm grating the other detection system of a monochromator and spectrograph (Oriel; MS 257) with a 300 lines/mm grating and a ICCD camera (Andor). The emission spectra of Eu(III) were recorded in the 520–680 nm range, within a constant time window of 1 ms width, exciting at 396.6 nm (laser dye: Exalite 398) or at 395 nm respectively. For measuring the time dependent emission decay, the delay time between laser pulse and camera gating was scanned with time intervals of 10 µs.

Results and discussion

Sorption edge

The $\log K_D$ was obtained for Eu(III) as a function of pH for the two clay minerals at low ionic strength. We did not observe any significant difference between the two experiments conducted with or without dissolved CO_2 (glove box or atmospheric conditions). At low ionic strength the K_D values for kaolinite and smectite show a small pH dependence. However, the sorption pH dependence is more important for kaolinite than for smectite. In the case of kaolinite the sorption coefficient exhibits a linear increase with increasing pH over all the studied pH range. In case of smectite three different trends can be observed: between pH 2.39 and 5.89 the sorption of Eu(III) is weakly pH dependent, while above pH 6 it shows a slight decrease from 5.34 (pH 6) to 4.03 (pH 7.7) to increase again to 5.1 (pH 9.79).

In contrast to the results at high ionic strength the logarithm of sorption coefficients for smectite and kaolinite show an important pH dependence with a significant increase between pH 5.9 and 8.6. In this pH range the $\log K_D$ values increase from 2 to 5.8 for kaolinite and from 2.1 to 5.6 for smectite. Below pH 6 the sorption coefficients remain constant around 1.86 for kaolinite and evolve weakly as a function of pH for smectite from 1.5, (pH 2.7) to 2.6 (pH 5.76) with a majority of values around 2.

TRLFS measurements

Spectroscopic characterization of Eu(III) sorption species in presence of carbonate at low ionic strength

In Fig. 1 the fluorescence emission spectra of 3.3×10^{-6} mol/L Eu(III) in a 6.7×10^{-4} mol/L smectite suspension at an ionic strength of 0.025 mol/L at various pH are shown. With increasing pH the intensity of the peak corresponding to the $^5D_0 \rightarrow {}^7F_2$ transition increases. The $^7F_1/{}^7F_2$ ratio changes from 2.00 ± 0.03 at pH 3.50 (2.00 is measured for the europium aquo ion at pH 4) to 0.24 ± 0.03 at pH ≥ 7.11 (Table 1). The same evolution of the spectra was observed for 3.3×10^{-6} mol/L Eu(III) in a 9.7×10^{-4} mol/L kaolinite suspension. With increasing pH the intensity of the 619 nm peak increases and the $^7F_1/{}^7F_2$ ratio reaches the final value of 0.21 ± 0.03 at pH ≥ 7.02. It is remarkable that the spectra of the Eu(III) species sorbed onto smectite and kaolinite at pH 3.5 are the same as the spectra of the Eu(III) aquo ion although at this

Table 1. 3.3×10^{-6} mol/L Eu(III) in 6.7×10^{-4} mol/L smectite suspension under atmospheric conditions, $I = 0.025$ mol/L $NaClO_4$; Ratio between the transition peaks $^5D_0 \rightarrow {}^7F_1$ and $^5D_0 \rightarrow {}^7F_2$ at various pH.

pH	3.50	5.57	5.89	6.07	6.65	7.11	7.34	8.76
$^7F_1/{}^7F_2$ ratio	2.00	1.50	1.27	0.48	0.42	0.24	0.26	0.24

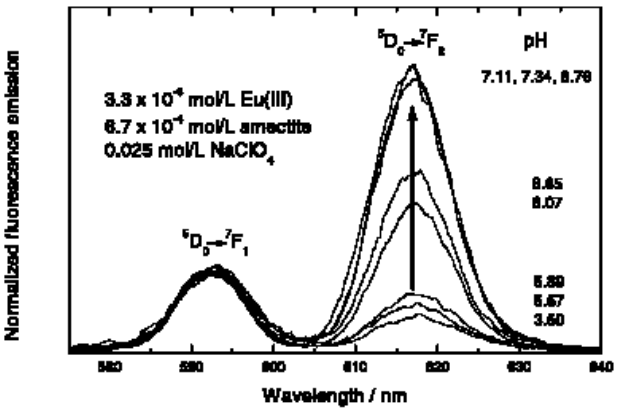

Fig. 1. Normalized fluorescence emission spectra of 3.3×10^{-6} mol/L Eu(III) in 6.7×10^{-4} mol/L smectite suspension at various pH, $I = 0.025$ mol/L $NaClO_4$.

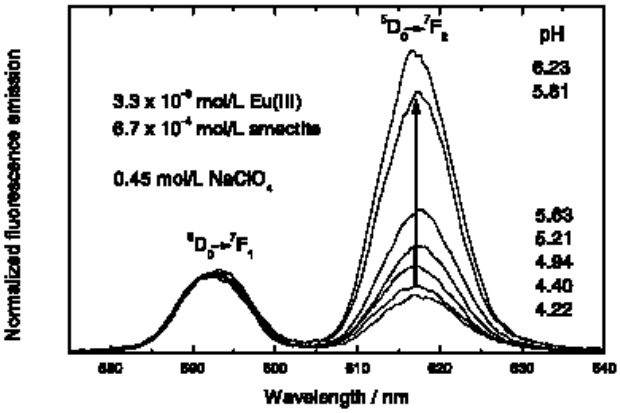

Fig. 3. Normalized fluorescence emission spectra of 3.3×10^{-6} mol/L Eu(III) in 6.7×10^{-4} mol/L smectite suspension at various pH, $I = 0.45$ mol/L $NaClO_4$.

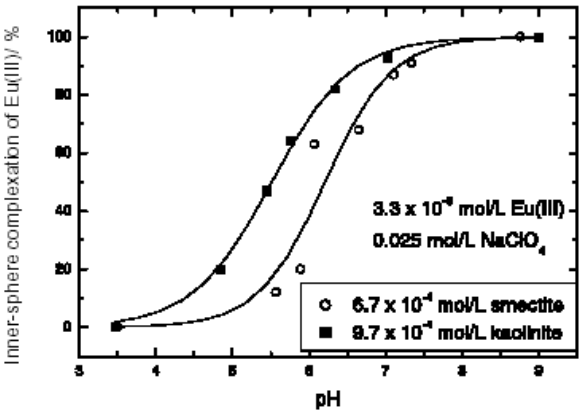

Fig. 2. pH edges as the result of peak deconvolution, illustrating inner-sphere complexation of 3.3×10^{-6} mol/L Eu(III) in 6.7×10^{-4} mol/L smectite suspension and in 9.7×10^{-4} mol/L kaolinite suspension.

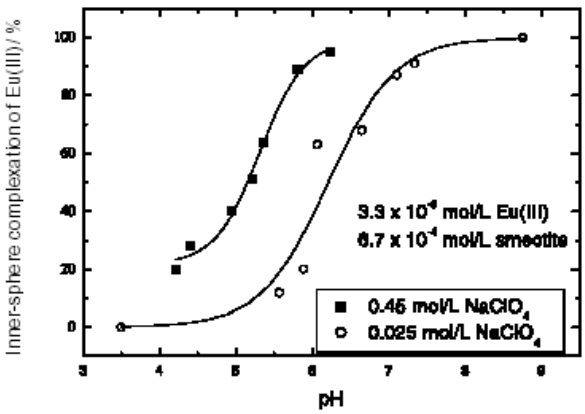

Fig. 4. pH edges as the result of peak deconvolution, illustrating inner-sphere complexation at different ionic strength ($I = 0.025$ mol/L $NaClO_4$ and $I = 0.45$ mol/L $NaClO_4$).

pH considerable amounts of the Eu(III) are sorbed according to the K_D values discussed before. In the case of smectite 95% of the Eu(III) is sorbed onto the mineral surface at pH 3.5 whereas in the case of kaolinite only 13% is sorbed at this pH value. These observations indicate that at low pH the sorbed Eu(III) ion is bonded as an outer-sphere complex.

The change of the (transition) ratio of the fluorescence emission of Eu(III) at higher pH (> 3.5) in the kaolinite and smectite suspensions is caused by a change in the ligand field of the europium ion and indicates inner-sphere complex formation. A peak deconvolution was carried out to quantify the inner-sphere sorption process. The spectrum of the Eu^{3+} aquo ion and the spectrum of Eu(III) in the smectite suspension at pH 8.76 ($^7F_1/^7F_2$ ratio 0.24 ± 0.03; 100% sorbed europium) were used as components in the deconvolution of all measured spectra. The results presented as pH-edges are illustrated in Fig. 2. Inner-sphere complex formation starts in the kaolinite suspension at lower pH than in the case of smectite.

Spectroscopic characterization of Eu(III) sorption species in presence of carbonate at high ionic strength

Variation of the ionic strength provides additional information on the sorption process. In Fig. 3 fluorescence emission spectra of 3.3×10^{-6} mol/L Eu(III) in a 6.7×10^{-4} mol/L smectite suspension at various pH at an ionic strength of 0.45 mol/L $NaClO_4$ are shown. The evolution of the emission spectra with increasing pH are very similar to the progress found for the sorption process at low ionic strength. With increasing pH the intensity of the peak with the maximum at 619 nm, that corresponds to the hypersensitive $^5D_0 \rightarrow {}^7F_2$ transition, increases. At the point where all Eu(III) is sorbed onto smectite the final value for the $^7F_1/^7F_2$ ratio is found to be 0.24 ± 0.3 again. But the sorption reaction at high ionic strength is shifted to lower pH values. Inner-sphere complex formation at an ionic strength of 0.45 mol/L $NaClO_4$ starts below pH 4.22 and is completed at pH 6.23. This is a difference of nearly one pH unit compared to the obtained sorption progress at low ionic strength. The influence of ionic strength on the sorption reaction is illustrated by pH-edges shown in Fig. 4.

Lifetime (fluorescence decay) of Eu(III) emission

Besides the ratio of the $^7F_1/^7F_2$ transitions the fluorescence emission lifetime contains information about the coordination sphere of Eu(III). The fluorescence decay behaviour of different europium species contains information about the kinetics of the complex formation reaction and about

the number of co-ordinated water molecules in the first co-ordination shell [17]. If the ligand exchange reaction rate is high compared to the fluorescence decay rate of the excited Eu(III) species, an average lifetime of the species and a mono-exponential decay is expected. If the ligand exchange rate is low in comparison to the fluorescence decay rate, a bi-exponential decay follows. The emission decay of Eu(III) in the clay suspensions between pH 4 and 7 is bi-exponential, indicating slow exchange of Eu^{3+} with surface bond Eu(III) species. Single component spectra with mono-exponential decay behaviour are found at pH < 4 corresponding to the Eu^{3+} aquo ion and at pH > 7 corresponding to the Eu(III) surface complex with fluorescence emission lifetimes of 110 ± 6 μs and 330 ± 20 μs. The rate of the fluorescence decay depends on radiative and non-radiative processes. Non-radiative decay is due mainly to energy transfer from the excited state to ligand vibrations, *e.g.* OH vibration of co-ordinated H_2O molecules. The experimental lifetime for the Eu^{3+} aquo ion is 110 ± 5 μs in water [15–19]. A linear correlation is observed between the decay rate and the number of H_2O molecules in the first co-ordination sphere of Eu(III), where a lifetime of 110 μs, corresponds to 9, and 1725 μs to zero H_2O molecules [17]. The increase in lifetime by increasing surface complexation reflect the stepwise exclusion of water molecules from the first co-ordination shell of Eu(III). According to the method developed by Horrocks [17] the number of water molecules in the first co-ordination shell decreases from a calculated value of 9 at pH < 4 to 2.6 ± 0.3 at pH > 7.

Spectroscopic characterization of Eu(III) sorption species in absence of carbonate

In Fig. 5 fluorescence emission spectra of 3.3×10^{-6} mol/L Eu(III) in carbonate free smectite suspension at an ionic strength of 0.025 mol/L $NaClO_4$ are shown. With increasing pH also the intensity of the peak corresponding to the $^5D_0 \rightarrow {}^7F_2$ transition increases. Aside from small differences in the peak form of the $^5D_0 \rightarrow {}^7F_1$ transition at pH ≥ 6.65 the peak evolution with pH looks similar to the spectra observed under natural conditions. But a closer look into the ${}^7F_1/{}^7F_2$ ratios (shown in Table 2) provides significant differences to values of the Eu(III) sorption in the presence of CO_2 (Table 1). For both systems a ratio of 2.0 is found at pH < 4 corresponding to the value of the Eu^{3+} aquo ion. The ratio evolution in the pH range from 4 to 6 is comparable. At pH ≥ 6.65 the ${}^7F_1/{}^7F_2$ ratios of the two systems differ. The increase in intensity of the ${}^7F_2$ transition is more pronounced in presence of carbonate than in absence. This observation indicates that different Eu(III) complexes are formed in the two systems. A further information that can be extracted from this data is that the change in the ligand field of the europium during the sorption process is

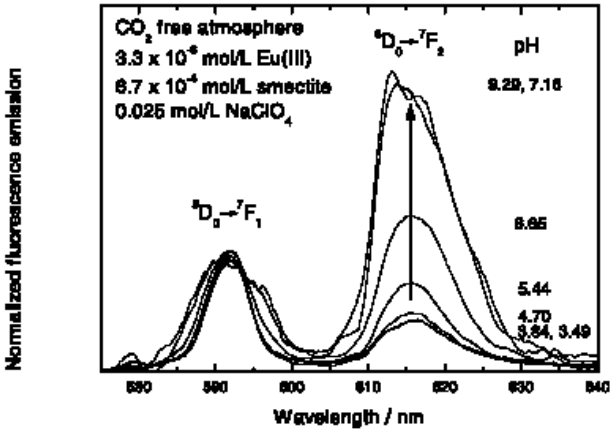

Fig. 5. Normalized fluorescence emission spectra of 3.3×10^{-6} mol/L Eu(III) in 6.7×10^{-4} mol/L smectite suspension at various pH in carbonate free atmosphere, $I = 0.025$ mol/L $NaClO_4$.

bigger in the presence of CO_2. From this we suggest that under natural conditions ternary surface/Eu(III)/carbonate complexes are formed. To validate the suggestion we compared the fluorescence emission lifetimes of sorbed europium species at pH 7.1 prepared under atmospheric conditions with that obtained in a carbonate free surrounding. The result is illustrated in Fig. 6. The fluorescence emission lifetime of sorbed Eu(III) under atmospheric conditions is determined to be 333 ± 20 μs corresponding to 2.6 ± 0.3 H_2O molecules in the first co-ordination shell of the lanthanide ion. For the lifetime of the surface sorbed Eu(III) species in a CO_2 free atmosphere 188 ± 20 μs is measured. Using the Horrocks correlation 5.1 ± 0.6 water molecules are calculated for the first co-ordination sphere

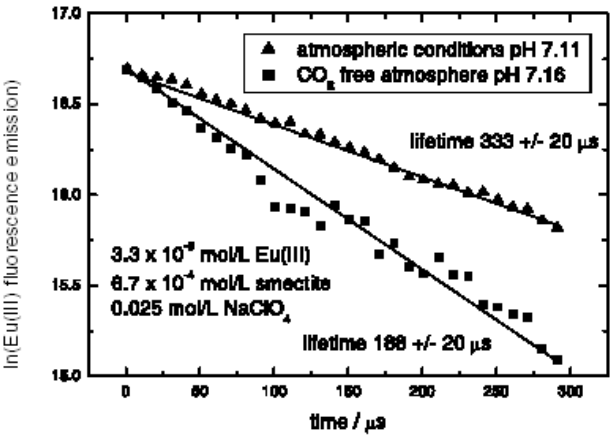

Fig. 6. Fluorescence emission lifetimes of 3.3×10^{-6} mol/L Eu(III) in 6.7×10^{-4} mol/L smectite suspension at pH 7.1 under atmospheric conditions and in carbonate free atmosphere, $I = 0.025$ mol/L $NaClO_4$.

Table 2. 3.3×10^{-6} mol/L Eu(III) in 6.7×10^{-4} mol/L smectite suspension in carbonate free atmosphere, $I = 0.025$ mol/L $NaClO_4$; Ratio between the transition peaks $^5D_0 \rightarrow {}^7F_1$ and $^5D_0 \rightarrow {}^7F_2$ at various pH.

pH	3.49	3.84	4.70	5.44	6.65	7.16	9.29
${}^7F_1/{}^7F_2$ ratio	2.01	2.00	1.67	1.27	0.74	0.63	0.59

of the sorbed Eu(III) species. This result is in good agreement with values found for Eu(III) and Cm(III) surface complexes with alumina and clays [19–21]. The explanation for a difference of 2–3 water molecules in the first coordination sphere of the sorbed europium in absence and presence of carbonate suggests the formation of ternary surface complexes. Under atmospheric conditions two to three water molecules are displaced from the first hydration sphere by carbonate molecules to form a clay/Eu(III)/carbonate species.

Conclusions

The results obtained give a description of the sorption process of Eu(III) onto kaolinite and smectite in the trace concentration range as a function of pH and of different ionic strengths. The results of sorption edges combined with TRLFS studies indicate the formation of outer-sphere and inner-sphere surface complexation of Eu(III) by smectite and kaolinite. The stability of ternary clay/Eu(III)/carbonate complexes was demonstrated by the emission spectra and the fluorescence emission lifetime of surface sorbed europium in presence and absence of CO_2. Because of the similarity of Eu(III) with trivalent actinides the results should be applicable to the sorption process of those radionuclides.

References

1. Bayens, B., Bradbury, M. H.: A mechanistic description of Ni and Zn sorption on Na-montmorillonite. Part I: Titration and sorption measurements. J. Contam. Hydrol. **27**, 199 (1997).
2. Strawn, D. G., Sparks, D. L.: The use of XAFS to distinguish between inner- and outer-sphere lead adsorption complexes on montmorillonite. J. Colloid Interface Sci. **216**, 257 (1999).
3. Carnall, W. T., Goodman, G. L., Rajnak, K., Rana, R. S.: A systematic analysis of the spectra of the lanthanides doped into single crystal LaF_3. Report ANL-88-8, Argonne National Laboratory, Argonne (1988).
4. Carnall, W. T.: The absorption and fluorescence spectra of rare earth ions in solution. *Handbook on the Physics and Chemistry of Rare Earth*. North Holland Publishing, Amsterdam (1976).
5. Jörgensen, C. K., Judd, B. R.: Hypersensitive pseudoquadrupole transitions in lanthanides. Mol. Phys. **8**, 281 (1964).
6. Dobbs, J. C., Susetyo, W., Knight, F. E., Castles, M. A., Carreira, L. A., Azarraga, L. V.: Characterization of metal binding sites in fulvic acids by lanthanide ion probe spectroscopy. Anal. Chem. **61**, 483 (1989).
7. Richardson, F. S.: Terbium(III) and europium(III) ions as luminescent probes and stains for biomolecular systems. Chem. Rev. **82**, 541 (1982).
8. Meier, L., Kahr, G.: Determination of the cation exchange capacity (CEC) of clay minerals using the complexes of copper (II) ion with triethylenetetramine and tetraethylenepentamine. Clays Clay Miner. **47**, 386 (1999).
9. Bauer, A., Berger, G.: Kaolinite and smecite dissolution rate in high molar KOH solutions at 35 and 80 °C. Appl. Geochem. **13**, 905 (1998).
10. Coppin, F., Berger, G., Bauer, A., Castet, S., Loubet, M.: Sorption of lanthanides on smectite and kaolinite. Chem. Geol. **182**, 57 (2002).
11. Klenze, R., Kim, J. I., Wimmer, H.: Speciation of aquatic actinide ions by pulsed laser spectroscopy. Radiochim. Acta **52/53**, 97 (1991).
12. Wimmer, H., Klenze, R., Kim, J. I.: A study of hydrolysis reaction of curium(III) by time resolved laser fluorescence spectroscopy. Radiochim. Acta **56**, 79 (1992).
13. Fanghänel, T., Kim, J. I., Pavie, P., Klenze, R., Hauser, W.: Thermodynamics of radioactive trace elements in concentrated electrolyte solutions: hydrolysis of Cm(III) in NaCl-solutions. Radiochim. Acta **66/67**, 81 (1994).
14. Fanghänel, T., Kim, J. I., Klenze, R., Kato, J.: Formation of Cm(III) chloride complexes in $CaCl_2$ solutions. J. Alloys Compd. **225**, 308 (1995).
15. Paviet, P., Fanghänel, T., Klenze, R., Kim, J. I.: Thermodynamics of Cm(III) in concentrated electrolyte solutions: formation of sulfate complexes in $NaCl/Na_2SO_4$ solutions. Radiochim. Acta **74**, 99 (1996).
16. Fanghänel, T., Weger, H. T., Schubert, G., Kim, J. I.: Bicarbonate complexes of trivalent actinides – stable or unstable? Radiochim. Acta **82**, 55 (1998).
17. Horrocks, W. DeW., Sudnick, D. R.: Lanthanide ion probes of structure in biology. Laser induced luminescence decay constants provide a direct measure of the number of metal-coordinated water molecules. J. Am. Chem. Soc. **101**, 334 (1979).
18. Takahashi, Y., Kimura, T., Kato, Y., Minai, Y., Tominaga, T.: Characterization of Eu(III) species sorbed on silica and montmorillonite by laser-induced fluorescence spectroscopy. Radiochim. Acta **82**, 227 (1998).
19. Rabung, Th., Stumpf, Th., Geckeis, H., Klenze, R., Kim, J. I.: Sorption of Am(III) and Eu(III) onto γ-alumina: experimental results and modelling. Radiochim. Acta **88**, 711 (2000).
20. Stumpf, Th., Rabung, Th., Klenze, R., Geckeis, H., Kim, J. I.: A spectroscopic study of the Cm(III) sorption onto γ-alumina. J. Colloid Interface Sci. **238**, 219 (2001).
21. Stumpf, Th., Bauer, A., Coppin, F., Kim, J. I.: Time-resolved laser fluorescence spectroscopy (TRLFS) study of the sorption of Cm(III) onto smectite and kaolinite. Environ. Sci. Technol. **35**, 3691 (2001).

Environ. Sci. Technol. 2006, 40, 3522–3528

Sorption of Am(III) onto 6-Line-Ferrihydrite and Its Alteration Products: Investigations by EXAFS

SILVIA STUMPF,*,† THORSTEN STUMPF,§ KATHY DARDENNE,‡ CHRISTOPH HENNIG,∥,⊥ HARALD FOERSTENDORF,∥ REINHARDT KLENZE,‡ AND THOMAS FANGHÄNEL‡,§

Institut de Recherches Subatomiques, 23 Rue du Loess, P.O. Box 28, 67037 Strasbourg, France, Forschungszentrum Karlsruhe, Institut für Nukleare Entsorgung, P.O. Box 3640 76021 Karlsruhe, Germany, Physikalisch-Chemisches Institut, Ruprecht-Karls-Universität Heidelberg, Im Neuenheimer Feld 253, 69120 Heidelberg, Germany, Forschungszentrum Rossendorf, Institut für Radiochemie, P.O. Box 510119, D-01314 Dresden, Germany, and ROBL-CRG, European Synchrotron Radiation Facility, BP 220, F-38043, Grenoble, France

For the long-term performance assessment of nuclear waste repositories, knowledge about the interactions of actinide ions with mineral surfaces such as iron oxides is imperative. The mobility of released radionuclides is strongly dependent on the sorption/desorption processes at these surfaces and on their incorporation into the mineral structure. In this study the interaction of Am(III) with 6-line-ferrihydrite (6LFh) was investigated by EXAFS spectroscopy. At low pH values (pH 5.5), as well at higher pH values (pH 8.0), Am(III) sorbs as a bidentate corner-sharing species onto the surface. Investigations of the interaction of Am(III) with Fh coated silica colloids prove the sorption onto the iron coating and not onto the silica substrate. Hence, the presence of Fh, even as sediment coating, is the dominant sorption surface. Upon heating, Fh is transformed into goethite and hematite as shown by TEM and IR measurements. The results of the fit to the EXAFS data indicate the release of sorbed Am(III) at pH 5.5 during the transformation and likely a partial incorporation of Am into the Fh transformation products at pH 8.0.

Introduction

Iron oxides occur as corrosion products and naturally as sediment coatings or colloids (*1*). Due to its high specific area (200–800 m^2/g) (*2*, *3*) and strong interaction with metal ions, very small amounts of the amorphous 6-line-ferrihydrite (6LFh) have a strong influence on the migration behavior of metal ions. This property of Fh combined with its omnipresence implies that this amorphous metastable iron phase may play an important role in the retardation of radionuclides, in particular actinides, in the near-field as well as in the far-field of a nuclear waste repository.

* Corresponding author e-mail: silvia.stumpf@ires.in2p3.fr.
† Institut de Recherches Subatomiques.
‡ Institut für Nukleare Entsorgung.
§ Ruprecht-Karls-Universität Heidelberg.
∥ Institut für Radiochemie.
⊥ European Synchrotron Radiation Facility.

EXAFS investigations of Cu, Pb, and Zn sorption onto Fh show the formation of bidentate inner-sphere complexes at the mineral surface (*4*, *5*). For the sorption of Lu onto Fh, the formation of mono- and bidentate surface complexes depending on pH is observed (*6*). Fh is a metastable phase and converts to crystalline goethite and/or hematite. The relative proportion of both crystalline phases depends on the experimental conditions such as pH value, temperature, or concentration of metal ions (*7*) during the Fh transformation. To accelerate the alteration under laboratory conditions the temperature is increased to 85 °C. A pH decrease during the transformation process is reported in the literature (*8*). Moreover the transformation of the Fh phase affects the sorption behavior of various metal ions. Whereas Cu, Mn, and Ni are strongly bound to the surface, Pb and Cd are released during the transformation process (*9*, *10*). Al is incorporated into the crystal lattice (*11*). The incorporation of the trivalent lanthanide Lu into a hematite-like structure lattice during the Fh transformation is reported in the literature (*12*).

This study aims to understand and determine the importance of Fh as a sorbent in the near-field as well as in the far-field of a nuclear waste repository. The influence of the Fh transformation on the speciation of the adsorbed Am(III) is studied at different pH values using XAS spectroscopy.

Experimental Section

1. Method. Americium L_3 edge EXAFS spectra were recorded at the European Synchrotron Radiation Facility (ESRF, France), operating at 6 GeV with a maximum current of 200 mA, at the Rossendorf beamline (ROBL) (*13*). The double-crystal monochromator was equipped with a pair of Si(111) crystals. Two Pt coated mirrors were used to reject higher harmonics. The radioactive samples were sealed with polyethylene foils and put into lead containers with windows for the probe beam and fluorescence signal. All measurements were performed at room temperature. The samples were measured in fluorescence mode using a four-pixel Ge detector with a sample orientation of 45° to the incident beam.

The Am L_3 edge EXAFS spectra of the Am(III) aquo species reference were recorded at the Angströmquelle Karlsruhe (ANKA, Forschungszentrum Karlsruhe, Germany) operating at 2.5 GeV with a maximum of current of 180 mA. The spectra were recorded at the INE-Beamline for actinide research (*14*) using a pair of Ge(422) crystals ($2d$ = 3.412 Å) in the Lemonnier-type double crystal monochromator (DCM). The INE-Beamline was equipped with a collimating first and a focusing second mirror and the beam spot used was 5 × 1 mm^2. Higher harmonic radiation in the incident beam was suppressed by detuning the parallel alignment of the DCM crystals to 65% of photon flux peak intensity. Fluorescence spectra were recorded using a 5-pixel energy-dispersive solid-state Ge detector (Canberra LEGe).

The energy was calibrated by assigning the first inflection point at the K-edge absorption spectrum of a Zr metal foil to 17 998 eV (*15*). The data were analyzed by using standard procedures (*16*) and software packages. The EXAFSPAK program (*17*) was used to fit the data for the sorption of Am(III) onto iron coated colloids using a k range of 3.3–9.0 $Å^{-1}$.

The data of Am(III) aquo species, Am(III) sorption onto 6LFh, and its transformation under tempering experiment were analyzed using WINXAS97 (*18*) for extracting $\chi(k)$ from the absorption spectrum and the FEFFIT program of the UWXAFS (*19*) package for the fit. Fit to the data was carried

10.1021/es052518e CCC: $33.50 © 2006 American Chemical Society
Published on Web 04/29/2006

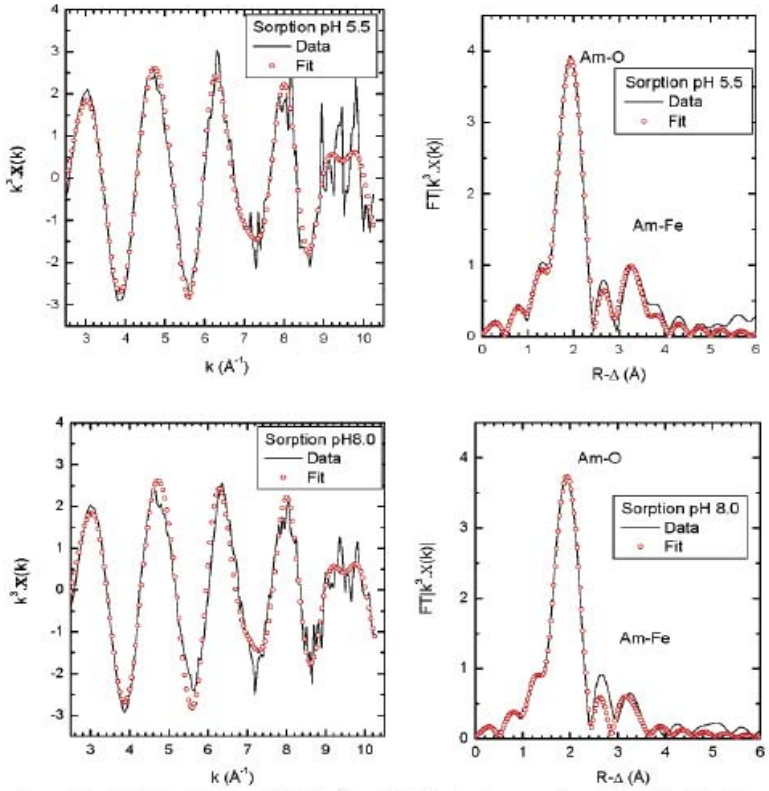

FIGURE 1. Am sorption onto ferrihydrite at pH 5.5 and 8.0. Left: k^3-weighted Am L_3 edge experimental EXAFS and back transformed *R*-space fit results. Right: corresponding Fourier transformed spectra. Experimental data are lines and fit data are circles.

out in the *R* space (1.5−4.0 Å). The *k*-space range was set from 2.7 to 10.3 $Å^{-1}$. Theoretical backscattering amplitude and phase functions for fitting the experimental data were calculated with the FEFF8 (*20*) code. Single scattering FEFF files are used for the fit. The overall scaling factor, S_0^2, was held constant at 1. Distances and coordination number are determined with EXAFS within typical errors of ±0.02 Å on the distance and ± 10−20% on coordination numbers.

2. Materials. *2.1. 6-line-Ferrihydrite (6LFh).* A dispersion of Fh was freshly prepared according to Schwertmann and Cornell (*21*). All chemicals were of analytical grade. The product was dialyzed (Spectra Por Membrane, 4, MWCO: 12−14.000) in a Milli-Q water bath for 3 days in the dark. The bath water was periodically changed. The resulting Fh stock solution had a concentration of approximately 1.5 g/L. Fh was characterized by powder X-ray diffraction (XRD), infrared spectroscopy (IR), surface area determination (BET), and transmission electron microscopy (TEM).

The XRD patterns of powder samples were recorded using a Seifert 3000TT diffractometer with Cu Kα radiation. The pattern of 6LFh shows characteristic peaks at 0.15, 0.17, 0.2, 0.22−0.23, and 0.25 nm as described in the literature (*21*, *22*).

The IR analysis on KBr pellets using a Perkin-Elmer Spectrum 2000 shows characteristic absorption bands at 450 and 650 cm^{-1} (bulk OH deformations), 1620 cm^{-1} (molecular water), and 3440 cm^{-1} (bulk OH stretch). The product contains a trace of nitrate (absorption band at 1380 cm^{-1}).

Specific surface area measurements were performed by the BET method using N_2 absorption (Quantochrome Autosorb) (*23*). The surface area obtained after drying the samples was approx. 235 m^2/g, which is in good agreement with published values (*24*).

The TEM images were recorded at a Philips CM300 SuperTWIN. EDAX SuperUTW samples were prepared by placing a droplet of the ferrihydrite stock solution on a holey-carbon film supported by a copper-mesh TEM grid. The electron microscope shows isometric particles 6 nm in size, which is in agreement with the literature (*22*).

2.2. Preparation of Coated Colloids. A solution of 6LFh was freshly prepared in the presence of silica particles 450 nm in diameter (Silica Microspheres; 5.6% silica suspension; Polysciences Europe GmbH) using 100 μL of the silica suspension added to 10 mL of a 15 mg/L Fe$(NO_3)_3$ solution. The mixture was then hydrolyzed and the resulting dispersion was centrifuged three times at 1700*g* for 10 min. The supernatant solutions were discarded and the particles were then re-suspended in Milli-Q water. The coated colloids were characterized by using TEM and EDX analysis. The TEM samples images show silica particles coated with a thin film of particles each 6 nm in size identified as Fh. This was confirmed by the presence of the Fe K lines (Kα Fe 6.4 keV; Kβ Fe 7.06 keV) in the EDX spectrum.

2.3. Preparation of EXAFS Samples. The long-lived americium isotope Am-243 ($t_{1/2}$ = 7370 years) was provided by

TABLE 1. EXAFS Parameter Resulting from the Fit of the EXAFS Data of the Sorption of Am(III) onto Ferrihydrite at pH 5.5 and pH 8.0 Before and After Transformation as Well as for an Aquo Species (Reference)

sample	shell	R [Å][a]	N	σ^2 [Å^2][b]	ΔE_0 [eV][d,e]
Am aquo species	Am−O	2.477(3)	7.4	0.0069	−2.15
Am/Ferrihydrite pH 5.5	Am−O	2.480(5)	6.3	0.0084	−2.73[d]
	Am−Fe	3.70(2)	1.0[c]	0.0046	5.47[e]
Am/Ferrihydrite pH 8.0	Am−O	2.478(3)	6.1	0.0086	−2.73[d]
	Am−Fe	3.69(2)	1.0[c]	0.0112	5.47[e]
Am/Goethite pH 5.5 after Fh transformation	Am−O	2.478(3)	7.2	0.0079	−2.73[d]
	Am−Fe	3.75(3)	0.3	0.0020[f]	5.47[e]
Am/Goethite pH 8.0 after Fh transformation	Am−O	2.466(4)	4.1	0.0081	−2.73[d]
	Am−Fe	3.59(1)	4.4	0.0200[f]	2.28
	Am−Fe	3.32(1)	1.4	0.0108	2.28

[a] Standard deviation from the fit in parentheses. [b] Debye−Waller factor. [c] Fixed value (when allowed to vary, N values of 1.0 ± 0.2 are obtained). [d] Same for all four samples. [e] Same for all three samples. [f] Constrained value.

the Oak Ridge National Laboratory. The isotopic composition of the Am oxide dissolved in 1.0 M $DClO_4$ was 99.987% Am-243, <0.001% Am-242, and 0.012% Am-241. The EXAFS samples at pH 5.5 and 8.0 were prepared in a glovebox under a nitrogen atmosphere at 25 ± 1 °C. $NaClO_4$ (35 mg) and 50 μL of a 2×10^{-2} mol/L $Am(ClO_4)_3$ stock solution were added to 10 mL of 6LFh and coated colloid stock solution. The pH was slowly adjusted over one week from 3.5 to the final values of 5.5 and 8.0, respectively. The samples were centrifuged 2 h at 500g. The supernatant was discarded and pastes with final concentrations of 0.025 mol/L $NaClO_4$ and 10^{-3} mol/L Am(III) were transferred into 1 mL vials. For the Am(III) aquo species reference, a 4×10^{-3} mol/L Am(III) in 0.05 M $HClO_4$ was used. For further characterization, additional samples with Eu(III) as a non-radioactive Am(III) analogue were prepared in an identical manner.

2.3. Transformation. Am(III) and Eu(III) samples were heated for 67 days at 85 °C using a water bath. Aliquots of the Eu(III) sample were taken before and after 16, 51, and 67 days of transformation (*7*, *25*, *26*) for IR characterization. The IR spectra were recorded with a resolution of 4 cm^{-1} using a Perkin-Elmer Spectrum 2000 (GX Series) by accumulating 32 scans. The detector was a DTGS. TEM images were recorded after heating for 67 days.

Results and Discussion

Sorption of Am(III) onto 6-L-Ferrihydrite at pH 5.5 and 8.0. From the literature it is known that Lu(III), which can be regarded as Am(III) homologue, sorbs onto Fh already at pH 4.3 with a very low ratio of approx. 20%. This ratio increases with the pH and yields values over 80% for pH values over 5.5. To get a quantitative sorption but avoid hydrolysis of the sorbed species we chose for the first sample in this study a pH of 5.5. Additionally the sorption at pH 8.0 was investigated.

Figure 1 shows the EXAFS and Fourier transformed (FT) spectra of Am(III) sorbed onto ferrihydrite at pH 5.5 and 8.0. The fit to the EXAFS data is simultaneously done for all 4 samples before and after transformation (Table 1). All four samples exhibit a FT peak at ~3.2 Å. Although the intensity of this peak is small, its presence corresponds to the perturbation of the main oscillation frequency in the EXAFS spectra at around 7.0 and 9.5 $Å^{-1}$. The coordination number, N, interatomic distance, R, and EXAFS Debye−Waller factor, σ^2, obtained from the fits are listed in Table 1. The fit to the

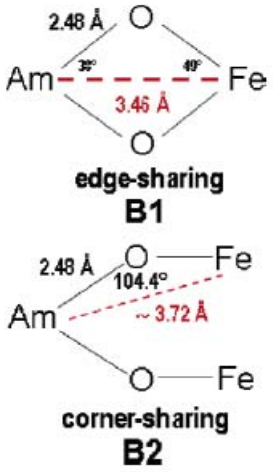

FIGURE 2. Models of the bidentate bonding of Am(III) onto the ferrihydrite surface.

EXAFS data yields an Am−O distance of 2.48 ± 0.02 Å at both pH values. It is not possible to distinguish between the Am−O distances from the hydration sphere and the Am−O originating from interactions of Am and oxygen atoms at the surface. The found Am−O distance of 2.48 Å at both pH values is an average distance composed of the surface Am−O contribution and the contribution of the hydration sphere Am−OH_2. It corresponds to the Am−O distance from the Am^{3+} aquo ion with a hydration sphere of 9 H_2O molecules (*27*, *28*). Using the same fit conditions, the fit to the Am^{3+} aquo species data yields 7.4 oxygen atoms (Table 1). The error in determining coordination numbers by the use of EXAFS spectroscopy is in general about 10−20%. A reduction of the O-coordination from 7.4 to 6.3 is nevertheless significant as we compare samples within a series, fit with the same conditions. The variation of N from 6.3 to 6.1 for the samples at pH 5.5 and pH 8.0 is not significant. The peak intensity of the Am−Fe interaction at pH 8.0 is decreased compared to the interaction at pH 5.5. The apparent difference of the Am−Fe interaction can be explained by the larger value of the Debye−Waller factor σ^2 for the sample at pH 8.0 compared to the sample at pH 5.5. The mean Am−Fe distance of 3.69 ± 0.02 Å found in the fits is the same for both sorption samples.

To interpret the results for the Am−Fe parameters listed in Table 1 a discussion of the possible Am−Fe interactions is required. Possible binding sites for Am(III) onto an FeO_6-octahedron located on the 6LFh surface are a monodentate species (**M**) and two possible bidendate species (bidentate edge-sharing **B1** and bidentate geminal corner-sharing **B2**). The latter are presented schematically in Figure 2. The expected Am−Fe distances for the different binding modes are also partially indicated in Figure 2. They are based on the proposed structure for 6LFh (*22*) (Fe−O approx. 2.12 Å and O−O distances of 3.0 Å for **B1**; 3.0 Å and 4.7 Å for **B2**) and the Am−O bond length from our EXAFS analysis. Based on this model the **B1** species is expected to have Am−Fe distances of around 3.46 Å while species **B2** is expected to have Am−Fe distances near 3.72 Å for a geminal site with O−O of 4.7 Å (∠ Fe−O−Am: 104.4°). Relatively long Am−Fe distances in the 3.77−4.6 Å range, depending on binding angle (∠ Fe−O−Am), are expected for **M**. The interpretation of Am(III) sorbed onto 6LFh EXAFS fit rules out the possibility of a monodentate sorption species **M** because the observed

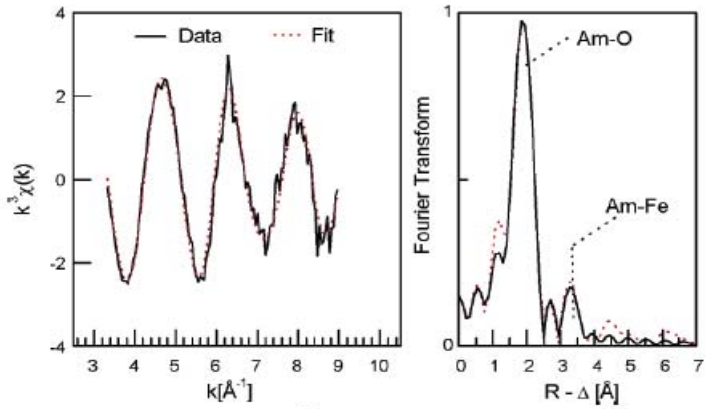

FIGURE 3. Am sorption onto coated colloids at pH 8.0. Left: k^3-weighted Am L_3 edge experimental EXAFS and back transformed R-space fit results. Right: corresponding Fourier transformed spectra.

TABLE 2. EXAFS Parameters Resulting from the Fit of the EXAFS Data for the Sorption of Am(III) onto Coated Colloids

sample	shell	R [Å][a]	N	σ^2 [Å²][b]	ΔE [eV]	k [Å⁻¹]
Am/Coated Colloids	Am−O	2.474(4)	6.4	0.0087(6)	−2.9	3.3−9.0
	Am−Fe	3.71(2)	1[c]	0.011(2)	10.5	

[a] Standard deviation in parentheses. [b] Debye−Waller-Factor. [c] Fixed value.

Am−Fe distance is too short for a monodentate binding. Moreover, due to both the long distance expected for monodentate interaction and the dynamic atomic displacements possible for **M** binding, an Am−Fe interaction is not anticipated in the EXAFS. The species **B1** and **B2** have shorter Am−Fe distances than species **M**, as well as a more rigid structure so that an Am−Fe interaction should be observed in the EXAFS. The Am−Fe interaction observed at 3.69 ± 0.02 Å suggests that Am(III) sorbs onto 6LFh by forming mainly a bidendate geminal corner-sharing bonding species (**B2**). This distance matches very well with the expected bond distance of 3.72 Å (Figure 2). The other bidendate site **B1** yields Am−Fe distances that are too short.

No reliable fit of the data using Am−Am phase and amplitude scattering function is possible. The lack of an Am−Am interaction excludes the presence of sorbed polynuclear surface species or significant surface precipitation. However, a minor fraction of poorly ordered Am precipitate might not be detected.

These results are in agreement with investigations of the Lu(III) sorption onto ferrihydrite (*6*). Here, a bidentate species too (but edge-sharing) is formed at pH > 5.

Sorption of Am(III) onto Coated Colloids. Figure 3 shows the EXAFS and Fourier transformed spectra of sorbed Am(III) onto coated colloids at pH 8.0. The EXAFS spectra show a good signal-to-noise ratio. The main oscillation of the Am−O interaction in the EXAFS spectrum is superimposed with a different oscillation than for the sorption of Am(III) onto ferrihydrite at pH 5.5 and 8.0. This results in fine structure in the EXAFS spectrum from 7.0 to 7.5 Å^{-1}. The peak around 3.2 Å in the FT cannot be explained by an Am−Si interaction. In fact, it is identified as a backscattering contribution through the iron atoms. The first peak in the FT can be attributed to an Am−O distance of 2.47 Å while the second one is attributed to an Am−Fe distance of 3.71 Å (Table 2). The sorption of Am(III) onto coated colloids yields again an apparent reduction of the coordination

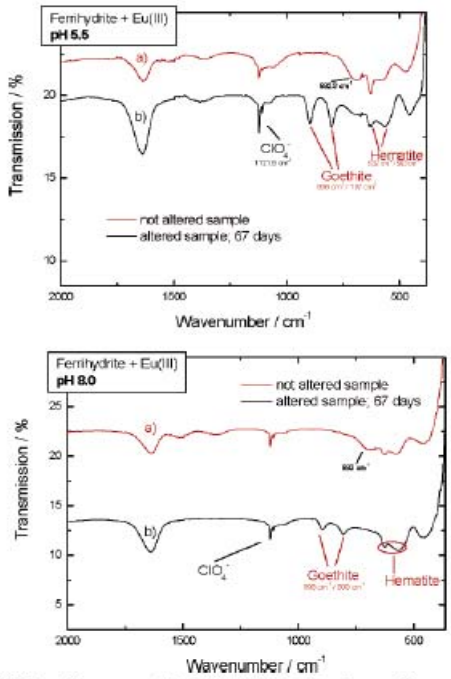

FIGURE 4. IR spectra of Eu(III)/ferrihydrite samples at pH 5.5 and 8.0 (a) before and (b) after transformation.

number and indicates the formation of an inner-sphere complex. The results of the fit to the sorption data are similar to the results obtained by direct sorption onto 6LFh and thus yield the same conclusion. Am(III) sorbs onto 6LFh by forming a bidendate geminal corner-sharing bonding species on the site with O−O of 4.7 Å. Hence, the Fh even present as coating is the predominant sorption surface. This result is supported indirectly by TRLFS (time-resolved laser fluorescence spectroscopy) investigations of the Cm(III) sorption onto Fh (not published yet). The authors have observed a

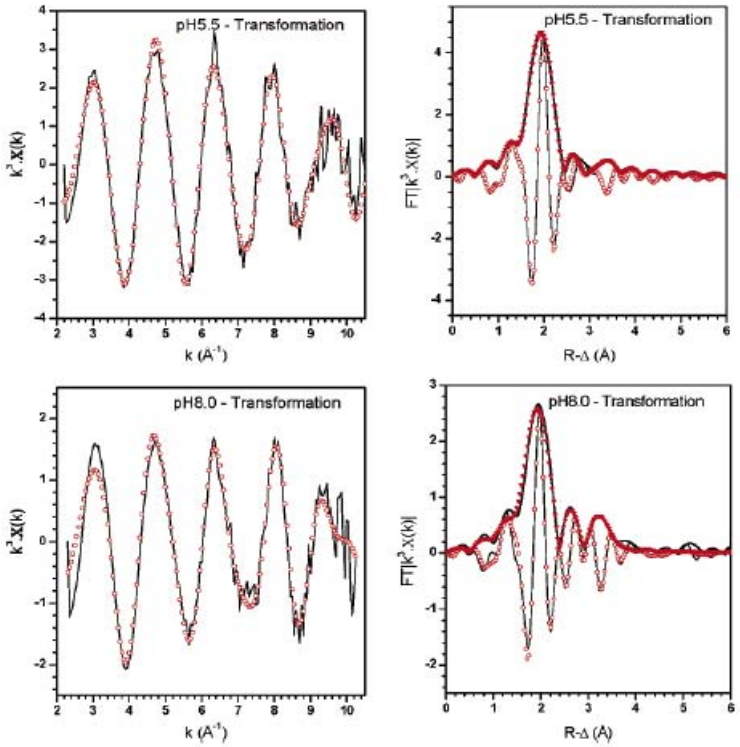

FIGURE 5. Am sorption onto ferrihydrite at pH 5.5 and 8.0 after transformation. Left: k^3-weighted Am L_3 edge experimental EXAFS and back transformed *R*-space fit result. Right: corresponding Fourier transformed spectra. Experimental data are lines and fit data are circles or triangles.

quenching of the Cm (III) fluorescence in this study on Fh coated colloids as it is the case for Cm(III) sorbed directly onto Fh. The Cm(III) fluorescence is not quenched for the sorption onto silica.

The results indicate the dominance of the sorption on the Fh surface even if the Fh is present as sediment coating. This is in good accordance with investigations of Arnold et al., who have shown that a Fh coating on phyllite, formed by weathering of this mineral, dominates the sorption process of uranium (*29*).

Transformation of Ferrihydrite at pH 5.5 and pH 8.0. The transformation product of ferrihydrite at pH 5.5 and 8.0 was characterized by IR and TEM measurements. The TEM images show the formation of crystalline phases that can be attributed to both goethite and hematite. It is not possible to ascertain which product represents the dominant phase. Figure 4 shows the IR spectra of both samples before and after the transformation. There is a definite change in the fingerprint area of the spectra after the transformation at pH 5.5 and 8.0. The characteristic peak for the amorphous iron mineral phase at 693 cm^{-1} is not longer detectable after the transformation. Moreover there are new peaks at 898 and 809 cm^{-1} that can be attributed to goethite while the peaks at ~632 and ~563 cm^{-1} indicate the formation of hematite. Again this method does not allow the full quantification of both mineral phases.

Figure 5 shows the EXAFS and Fourier transform (FT) spectra of the altered samples at pH 5.5 and 8.0 with the graphical fit results. The structural parameters obtained from the fit to the EXAFS data are also listed in Table 1 for easy comparison to the Fh results. At pH 5.5 the amplitude of the main Am−O oscillation increases in the transformed sample while the amplitude of the Am−Fe oscillation observed in the *k*-range from 7.0 to 7.5 $Å^{-1}$ and 9.0 to 10.5 $Å^{-1}$ is reduced. This is more evident while comparing the FT spectra on the right parts of Figures 1 and 5. The intensity of the Am−O FT peak increases for the altered sample while the Fe−O FT peak intensity is strongly reduced. The result of the fitted data show that the number of O coordinating ligands at 2.48 Å increases from 6.3 to 7.2 (~ value for aquo species) for the transformation sample while the coordination number of Fe neighboring the Am decreases from 1 to 0.3 (Table 1). The Am−Fe distance becomes slightly longer in the transformed sample but still lies in the expected range for a bidendate corner-sharing sorption complex. This result can be explained by the release of Am during the transformation of Fh. Indeed during the transformation, the pH of the solution decreases (pH < 4) and a large part of the Am(III) is desorbed and stabilized in the solution as aquo-species before the Fh transformation is completed. This was observed in a previous study (*6*) on Lu where we show that 48% of the initially sorbed Lu onto Fh is released during the transformation at pH 6. In the present work, as the sample is investigated without prior separation of the aqueous phase, we measure a mixture containing a large part of aquo-species having a higher oxygen coordination number in the first coordination sphere (2.48 Å) and no Fe neighbor. That explains the EXAFS results obtained for this sample. As the Am−O distance of the sorbed

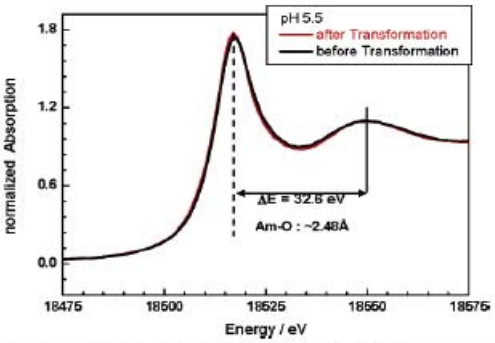

FIGURE 6. XANES spectra: comparison of the Am L_3 edge of the ferrihydrite samples at pH 5.5 before and after transformation.

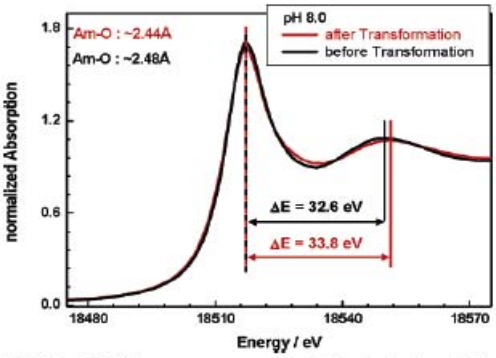

FIGURE 7. XANES spectra: comparison of the Am L_3 edge of the ferrihydrite samples at pH 8.0 before and after transformation.

species and the aquo ion is the same, the XANES spectrum of the transformed sample at pH 5.5 (Figure 6) does not show any structural change compared to the spectrum of the sorption sample at pH 5.5.

The EXAFS spectra of the sorption and transformed sample at pH 8.0 show a significant difference in both the fine structure and amplitude (Figures 1 and 5, bottom). We can see a broadening of the EXAFS oscillation for the transformation sample especially visible in the *k*-range from 7.0 to 7.5 $Å^{-1}$. We also note the splitting of the oscillation between 9.0 and 10.5 $Å^{-1}$ that can be attributed to the Am−Fe interaction. The fraction of oxygen in the FT spectrum of the transformation sample at pH 8.0 is strongly reduced (~5.0 after rescaling relative to the aquo species 7.4→9). This can be explained by the reduction of the number of coordinated oxygen ligands during the transformation. A coordination by 6 oxygen atoms would be comparable to a replacement of octahedral coordinated Fe(III) by Am(III) in the mineral. In contrast to the pH 5.5 sample, the XANES spectra of the pH 8.0 sample given in Figure 7 show differences in the position of the maximum of the multiple scattering features around 18 550 eV. The energy shift of the scattering resonance allows calculating the distance between Am and the O atoms in the first coordination sphere.

The scattering resonances shift is related to the bond distance by (*30*)

$$\Delta E R^2 = C \qquad (1)$$

C is a constant determined by using known compounds with known bond distances. From spectra issued of literature data (*31*) (Am(III) in 0.25 M HCl, XANES in the Supporting Information of ref 31) and our own measurements (aquo species and sorption species) we get an estimation for the *C* value of 201 ± 6 eV × $Å^2$.

After transformation the maximum of scattering resonance around 18 550 eV is shifted by ~1.2 eV which corresponds to an Am−O bond distance of ~2.44 Å, i.e., ~0.04 Å shorter than for the sorption sample (2.48 Å). A shortening of the mean bond distance indicates a reduction of the coordination number according to the bond valence theory (*32*, *33*). This slight trend to shorten the Am−O distance is observed for the pH 8.0 transformed samples in both EXAFS and XANES. This indicates a possible partial incorporation of Am(III) into the iron mineral phase during transformation at pH 8.0. When incorporation occurs shorter Am−Fe distances are expected because of a stronger Am−Fe interaction. The fit to the EXAFS data yields Am−Fe distances of 3.32 and 3.59 Å. In the literature two models for the incorporation of lutetium into transformed Fh are described (*34*). In the case of a Lu incorporation into a goethite-like structure three Lu−Fe distances with values of ~3.04, ~3.24, and ~3.45 Å are expected, whereas the incorporation into a hematite like structure would yield bond distances of ~3.08, ~3.41, and ~3.88 Å. If we take into account the difference of ionic radii between Lu^{3+} (0.86 Å) and Am^{3+} (0.97 Å), we can estimate that the distance for Am would be ~0.11 Å longer than the one for Lu. This gives Am−Fe distances of approx. 3.15, 3.35, and 3.56 Å for the incorporation of Am(III) into goethite and approx. 3.19, 3.52, and 3.99 Å for the incorporation into hematite. The obtained values of 3.32 and 3.59 Å suggest the incorporation of Am(III) in either a more goethite-like structure or as defect (mononuclear inclusion) in the goethite/hematite phases during the transformation of Fh at pH 8.0.

Acknowledgments

We thank A. Rossberg, H. Funke, and H. Moll for their experimental assistance at the European Synchrotron Radiation Facility.

Literature Cited

(1) Dario, M.; Ledin, A. Sorption of Cd to colloidal ferric hydroxides − Impact of pH and organic acids. *Chem. Spec. Bioavail.* **1997**, *9* (1), 3−14.
(2) Janney, D. E.; Cowley, J. M.; Buseck, P. R. Transmission electron microscopy of synthetic 2-and 6-line ferrihydrite. *Clays Clay Miner.* **2000**, *48* (1), 111−119.
(3) Cornell, R. M.; Schwertmann, U. *The Iron Oxides: Structure, Properties, Reactions, Occurrence and Uses*; VCH Verlagsgesellschaft: Weinheim, 1996.
(4) Scheinost, A. C.; Abend, S.; Pandya, K. I.; Sparks, D. L. Kinetic controls on Cu and Pb sorption by ferrihydrite. *Environ. Sci. Technol.* **2001**, *35* (6), 1090−1096.
(5) Waychunas, G. A.; Fuller, C. C.; Davis, J. A. Surface complexation and precipitate geometry for aqueous Zn(II) sorption on ferrihydrite I: X-ray absorption extended fine structure spectroscopy analysis. *Geochim. Cosmochim. Acta* **2002**, *66* (7), 1119−1137.
(6) Dardenne, K.; Schäfer, T.; Denecke, M. A.; Rothe, R.; Kim, J. I. Identification and characterization of sorbed lutetium species on 2-line ferrihydrite by sorption data modeling, TRLFS and EXAFS. *Radiochim. Acta* **2001**, *89* (7), 469−479.
(7) Martínez, C. E.; Sauvé, S.; Jacobson, A.; McBride, M. B. Thermally induced release of adsorbed Pb upon aging ferrihydrite and soil oxides. *Environ. Sci. Technol.* **1999**, *33* (12), 2016−2020.
(8) Schwertmann, U.; Friedl, J.; Stanjek, H.; Schulze, D. G. The effect of Al on Fe oxides. XIX. Formation of Al-substituted hematite from ferrihydrite at 25 degrees C and pH 4 to 7. *Clays Clay Miner.* **2000**, *48* (2), 159−172.
(9) Ford, R. G.; Bertsch, P. M.; Farley, K. J. Changes in transition and heavy metal partitioning during hydrous iron oxide aging. *Environ. Sci. Technol.* **1997**, *31* (7), 2028−2033.

(10) Karthikeyan, K. G.; Elliott, H. A.; Cannon, F. S. Adsorption and coprecipitation of copper with the hydrous oxides of iron and aluminum. *Environ. Sci. Technol.* **1997**, *31* (10), 2721−2725.
(11) Lewis, D. G.; Schwertmann, U. The influence of Al on iron oxides; Part III, Preparation of Al goethites in M KOH. *Clays Clay Miner.* **1979**, *27* (3), 195−200.
(12) Dardenne, K.; Schäfer, T.; Lindqvist-Reis, P.; Denecke, M. A.; Plaschke, M.; Rothe, J.; Kim, J. I. Low-temperature XAFS investigation on the lutetium binding changes during the 2-line ferrihydrite alteration process. *Environ. Sci. Technol.* **2002**, *36* (23), 5092−5099.
(13) Matz, W.; Schell, N.; Bernhard, G.; Prokert, F.; Reich, T.; Claussner, J.; Oehme, W.; Schlenk, R.; Dienel, S.; Funke, H.; Eichhorn, F.; Betzl, M.; Pröhl, D.; Strauch, U.; Hüttig, G.; Krug, H.; Neumann, W.; Brendler, V.; Reichel, P.; Denecke, M. A.; Nitsche, H. ROBL − a CRG beamline for radiochemistry and materials research at the ESRF. *J. Synchrotron Radiat.* **1999**, *6*, 1076−1085.
(14) Denecke, M. A.; Rothe, J.; Dardenne, K.; Blank, H.; Hormes, J. The INE-Beamline for Actinide Research at ANKA. *Phys. Scripta* **2005**, *T115*, 1001−1003.
(15) McMaster, W. H.; Kerr Del Grande, N.; Mallett, J. H.; Hubbell, J. H. *Compilation of X-ray Cross Sections*; Report UCRL-50174; Section II; Revision I; Lawrence Livermore National Laboratory: Livermore, CA, 1969.
(16) Koningsberger, D. E.; Prins, R. *X-ray Absorption: Principles, Applications, Techniques for EXAFS, SEXAFS and XANES*; Wiley-Interscience: New York, 1988.
(17) George, G. N.; Pickering, I. J. *EXAFSPAK: A suite of computer programs for analysis of X-ray absorption spectra*; Stanford Synchrotron Radiation Laboratory: Stanford, CA, 1995.
(18) Ressler, T. J. WinXAS: A new software package not only for the analysis of energy-dispersive XAS data. *Physique IV* **1997**, *7* (C2), 269−270.
(19) Newville, M.; Livins, P.; Yacoby, Y.; Rehr, J. J.; Stern, E. A. Near-Edge X-ray absorption fine structure of Pb − a comparison of theory and experiment. *Phys. Rev. B* **1993**, *47* (21), 14126−14131.
(20) Ankudinov, A. L.; Ravel, B.; Rehr, J. J.; Conradson, S. D. Real-space multiple scattering calculation and interpretation of X-ray-absorption near-edge structure. *Phys. Rev. B* **1998**, *58*, 7565−7576.
(21) Schwertmann, U.; Cornell, R. M. *Iron Oxides in the Laboratory (Preparation and Characterization)*; VCH-Verlag: Weinheim, 1991.
(22) Janney, D. E.; Cowley, J. M.; Buseck, P. R Structure of synthetic 6-line ferrihydrite by electron nanodiffraction. *Am. Mineral.* **2001**, *86* (3), 327−335.
(23) Brunauer, S.; Emmett, P. H.; Teller, F. *J.* Adsorption of gases in multimolecular layers. *J. Am. Chem. Soc.* **1938**, *60*, 309−319.
(24) Eggleton, R. A.; Fitzpatrick, R. New data and a revised structural model for ferrihydrite. *Clays Clay Miner.* **1988**, *36* (2), 111−124.
(25) Sherman, D. M.; Waite, T. D. Electronic spectra of Fe (super 3+) oxides and oxide hydroxides in the near-IR to near UV. *Am. Mineral.* **1985**, *70* (11−12), 1262−1269.
(26) Musić, S.; Šarić, A.; Nomura, K.; Popović, S. Chemical and microstructural properties of oxide phases obtained by forced hydrolysis of Fe3+ ions. *ACH - Models Chem.* **1999**, *136* (4), 457−476.
(27) Stumpf, T.; Hennig, C.; Bauer, A.; Denecke, M. A.; Fanghänel, T. An EXAFS and TRLFS study of the sorption of trivalent actinides onto smectite and kaolinite. *Radiochim. Acta* **2004**, *92* (3), 1−6.
(28) Allen, P. G.; Bucher, J. J.; Shuh, D. K.; Edelstein, N. M.; Craig, I. Coordination chemistry of trivalent lanthanide and actinide ions in dilute and concentrated chloride solutions. *Inorg. Chem.* **2000**, *39* (3), 595−601.
(29) Arnold, T.; Zorn, T.; Zänker, H.; Bernhard, G.; Nitsche, H. Sorption behavior of U(VI) on phyllite: experiments and modelling. *J. Contam. Hydrol.* **2001**, *47* (2−4), 219−231.
(30) Natoli, C. R. EXAFS and near edge Structure. In *Chemical Physics*; Bianconi, A.; Incoccia, L.; Stipcich, S.; Springer-Verlag: Berlin, 1984.
(31) Allen, P. G.; Bucher, J. J.; Shuh, D. K.; Edelstein, N. M.; Craig, I. Coordination chemistry of trivalent lanthanide and actinide ions in dilute and concentrated chloride solutions. *Inorg. Chem.* **2000**, *39* (3), 595−601.
(32) Altermatt, D.; Brown, I. D. The automatic searching for chemical bonds in inorganic crystal structures. *Acta Crystallogr. B* **1985**, *41*, 240−244.
(33) Brown, I. D.; Altermatt, D. Bond-valence parameters obtained from a systematic analysis of the Inorganic Crystal Structure Database. *Acta Crystallogr. B* **1985**, *41*, 244−247.
(34) Dardenne, K.; Denecke, M. A.; Schäfer, T. *Advanced Photon Source Activity Report 2002*; ANL-03/21; Argonne National Laboratory: Argonne, IL, December 2003.

Received for review December 16, 2005. Revised manuscript received March 15, 2006. Accepted March 22, 2006.

ES052518E

4. Kristallchemischer Einbau von dreiwertigen Actiniden in Mineralphasen

Die Wechselwirkung von dreiwertigen Actiniden mit Mineralphasen kann neben der Bildung von outer-sphere und inner-sphere Komplexen zur Aufnahme der Metallionen in die Struktur des Minerals führen. Ein solcher kristallchemischer Einbau könnte zu einer effektiven Retardierung von Radionukliden im Nah- und Fernfeld eines nuklearen Endlagers beitragen. Aus diesem Grund ist der Nachweis der Bildung, die strukturelle Charakterisierung und die Quantifizierung sog. "solid solutions" von großem Interesse. Hierzu konnten Cm(III) TRLFS Untersuchungen der Systeme Cm/Calcit; Cm/CSH Phasen und Cm/Zement einen Beitrag liefern. Eine Zusammenfassung der erarbeiteten Ergebnisse findet sich in den folgenden Publikationen.

"A Time-Resolved Laser Fluorescence Spectroscopy (TRLFS) Study of the Interaction of Trivalent Actinides (Cm(III)) with Calcite"; Thorsten Stumpf, Thomas Fanghänel; J. Colloid Interface Sci., 2002, 249, 119-122.

“Structural characterization of Am incorporated into calcite: A TRLFS and EXAFS study”; Thorsten Stumpf, Maria Marques Fernandes, Clemens Walther, Kathy Dardenne, Thomas Fanghänel; J. Colloid Interface Sci., 2006, 302, 240-245.

"Uptake of Cm(III) and Eu(III) by Calcium Silicate Hydrates: A Solution Chemistry and Time-Resolved Laser Fluorescence Spectroscopy (TRLFS) Study"; Jan Tits, Thorsten Stumpf, Thomas Rabung, Erich Wieland, Thomas Fanghänel; Environ. Sci. Technol., 2003, 37, 3568-3573.

"Uptake of Trivalent Actinides (Cm(III)) by Hardened Cement Paste: A Time-Resolved Laser Fluorescence Spectroscopy (TRLFS) Study"; Thorsten Stumpf, Jan Tits, Clemens Walther, Erich Wieland, Thomas Fanghänel; J. Colloid Interface Sci., 2004, 276, 118-124.

Calcit stellt eine wichtige Komponente der meisten geologischen Gesteinsformationen dar. In den Tonmineralen, die als potentiell endlagerrelevante Gesteinsformation in Frankreich (Argilites de Bure), in Belgien (Boom Clay) und in der Schweiz (Opalinus Ton) für die Lagerung sowohl hochradioaktiver als auch

langlebig mittelradioaktiver Abfälle untersucht werden, liegt der Calcitgehalt bei mindestens zehn Prozent. Darüber hinaus ist Calcit das wichtigste sekundäre Alterationsprodukt bei der Auflösung von zementgebundenen Materialien (technische Barriere). Da die Freisetzung von Radionukliden aus einem nuklearen Endlager im Spurenkonzentrationsbereich stattfinden wird, wurde bei der vorliegenden Untersuchung Curium im Spurenkonzentrationsbereich eingesetzt (9×10^{-8} mol/L). Unter diesen umweltrelevanten Bedingungen konnten zwei Cm(III)/Calcit Spezies nachgewiesen und charakterisiert werden. Cm/Calcit Spezies 1 zeigt ein Peakmaximum bei 607.5 nm während Cm/Calcit Spezies 2 ein um weitere 10.5 nm rotverschobenes Signal aufweist. Die Kinetik des Auftretens der beiden Komponenten ließ sich mit Hilfe der TRLFS verfolgen. Mit zunehmender Cm(III)/Calcit Kontaktzeit nimmt die Stärke des Signals mit einem Emissionsmaximum bei 607.5 nm sukzessive ab und das sehr weit rotverschobene Signal der zweiten Cm/Calcit Spezies wird sichtbar. Wie bereits mehrfach erwähnt, lässt sich aus den Fluoreszenzlebensdauern die Zahl der Wassermoleküle, die das Curiumatom umgeben, errechnen und somit auf die Art der Bindung an die Mineraloberfläche rückschließen. Während das freie Cm(III) Aquoion von neun Wassermolekülen umgeben ist (Lebensdauer 68 $\pm$ 3 μs), deutet die für Cm/Calcit Spezies 1 ermittelte Fluoreszenzlebensdauer von 314 $\pm$ 6 μs auf nur noch ein Wassermolekül in der ersten Koordinationssphäre des Curiums hin. Für Cm/Calcit Spezies 2 wurde die sehr lange Fluoreszenzlebensdauer von 1302 $\pm$ 75 μs gemessen. 1.3 ms entsprechen dem theoretischen Wert für die Fluoreszenzlebensdauer von Curium bei völliger Abwesenheit von Wasser. Die für Cm/Calcit Spezies 2 ermittelte Fluoreszenzlebensdauer und die starke Verschiebung des Cm(III) Spektrums mit zunehmender Kontaktzeit lassen auf einen Einbau des Curiums in das Calcitgitter schließen.

Um Strukturparameter wie Bindungslängen und Koordinationszahlen für die in Calcit eingebaute Actinidspezies zu erhalten, wurden EXAFS Untersuchungen an gezielt mit Am(III) dotierten Calcit durchgeführt. Da auch Am(III) über eine Fluoreszenzemission verfügt und zudem Curium als Verunreinigungen in der Americium Stammlösung vorhanden war, war es möglich neben der Untersuchung mit Hilfe der Röntgenabsorptionsspektroskopie, die Am(III)/Calcit und Cm(III)/Calcit Spezies mit Hilfe der TRLFS zu charakterisieren und zu quantifizieren. Sowohl für Cm(III) als auch für Am(III) konnten zwei Spezies bestimmt werden, die analog zu

den in (Stumpf und Fanghänel; 2002) vorgestellten Ergebnissen als eine Oberflächen und eine Einbau Spezies identifiziert werden konnten. Ferner zeigte sich, dass bei dem synthetisierten Calcit der überwiegende Teil des Actinids in die Struktur eingebaut vorliegt. Am(III) EXAFS Untersuchungen ergaben für die erste Am-O Koordinationsschale eine Bindungslänge von 2.40 ± 0.01 Å und die Koordinationszahl von 6.3 ± 0,6. Die nächsten Schalen (Am-C und Am-O) konnten nicht angepasst werden. Die ermittelte Bindungslänge von 2.40 Å ist wesentlich kürzer als die Am-O Abstände, die für das 8 bis 9 -fach Sauerstoff koordinierte Am(III) Aquoion (2.49) (Stumpf et al.; 2004) und für die Am(III) Smectit/Kaolinit Sorptionsspezies gefunden wurden (2.47, 2.49 Å) und stimmt sehr gut mit denen von (Elzinga et al.; 2002) und (Withers et al.; 2003) publizierten Bindungslängen für Ln(III) dotierten Calcitkristallen überein. Der gemessene Am-O Abstand im Am/Calcit ist etwas größer als die Ca-O Bindungslängen (2.36 Å) in der idealen Calcitstruktur. Diese leichte erhöhte Am-O Bindungslänge im Vergleich zur Ca-O Bindungslänge im Calcitgitter ist durch die Gegenwart der oberflächenkomplexierten Am(III) Spezies bedingt. Eine Aufspaltung der Am-O Schale im EXAFS Spektrum, die das Vorhandensein von zwei unterschiedlich koordinierten Am(III)/Calcit Spezies bestätigen würde, ist nicht zu beobachten. Dies lässt sich durch die bei der TRLFS Messung festgestellten Dominanz der im Calcit eingebauten Komponente erklären. Die mit Hilfe der EXAFS Untersuchung ermittelten Werte für die Am-O Bindungslänge (2.40 Å) und Koordinationszahl (N = 6.3) bestätigen, dass sich das Am^{3+} an der Stelle des Ca^{2+} in der Calcitstruktur befindet.

Der spektroskopische Beweis des Austausches von Calcium gegen ein dreiwertiges Actinid am Beispiel von Calcit führte zur Untersuchung der Wechselwirkung von Curium mit Zement. Obwohl Zement aus einer Vielzahl diverser Mineralphasen besteht und somit ein sehr kompliziertes System darstellt, konnte die Sorption von Curium und der nachfolgende zeitabhängige Einbau des Radionuklids in die Festphase spektroskopisch verfolgt und quantifiziert werden. In der Lösung, die aus hochalkalischem (pH 13.3) künstlichem Zementporenwasser bestand, konnte nach Zugabe von Cm(III) die Bildung von Curiumeigenkolloiden mit Hilfe der TRLFS sowie der Laser-induzierten Breakdown Detektion (LIBD) nachgewiesen werden. Diese Kolloide lösten sich nach einigen Tagen auf und es bildet sich eine Cm/Zement Spezies mit einem Peakmaximum bei 613.6 nm und einer Fluoreszenzemissionslebensdauer von 66 ± 1 μs. Diese Komponente konnte als eine

Cm/Portlandit ($CaOH_2$) Spezies identifiziert werden. Mit zunehmender Cm/Zement Kontaktzeit nimmt die Intensität des Emissionssignals dieser Spezies ab und eine starke Rotverschiebung des Peaks sowie ein deutlicher Anstieg der Emissionslebensdauer sind zu beobachten. Cm(III) TRLFS Untersuchungen einiger Mineralphasen aus denen sich Zement zusammensetzt zeigen, dass die beobachtete starke Rotverschiebung des Emissionssignals im Cm/Zement System mit Spektren inkorporierten Curiums im Cm/CSH System erklärt werden kann. Darüber hinaus finden sich in beiden Systemen vergleichbare Emissionslebensdauern. Dies deutet auf einen zeitabhängigen Einbau des Radionuklids in die CSH Phase des Zements hin. Das Aufnehmen von Radionukliden in Minerale bietet statt der stets reversiblen Oberflächensorption die Möglichkeit, Actinide aus der Geosphäre nachhaltiger zu entfernen. Das Wissen um den Einbaumechanismus von dreiwertigen Actiniden in calciumhaltige Minerale könnte zu einer langfristigen Immobilisierung der Radionuklide in einem Endlager genutzt werden.

Durch den Einbau von Lanthaniden und Actiniden in Kristallstrukturen (z. B. von Sekundärphasen wie Calcit) erhalten die Metallionen ein definiertes, zeitlich fixiertes Ligandenfeld. Dadurch wird es möglich, hochauflösende Fluoreszenzspektroskopie bei tiefen Temperaturen zu betreiben. Während die Auflösung der einzelnen chemisch relevanten Energieniveaus wegen der vibronischen Bandenverbreitung bei Raumtemperatur nicht möglich ist, können bei Tieftemperaturmessungen einzelne Spezies , die verschiedene „sites“ im Wirtsgitter belegen, aufgelöst werden. Dies gilt sowohl für die Spektroskopie mit Cm(III) als auch mit Eu(III). Die anfügten Publikationen befassen sich mit jeweils Lanthanid dotierten Calciten und Hydrotalciten, die mit Hilfe der TRLFS bei tiefen Temperaturen untersucht wurden.

“Site-selective time resolved Laser fluorescence spectroscopy study of Eu(III) doped calcite”; Maria Marques Fernandes , Moritz Schmidt, Thorsten Stumpf, Clemens Walther, Dirk Bosbach, Thomas Fanghänel, Geochim. Cosmochim. Acta, 2007 submitted.

“Incorporation of Eu(III) into hydrotalcite: a TRLFS and EXAFS study”; Thorsten Stumpf, Hilde Curtius, Clemens Walther, Kathy Dardenne, Karsten Ufer, Thomas Fanghänel, Environ. Sci. Technol. 2007, 41, 3186-3191.

Wie bereits in der Einleitung erwähnt, lassen sich bei der nicht selektiven Anregung des Eu(III) $^5L_6$ Niveaus nur wenig Informationen zu Anzahl und Art der vorhandenen Lanthanid Spezies erhalten. Die selektive Anregung des $^5D_0 \rightarrow {}^7F_0$ Übergangs bei tiefen Temperaturen bietet dagegen die Möglichkeit, diverse Eu(III) Spezies mit definiertem Ligandenfeld von einander zu unterscheiden. Der Grund dafür ist, dass der $^7F_0$ Grundzustand nicht entartet ist, also jeder detektierte $^5D_0 \rightarrow {}^7F_0$ Übergang genau einer diskreten Lanthanid Spezies zugeordnet werden kann (Bünzli und Choppin 1989; Gröller-Walrand und Binnemans 1996). Die gezielte Anregung der diskreten $^5D_0$ – $^7F_0$ Übergänge verschiedener Eu(III) Spezies erlaubt durch die Auswertung der erhaltenen Emissionsspektren eine Aussage zur Punktsymmetrie des jeweiligen Eu(III)-Zentrums.

In Tabelle 2 sind die maximalen Aufspaltung der F_J-Zustände in Abhängigkeit von der Quantenzahl J für verschiedene Symmetrien dargestellt. Es wird deutlich, dass eine Erhöhung der Symmetrie stets zu einer verringerten Anzahl beobachtbarer Banden im Emissionsspektrum führt. So spaltet die F_1-Bande in kubischer Symmetrie nicht auf, bei hexa-, tri- oder tetragonaler Symmetrie beobachtet man zwei, bei noch geringerer Symmetrie drei Banden (Bünzli und Choppin; 1989).

Symmetrie	J= 0	1	2	3	4	5	6	Punktgruppen
Ikosaeder	1	1	1	2	2	3	4	
Kubisch	1	1	2	3	4	4	6	O_h, O, T_d, T_h, T
Hexagonal	1	2	3	5	6	7	9	D_{6h}, D_6, C_{6v}, D_{3h}, C_{3h}, D_{3d}, D_3, C_{3v}, C_{3i}, C_3
Pentagonal	1	2	3	4	5	7	8	D_{5h}, C_{5h}, C_{5v}, C_5, D_5
Tetragonal	1	2	4	5	7	8	10	D_{4h}, D_4, C_{4v}, C_{4h}, C_4, D_{2d}, S_4
Gering	1	3	5	7	9	11	13	D_{2h}, D_2, C_{2v}, C_{2h}, C_s, S_2, C_1, C_i

Tabelle 2 Aufspaltung der J-Übergänge in Abhängigkeit von J bei verschiedenen Symmetrien

Die Ergebnisse der Untersuchungen von Eu(III) dotierten Calciten bei Probentemperaturen von < 20 K und bei Variation der Anregungswellenlänge des Lasers sind in der Publikation “Site-selective time resolved Laser fluorescence spectroscopy study of Eu(III) doped calcite” zusammengefasst.

Drei verschiedene Eu(III)/Calcit Spezies wurden gefunden, denen eine oberflächenkomplexierte (A) und zwei eingebaute Lanthanid Spezies (B und C) zugeordnet werden konnten. Lanthanid Spezies C zeigt die stärkste Rotverschiebung des $^5D_0 \rightarrow {}^7F_0$ Signals zu einem Peakmaximum bei 17253 cm^{-1} (579.6 nm) und konnte als ein auf dem Ca^{2+} Gitterplatz eingebautes Eu^{3+} identifiziert werden, welches von sechs Carbonat Sauerstoffen oktaedrisch koordiniert ist und, wie aus dem Aufspaltungsmuster des Emissionsspektrums abgeleitet werden konnte, die Punktsymmetrie C_{3i} aufweist. Diese dominierende Einbauspezies zeigt eine lange Emissionslebensdauer von über 2.5 ms. Dieser Wert korreliert mit vollständigen Verlust der Hydrathülle.

Die zweite Einbauspezies B ist im Excitationsspektrum ($^5D_0 \rightarrow {}^7F_0$ Übergang) weniger stark rotverschoben (17289 cm^{-1}; 578.4 nm) als Spezies C und das zugehörige Emissionsspektrum zeigt eine niedrigere Symmetrie. Die gefundene Emissionslebensdauer weist allerdings auch bei dieser Spezies auf den Verlust der kompletten Hydrathülle hin, was ein klares Indiz für ein in die Kristallstruktur inkorporiertes Eu^{3+} ist. Als dritte Eu(III) Komponente findet sich eine Oberflächeneinbauspezies A, deren Signal im Excitationsspektrum bei 17296 cm^{-1} (578.2 nm) eine geringere Rotverschiebung als Spezies B und C zeigt und die noch über ein bis zwei Wassermoleküle in der ersten Koordinationssphäre verfügt. Sowohl die starke Aufspaltung der Banden des Emissionsspektrums von Spezies A als auch die vergleichsweise kurze Emissionslebensdauer von ~ 0.4 ms deuten auf eine Oberflächeneinbauspezies hin.

Ferner konnte spektroskopisch gezeigt werden, dass beim Ersatz von Na^+ durch K^+ bei der Synthese des Eu(III) dotierten Calcits die Koordination der Spezies C von der oktaedrischen Symmetrie des Ca^{2+} Platzes abweicht. Folglich führt ein Mangel an Na^+ zu einer Verzerrung des Ligandenfeldes dieser Lanthanid Spezies. Dies bedeutet, dass aus Gründen der Ladungskompensation ein gekoppelter Na^+ und Eu^{3+} Einbaumechanismus vorliegt. Allerdings findet auch bei einer zur Ladungskompensation nicht ausreichenden Menge an Na^+ ein Einbau des Europiums statt. Die Triebkraft zur Bildung einer „solid solution“ scheint so groß zu sein, dass es auch zu einem Einbau des Lanthanids unter erschwerten Bedingungen kommt.

Weitere endlagerrelevante Sekundärphasen stellen Mg-Al-LDH (layered double hydroxide) Phasen dar. Solche „Hydrotalcite“ konnten als Korrosionsprodukte von

verschiedenen Brennelementen sowohl vor als auch nach dem Abbrannt identifiziert werden. Ferner konnte gezeigt werden, dass diese Sekundärphasen bei der Retardierung von Actiniden im Nahfeld eines Endlagers eine Rolle spielen (Mazeina et al.; 2003). Die Untersuchung von in Gegenwart von Eu(III) synthetisiertem Hydrotalcit mit Hilfe der TRLFS bei Temperaturen <10 K führten zur Identifizierung zweier Eu(III)/Hydrotalcit Spezies. Das dominierende Signal bei der Aufnahme des Excitationsspektrums im Bereich des $^5D_0 \rightarrow {}^7F_0$ Übergangs zeigt ein Maximum bei 580.0 nm. Das zugehörige Emissionsspektrum ist wenig strukturiert und die detektierte Fluoreszenzemissionslebensdauer beträgt 305 +/- 5 µs. Diese Lebensdauer entspricht nach der von Horrocks veröffentlichten Gleichung drei Wassermolekülen bzw. sechs Hydroxylgruppen in der ersten Koordinationsschale des Europiums. Eu(III)/Hydrotalcit Spezies 2 zeigt für den $^5D_0 \rightarrow {}^7F_0$ Übergang ein Peakmaximum bei 581,6 nm. Im Vergleich zu Spezies 1 sind die zu J = 1 und J = 2 gehörenden Banden des zugehörigen Emissionsspektrums stark aufgespalten. Die $^7F_1$ Bande zeigt die maximale Aufspaltung in drei Peaks, so dass diesem Eu(III) Zentrum eine geringe Punktsymmetrie zugeordnet werden kann. Die detektierte Emissionslebensdauer für Eu(III) Spezies 2 beträgt 193 +/- 6 µs. Dieser Wert entspricht einer Hydrathülle von fünf H_2O Molekülen und ist typisch für Europium inner-sphere Komplexe an Mineraloberflächen (siehe Kapitel 2 und 3). Aufgrund der gemessenen Emissionslebensdauer und der starken Aufspaltung des Emissionsspektrums liegt es nahe, dass es sich bei Spezies 2 um einen Eu(III)/Hydrotalcit Oberflächenkomplex handelt. Ferner kann aus ähnlichen Überlegungen für Spezies 1 geschlossen werden, dass es sich dabei um eine Einbauspezies handelt, bei der Al(III) im Kristallgitter durch Eu(III) ersetzt wird. Die geringere Aufspaltung des Emissionsspektrums spricht für eine höhere Punktsymmetrie des Eu(III) Zentrums im Vergleich zur Sorptionsspezies und die gemessene Emissionslebensdauer spiegelt die Umgebung von sechs OH Gruppen des Aluminiumplatzes im Hydrotalcitgitter wider. EXAFS Messungen der Probe konnten die Annahme, dass der überwiegende Teil des Europiums im Hydrotalcitgitter eingebaut vorliegt und dabei den Aluminumplatz belegt, bestätigen. Für Eu(III) wurde ein mittlerer Sauerstoffabstand von 2,42 Å und eine durchschnittliche Koordinationszahl von 6,9 ermittelt. Diese Werte entsprechen sehr gut denen, die, für eine Hydrotalcitstruktur bei der Aluminium durch Europium ersetzt ist, berechnet wurden. Die Kombination von Röntgenabsorptionsspektroskopie und

TRLFS erlaubte es, den Rückhaltemechanismus für dreiwertige Actiniden bzw. Lanthaniden bei der Bildung der Sekundärphase Hydrotalcit aufzuklären. Der überwiegende Teil der dreiwertigen Fremdionen (hier Eu(III)) wird bei der Kristallisation der LDH Phase unter Ausbildung einer „solid solution“ eingebaut und ersetzt in der Struktur das dreiwertige Aluminium.

Die erhaltenen Ergebnisse zum Einbau bzw. zur Sortion von Europium in bzw. an Hydrotalcit sind in der Publikation “Incorporation of Eu(III) into hydrotalcite: a TRLFS and EXAFS study” veröffentlicht.

Journal of Colloid and Interface Science 249, 119–122 (2002)
doi:10.1006/jcis.2002.8251, available online at http://www.idealibrary.com on IDEAL®

A Time-Resolved Laser Fluorescence Spectroscopy (TRLFS) Study of the Interaction of Trivalent Actinides (Cm(III)) with Calcite

Thorsten Stumpf[1] and Thomas Fanghänel

Forschungszentrum Rossendorf, Institute of Radiochemistry (IRC), P.O. Box 510119, D-01314 Dresden, Germany

E-mail: T.stumpf@fz-rossendorf.de

Received August 13, 2001; accepted January 24, 2002; published online March 26, 2002

Cm(III) interaction with calcite was investigated by time-resolved laser fluorescence spectroscopy (TRLFS) in the trace concentration range. Two different Cm(III)/calcite sorption species were found. The first Cm(III) sorption species consists of a curium ion bonded onto the calcite surface. The second Cm(III) sorption species has lost its complete hydration sphere and is incorporated into the calcite bulk structure. The Cm(III)/calcite complexes are characterized by their emission spectra (peak maxima at 607.5 and 618.0 nm) and their fluorescence emission lifetimes (314 ± 6 and 1302 ± 75 μs). © 2002 Elsevier Science (USA)

Key Words: curium; calcite; surface complexation; solid solutions; TRLFS.

INTRODUCTION

Sorption and desorption of radionuclides onto mineral surfaces is accepted to be one of the most important retardation processes in natural aquifer systems. Several studies have been performed in recent times in order to understand the interaction mechanisms of radionuclides and other metal ions on mineral surfaces (1–6). Emphasis is placed on the identification of the relevant species formed on the aqueous/mineral surface. Although the incorporation of radionuclides into the bulk structure represents another very important mechanism for their retardation, very little is known about these processes. Only a very few systematic studies for investigating the incorporation mechanisms in the trace concentration range have been performed (7–9). As a consequence these processes are in general neglected in the performance assessment of a nuclear waste repository.

Carbonates are among the most important secondary alteration products that are formed during the degradation of cement in radioactive waste repositories. More over calcite is a constituent of bentonite backfill materials, and it is an omnipresent solid phase in the geosphere.

Previous studies have shown that divalent and trivalent metal ions like Mg^{2+} (10, 11), Cd^{2+} (12–14), and Eu^{3+} (15) interact strongly with calcite surfaces and are thus efficiently removed from the aqueous phase.

It is the aim of the present work to study by time-resolved laser fluorescence spectroscopy (TRLFS) the mechanism of the Cm(III) uptake by calcite. Cm(III) was chosen as a representative for trivalent actinides and lanthanides. Its high fluorescence spectroscopy sensitivity enable speciation studies in the nanomol concentration range (22). In previous spectroscopic studies of the Cm(III) sorption onto γ-alumina (7), smectite, kaolinite (8), and silica (9) different surface-sorbed curium species have been identified. As TRLFS makes it possible also to study the hydration status of the Cm species it hence makes it possible to distinguish between surface sorption and incorporation into the lattice. This has been demonstrated for the interaction of Cm(III) with silica. Lifetime measurements show that at pH ≥ 6 curium has lost all water molecules of the primary hydration sphere and is hence incorporated into the bulk structure of the silica.

EXPERIMENTAL

A grained (≤20 μm) natural calcite from Creel/Mexico was used because of its very small impurities. The specific surface area measured by the N_2 BET method was found to be 1.8 m^2/g. The calcite samples (1 g/L) were equilibrated for one week. $NaClO_4$ solutions ($I = 0.1$ mol/L) were prepared from analytical grade chemicals as background electrolyte. Cm-248 ($t_{1/2} = 3.4 \times 10^5$ years) was used for the experiment. The stock solution consists of 97.3% Cm-248, 2.6% Cm-246, 0.04% Cm-245, 0.02% Cm-247, and 0.009% Cm-244 in 1.0 mol/L $HClO_4$. The initial curium concentration was adjusted to 8.9×10^{-8} mol/L and controlled in the starting solution by ICP mass spectroscopy. Sorption experiments were performed at room temperature in 20 ml polypropylene vials in a glove box under argon atmosphere. During the curium/calcite contact time the samples were shaken periodically. The suspension was centrifugated (15,000 rpm; 15 min), and the supernatant was measured by ICP-MS and TRLFS in order to confirm that the curium is completely sorbed onto the calcite. In the supernatant aqueous phase no curium was detectable.

[1] To whom correspondence should be addressed. Fax: (0049)351-260 3553.

0021-9797/02 $35.00
© 2002 Elsevier Science (USA)
All rights reserved.

TRLFS measurements were performed using a pulsed Nd:YAG pumped dye laser system (Continuum, Powerlite 9030, ND 6000). Details on the experimental setup are given elsewhere (17–22). The system consists of a polychromator (Chromex 250) with a 1200 lines/mm grating. The emission spectrum of Cm(III) was recorded in the range 580–620 nm, within a constant time window of 1 ms, exciting at 396.6 nm (laser dye: Exalite 398). For measuring the emission decay, the delay time between laser pulse and camera gating was scanned with time intervals of 50 μs.

RESULTS AND DISCUSSION

Spectroscopic characterization. Selected fluorescence emission spectra of Cm(III) (8.9×10^{-8} mol/L) in calcite suspension (1.0 g/L) measured at different contact times are presented in Fig. 1. All spectra show two emission bands at 607.5 nm [1] and 618.0 nm [2]. That can be assigned to two different Cm(III) species sorbed onto calcite, as there is no component at lower wavelength one would expect for aqueous Cm(III) species under the conditions of this study. With increasing contact time the fluorescence intensity of the first species [1] decreases and the intensity of the second species [2] increases. All measured spectra can be deconvoluted into two components for each of the two Cm(III) sorption species. The fluorescence emission spectra of these pure Cm(III) species are plotted in Fig. 2. For comparison the spectrum of the aqueous Cm^{3+} ion measured at pH 1.9 is given in addition in Fig. 2. In contrast to the emission maxima of sorbed Cm(III) species found in previous studies for γ-alumina, kaolinite and smectite (603.3 nm), and silica (604.9 nm) at pH > 8 the emission maximum of the first Cm(III) sorption species onto calcite appears at a higher wavelength (607.5 nm). The spectrum of this first sorption complex in the calcite system is very similar to the spectrum of the Cm(III)

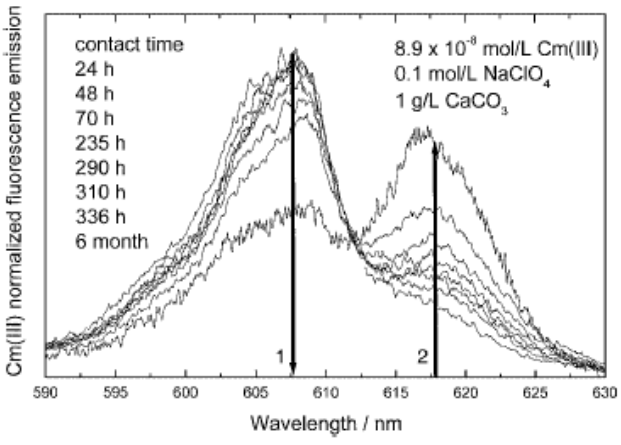

FIG. 1. Fluorescence emission spectra of 8.9×10^{-8} mol/L Cm(III) in aqueous calcite suspension at various contact times; spectra are scaled to the same peak area.

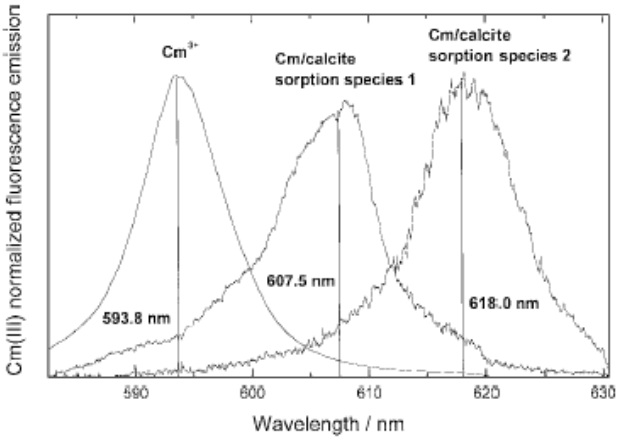

FIG. 2. Fluorescence emission spectra of Cm^{3+} aquo ion, Cm/calcite sorption species 1 and Cm/calcite sorption species 2 derived by peak deconvolution; spectra are scaled to the same peak area.

tetracarbonato complex in solution (22). However, the formation of $Cm(CO_3)_4^{5-}$ can be ruled out under the present conditions. The formation of detectable amounts of the tetracarbonato complex in solution requires orders of magnitude higher carbonate concentration ($\log[CO_3^{2-}] > -2$) as present in the calcite suspension. As both species, the first Cm(III)/calcite sorption species and the Cm(III) tetracarbonato complex in solution, show almost identical emission bands we conclude that the ligand field and hence the first coordination sphere should be very similar in both species. The unusual extraordinary red shift of the fluorescence emission of the second Cm/calcite complex with a peak maximum at 618.0 nm indicates a considerable large change of the ligand field of the actinide ion, which could be caused by a change in the coordination number of Cm(III).

Lifetime (fluorescence decay) of Cm(III). Fluorescence emission lifetime measurements have been performed in order to study the hydration status of the identified Cm(III) species. Fluorescence decay rates are caused by radiative and nonradiative processes. For the $^6D_{7/2} \rightarrow {}^8S_{7/2}$ transition of Cm(III) in 1 M $HClO_4$, the decay rate is calculated to be 770 s^{-1} (23); this corresponds to a radiative lifetime (reciprocal decay rate) of 1.3 ms. Nonradiative decay is mainly due to energy transfer from the excited state to ligand vibronics, e.g., OH vibration of co-ordinated H_2O or OH^- molecules. A lifetime of 68 ± 3 μs is determined for the Cm(III) aquo ion (24–27), while in D_2O the lifetime is increased to 1250 ± 80 μs (28), which is close to the above calculated radiative lifetime. There exists a linear correlation between the decay rate and the number of H_2O molecules in the first coordination shell of Cm(III) complexes (16). A lifetime of 68 μs, determined for the Cm(III) aquo ion, corresponds to 9 water molecules and a value of 1.3 ms corresponds to zero H_2O molecules in the first coordination shell of Cm(III).

Selected fluorescence emission spectra of one of the Cm/calcite samples measured after a contact time of 460 h at different

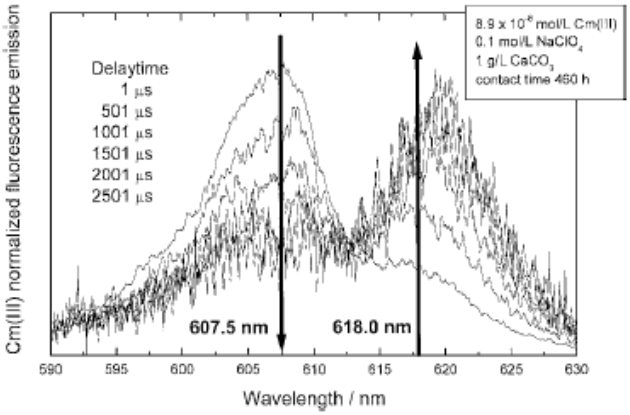

FIG. 3. Fluorescence emission spectra of Cm(III) in aqueous calcite suspension after a contact time of 460 h at different delay times.

delay times are shown in Fig. 3. By varying the delay time the ratio of the fluorescence intensities of the first and the second Cm(III) sorption species changes. With increasing delay time the fluorescence signal with the peak maximum at 607.5 nm decreases while in parallel the peak of the second Cm(III) species at 618.0 nm increases. This result indicates that the two Cm(III) species have different lifetimes. In Fig. 4 the fluorescence intensities (in logarithmic scale) are plotted as a function of the delay time. The relaxation follows a biexponential decay law. For the first Cm(III) sorption species a lifetime of $\tau = 314 \pm 6\ \mu s$ and for the second species $\tau = 1302 \pm 75\ \mu s$ have been determined. The second value is very close to the above calculated radiative lifetime for Cm(III). Hence, the excited state is not quenched by OH vibrations. It follows that the Cm(III) of the second sorption species does not contain water molecules in its first coordination sphere. Applying the linear correlation between the decay rate k_{obs} [ms^{-1}] (reciprocal lifetime of the excited state) and the number of water molecules in the first coordination sphere of the Cm(III) species

$$n(H_2O) = 0.65k_{obs} - 0.88 \quad (16)$$

it follows that the first species contains one water molecule in the first coordination sphere, while the second species has lost its complete hydration sphere. This is a clear indication for the incorporation of the Cm(III) into the bulk structure of the calcite lattice.

The biexponential decay behavior (Fig. 4) indicates that the exchange reaction rate between the different curium species is low compared to the fluorescence decay rate of the excited Cm(III) species. A high exchange reaction rate in comparison to the fluorescence decay rate causes an average lifetime of the species and the relaxing follows a mono-exponential decay law. This behavior is typical for most of the complexation reactions of Cm(III) with inorganic ligands in the aqueous phase (29). In contrast, the relatively slow exchange reaction rate found in the present study is in agreement with the expected behavior for sorption processes and in particular for the formation of solid solutions. This observation supports our model.

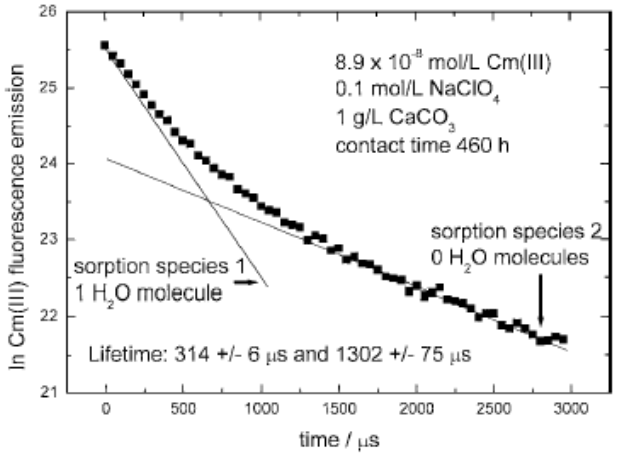

FIG. 4. Time dependency of the fluorescence emission decay of 8.9×10^{-8} mol/L Cm(III) in aqueous calcite suspension.

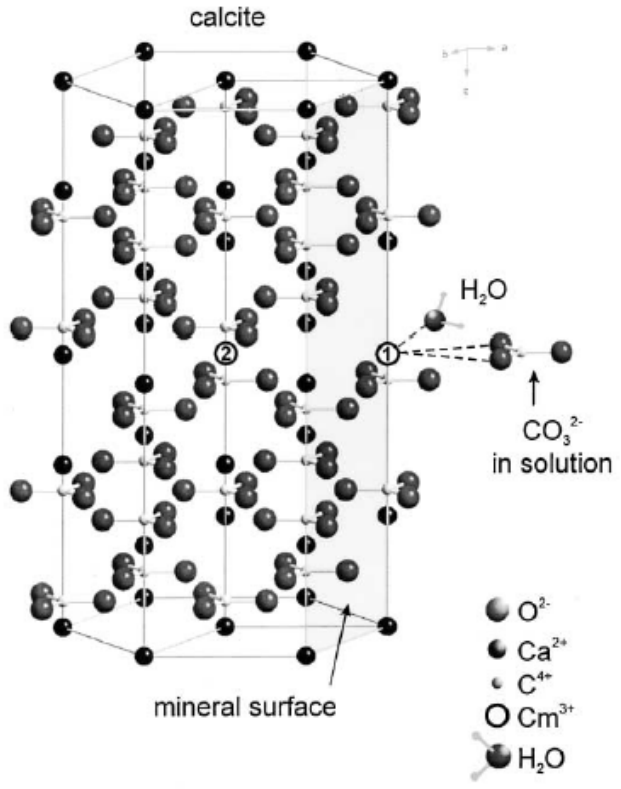

FIG. 5. Schematic diagram of the structure of the Cm(III)/calcite sorption species.

Mechanism of the sorption process. In a first step a Ca^{2+} ion of the calcite surface layer is exchanged against Cm^{3+}. The Cm^{3+} ion is surrounded by six oxygens from the carbonate of the calcite lattice and two oxygens of a surface-bonded carbonate from the aqueous phase. In addition one water molecule from the aqueous solution is bonded to the Cm(III). The coordination geometry of this Cm(III) species is in principle similar to that of a tetracarbonato complex in aqueous solution (coordination number 9) as indicated by the emission spectra and the lifetime of this species.

With increasing contact time Cm^{3+} is incorporated into the bulk mineral structure of the calcite as indicated by the formation of the second Cm(III) sorption species. Ca^{2+} in the calcite lattice is replaced by Cm^{3+}. The coordination geometry of this Cm^{3+} ion is different from that of the first surface species. The coordination number is lowered to six oxygens from the carbonates of the calcite lattice. This Cm^{3+} ion has no direct contact to water molecules of the aqueous solution. Both the large red shift of the emission spectra and the long lifetime of the excited state support this evaluated structural unit (Fig. 5).

ACKNOWLEDGMENTS

This work has been financially supported by the EC, "Aquatic Chemistry and Thermodynamics of Actinides and Fission Products Relevant to Nuclear Waste Disposal (ACTAF)—Project FIS5-1999-00157." The authors are indebted for the use of Cm-248 to the Office of Basic Energy Sciences, U.S. Department of Energy, through the transplutonium element production facilities at the Oak Ridge National Laboratory. We thank the Institute for Nuclear Waste Management (INE) at the Forschungs-zentrum Karlsruhe for their support and the supply of the laser equipment.

REFERENCES

1. Sposito, G., *in* "Geochemical Processes at Mineral Surfaces" (J. A. Davis and K. F. Hayes, Eds.), ACS Symposium Series 323, p. 217. Am. Chem. Soc. Washington, DC, 1986.
2. Geckeis, H., Klenze, R., and Kim, J. I., *Radiochim. Acta* 87, 13 (1999).
3. Rabung, Th., Geckeis, H., Kim, J. I., and Beck, H. P., *J. Colloid Interface Sci.* 208, 153 (1998).
4. Bradbury, M. H., and Baeyens, B., *J. Contam. Hydrol.* 27, 223 (1997).
5. Kosmulski, M., *J. Colloid Interface Sci.* 192, 215 (1997).
6. Nordèn, M., Ephraim, J. H., and Allard, B., *Radiochim. Acta* 65, 265 (1994).
7. Stumpf, Th., Rabung, Th., Klenze, R., Geckeis, H., and Kim, J. I., *J. Colloid Interface Sci.* 238, 219 (2001).
8. Stumpf, Th., Bauer, A., Coppin, F., and Kim, J. I., *Environ. Sci. Technol.* 35, 3691 (2001).
9. Chung, K. H., Klenze, R., Park, K. K., Paviet-Hartmann, P., and Kim, J. I., *Radiochim. Acta* 82, 215 (1998).
10. Mucci, A., and Morse, J. W., *Geochim. Cosmochim. Acta* 47, 217 (1983).
11. Dromgoole, E. L., and Walter, L. M., *Chem. Geol.* 81, 311 (1990).
12. Stipp, S. L., Hochella, Jr., M. F., Parks, G. A., and Leckie, J. O., *Geochim. Cosmochim. Acta* 56, 1941 (1992).
13. Davis, J. A., Fuller, C. C., and Cook, A. D., *Geochim. Cosmochim. Acta* 51, 1477 (1992).
14. Curti, E., *Appl. Geochem.* 14, 433 (1999).
15. Piriou, B., Fedoroff, M., Jean, J., and Bercis, L., *J. Colloid Interface Sci.* 194, 440 (1997).
16. Kimura, T., and Choppin, G. R., *J. Alloys Comp.* 213/214, 313 (1994).
17. Wimmer, H., Klenze, R., and Kim, J. I., *Radiochim. Acta* 56, 79 (1992).
18. Klenze, R., Kim, J. I., and Wimmer, H., *Radiochim. Acta* 52/53, 97 (1991).
19. Fanghänel, T., Kim, J. I., Paviet, P., Klenze, R., and Hauser, W., *Radiochim. Acta* 66/67, 81 (1994).
20. Paviet, P., Fanghänel, T., Klenze, R., and Kim, J. I., *Radiochim. Acta* 74, 99 (1996).
21. Fanghänel, T., Weger, H. T., Schubert, G., and Kim, J. I., *Radiochim. Acta* 82, 55 (1998).
22. Fanghänel, T., Weger, H. T., Könnecke, T., Neck, V., Paviet-Hartmann, P., Steinle, E., and Kim, J. I., *Radiochim. Acta* 82, 47 (1998).
23. Carnall, W. T., and Crosswhite, H. M., Report ANL-84-90 (1995).
24. Wimmer, H., Klenze, R., and Kim, J. I., *Radiochim. Acta* 56, 79 (1992).
25. Fanghänel, T., Kim, J. I., Klenze, R., and Kato, J., *J. Alloys Comp.* 225, 308 (1995).
26. Beitz, J. V., and Hessler, J. P., *Nucl. Technol.* 51, 169 (1980).
27. Beitz, J. V., Bowers, D. L., Doxtader, M. M., Maroni, V. A., and Reed, D. T., *Radiochim. Acta* 44–45, 87 (1988).
28. Fanghänel, T., unpublished results.
29. Fanghänel, T., and Kim, J. I., *J. Alloys Comp.* 271–273, 728 (1998).

Available online at www.sciencedirect.com
ScienceDirect
Journal of Colloid and Interface Science 302 (2006) 240–245
JOURNAL OF Colloid and Interface Science
www.elsevier.com/locate/jcis

Structural characterization of Am incorporated into calcite: A TRLFS and EXAFS study

T. Stumpf [a,b,*], M. Marques Fernandes [a], C. Walther [a], K. Dardenne [a], Th. Fanghänel [a,b]

[a] Forschungszentrum Karlsruhe, Institut für Nukleare Entsorgung, P.O. Box 3640, D-76021 Karlsruhe, Germany
[b] Ruprecht-Karls-Universität Heidelberg, Physikalisch-Chemisches Institut, Im Neuenheimer Feld 253, 69120 Heidelberg, Germany

Received 28 April 2006; accepted 7 June 2006
Available online 17 July 2006

Abstract

Calcite homogeneously doped with Am(III) and Cm(III) was synthesized in a mixed-flow reactor. The mechanism of incorporation of these actinides (An) into calcite was investigated by time-resolved laser fluorescence spectroscopy. Two different An(III)/calcite species were found. One has been identified as ions bonded onto the calcite surface. The second An(III) species has lost its complete hydration sphere and is incorporated into the calcite bulk structure. Both Cm(III)/calcite and Am(III)/calcite complexes have been characterized by their fluorescence emission spectra and lifetimes. Structural parameters of the incorporated Am(III) species determined by EXAFS indicate a coordination number of 6.3 ± 0.6 and distances of 2.40 ± 0.01 Å for the first Am–O shell.
© 2006 Elsevier Inc. All rights reserved.

Keywords: Americium; Curium; Calcite; Surface complexation; Solid solutions; Time-resolved laser fluorescence spectroscopy (TRLFS); Extended X-ray absorption fine structure (EXAFS)

1. Introduction

The behavior of radionuclides in the environment is to a large extent governed by heterogeneous reactions such as adsorption, ion exchange, and incorporation processes. The incorporation of actinides into secondary phases and the formation of solid solutions play a key role in the retardation process. In the literature, the interaction of radionuclides with mineral surfaces is often described by operational distribution coefficients. These distribution coefficients (K_d values) are macroscopic parameters that are valid only for the mineral and solute composition of a given system. Their application is rather limited. For this purpose, interaction mechanisms and the process of the formation of solid solutions need to be understood on a molecular level. A substantial contribution can be achieved by the application of spectroscopic methods.

Because of the reductive conditions in the environment of waste repositories in deep geologic formations, metal ions are present in their low oxidation states. Americium, which contributes to radiotoxicity to a high degree, and curium occur in the trivalent state. Even plutonium can exist in the trivalent state under reducing conditions. Time-resolved laser fluorescence spectroscopy (TRLFS) has proven to be a versatile tool for Cm(III) speciation studies (e.g., [1–4]) and for sorption studies on various solids [5–11]. It is capable of identifying different species as well as determining their hydration status [12–14], thus making it possible to distinguish whether an inner-sphere surface complex or a species incorporated into the crystal lattice of the solid is formed. The application of TRLFS to studying Am(III) is limited because of the much lower fluorescence intensity and much shorter lifetime of the Am(III) fluorescence emission in comparison to the Cm(III) emission. Nevertheless, the emission of the Am(III) $^5D_0 \rightarrow {}^7F_1$ transition was used for speciation studies of americium in aqueous solution [14–17]. Emission spectra of Am(III) incorporated into solid phases have been published by Thouvenot et al. [16] and Hubert et al. [18]. In both cases Am(III) is incorporated into a ThO_2 matrix. At low temperature (10 K), several narrow peaks between 680 and 750 nm were obtained, indicating that Am(III) occupies defined sites in the ThO_2 crystal.

* Corresponding author. Fax: +49 (0) 7247 82 3927.
E-mail address: thorsten.stumpf@ine.fzk.de (T. Stumpf).

0021-9797/$ – see front matter © 2006 Elsevier Inc. All rights reserved.
doi:10.1016/j.jcis.2006.06.010

The interaction of radionuclides with the mineral calcite ($CaCO_3$) is of interest for the long-term performance assessment of a nuclear waste repository. On one hand, calcite is omnipresent in many potential nuclear waste repository host rock formations. On the other hand, many waste repository designs include cement-based components. Taking geological timescales into account, calcite is one of the major secondary alteration products that are formed during the degradation of cement.

Limited data are available in the literature concerning rare earth element (REE) and actinide sorption/uptake by calcite. Most of these studies were performed to determine partition coefficients [19–23]. The high values of the partition coefficients found for Am(III) [24] and REE [19–23] uptake by calcite indicate that trivalent actinides and lanthanides interact very strongly with the calcite surface. However, as mentioned before, partition coefficients do not give structural information on the sorption and incorporation mechanism.

Some spectroscopic studies have been performed to get structural information about the sorption and incorporation species of REE [25–27] and Cm(III) [9] onto/into calcite. Extended X-ray absorption fine structure (EXAFS) investigations on REE-doped calcites confirmed the replacement of Ca^{2+} by lanthanide ions. It was shown that the coordination number of the lanthanide increases with increasing REE ionic radius [25]. The additional O-ligation is explained by a bidentate linkage of one carbonate group or by the loss of one OH^-/H_2O molecule out of the REE hydration shell [25,26]. Eu(III) and Cm(III) sorption onto calcite was investigated by TRLFS. Piriou et al. [27] found that a minority of the Ca^{2+} was replaced by Eu^{3+}; predominantly they observed two hydrated Eu(III) species. TRLFS investigation of the Cm(III)/calcite system [9] showed that Cm(III) is initially sorbed at the calcite surface, forming a partially hydrated Cm(III) species with one H_2O molecule in the first coordination sphere. With increasing Cm(III) calcite contact time the actinide ion was incorporated into the calcite structure, accompanied by the loss of its hydration sphere.

Beside these spectroscopic studies, Curti et al. [28] modeled the Eu(III)/calcite solid solution formation using the Gibbs energy minimization (GEM) code. Three different experimental data sets could be reproduced simultaneously only with the formation of the ternary ideal solid solution $EuH(CO_3)_2$–$EuO(OH)$–$CaCO_3$.

In this paper we discuss the structural information determined using two independent spectroscopic methods directly on a specific actinide ion (Am(III)).

2. Experimental

The Am/Cm-doped calcite crystals were synthesized using a mixed-flow reactor (MFR) under conditions similar to those used by Zhong and Mucci [19]. MFRs are particularly useful because they allow crystal growth under constant and controlled conditions (saturation state, pH, ionic strength). In a stirred MFR, the concentrations of the precipitating and co-precipitating components are expected to be constant during the experiment and a homogeneous precipitate should be obtained. Also, co-precipitation was conducted over extended periods of time (up to four weeks). The MFR was fed by three independent solutions introduced separately by a peristaltic pump (0.333 ml/min) from reservoir bottles. The input solutions were delivered from the reservoir bottles to the reactor at a constant rate so that the concentrations of the precipitating and co-precipitating components reached steady state and remained constant. The reactor had an internal volume of 45 ml. Input solutions entered and left the reactor through a 0.45-μm pore size hydrofoil Teflon membrane. Grained natural calcite was used as seed material for calcite precipitation. The specific surface area of the seed calcite measured by the N_2 BET method was found to be 2.7 $m^2\,g^{-1}$. In the case of seeded co-precipitation, it is assumed that growth occurred only on the crystallites. The following input solutions (closed system, ionic strength $I =$ 0.01 mol/L, background electrolyte $NaClO_4$) saturated with respect to calcite were used for Am/Cm(III) co-precipitation experiments: (1) $CaClO_4$, (2) an appropriate mixture of $NaHCO_3$ and Na_2CO_3, and (3) an Am-243 ($t_{1/2} = 7370$ yr) solution. The Am(III) stock solution (4.22×10^{-6} mol/L Am(III)) contains 0.1% Cm-246 in 1.0 mol/L $HClO_4$. The Am(III) concentration of the doped calcite was measured to be 9.4×10^{-6} g/g. Concentrations of calcium, sodium, and americium were analyzed by ICP-MS.

TRLFS measurements were performed using a pulsed Excimer pumped dye laser system. Details are given elsewhere [1,10,11]. The system consists of a polychromator with 300/600/1200 lines/mm grating. The fluorescence emission spectra of Cm(III) were recorded in the range 575–640 nm, within a constant time window of 1 ms, exciting at 493 and 497 nm. The Cm(III) emission decay was recorded within a constant time window of 10 ms. The delay time between laser pulse and camera gating was scanned with time intervals of 50 μs.

The fluorescence emission of Am(III) was recorded from 650 to 740 nm after excitation at 501 to 507 nm. Due to the shorter emission lifetime of Am in comparison to Cm(III), the americium decay was recorded within a constant time window of 1.44 μs. The delay time between laser pulse and camera gating was scanned with time intervals of 20 ns.

The Am(III) L3 EXAFS spectra were recorded at the INE Beamline at the ANKA synchrotron light source in Karlsruhe, Germany. For these measurements, the dried calcite microcrystallites were placed into a 400-μl polyethylene vial and mounted in the INE Beamline standard sample holder. All spectra were recorded at room temperature in fluorescence mode using a Canberra LEGe five-element solid state detector. The incoming intensity was measured using an argon-filled ionization chamber. The double-crystal monochromator was equipped with a pair of Ge⟨422⟩ crystals. The spectra were calibrated against the first derivative of the XANES spectrum of a Zr metal foil, defined as 17,998 eV. EXAFS data analysis was based on standard least-squares fit techniques [29] using the WinXAS [30] and the UWXAFS [31] program packages. The WinXAS program was used for extracting $\chi(k)$ from the absorption spectrum and the FEFFIT software for modeling data from the UWXAFS package. The ionization energy E_0, the origin for calculation of the

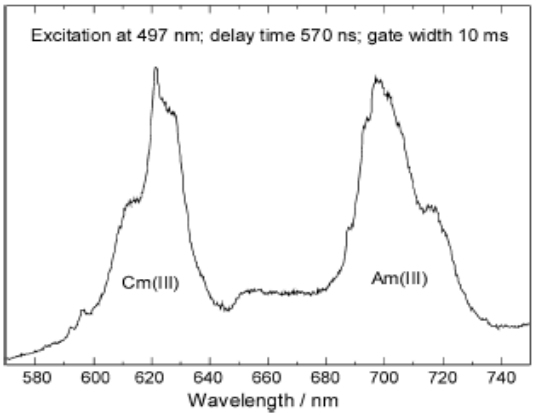

Fig. 1. Fluorescence emission spectrum of Cm(III) and Am(III) in doped calcite.

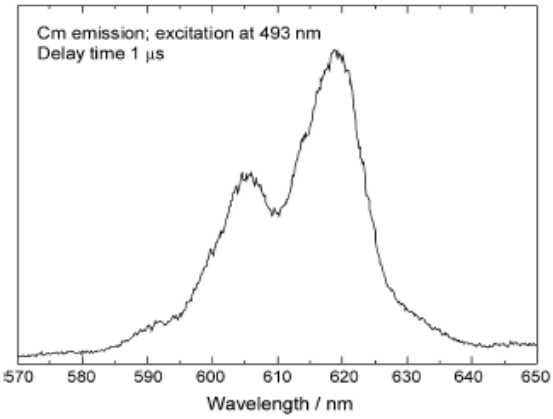

Fig. 2. Fluorescence emission spectrum of sorbed and incorporated Cm(III) in doped calcite.

$\chi(k)$-function, was fixed at the maximum of the most intense absorption feature—the white line (WL).

Theoretical back-scattering amplitude and phase functions for fitting the experimental data from the Am-doped calcite samples were calculated with the multiple scattering code FEFF8 [32] using single scattering paths. Fits were carried out in R-space between 0.5 and 2.2 Å (k range 1.5–9 Å^{-1}).

3. Results and discussion

3.1. TRLFS measurements

Using suitable laser and camera parameters (excitation wavelength 497 nm; delay time 570 ns; gate width 10 ms), we were able to observe simultaneously the Am(III) $^5D_1 \rightarrow {}^7F_1$ and the Cm(III) $^6D_{7/2} \rightarrow {}^8S_{7/2}$ transitions. Fig. 1 shows the emission spectra of Cm(III) and Am(III) in doped calcite. In Fig. 2 the emission spectrum of the Cm/calcite species is plotted in detail. Two different peak maxima at 606 and 619 nm are detected. As known from the literature, these two signals can be attributed to different Cm/calcite species [9,33]. The peak at lower wavelength belongs to a surface-sorbed actinide compound, whereas the strongly red-shifted peak (619 nm) can be attributed to a curium ion that is incorporated into the calcite lattice. The signal intensities show that the major part of the actinide is incorporated into the calcite bulk structure. The decay of the Cm(III) fluorescence emission upon excitation of the P-state at 493 nm (Fig. 3) supports these findings. Biexponential decay behavior is observed. The two calculated lifetimes are 408 ± 10 and 1941 ± 25 μs. These values are in good agreement with the mean fluorescence emission lifetimes found for Cm(III) that is sorbed (386 ± 40 μs) and that is incorporated (1874 ± 200 μs) into the calcite frame [9,32]. Applying the linear correlation between the decay rate k_{obs} [ms^{-1}] (reciprocal lifetime of the excited state) and the number of water molecules in the first coordination sphere of the Cm(III) species,

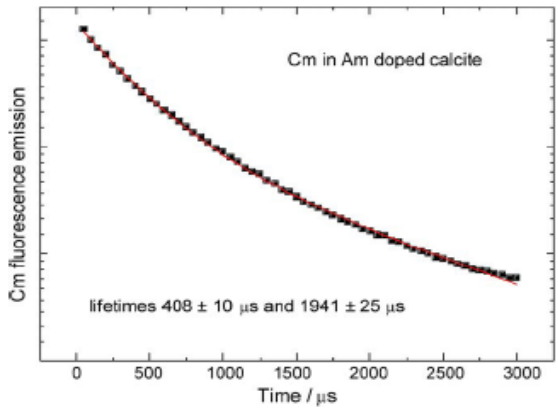

Fig. 3. Time dependence of Cm(III) fluorescence emission decay in doped calcite. Biexponential decay behavior is obtained with lifetimes $t_1 = 408 \pm 10$ μs and $t_2 = 1941 \pm 25$ μs, suggesting the presence of both sorbed and incorporated Cm(III).

$$n(H_2O) = 0.65k_{obs} - 0.88,$$

developed by Kimura and Choppin [13], it follows that the first species contains one water molecule in the first coordination sphere, while the second species has lost its complete hydration sphere.

From 670 to 730 nm the Am(III) fluorescence emission can be observed. To distinguish between surface-sorbed and incorporated americium, the doped calcite was cooled down to 18 K. At this low temperature, structurally incorporated Am(III) should show a crystal field splitting, accompanied by a strong narrowing of the emission bands. In contrast, the influence of temperature on the fluorescence signal of the surface sorbed actinide species should be negligible, since the orientation according to the calcite crystal structure of the sorbed and within partly hydrated Am(III) should be highly

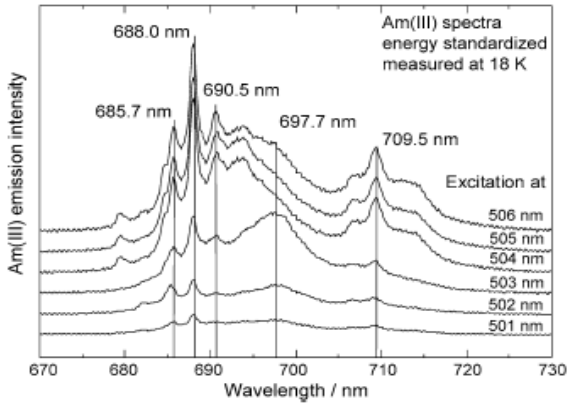

Fig. 4. Fluorescence emission spectrum of Am(III) in doped calcite at various excitation wavelengths. Measurements were done at 18 K.

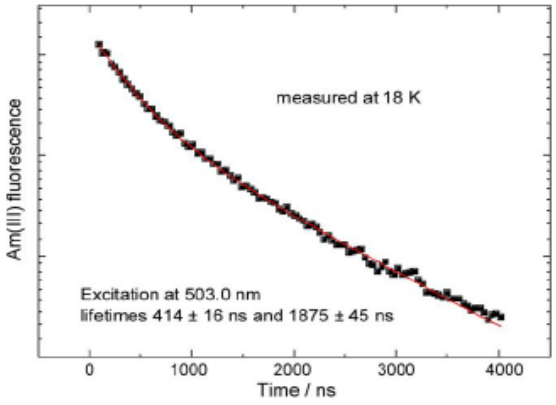

Fig. 5. Time dependence of Am(III) fluorescence emission decay in doped calcite. Biexponential decay behavior is obtained with lifetimes $t_1 = 414 \pm 16$ ns and $t_2 = 1875 \pm 45$ ns, suggesting the presence of both sorbed and incorporated Am(III).

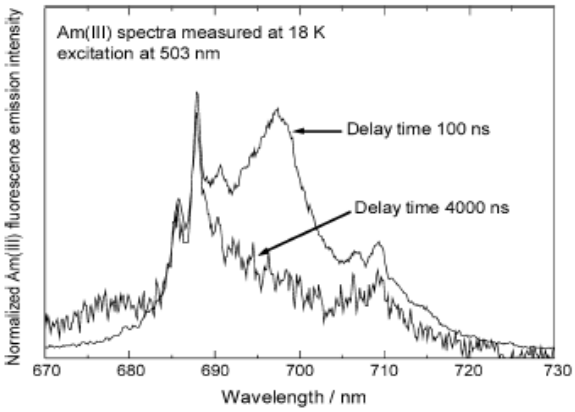

Fig. 6. Fluorescence emission spectra of Am(III) in doped calcite at different delay times. The spectra are scaled to the same peak area.

disordered. Fig. 4 shows Am(III) fluorescence emission spectra of the doped calcite measured at 18 K. The spectra differ with the variation of the excitation wavelength, indicating that different Am/calcite species exist. In all spectra peak maxima at 685.7, 688.0, and 709.5 nm are observed. The intensity of these signals increases with increasing excitation wavelength. At 503 nm a further emission peak at 690.5 nm appears, which becomes more pronounced at higher excitation wavelengths. The four signals are sharp and show a full width at half maximum of ~1 nm. These narrow peaks can be attributed to Am(III) species, which have a well-defined orientation according to the calcite crystal structure. Hence, we suggest that these signals belong to Am(III) that is incorporated into the calcite bulk structure. When the actinide ion is excited at 503 nm, another broad peak at 697.7 nm appears (full width at half maximum ~5 nm). We suggest that this peak belongs to an Am(III) species that is sorbed onto the calcite surface.

The decay of the Am(III) fluorescence emission was measured for different excitation wavelengths. In all cases the decay behavior was biexponential. As a representative illustration, the emission decay after excitation at 503 nm is shown in Fig. 5. The measured lifetimes are 414 ± 16 and 1875 ± 45 ns. Two normalized spectra measured at different delay times are plotted in Fig. 6. At a delay time of 100 ns the emission peak at 697.7 nm is very pronounced, whereas this signal is almost absent after a delay time of 4000 ns. In contrast, the strong peak with a peak maximum at 688 nm is clearly observable in both spectra measured after short and long delay times. These findings indicate that the shorter lifetime belongs to the sorbed Am/calcite species and that the long lifetime can be attributed to the incorporated actinide ion.

In summary, TRLFS investigations on two trivalent actinides, Cm(III) and Am(III), in one doped calcite led to the suggestion that the major part of the actinide is incorporated into the calcite bulk structure. To get additional information about the structural parameters of this incorporated species, Am(III) EXAFS measurements with this doped calcite were done.

3.2. EXAFS measurements

The Fourier transform (FT) of the k^2-weighted EXAFS function is shown in Fig. 7, together with the k^2-weighted EXAFS. R-space fit results are depicted as symbols. The FT spectrum exhibits a single low-R peak at $R - \Delta$ near 1.8 Å, which can be modeled as a single oxygen shell ($N = 6.3 \pm 0.6$ O at 2.40 ± 0.01 Å); see Table 1. This coordination number is much lower than the N that is found for the Am^{3+} aquo ion (8–9 oxygen atoms) and for Am sorbed onto mineral surfaces [34]. In the case of Am(III) sorbed onto clay minerals such as smectite and kaolinite, the coordination number is found to be between 7 and 9. Furthermore, the Am–O distance measured for Am in

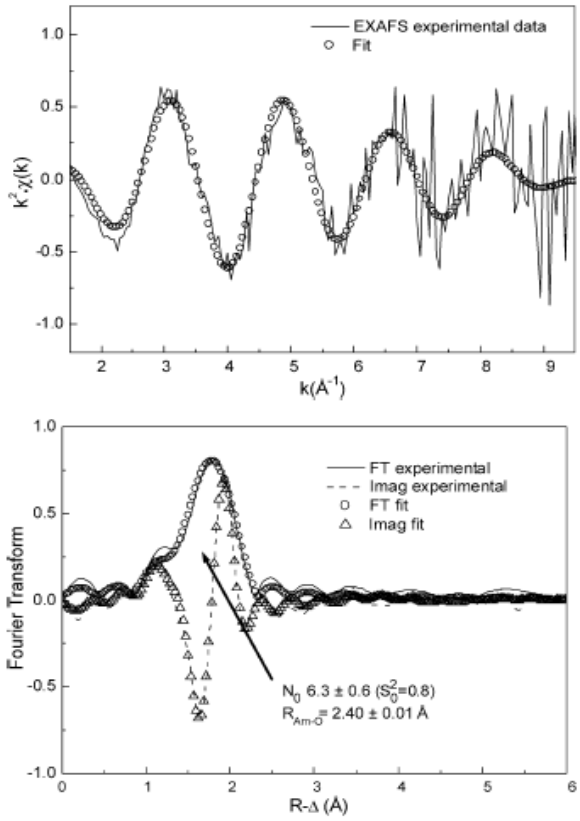

Fig. 7. L_{III}-edge k^2-weighted EXAFS spectra and corresponding FT of Am(III) in doped calcite (solid line—experiment; dotted line—theoretical fit results from fits to $\chi(k)$ as described in the text).

calcite is significantly shorter than the distance that is found for $Am(H_2O)_{8-9}$ (2.49 Å) and that was detected for the Am/clay sorption species (2.47–2.49 Å). No shell splitting, as might be expected from the different TRLFS species, is observed. As is known from the TRLFS data, the incorporated Am/calcite species is the predominant component in the system. We suggest that the signal of the Am/calcite sorption species is covered by the EXAFS signal of the dominating Am/calcite incorporation species. Furthermore, there is no Am–Am interaction, excluding the presence of separate Am mineral phases. The Am–O distance differs slightly from the Ca–O distance (2.36 Å) in calcite but is in good agreement with structural parameters obtained in EXAFS studies on rare-earth-element-doped calcite [25,26].

In summary, Am(III) TRLFS and EXAFS measurements of an actinide-doped calcite show that americium is incorporated into the calcite bulk structure. A "solid solution" is formed and the structural parameters indicate that Am(III) replaces Ca(II) in the calcite lattice. This result was confirmed by analyzing the fluorescence emission of Cm(III) in the same sample.

Table 1
Results of the fits to the EXAFS data

Sample	Shell	S_0^2	N	R [Å]	σ^2 [10^{-3} Å^2]	ΔE_0 [eV]	R-factor [%]
$Am(III)_{aq}$	O	0.8	9[a]	2.47(1)	6.3	−2.2	1.4
Am(III) in doped calcite	O	0.8[a]	6.3(6)	2.40(1)	6.6	−2.5	0.9

[a] Fixed.

Acknowledgments

We gratefully acknowledge the assistance of Annick Froideval during the EXAFS measurements. Thanks to Dirk Bosbach and Felix Brandt for fruitful discussions and for making the flow-through reactor available. This work was financed by the Helmholtz Gemeinschaft Deutscher Forschungszentren (HGF) by supporting the Helmholtz-Hochschul-Nachwuchsgruppe "Aufklärung geochemischer Reaktionsmechanismen an der Wasser/Mineralphasen Grenzfläche."

References

[1] H. Wimmer, R. Klenze, J.I. Kim, Radiochim. Acta 56 (1992) 79.
[2] V. Moulin, J. Tits, C. Moulin, P. Decambox, P. Mauchien, O. De Ruty, Radiochim. Acta 58/59 (1992) 121.
[3] Th. Fanghänel, J.I. Kim, P. Pavie, R. Klenze, W. Hauser, Radiochim. Acta 66/67 (1994) 81.
[4] Th. Fanghänel, J.I. Kim, J. Alloys Compd. 271–273 (1998) 728.
[5] K.H. Chung, R. Klenze, K.K. Park, P. Paviet-Hartmann, J.I. Kim, Radiochim. Acta 82 (1998) 215.
[6] T. Rabung, T. Stumpf, H. Geckeis, R. Klenze, J.I. Kim, Radiochim. Acta 88 (2000) 711.
[7] T. Stumpf, T. Rabung, R. Klenze, H. Geckeis, J.I. Kim, J. Colloid Interface Sci. 238 (2001) 219.
[8] T. Stumpf, A. Bauer, F. Coppin, J.I. Kim, Environ. Sci. Technol. 35 (2001) 3691.
[9] T. Stumpf, Th. Fanghänel, J. Colloid Interface Sci. 249 (2002) 119.
[10] J. Tits, T. Stumpf, T. Rabung, E. Wieland, Th. Fanghänel, Environ. Sci. Technol. 37 (2003) 3568.
[11] T. Stumpf, J. Tits, C. Walther, E. Wieland, Th. Fanghänel, J. Colloid Interface Sci. 276 (2004) 118.
[12] W. DeW Horrocks, D.R. Sudnick, J. Am. Chem. Soc. 101 (1979) 334.
[13] T. Kimura, G.R. Choppin, J. Alloys Compd. 213/214 (1994) 313.
[14] J.V. Beitz, G. Jursich, G. Sullivan, J. Less. Comm. Met. 126 (1986) 301.
[15] A.B. Yusov, J. Radioanal. Nucl. Chem. 143 (1990) 287.
[16] P. Thouvenot, S. Hubert, C. Moulin, P. Decambox, P. Mauchien, Radiochim. Acta 61 (1993) 15.
[17] T. Kimura, Y. Kato, J. Alloys Compd. 271–273 (1998) 867.
[18] S. Hubert, P. Thouvenot, N. Edelstein, Phys. Rev. B 48 (1993) 5751.
[19] S.J. Zhong, A. Mucci, Geochim. Cosmochim. Acta 59 (1995) 443.
[20] Y. Terakado, A. Masuda, Chem. Geol. 69 (1988) 103.
[21] S.L.S. Stipp, L.Z. Lakshtanov, J.T. Jensen, J.A. Baker, J. Contaminant Hydrol. 61 (2003) 33.
[22] L.Z. Lakshtanov, S.L.S. Stipp, Geochim. Cosmochim. Acta 68 (2004) 819.
[23] E. Curti, Appl. Geochem. 14 (1999) 433.
[24] P.M. Shanbhag, J.W. Morse, Geochim. Cosmochim. Acta 46 (1982) 241.
[25] E.J. Elzinga, R.J. Reeder, S.H. Withers, R.E. Peale, R.A. Mason, K.M. Beck, W.P. Hess, Geochim. Cosmochim. Acta 66 (2002) 2875.
[26] S. H Withers, R.E. Peale, A.F. Schulte, G. Braunstein, K.M. Beck, W.P. Hess, R.J. Reeder, Phys. Chem. Miner. 30 (2003) 448.
[27] B. Piriou, M. Fedoroff, J. Jeanjean, L. Bercis, J. Colloid Interface Sci. 194 (1997) 447.
[28] E. Curti, D.A. Kulik, J. Tits, Geochim. Cosmochim. Acta 69 (2005) 1721.

[29] D.E. Sayers, B.A. Bunker, in: D.C. Koningsberger, R. Prins (Eds.), X-Ray Absorption: Techniques of EXAFS, SEXAFS and XANES, Wiley & Sons, New York, 1988, pp. 211–253.
[30] T. Ressler, J. Phys. IV 7-C2 (1997) 269.
[31] E.A. Stern, M. Newville, B. Ravel, Y. Yacoby, D. Haskel, Physica B 208/209 (1995) 117.
[32] L.A. Ankudinov, B. Ravel, J.J. Rehr, S.D. Conradson, Phys. Rev. B 58 (1998) 7565.
[33] M. Marques Fernandes, T. Stumpf, T. Rabung, D. Bosbach, Th. Fanghänel, Geochim. Cosmochim. Acta, submitted for publication.
[34] T. Stumpf, C. Hennig, A. Bauer, M.A. Denecke, Th. Fanghänel, Radiochim. Acta 92 (2004) 133.

Environ. Sci. Technol. **2003**, *37*, 3568−3573

Uptake of Cm(III) and Eu(III) by Calcium Silicate Hydrates: A Solution Chemistry and Time-Resolved Laser Fluorescence Spectroscopy Study

JAN TITS,[†] THORSTEN STUMPF,*[,‡,§] THOMAS RABUNG,[§] ERICH WIELAND,[†] AND THOMAS FANGHÄNEL[§]

Paul Scherrer Institute, Waste Management Laboratory, CH-5232 Villigen-PSI, Switzerland, Forschungszentrum Rossendorf, Institut für Radiochemie, P.O. Box 510119, D-01314 Dresden, Germany, and Forschungszentrum Karlsruhe, Institut für Nukleare Entsorgung, P.O. Box 3640, D-76021 Karlsruhe, Germany

The interaction of the two chemical homologues [Cm(III) and Eu(III)] with calcium silicate hydrates (CSH phases) at pH 13.3 has been investigated in batch-type sorption studies using Eu(III) and complemented with time-resolved laser fluorescence spectroscopy (TRLFS) using Cm(III). The sorption data for Eu(III) reveal fast sorption kinetics and a strong uptake by CSH phases with distribution ratios of $(6 \pm 3) \times 10^5$ L kg^{-1}. Three different Cm(III) species have been identified: A nonfluorescing species, which was identified as a curium hydroxide (surface) precipitate, and two fluorescing Cm(III)/CSH-sorbed species. The fluorescing sorbed species have characteristic emission spectra with main peak maxima at 618.9 and 620.9 nm and fluorescence emission lifetimes of 289 ± 11 and 1482 ± 200 μs, respectively. From the fluorescence lifetimes, it was calculated that the two fluorescing Cm(III) species have one or two and no water molecules left in their first coordination sphere, suggesting that these species are incorporated into the CSH structure. A structural model for Cm(III) and Eu(III) incorporation into CSH phases is proposed based on the substitution for Ca at two different types of sites in the CSH structure.

Introduction

Cementitious materials are commonly used worldwide for the immobilization of low and intermediate level (L/ILW) radioactive waste. In a (L/ILW) nuclear waste repository, the immobilization of radionuclides by cementitious materials takes place both in the waste containers and in the construction materials, such as backfill, liners, etc. A large number of studies have demonstrated the waste loading potential of cement materials and their performance in leaching tests (e.g., see reviews in refs *1*−*4*). However, the chemical mechanisms governing radionuclide immobilization are not well understood. A mechanistic understanding of the underlying chemical processes is necessary for the long-term performance assessment of a nuclear waste repository.

Hardened cement paste (HCP) is a complex mixture of different phases. The immobilization potential of HCP originates from the selective binding properties of these phases for metal cation and anion species. Calcium aluminates (e.g., ettringite or monosulfate) and calcium silicate hydrates (CSH phases) are considered to be among the most important phases governing immobilization processes because of their abundance and appropriate structures for cation and anion binding (e.g., refs *3* and *4*).

The chemical conditions in a cementitious environment are controlled by the interaction of HCP with groundwater resulting in the degradation of HCP. The first phase of HCP degradation is characterized by the dissolution of the alkali oxides in the cement resulting in a pH of approximately 13.3 and Na and K concentrations of approximately 0.11 and 0.18 M, respectively.

The objective of this study is to investigate the interaction of trivalent actinides and their analogues with CSH phases under conditions relevant to a cementitious repository for radioactive waste by combining macroscopic information from batch sorption experiments and molecular level spectroscopic information using time-resolved laser fluorescence spectroscopy (TRLFS).

Cm(III) was chosen as a representative of the trivalent actinides because its fluorescence spectroscopic sensitivity allows sorbed species to be studied on a molecular level at very low concentrations. TRLFS has been proven to be a versatile tool for Cm(III) speciation studies (*5*−*9*) and for sorption studies on various solids (*10*−*14*). It is capable of identifying different species as well as determining their hydration status (*15*), thus allowing outer- and inner-sphere surface complexes and species incorporated in the crystal lattice of the solid to be distinguished.

Eu(III) was used as an analogue for the trivalent actinides in the wet chemistry studies. On the basis of the similarities in the complexation behavior of trivalent lanthanides and actinides with comparable ionic radius (*16*), it is anticipated that Eu(III) is a suitable analogue for Cm(III).

Experimental Section

Materials. Solutions were prepared from reagent-grade chemicals in deionized water. All experiments were performed in an artificial cement pore water (ACW) simulating the chemical conditions during the first phase of the HCP degradation. The ACW contained 0.18 M KOH and 0.114 M NaOH and had a pH of 13.3. The Ca and Si concentrations in this pore water were fixed at levels such that the solution was in equilibrium with the CSH phase.

An acidic radionuclide solution of ^{152}Eu was purchased from Amersham International Plc. This ^{152}Eu solution was diluted in 50 mL of 5% HCl to obtain a stock solution with an Eu(III) concentration of 2×10^{-6} M. The ^{248}Cm ($t_{1/2} = 3.4 \times 10^5$ yr) stock solution had a concentration of 2.36×10^{-4} M and was prepared in 1.0 M $HClO_4$.

CSH phases were prepared using the so-called "direct reaction" method (*17*). CSH preparation was carried out in a glovebox under N_2 atmosphere. AEROSIL 300 (SiO_2) was mixed with CaO in polyethylene centrifuge tubes to give a target Ca/Si weight ratio (C:S) of 1.0. To this, ACW was added to obtain a solid to liquid (S:L) ratio of 24 g L^{-1}. After an aging period of 4 weeks, the slurries were filtered through Whatman

* Corresponding author phone: +49 7247-826023; fax: +49 7247-82 3927; e-mail: Thorsten.Stumpf@ine.fzk.de.
† Paul Scherrer Institute.
‡ Institut für Radiochemie.
§ Institut für Nukleare Entsorgung.

10.1021/es030020b CCC: $25.00 © 2003 American Chemical Society
Published on Web 07/04/2003

ashless 541-grade filter paper using a Buchner funnel with vacuum pump. The supernatant solution was analyzed to obtain the Na, K, Ca, and Si concentrations. The solid material was then resuspended in fresh ACW and equilibrated for a further week. The filtration and resuspension procedures were repeated until the Na and K concentrations in the filtrate were identical to their respective concentrations in fresh ACW. The CSH phase is then in equilibrium with ACW. In preparation of the drying step, the slurries were washed with Milli-Q water to remove the remaining NaOH and KOH. The contact time of the slurries with Milli-Q water was kept as short as possible (i.e., less than 1 min to minimize changes in composition).

In a few experiments, a CSH phase supplied by the University of Aberdeen was used. This CSH phase was prepared in Milli-Q water and afterwards conditioned with ACW. After being conditioned, the Ca:Si ratio was determined to be 1.09. The CSH phase prepared "in house" will be denoted as CSHa, and the CSH phase from Aberdeen will be denoted as CSHb. The CSH phases were dried to constant weight in a desiccator over a saturated $CaCl_2$ solution, which maintains a relative humidity of 30%.

Methods. Sorption values for ^{152}Eu were determined using the batch technique. All experiments were carried out at 25 $\pm$ 1 °C in gloveboxes under N_2 atmosphere. CSH suspensions were prepared by mixing a quantity of fresh CSHa or CSHb from the desiccator with 1 L of synthetic CSH solution. The composition of this solution is based upon the chemical analysis of the last filtrate obtained during conditioning of the CSH phase with ACW (see Materials). A total of 40 mL of the preequilibrated suspensions was transferred into centrifuge tubes, and an aliquot of the radionuclide solution was added. The suspensions were then equilibrated on an end-over-end shaker for a given period of time depending on the type of experiment. Experiments were performed in duplicate or triplicate. Phase separation was carried out by centrifugation (1 h at 95000*g*). The concentrations of the radionuclides in the suspension and in the equilibrium solution were assayed with a Canberra Packard Tri-Carb 2250CA liquid scintillation counter using an energy window between 6 and 70 keV.

The sorption data are presented in terms of a distribution ratio, R_d (L kg^{-1}), relating the quantity of radionuclide sorbed (mol kg^{-1}) to the equilibrium radionuclide concentration in solution (M). The difference in concentration between the total activity in the suspension and the activity in the supernatant solution after centrifugation was taken as a measure of the tracer activity on the solid. In this manner, artifacts due to wall sorption effects were avoided. TRLFS measurements were performed as described by Stumpf et al. (*18*).

For the spectroscopic studies conducted at low temperature, 180 μL of the Cm(III)/CSH suspension was transferred into an in-house constructed copper cell (total cell volume of 200 μL) with a sapphire window sealed with a Teflon disk. The cooling system (Cryodyne Cryocooler model 22C, compressor 8200, CTI-Cryogenics, USA) uses helium as the refrigerant and allows continuous closed-cycle cooling of the copper sample holder at the cold head down to about 10 K in a two-stage decompression step. The cold head with the sample holder was surrounded by a vacuum chamber with four quartz glass windows. The pressure at low temperatures was in the range between 10^{-4} and 10^{-5} mbar. An auto-tuning controller (model 330-1X, Lake Shore, USA) with a silicon dioxide sensor was used for temperature control. All temperatures between 10 and 370 K can be adjusted using the heater. For sample excitation, the laser beam was focused on the copper cell in the vacuum chamber. The fluorescence signal was collected via a quartz fiber and directed into the monochromator.

In a series of preliminary tests, the fluorescence behavior of aqueous Cm(III) under highly alkaline conditions was studied. In one experiment, 15 μL of Cm(III) stock solution was added to 2 mL of 0.1 N NaOH in a quartz cuvette to obtain a total Cm(III) concentration of 2×10^{-6} M, and the Cm(III) fluorescence emission spectrum was recorded. The solution was decanted, and the quartz cuvette was filled with 2 mL of 1 M $HClO_4$. The decanted Cm(III) solution was acidified with 2 mL of 1 M $HClO_4$. Fluorescence emission spectra of both acidic solutions were recorded as well. In a second experiment, 10 μL of Cm(III) stock solution was mixed with 0.25 mL of a 0.5 M Gd(III) solution in 2.75 mL of 1 M $HClO_4$ and in 2.75 mL of 1 M NaOH, respectively. Fluorescence emission spectra of Cm(III) in both systems were recorded. The final Cm(III) and Gd(III) concentrations in these solutions were 8×10^{-7} and 0.042 M, respectively.

For the TRLFS investigations of the Cm(III) sorption on CSH phases, CSHa suspensions were prepared as described above. Sample preparation was carried out in a glovebox under Ar atmosphere. An aliquot of Cm(III) stock solution was added to the CSH suspensions to obtain a total Cm(III) concentration of 10^{-7} M. The suspensions were then equilibrated for a given period of time depending on the type of experiment. The samples were shaken periodically during equilibration. At chosen time intervals, Cm(III) emission spectra were recorded. In addition, one of the parallel samples was centrifuged (15000 rpm; 15 min), and the supernatant was measured by ICP-MS and TRLFS in order to check whether Cm(III) was completely sorbed onto the CSH phase. Cm(III) concentrations in the supernatant were found to be below the detection limit ($\sim 4 \times 10^{-10}$ M).

Results

Sorption Kinetics. Eu(III) sorption kinetics were studied on CSHa and CSHb at S:L ratios (based on the dry weight) of 3.8 $\times$ 10^{-4} and 5.4 $\times$ 10^{-3} kg L^{-1}, respectively, and a total Eu(III) concentration of 2×10^{-9} M. The results indicate fast sorption kinetics. Steady state was reached within 1 d; R_d values were found to remain constant over a time period of 90 d. Relatively high distribution ratios [$R_d = (6.0 \pm 3) \times 10^5$ L kg^{-1}] identical for the two CSH phases were determined. The uncertainty on the experimental data was determined from the evaluation of a series of 10 replicates of a typical sorption test. The resulting relative uncertainty of 60% on the R_d value and 40% on the equilibrium concentration was applied to all sorption data. The high uncertainty of the measured R_d values presumably originates from the extremely strong sorption of Eu(III) on the CSH phases; therefore, incomplete phase separation (e.g., colloidal material remaining in solution or partial resuspension after centrifugation by accidental shaking) may have a significant effect on the measured concentration in the supernatant.

The measurement of the Eu(III) concentration in the suspension before centrifugation allows an evaluation of the fraction sorbed onto the walls of the centrifuge tubes. The measurements indicated that this fraction was negligible (below 1%) in the experiments.

Sorption Isotherm. An Eu(III) sorption isotherm was determined for CSHb at a S:L ratio of 5×10^{-4} kg L^{-1} and an equilibration time of 1 week. The total Eu(III) concentration in the experiments was varied between 10^{-10} and 7×10^{-7} M. The data are shown in Figure 1. The isotherm was found to be linear over the entire concentration range investigated (least-squares analysis yielded a slope for the log–log plot of 1.05 $\pm$ 0.06).

Spectroscopic Characterization of Alkaline Cm(III) Solutions. A 2×10^{-6} M Cm(III) solution in 0.1 M NaOH did not show any fluorescence signal (Figure 2). Note that this solution is strongly oversaturated with respect to $Cm(OH)_3$(s). The acidic solution used to rinse the cuvette

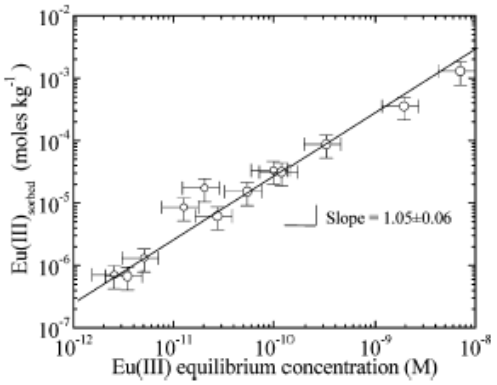

FIGURE 1. Eu(III) sorption isotherm on CSHb. The S:L ratio was 5.0 × 10^{-4} kg L^{-1}. The equilibration time was 1 week.

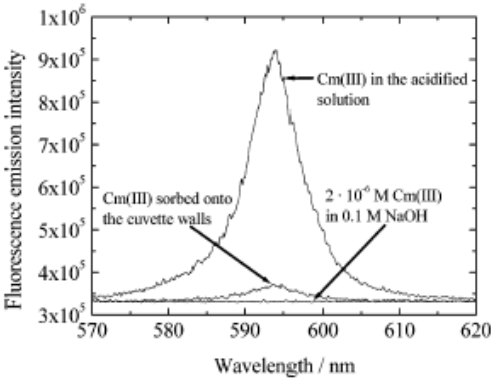

FIGURE 2. Characterization of the behavior of 5 × 10^{-7} M Cm(III) in a quartz cuvette. Fluorescence emission spectra of Cm(III) in a 0.1 M NaOH solution, of Cm(III) in an 1 M $HClO_4$ used to wash the cuvette after decanting the original alkaline solution, and of Cm(III) after acidifying the original alkaline solution with 1 M $HClO_4$.

after decanting the original solution revealed only a small fluorescence signal, indicating that only a small fraction of the Cm(III) was sorbed on the cuvette walls. When the original alkaline Cm(III) solution was acidified, an intense fluorescence signal was observed, suggesting that in the original alkaline solution all Cm(III) was present in solution as nonfluorescing species.

Mixing 8 × 10^{-7} M Cm(III) with 0.042 M Gd(III), a nonfluorescing homologue of Cm(III), in 1 M $HClO_4$ gave a fluorescence emission spectrum with a peak maximum at 593.8 nm characteristic for the Cm(III) aquo ion (*6*) (Figure 3). When 8 × 10^{-7} M Cm(III) was mixed with 0.042 M Gd(III) in 1 M NaOH, a red-shift to a peak maximum at 607.1 nm was observed in the fluorescence emission spectrum. Under these conditions, Cm(III) is assumed to coprecipitate with $Gd(OH)_3$(s). The differences in the emission intensity between the two spectra are the result of light absorption in the weak-milky suspension at high pH. The fluorescence emission lifetimes were found to be 68 ± 1 μs for the acidic Cm(III)/Gd(III) solution and 56 ± 2 μs for the alkaline Cm(III)/Gd(III) solution.

Spectroscopic Characterization of Cm(III) in CSH Suspensions in ACW at pH 13.3. Selected fluorescence emission spectra of Cm(III) (1 × 10^{-7} M) in CSH suspension (5.0 × 10^{-5} kg L^{-1}) measured at different contact times are shown

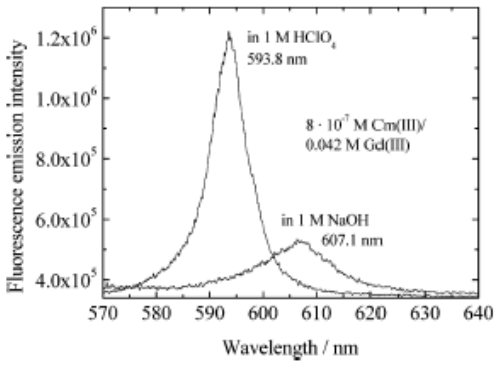

FIGURE 3. Fluorescence emission spectra of a solution containing 8 × 10^{-7} M Cm(III) mixed with 0.042 M Gd(III) in 1 M $HClO_4$ and in 1 M NaOH.

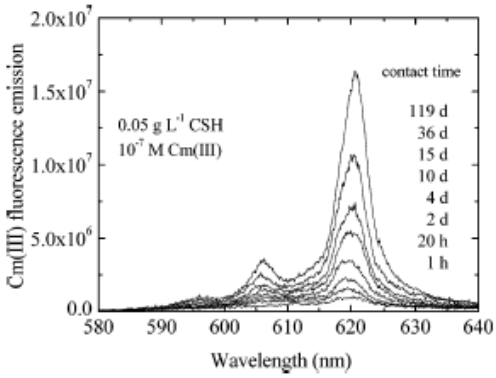

FIGURE 4. Fluorescence emission spectra of 10^{-7} M Cm(III) in CSH suspension (0.05 g L^{-1}) measured at different Cm(III)/CSH contact times.

in Figure 4. Two different peak maxima at ~606.0 and ~620 nm appear in the spectra. Similar spectra were observed for 1 × 10^{-7} M Cm(III) and a different S:L ratio of 5 × 10^{-4} kg L^{-1} CSH suspension. The intensity of the Cm(III) fluorescence emission spectra increased with increasing contact time between Cm(III) and CSH phases.

In all spectra, a peak with a maximum at ~606.0 nm was observed. Its position and intensity ratio with respect to the main peak does not change with increasing Cm(III)/CSH contact time. A Cm(III) emission spectrum of a system containing 10^{-7} M Cm(III) and 10^{-4} kg L^{-1} CSH was recorded at a temperature of 20 K and compared with spectra of the same system obtained at 298 K. The peak at 606.0 nm present in the latter spectra was not detected in the spectrum at 20 K (Figure 5). Therefore, it was concluded that this peak is the result of visible transitions of thermally populated states at room temperature and has no chemical relevance. This conclusion is confirmed by the following theoretical considerations.

The difference in energy between 606 and 620 nm is 370 cm^{-1}. This value is of the same order of magnitude as the thermal energy (kT) at 298 K (207 cm^{-1}). According to the Maxwell−Boltzmann equation:

$$\frac{N_a}{N} = e^{-E_a/kT} \quad (1)$$

with N_a as the number of atoms with the energy E_a, N as the

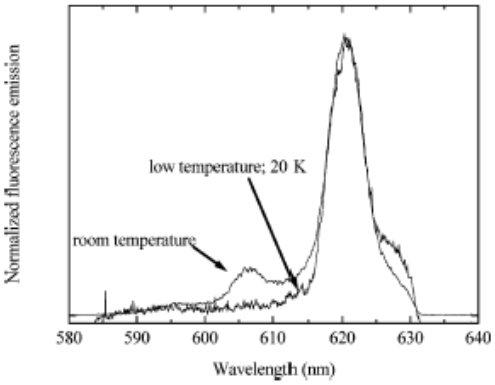

FIGURE 5. Emission spectra of 10^{-7} M Cm(III) CSH suspension (0.1 g L^{-1}) after a contact time of 10 month obtained at 20 and 298 K showing the absence of the peak maximum at 606.0 nm at low temperature. The spectra were scaled to the same peak height.

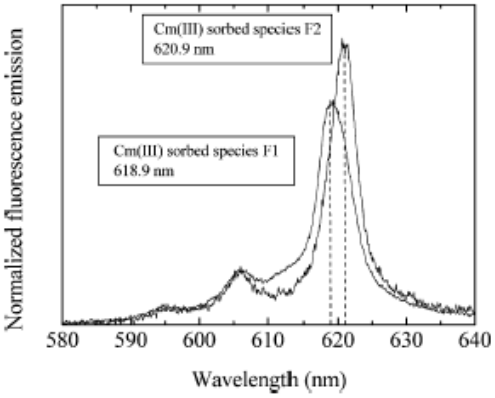

FIGURE 6. Fluorescence emission spectra of the fluorescing Cm(III) sorbed species F1 and F2 as derived by peak deconvolution. The spectra were scaled to the same peak area.

total number of atoms, and k as the Boltzmann constant, 17% of the Cm(III) atoms should possess the energy to occupy the transition state at 606 nm. A comparison of the peak areas of the two signals at 606 and 620 nm showed that the peak with a maximum at 606 nm has 17.1% of the total fluorescence emission intensity. This calculation supports the conclusion that the peak with the maximum at 606 nm belongs to a hot band; hence, in further analysis of the spectra this peak will be treated as a part of the background of all measured spectra. This peak was not observed in the spectra of alkaline or acidic Cm(III) solutions because it disappears behind the peak of the Cm(III) aquo ion or the $Cm(OH)_3$ peak.

To determine the number of Cm(III) species and quantify their concentrations, a factor analysis was performed using the set of spectra at different contact times and the procedure described by Rossberg et al. (*19*). Two different fluorescing Cm(III) species were identified with peak maxima at 618.9 nm (F1) and 620.9 nm (F2) (Figure 6). The batch sorption experiments with Eu(III) showed that under the present experimental conditions more than 99% of the Cm(III) is sorbed on the CSH phases. Hence the two Cm(III) species identified with TRLFS must be sorbed species.

Lifetime (Fluorescence Decay) of Cm(III) in CSH Suspensions. The fluorescence lifetime provides information

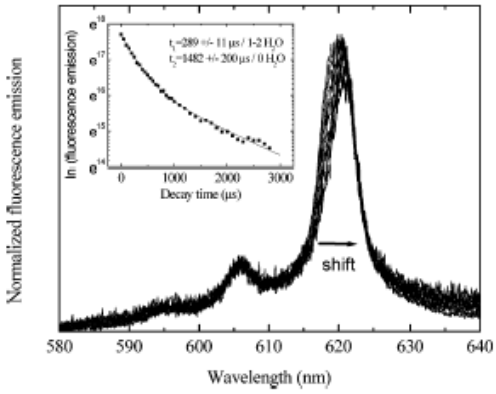

FIGURE 7. Fluorescence emission spectra of 10^{-7} M Cm(III) in a CSH suspension (0.5 g L^{-1}) after a Cm(III)/CSH contact time of 58 d at different delay times. The spectra were scaled to the same peak area. The time dependency of emission decay shows a biexponential decay behavior.

on the composition of the first coordination sphere of the fluorescing species. According to the method developed by Horrocks and Sudnick (*20*) for Eu(III) and later applied to Cm(III) by Kimura and Choppin (*15*), the following linear correlation between the observed decay rate and the number of H_2O molecules in the first coordination sphere applies:

$$n(H_2O) = 0.65k_{obs} - 0.88 \quad (2)$$

with $n(H_2O)$ as the number of coordinated water molecules and k_{obs} as the observed decay rate (reciprocal lifetime) of the excited state (ms^{-1}).

$Cm(H_2O)_9^{3+}$ has a lifetime of 68 ± 3 µs (*5*, *21*–*23*). When no water molecules are coordinated, the lifetime is 1250 ± 80 µs (*15*, *24*).

Selected normalized fluorescence emission spectra of a Cm(III)/CSH sample [10^{-7} M Cm(III) and 5.0 × 10^{-4} kg L^{-1}CSH] measured after a contact time of 58 d at different delay times are shown in Figure 7. With increasing delay time, the peak with a peak maximum at ~620 nm shows a red shift from 619.6 to 620.9 nm. A peak deconvolution was carried out to separate the individual species from the composite fluorescence emission spectra. Again, as result the two different Cm(III) species sorbed on CSH with peak maxima at 618.9 nm (F1) and 620.9 nm (F2) are derived. The Cm(III) fluorescence emission intensity (on a logarithmic scale) as a function of the delay time is also shown in Figure 7. The decay behavior follows a biexponential decay law. The lifetimes of F1 and F2 were determined to be τ = 289 ± 11 and 1482 ± 200 µs, respectively. According to eq 2, a lifetime of 289 ± 11 µs corresponds to 1.4 water molecules in the first coordination shell of the Cm(III) F1 complex, whereas a lifetime of 1482 ± 200 µs indicates the total loss of the hydration sphere of the Cm(III) F2 complex.

Discussion

Characterization of Cm(III) Species in Alkaline Solutions. Speciation calculations using the Nagra/PSI Thermodynamic Database (*25*) indicate that initially all experimental systems are oversaturated with respect to $Eu(OH)_3(s)$ and $Cm(OH)_3(s)$. The dominating species in solution are $Eu(OH)_4^-$ and $Cm(OH)_3$. Spectroscopic characterization of alkaline Cm(III) solutions in a quartz cuvette showed that, notwithstanding the absence of any fluorescence signal, most of the Cm(III) was present in solution.

When Cm(III) (2×10^{-7} M) was diluted in 0.042 M Gd(III), a nonfluorescing homologue of Cm(III), and coprecipitated with gadolinium hydroxide in 1 M NaOH a clear Cm(III) fluorescence signal with a peak maximum at 607.1 nm was obtained. Hence, the absence of a fluorescence signal in the pure alkaline Cm(III) solutions has to be attributed to concentration quenching involving nonradiative energy transfer to adjacent Cm(III) ions in $Cm(OH)_3$ colloids. Coprecipitation with $Gd(OH)_3$ isolates the Cm(III) ions from each other, which reduces energy transfer to adjacent Cm(III) ions. These observations suggest that Cm(III) is present in alkaline solutions as curium(III) hydroxide colloids.

Time-Dependent Fluorescence Intensity of Cm(III) in CSH Suspensions. At the beginning of the sorption kinetic experiments no fluorescence signal could be detected. With increasing equilibration time, an increasing fluorescence intensity was observed. The absence of a fluorescence signal must be attributed to similar effects as in the alkaline Cm(III) solutions [i.e., concentration quenching due to precipitation of $Cm(OH)_3$ colloids that might be sorbed at the CSH surfaces (surface precipitation)]. The concentration of the nonfluorescing species $Cm(OH)_3$ decreases with time, and the concentration of the fluorescing species is increased by time. This is a clear indication for different thermodynamic stabilities of the involved curium compounds. $Cm(OH)_3(s)$ is obviously unstable and dissolves to form the fluorescing Cm(III) species F1 and F2.

Identification of the Different Sorption Sites. The low number of H_2O molecules in the first coordination sphere of the sorbed species F1 and F2 indicate that both species must be incorporated into the CSH structure. It is well-known that the crystal ionic radius of Eu(III) (0.95 Å) and Cm(III) (0.97 Å) are very close to the crystal ionic radius of Ca(II) (0.99 Å) (*26*). Hence, it is concluded that Eu(III) and Cm(III) substitute for Ca(II) in the CSH structure.

A structural model for Cm(III) and Eu(III) incorporation by CSH phases was developed based on a defect 11-Å tobermorite structure (*27*−*31*). The crystal structure of 11-Å tobermorite was reported by Hamid (*32*) (Figure 8). It consists of layers of Ca octahedra ("stable Ca") linked through nonbridging oxygens to chains of silicate tetrahedra on either side, forming Ca−silicate layers. In the interlayers between the Ca−silicate sheets, variable amounts of Ca atoms may be located ("labile" Ca). Thus, the tobermorite structure contains Ca atoms at three different types of sites: The "labile" Ca in the interlayers (labeled 1 in Figure 8) is coordinated with 7 oxygen atoms of which two originate from H_2O molecules. In the second type of sites (labeled 2 in Figure 8), Ca is coordinated with 6 oxygen atoms originating from Si tetrahedra and one oxygen from H_2O (stable Ca), and in the third type of sites (labeled 3 in Figure 8), Ca is coordinated with 7 oxygen atoms originating from Si tetrahedra (stable Ca). The fluorescing Cm(III) species, F1 corresponds to Cm(III) substituting for Ca in the interlayer (type 1 Ca) or Ca bound in the type 2 sites of the Ca octahedral layers, whereas the fluorescing Cm(III) species (F2) can be interpreted as being a Cm(III) substituting for Ca in the type 3 sites of the Ca octahedral layers.

The relative concentration of the incorporated Cm(III) species was estimated using the pure component spectra obtained for each contact time in Figure 4. The results obtained for 1×10^{-7} M Cm(III) in 0.5 g L^{-1} CSH suspension show that, with increasing equilibration time, the relative concentration of F1 decreases while the relative concentration of F2 increases. It is thus inferred that Cm(III) bound in Ca octahedral layers on type 3 sites is thermodynamically most favorable.

Pointeau et al. (*33*) found two types of sorbed Eu(III) species on a CSH phase with a C:S ratio of 0.83 at a pH of 11.6 with fluorescence lifetimes of 390 and 990 μs, respectively. According to the method developed by Horrocks and Sudnick (*20*), it can be calculated that these lifetimes correspond to 2 and 0 water molecules in the first coordination sphere of the sorbed Eu(III). Hence, these two species might be identical to the sorbed Cm(III) species, F1 and F2, found in the present study.

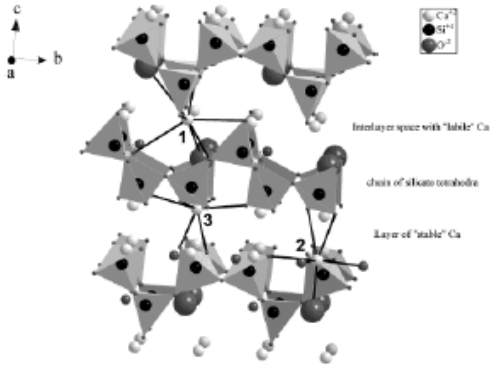

FIGURE 8. Three-dimensional view of the tobermorite structure according to Hamid (32). Note that oxygens of H_2O molecules are enlarged compared to the oxygens from the silica tetraedra. Cm(III) and Eu(III) substitute for three types of Ca with different coordination labeled 1−3.

Acknowledgments

We thank Andre Rossberg for providing the factoranalysis program code designed for the analysis of EXAFS, UV−vis, and TRLFS spectra. E. Curti and M. H. Bradbury are acknowledged for the many valuable discussions and careful reviews of the manuscript. Partial financial support was provided by the National Cooperative for the Disposal of Radioactive Waste (Nagra), by the European commission (Contract FIS5-1999-00157), and by the Swiss Federal Office for Education and Science (on behalf of the European Commission, Contract FIKW-CT-2000-00028).

Literature Cited

(1) Glasser, F. P. In *Chemistry and Microstructure of Solidified Waste Forms*; Spence, R. D., Ed.; Lewis Publishers: Boca Raton, FL, 1993; p 1.
(2) Bonen, D.; Sarkar, S. L. In *Advances in Cement and Concrete*; Grutzeck, W. M., Sarkar, S. L., Eds.; American Society of Civil Engineers: New York, 1994.
(3) Cocke, D. L.; Mollah, M. Y. A. In *Chemistry and Microstructure of Solidified Waste Forms*; Spence, R. D., Ed.; Lewis Publishers: Boca Raton, FL, 1993; p 187.
(4) Gougar, M. L. D.; Scheetz, B. E.; Roy, D. M. *Waste Manage.* **1996**, *16*, 295.
(5) Wimmer, H.; Klenze, R.; Kim, J. I. *Radiochim. Acta* **1992**, *56*, 79.
(6) Moulin, V.; Tits, J.; Moulin, C.; Decambox, P.; Mauchien, P.; De Ruty, O. *Radiochim. Acta* **1992**, *58/59*, 121.
(7) Fanghänel, Th.; Kim, J. I.; Paviet, P.; Klenze, R.; Hauser, W. *Radiochim. Acta* **1994**, *66/67*, 81.
(8) Fanghänel, Th.; Weger, H. T.; Könnecke, T.; Neck, V.; Paviet-Hartmann, P.; Steinle, E.; Kim, J. I. *Radiochim. Acta* **1998**, *82*, 47.
(9) Fanghänel, Th.; Kim, J. I. *J. Alloys Compd.* **1998**, *271*−*273*, 728.
(10) Chung, K. H.; Klenze, R.; Park, K. K.; Paviet-Hartmann, P.; Kim, J. I. *Radiochim. Acta* **1998**, *82*, 215.
(11) Raburg, T.; Stumpf, Th.; Geckeis, H.; Klenze, R. *Radiochim. Acta* **2000**, *88*, 711.
(12) Stumpf, Th.; Rabung, T.; Klenze, R.; Geckeis, H. *J. Colloid Interface Sci.* **2001**, *238*, 219.
(13) Stumpf, Th.; Bauer, A.; Coppin, F.; Kim, J. I. *Environ. Sci. Technol.* **2001**, *35*, 3691.

(14) Stumpf, Th.; Fanghänel, Th. *J. Colloid Interface Sci.* **2002**, *249*, 119.
(15) Kimura, T.; Choppin, G. R. *J. Alloys Compd.* **1994**, *213/214*, 313.
(16) Neck, V.; Fanghänel, T.; Kim, J. I. *Wissenschaftlicher Bericht FZKA 6110*; Forschungszentrum: Karlsruhe, Germany, 1998.
(17) Atkins, M.; Glasser, F. P.; Kindness, A. *Cem. Concr. Res.* **1992**, *22*, 241.
(18) Stumpf, Th.; Fanghänel, Grenthe, I. *J. Chem. Soc., Dalton Trans.* **2002**, 3799.
(19) Rossberg, A.; Reich, T.; Bernhard, G. *Anal. Bioanal. Chem.* (In press).
(20) Horrocks, W. D., Jr.; Sudnick, D. R. *J. Am. Chem. Soc.* **1979**, *101*, 334.
(21) Fanghänel, Th.; Kim, J. I.; Klenze, R.; Kato, J. *J. Alloys Compd.* **1995**, *225*, 308.
(22) Beitz, J. V.; Hessler, J. P. *Nucl. Technol.* **1980**, *51*, 169.
(23) Beitz, J. V.; Bowers, D. L.; Doxtader, M. M.; Maroni, V. A.; Reed, D. T. *Radiochim. Acta* **1988**, *44/45*, 87.
(24) Carnall, W. T.; Crosswhite, H. M. *J. Chem. Phys.* **1995**, *63*, 3510.
(25) Hummel, W.; Berner, U.; Curti, E.; Pearson, F. J.; Thoenen, T. *Nagra/PSI Chemical Thermodynamic Data Base 01/01*; Nagra: Wettingen, Switzerland, 2002.
(26) Cotton, F. A.; Wilkinson, G. *Advanced Inorganic Chemistry*; Interscience Publishers: New York, 1972.
(27) Young, J. F. *J. Am. Ceram. Soc.* **1988**, *71*, C118.
(28) Grützeck, M.; Benesi, A.; Fanning, M. *J. Am. Ceram. Soc.* **1989**, *72*, 665.
(29) Cong, X.; Kirkpatrick, R. J. *Cem. Concr. Res.* **1993**, *23*, 1065.
(30) Faucon, P.; Delaye, J. M.; Virlet, J. *J. Solid State Chem.* **1996**, *127*.
(31) Kirkpatrick, R. J.; Brown, G. E.; Xu, N.; Cong, X. *Adv. Cem. Res.* **1997**, *9*, 31.
(32) Hamid, S. A. *Z. Kristallogr.* **1981**, *154*, 189.
(33) Pointeau, I.; Piriou, B.; Fedoroff, M.; Barthes, M.-G.; Marmier, N.; Fromage, F. *J. Colloid Interface Sci.* **2001**, *236*, 252.

Received for review February 3, 2003. Revised manuscript received May 7, 2003. Accepted May 16, 2003.

ES030020B

Available online at www.sciencedirect.com
SCIENCE DIRECT
Journal of Colloid and Interface Science 276 (2004) 118–124
JOURNAL OF Colloid and Interface Science
www.elsevier.com/locate/jcis

Uptake of trivalent actinides (curium(III)) by hardened cement paste: a time-resolved laser fluorescence spectroscopy study

Thorsten Stumpf,[a,*] Jan Tits,[b] Clemens Walther,[a] Erich Wieland,[b] and Thomas Fanghänel [a]

[a] *Forschungszentrum Karlsruhe, Institut für Nukleare Entsorgung, P.O. Box 3640, D-76021 Karlsruhe, Germany*
[b] *Paul Scherrer Institute, Waste Management Laboratory, CH-5232 Villigen, Switzerland*

Received 3 October 2003; accepted 8 March 2004

Available online 27 April 2004

Abstract

The curium(III) interaction with cement was investigated using time-resolved laser fluorescence spectroscopy at trace concentrations. Four different Cm(III) species were identified: a nonfluorescing species which corresponds to curium hydroxide real colloids, which were characterized in detail by laser-induced breakdown detection (LIBD), a fluorescing Cm(III)/portlandite sorption species, and two fluorescing Cm(III)/calcium silicate hydrate (CSH) species. From the fluorescence emission lifetimes it is predicted that the two fluorescing Cm(III)/CSH species have one to two and no water molecules, respectively, left in their first coordination sphere, suggesting that these species are incorporated into the CSH structure.
© 2004 Elsevier Inc. All rights reserved.

Keywords: Curium; Cement; CSH; Sorption; Surface complexation; Incorporation; TRLFS; LIBD

1. Introduction

In many concepts for the storage of toxic and nuclear waste, cementitious materials are used for the solidification of the waste and for the construction of the engineered barrier system. A great number of studies have demonstrated the waste-loading potential of cement materials and their performance in leaching tests (e.g., [1–5] and references therein). However, the chemical mechanisms governing the immobilization of contaminants (heavy metals, radionuclides, anionic species) on the atomic/molecular scale are still not well understood. Hardened cement paste (HCP) can be considered as a complex mixture of different cement minerals. The immobilization potential of HCP originates from the selective binding properties of these phases for metal cations and anionic species. Calcium aluminates, e.g., ettringite or monosulfate, and calcium silicate hydrates (CSH) are regarded as being among the most important cement phases governing immobilization processes, because of their abundance and the availability of structural units for cation and anion binding (e.g., [3,4]). At present, however, it is still unknown which cement phases serve as sink for each individual contaminant in the complex cement matrix. Nevertheless, this information is needed for prediction of the long-term behavior of toxic and nuclear wastes embedded in a cementitious environment.

The chemical conditions in an underground repository foreseen for nuclear waste disposal are controlled by the interaction of HCP with groundwater. In the first stage of the HCP—groundwater interaction, alkali hydroxides are released from the HCP, resulting in Na and K concentrations of approximately 0.11 and 0.18 M, respectively, and a corresponding pH of 13.3 [6].

The objective of this study was to investigate the interaction of curium(III), a trivalent actinide, with HCP in order to discern which cement phases control the immobilization of the radionuclides at pH 13.3.

Cm(III) was chosen as a representative of the trivalent actinides, which are common in nuclear wastes, because its fluorescence spectroscopic sensitivity allows sorbed species to be studied on a molecular level at very low concentrations. Time-resolved laser fluorescence spectroscopy (TRLFS) has been proven to be a versatile tool for Cm(III) speciation studies (e.g., [7–11]) and for sorption studies on various solids [12–17]. It is capable of identifying different species

* Corresponding author. Fax: +49-7247-82-3927.
E-mail address: thorsten.stumpf@ine.fzk.de (T. Stumpf).

0021-9797/$ – see front matter © 2004 Elsevier Inc. All rights reserved.
doi:10.1016/j.jcis.2004.03.014

Table 1
Chemical composition of HCP

Chemical compound	Content in HCP (ppm)
Na	514
K	1580
Ca	3.92×10^5
Si	9.24×10^4
Al	1.13×10^4
Fe	1.59×10^4
Mn	171
Mg	4350
S	6110
Loss on ignition at 1000 °C (wt%)	18.8

as well as determining their hydration status [18], thus allowing outer-sphere and inner-sphere surface complexes and species incorporated in the crystal lattice of the solids to be distinguished from each other.

2. Experimental methods

2.1. Materials

The ^{248}Cm(III) ($t_{1/2} = 3.4 \times 10^5$ years) stock solution with a concentration of 2.36×10^{-4} M was prepared in 1.0 M $HClO_4$.

The cement samples were prepared from a commercial sulfate-resisting cement (Type CPA 55 HTS; Lafarge, France), denoted as HTS (haute teneur en silice). A special manufacturing procedure was developed to produce fully hydrated hardened cement paste under CO_2-free conditions [19]. The chemical composition of the HCP is listed in Table 1.

For the batch sorption experiments, a powder material was prepared by crushing the bulk material in a mortar under CO_2-free conditions and sieving the material to collect the fraction $\leqslant 70$ μm. The BET surface area of the cement powder was determined to be 46 ± 4 m^2/g.

In order to prevent any alteration of the HCP material during the sorption experiments an artificial cement pore water (ACW) was established based upon a series of stability tests with the HCP. A detailed description of this ACW and its preparation is given in [20]. Briefly, an alkaline solution containing 0.114 M NaOH and 0.18 M KOH was prepared. An excess of $Ca(OH)_2$ and $CaCO_3$ was added and this suspension was shaken for at least 1 week. Subsequently, the suspension was filtered through a 0.1-μm Criticap filter (Gelman Science) under CO_2-free conditions to remove all particulate material. Then 0.426 g L^{-1} Na_2SO_4 and 8.55×10^{-3} g L^{-1} $Al_2(SO_4)_3$ was added to the filtrate to obtain an Al concentration of 5×10^{-5} M and an SO_4^{2-} concentration of 3×10^{-3} M. Stability tests showed that the composition of this ACW (see Table 2) remained unchanged in contact with HCP over a period of at least 4 weeks. Cement suspensions were prepared by mixing a quantity of HCP powder with 40 ml of ACW in polypropylene containers to obtain solid to liquid ratios of 0.05, 0.1, and 0.5 g L^{-1}.

Table 2
Chemical composition of ACW

Chemical compound	Concentration (M)
Na	0.114
K	0.18
Ca	1.7×10^{-3}
Si	5.0×10^{-5}
Al	5.0×10^{-5}
SO_4^{2-}	3.0×10^{-3}

2.2. Methods

TRLFS measurements were performed using a flashlamp-pumped Ti:sapphire laser (Elight, Titania) or an Excimer pumped dye laser system (Lambda Physics). The laser pulse energy, at most 4 mJ, was controlled by a photodiode. The fluorescence emission was detected by an optical multichannel analyzer, which allows simultaneous detection of the total spectral range covered by the respective grating. The system consists of a monochromator and spectrograph (Oriel, MS 257) with a 300 or 1200 lines/mm grating and an ICCD camera (Andor). The excitation occurred at 395 nm and the emission spectra of Cm(III) were recorded in the 520–680 nm (300 lines/mm grating, lifetime measurements) and 580–640 nm (1200 lines/mm grating, high-resolution spectra for peak deconvolution) ranges using a constant time window of 1 ms. For measuring the time-dependent emission decay, the delay time between laser pulse and camera gating was scanned with time intervals between 10 and 50 μs.

For the TRLFS investigations of Cm(III) uptake by cement, an aliquot of Cm(III) stock solution was added to the HCP suspensions to obtain a total Cm(III) concentration of 10^{-7} M. The suspensions were then equilibrated for a period ranging between 1 h and 358 days. The samples were shaken periodically during equilibration. At chosen time intervals, Cm(III) emission spectra were recorded. In addition, one of the parallel samples was centrifuged (15,000 rpm, 15 min), and the supernatant was analyzed by ICP-MS and TRLFS. Cm(III) concentrations in the supernatant were found to be below the detection limit ($\sim 4 \times 10^{-10}$ M), suggesting that Cm(III) was completely removed from solution.

Laser-induced breakdown detection (LIBD) [21] was applied to assess the possibility of colloid formation with respect to size and concentration [22]. This method is based on plasma formation due to dielectric breakdown in the high field region of a focused pulsed (ns) laser beam. This process is selective and occurs only when a colloid is present in the focal volume. Each plasma event corresponds to one single colloid, and hence, the relative number of events per number of laser shots gives a measure of colloid concentration. The photon flux required for breakdown decreases with increasing number of molecules inside the colloid. By making

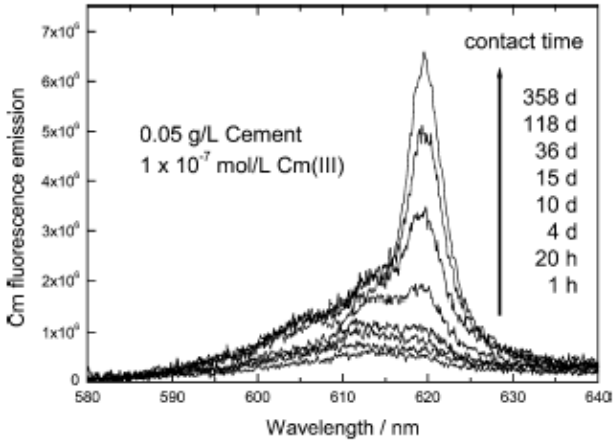

Fig. 1. Fluorescence emission spectra of 10^{-7} M Cm(III) in cement suspension (0.05 g L^{-1}) measured at different Cm(III)/cement contact times.

use of this relationship, the colloid size can be appraised by varying the laser pulse energy. Particles down to 5 nm in diameter can be detected in the low-ppt concentration range [22,23].

3. Results and discussion

3.1. Spectroscopic characterization

Selected fluorescence emission spectra of 10^{-7} M Cm(III) in 0.05 g L^{-1} cement suspension measured after different contact times are shown in Fig. 1. With increasing Cm(III)/cement contact time also the fluorescence emission intensity increases. At the beginning of the sorption kinetic experiments, only a broad peak is observed. With increasing Cm(III)/cement contact time a species with a peak maximum at 613.6 nm is identified. After longer equilibration times, a second peak with a maximum at 619.6 nm appears. This peak becomes more prominent with time and is dominating after 36 days. In the spectra in which the strong red-shifted peak at 619.6 nm prevails, an additional peak with a maximum at ~606.0 nm evolves. Its position and intensity ratio with respect to the main peak remain constant with increasing Cm(III)/cement contact time. In previous studies this peak has been shown to originate from visible transitions of thermally populated states at room temperature and has no chemical relevance [24].

The fluorescence intensity is very low at the beginning of the experiment but increases with increasing contact time. The very low fluorescence signal of Cm(III) in alkaline solutions has been reported in previous studies and was attributed to concentration quenching due to the formation of Cm(III) hydroxide colloids as shown by coprecipitation with the nonfluorescing homologue Gd(III) [24]. In the present experiments a more direct approach is used: an alkaline (pH 13) solution of 2×10^{-7} M Cm(III) was prepared by adding 3 µl stock solution to 3 ml 1 M NaOH which had been cleaned from colloidal impurities by multiple ultrafiltration. The formation of colloids in the freshly prepared solution was observed as a function of time by LIBD in constant pulse-energy mode, in which the breakdown probability, i.e., the relative number of colloids detected for a fixed number of laser shots, is a measure of total particle concentration. Starting from an almost colloid-free solution at $T = 0$ min, a rapid increase in colloid concentration is observed, which levels off after some 50 min (Fig. 2, top). While the constant energy mode is well suited for tracking colloid formation on a time scale of minutes, detailed size information cannot be obtained. To this end the breakdown probability is measured as a function of laser-pulse energy. Since small colloids require lower pulse energy for breakdown formation than larger ones, the onset of the probability curves ("threshold") reflects the colloid size (the higher the threshold, the lower the particle size). The slope of the curve is a measure of particle concentration. The NaOH contains only a minor amount of small colloids (<20 nm) (Fig. 2, bottom), considerably less than in the Cm(III) solution after 1 h (0 d). According to the calibration with polystyrene spheres [25], this solution contains colloids of 70–100 nm at a weight concentration of 40 ± 20 ppb corresponding to $(1.35 \pm 0.7) \times 10^{-7}$ M Cm(III). This agrees with the absence of fluorescence signals and is interpreted as Cm(III) being transformed quantitatively into colloidal phase. After 1 day (1 d) the threshold shifts to lower pulse energy, indicating colloid growth, while the total mass concentration of colloids remains constant. Further colloid growth at constant mass concentration (5 d) leads to a decrease in colloid concentration (since each colloid comprises a larger mass) and subsequently to a lower slope. Up to this time the sample is still spectroscopically blind—no fluorescence signal is obtained. However, after 3 weeks the slope decreases without further growth of the colloids (constant threshold, 21 d). This is clear evidence for colloid dissolution and conversion into fluorescing sorption species (onto the cuvette walls or the cement colloids, respectively). This conversion is in agreement with spectroscopic data, in which the 619-nm peak builds up after 15 days (Fig. 1). Presumably the colloids are a metastable species formed in the high pH gradients when the Cm(III) stock solution is added to the NaOH. In the long term the system evolves toward the thermodynamic equilibrium between colloidal and ionic species. The rate constant of dissolution depends on the concentration gradients and this process is accelerated by the presence of additional sinks for ionic species as are the cement phases.

From the series of composite fluorescence emission spectra measured at different time intervals, the pure components (pure Cm(III) species) were calculated using factor analysis [26]. A plot of the deconvoluted spectra is shown in Fig. 3. Two independent spectra with peak maxima at 613.6 and 619.6 nm are found, suggesting the formation of two different Cm(III) species sorbed on HCP.

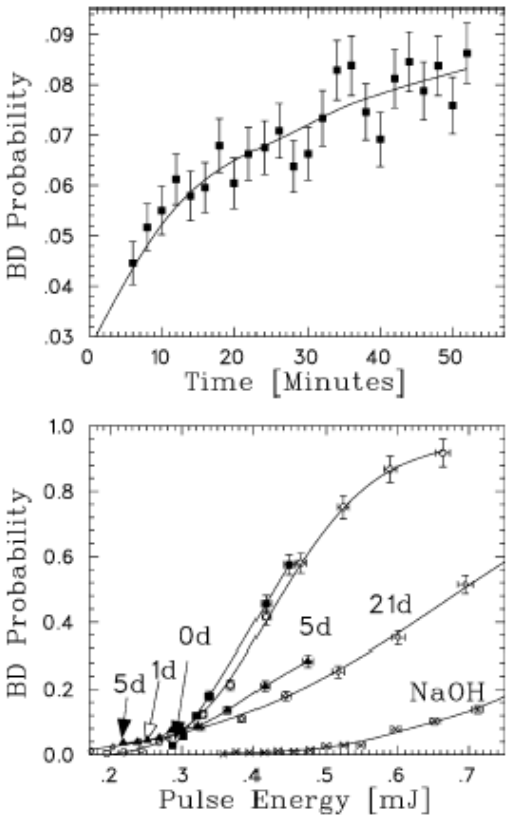

Fig. 2. Colloid formation detected by LIBD (top) in constant pulse-energy mode and (bottom) as a function of laser-pulse energy.

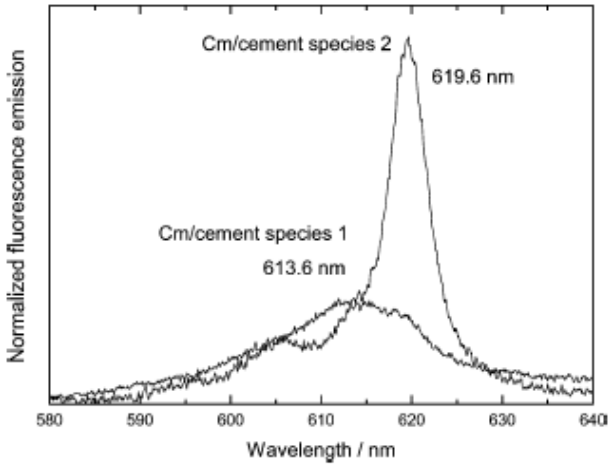

Fig. 3. Fluorescence emission spectra of the fluorescing Cm(III) sorbed species 1 and 2 as derived by peak deconvolution. The spectra were scaled to the same peak area.

3.2. Lifetime (fluorescence decay) of Cm(III)

The fluorescence emission lifetime provides information on the composition of the first coordination sphere. According to the method developed by Horrocks, Jr., and Sudnick [27] and Barthelemy and Choppin [28] for Eu(III) and later

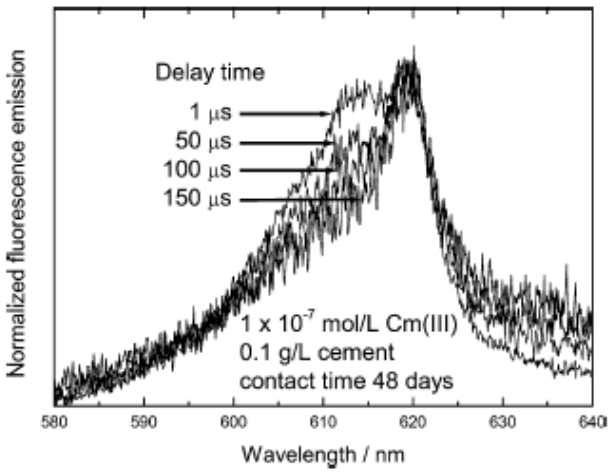

Fig. 4. Fluorescence emission spectra of 10^{-7} M Cm(III) in cement suspension (0.1 g L^{-1}) after a Cm(III)/cement contact time of 48 days at different delay times. The spectra were scaled to the same peak area.

applied to Cm(III) by Kimura and Choppin [18], there is a linear correlation between the observed decay rate and the number of H_2O or OH^- molecules in the first coordination sphere. In the case of Cm(III) this linear correlation takes the form of

$$n(H_2O/OH^-) = 0.65k_{obs} - 0.88, \quad (1)$$

where k_{obs} is the observed decay rate (reciprocal lifetime) of the excited state (ms^{-1}) and $n(H_2O/OH^-)$ is the number of coordinated water molecules or hydroxyl ions. $Cm(III)(H_2O)_9^{3+}$ corresponds to a lifetime of 68 ± 3 μs [7,29,30]. When all water molecules are removed from the first coordination sphere, the lifetime is 1250 ± 80 μs [31]. The decay rate is obtained by measuring the fluorescence signal at different delay times after the laser pulse.

Fluorescence emission spectra of 10^{-7} M Cm(III) in 0.1 g L^{-1} cement suspension after a contact time of 48 days measured at different delay times are shown in Fig. 4. A contact time of 48 days was chosen for the lifetime analysis because the spectrum at this contact time has a sufficiently high fluorescence intensity and the 613.6-nm peak has still an intensity that allows a statistically sound determination.

With increasing delay time the relative intensity of the peak with the maximum at 613.6 nm decreases compared to the peak with a maximum at 619.6 nm, suggesting the existence of two Cm(III) species with different fluorescence emission lifetimes. The shorter lifetime is attributed to a species showing a peak maximum at 613.6 nm, while the longer lifetime is attributed to the species with a peak maximum of 619.6 nm.

The Cm(III) fluorescence emission intensity with increasing delay time of 10^{-7} M Cm(III) in 0.1 g L^{-1} cement suspension after a contact time of 48 days is plotted on a log scale in Fig. 5. The fluorescence signal follows a biexponential decay law, indicating the existence of two different sorbed species with lifetimes of 66 ± 1 and 1208 ± 600 μs,

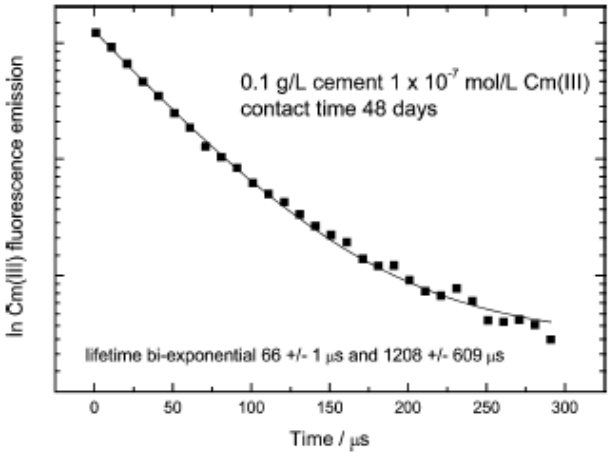

Fig. 5. Time dependency of emission decay of 10^{-7} M Cm(III) in cement suspension (0.1 g L^{-1}) after a Cm(III)/cement contact time of 48 days. The time dependency of emission decay shows a biexponential decay behavior.

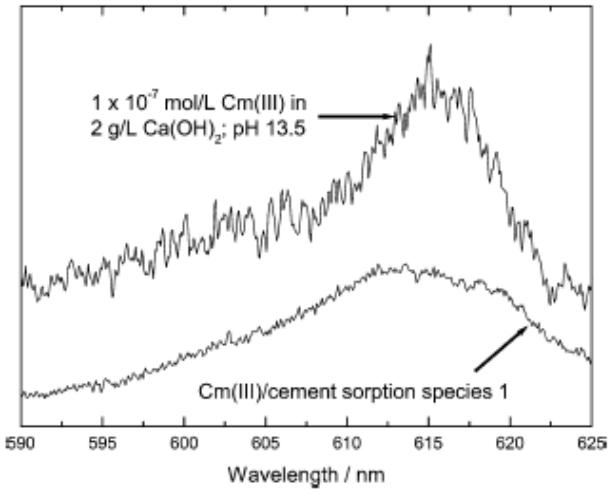

Fig. 6. Fluorescence emission spectrum of 10^{-7} M Cm(III) in portlandite suspension (2 g L^{-1}) at pH 13.5 together with the emission spectrum of Cm(III)/cement sorption species 1.

respectively, for the two sorbed species (Fig. 4). According to Eq. (1), a lifetime of 66 ± 1 µs corresponds to 9 water/OH^- molecules in the first coordination sphere of Cm(III), whereas a lifetime of 1208 ± 600 µs indicates the total loss of the hydration sphere of the second Cm(III) sorbed species. The substantial error of 600 µs on the calculated value for the lifetime of the second species originates from the low contribution of this species to the composite spectra after 48 days. However, according to Eq. (1) the lower limit would correspond to 0.2 water molecules in the first coordination sphere of the Cm(III) ion. Hence, we conclude that the second Cm(III) species consists of an actinide ion that is incorporated into the cement bulk structure.

Fig. 6 shows the spectrum of 1 × 10^{-7} M Cm(III) in 2 g L^{-1} portlandite suspension at pH 13.5 after actinide/$Ca(OH)_2$ contact time of 30 days in comparison to the spectrum of Cm(III)/cement sorption species 1. Both spectra show a broadened peak with a peak maximum at 613.6 nm, indicating that similar compounds are formed. In Fig. 7 the emission decay of Cm(III) fluorescence in $Ca(OH)_2$ suspension is plotted. The monoexponential decay behavior indicates that only one curium species is formed. The measured Cm(III) fluorescence emission lifetime of 62 ± 8 µs is very short and comparable to the lifetime of the completely hydrated $Cm(III)^{3+}$ aquo ion. But the peak maximum at 613.6 nm is strongly red-shifted compared to the peak maximum of the $Cm(III)^{3+}$ aquo ion (593.8 nm) and the Cm(III) hydroxo complexes ($Cm(III)(OH)^{2+}$aq 598.7 nm [8], $Cm(III)(OH)_2^+$aq 603.5 nm [9], and $Cm(III)(OH)_3$ 607.1 nm [24]). This suggests the formation of an inner-sphere Cm(III)/portlandite complex. A Cm(III) outer-sphere complex would show the same peak maximum as the Cm(III) aquo ion or as a Cm(III) hydroxo complex and can therefore be ruled out. The exceptional short lifetime of an inner-sphere Cm(III) complex can be explained by the coordination OH^- ions of the portlandite. Even if Cm(III) is sorbed onto the $Ca(OH)_2$ surface the actinide ion is surrounded by OH^- ligands, which are responsible for the quenching of the Cm(III) fluorescence emission and, hence, for the short emission lifetime of the Cm(III)/$Ca(OH)_2$ inner-sphere surface complex. The measured lifetime of the Cm(III)/portlandite sorption species is in good agreement with the lifetime t_1 of Cm(III)/cement sorption species 1. Because of the similarity of the spectra and of the fluorescence emission lifetimes we conclude that Cm(III)/cement sorption species 1 consists of Cm(III) sorbed onto portlandite.

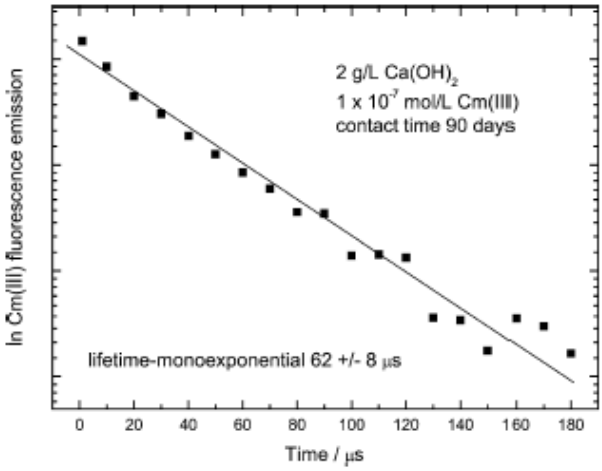

Fig. 7. Time dependency of emission decay of 10^{-7} M Cm(III) in portlandite suspension (2 g L^{-1}) at pH 13.5 after a Cm(III)/$Ca(OH)_2$ contact time of 90 days.

Fig. 8 shows the Cm(III) fluorescence emission intensity on a logarithmic scale with increasing delay time in 0.05 g L^{-1} cement suspension after a Cm(III)/HCP contact time of 358 days. The best fit of the experimental data using a biexponential decay model by assuming the presence of

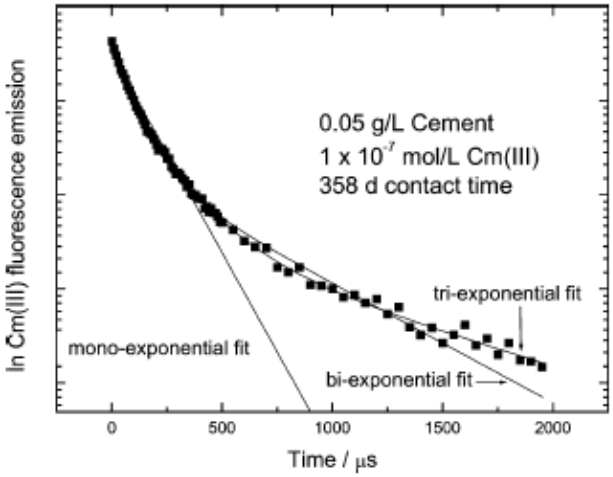

Fig. 8. Time dependency of emission decay of 10^{-7} M Cm(III) in cement suspension (0.05 g L^{-1}) after a Cm(III)/cement contact time of 358 days. Mono-, bi-, and triexponential decay behavior is fitted.

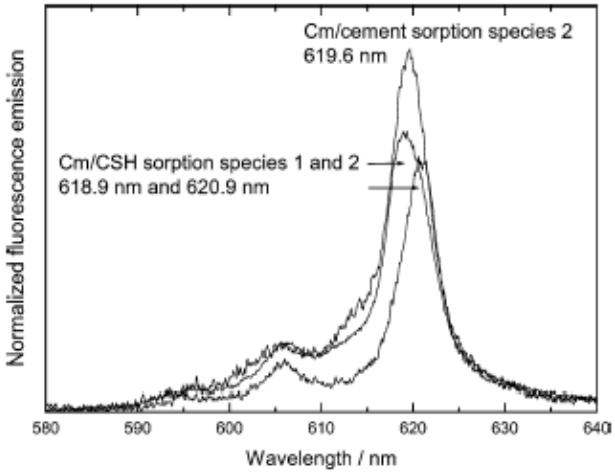

Fig. 9. Fluorescence emission spectra of Cm(III)/cement sorption species 1 together with the pure component spectra of Cm(III)/CSH sorption species 1 and 2.

two different sorbing Cm(III) species, yields the following lifetimes: $t_1 = 115 \pm 3$ µs and $t_2 = 786 \pm 31$ µs. According to Eq. (1) a lifetime of 115 µs corresponds to 4.8 and a lifetime of 786 µs corresponds to 0 water or hydroxide molecules in the first coordination sphere of the Cm(III). A visual analysis of Fig. 8 clearly reveals that this biexponential decay model does not fit the experimental data satisfactorily. More specifically, the experimental data beyond delay times of 500 µs are poorly described. Furthermore the calculated lifetimes after Cm(III)/HCP contact times of 48 and 358 days differ substantially, while the Cm(III)/HCP sorbed species involved are still the same (peak maxima 613.6 and 619.6 nm).

An acceptable agreement between the measured data points and the fit is reached by introducing a third lifetime in the decay model suggesting the presence of three different sorbing Cm(III) species. The best fit to the experimental data with this triexponential decay model yields the following lifetimes for the three sorbing Cm(III) species: $t_1 = 70 \pm 7$ µs, $t_2 = 226 \pm 26$ µs, and $t_3 = 1375 \pm 207$ µs. The corresponding numbers of water/OH^- molecules in the first Cm(III) shell are calculated to be approximately 8.5, 2, and 0. These values are close to the lifetimes found after 48 days Cm(III)/cement contact time.

TRLFS measurements of Cm(III) sorbed on CSH phases revealed two sorbed Cm(III) species, with peak maxima of 618.9 and 620.9 nm, respectively, and lifetimes of 289 ± 11 and 1482 ± 200 µs, corresponding to 1.4 and 0 water/OH^- molecules in the first coordination sphere of the actinide ion [24]. These lifetimes agree very well with lifetimes t_2 and t_3, for two of the three sorbing Cm(III) species in HCP found in the present study, suggesting that these two Cm(III) species are identical to the Cm(III) species sorbed on CSH phases described by Tits et al. [24]. The interferences of the Cm(III) fluorescence emission by foreign ions in the much more complex cement system do not allow the separation of the two Cm(III)/CSH peaks in the Cm(III)/cement system by peak deconvolution.

In Fig. 9 the second peak of the Cm(III)/cement spectrum with a peak maximum at 619.6 nm, obtained from the factor analysis, is compared with the pure spectra of two Cm(III) species sorbed on the CSH phase described by Tits et al. [24]. The Cm(III) HCP peak and the two Cm(III) CSH peaks are equally strongly shifted to wavelengths in the range of 619 to 620 nm. Such large shifts in wavelength are observed only for Cm(III) species incorporated in CSH phases, and therefore, this observation strongly supports the assumption that the peak at 619.6 nm in the Cm(III) HCP spectrum belongs to the two Cm(III) species incorporated in the CSH fraction of the HCP.

In summary, TRLFS spectroscopy measurements on Cm(III) HCP systems in ACW showed that, initially, Cm(III) is sorbed on the portlandite fraction of the HCP. With time, two new Cm(III) species appear and become dominant at the expense of the Cm(III) portlandite species. These two species were identified as Cm(III) being incorporated in the CSH fraction of HCP, where it occupies two different positions in the CSH structure, as described in detail by Tits et al. [24].

Acknowledgments

We thank André Rossberg for providing the factor analysis program code designed for the analysis of EXAFS, UV–vis, and TRLFS spectra and J.I. Yun and H.R. Cho for performing the LIBD measurements. We thank the Institut für Radiochemie at the Forschungszentrum Rossendorf for their support and the supply of the laser equipment. Partial financial support was provided by the Swiss National Cooperative for the Disposal of Radioactive Waste (Nagra).

References

[1] F.P. Glasser, in: R.D. Spence (Ed.), Chemistry and Microstructure of Solidified Waste Forms, Lewis Publishers, Boca Raton, FL, 1993, pp. 1–39.
[2] D. Bonen, S.L. Sarkar, in: W.M. Grutzeck, S.L. Sarkar (Eds.), Advances in Cement and Concrete, American Society of Civil Engineers, New York, 1994.
[3] D.L. Cocke, M.Y.A. Mollah, in: R.D. Spence (Ed.), Chemistry and Microstructure as Solidified Waste Forms, Lewis Publishers, Boca Raton, FL, 1993.
[4] M.L.D. Gougar, B.E. Scheetz, D.M. Roy, Waste Manage. 16 (1996) 295.
[5] S.E. Manahan, Industrial Ecology: Environmental Chemistry and Hazardous Waste, Lewis, New York, 1999.
[6] U. Berner, A Thermodynamic Description of the Evolution of Pore Water Chemistry and Uranium Speciation during the Degradation of Cement, Paul Scherrer Institut, Villigen, Switzerland, 1990.
[7] H. Wimmer, J.I. Kim, R. Klenze, Radiochim. Acta 58/59 (1992) 165.
[8] V. Moulin, J. Tits, C. Moulin, P. Decambox, P. Mauchien, O. De Ruty, Radiochim. Acta 58/59 (1992) 121.
[9] T. Fanghänel, J.I. Kim, P. Paviet, R. Klenze, W. Hauser, Radiochim. Acta 66/67 (1994) 81.
[10] T. Fanghänel, H.T. Weger, T. Könnecke, V. Neck, P. Paviet-Hartmann, E. Steinle, J.I. Kim, Radiochim. Acta 82 (1998) 47.
[11] T. Fanghänel, J.I. Kim, J. Alloys Compd. 271–273 (1998) 728.
[12] K.H. Chung, R. Klenze, K.K. Park, P. Paviet-Hartmann, J.I. Kim, Radiochim. Acta 82 (1998) 215.
[13] T. Rabung, T. Stumpf, H. Geckeis, R. Klenze, Radiochim. Acta 88 (2000) 711.
[14] T. Stumpf, T. Rabung, R. Klenze, H. Geckeis, J. Colloids Interface Sci. 238 (2001) 219.
[15] T. Stumpf, A. Bauer, F. Coppin, J.I. Kim, Environ. Sci. Technol. 35 (2001) 3691.
[16] T. Stumpf, T. Fanghänel, J. Colloids Interface Sci. 249 (2002) 119.
[17] I. Pointeau, B. Piriou, M. Fedoroff, M.-G. Barthes, N. Marmier, F.J. Fromage, J. Colloids Interface Sci. 236 (2001) 252.
[18] T. Kimura, G.R. Choppin, J. Alloys Compd. 213/214 (1994) 313.
[19] L.Döhring, W. Görlich, S. Rüttener, R. Schwerzmann, Herstellung von homogenen Zementsteinen mit hoher Hydraulischer Permeabilität, Nagra unpublished report, Wettingen, Switzerland.
[20] J. Tits, A. Jakob, E. Wieland, P. Spieler, J. Contam. Hydrol. 61 (2003) 45.
[21] T. Kitamori, K. Yokose, K. Suzuki, T. Sawada, Y. Goshi, Jpn. J. Appl. Phys. 27 (1988) L983.
[22] C. Walther, C. Bitea, W. Hauser, J.I. Kim, F.J. Scherbaum, Nucl. Instrum. Methods Phys. Res. B 195 (2002) 374.
[23] C. Walther, Colloids Surf. A 217 (2003) 81.
[24] J. Tits, T. Stumpf, T. Rabung, E. Wieland, T. Fanghänel, Environ. Sci. Technol. 37 (2003) 3568.
[25] F.J. Scherbaum, R. Knopp, J.I. Kim, Appl. Phys. B 63 (1996) 299.
[26] A. Rossberg, T. Reich, G. Bernhard, Anal. Bioanal. Chem., in press.
[27] W.D. Horrocks Jr., D.R. Sudnick, J. Am. Chem. Soc. 101 (1979) 334.
[28] P.P. Barthelemy, G.R. Choppin, Inorg. Chem. 28 (1989) 3354.
[29] J.V. Beitz, J.P. Hessler, Nucl. Technol. 51 (1980) 169.
[30] J.V. Beitz, D.L. Bowers, M.M. Doxtader, V.A. Maroni, D.T. Reed, Radiochim. Acta 44/45 (1980) 87.
[31] Carnall, W. T., Crosswhite, H. M., Report ANL, 84 (1995).

Site-selective time resolved laser fluorescence spectroscopy of Eu^{3+} doped calcite

M. Marques Fernandes[1], M. Schmidt[1], Th. Stumpf[1, 2], C. Walther[1], D. Bosbach[1], R. Klenze[1] and T. Fanghaenel[2, 3]

[1]Institut für Nukleare Entsorgung, Forschungszentrum Karlsruhe, P.O. Box 3640, Karlsruhe, 76021, Germany

[2]Ruprecht-Karls-Universität Heidelberg, Physikalisch-Chemisches Institut, Im Neuenheimer Feld 253, 69120 Heidelberg, Germany

[3]European Commission, Joint Research Center, Institute for Transuranium Elements, P.O. Box 2340, Karlsruhe, 76125, Germany

Author to whom correspondence should be addressed (maria.marques@ine.fzk.de)

Abstract

Three samples of calcite homogenously doped with Eu^{3+} were synthesized in a mixed-flow reactor. By means of selective excitation of the $^5D_0$ --> $^7F_0$ transition at low temperatures (T<18K) three different Eu^{3+} species (species A, B and C respectively) could be

discriminated. The thus found species were characterized by their emission spectra and lifetimes, obtained after selective excitation of the single species. On the basis of this data species C could be identified as Eu^{3+} incorporated into the calcite lattice on the (nearly) octahedral Ca^{2+} site. Species B is an incorporated species as well, but the ligand field shows a much weaker symmetry. Species A, however, is not incorporated into the crystal's bulk, having two H_2O ligands left in its first coordination sphere and showing very little symmetry, and is considered as Eu^{3+} incorporated into the calcite surface layer.

Comparing the emission spectra of species C in Eu:calcite (calcite I and III) which was grown in the presence of Na^+ with species C in an Eu:calcite, synthesized with K^+ (calcite II) revealed a strong distortion of the symmetry of species C in Eu:calcite II, which was not observed in sample I and III. This is strong spectroscopic evidence for the coupled substitution of Na^+ and Eu^{3+} for 2 Ca^{2+}, providing for the necessary charge compensation.

1. INTRODUCTION

Assessing the geochemical long-term safety of a nuclear waste repository requires a molecular level understanding of the radionuclides' behavior in the geosphere. This is needed in order to establish reliable thermodynamic data on the retention and transport mechanisms in groundwaters. In particular, the interaction of radionuclides with mineral phases (adsorption, structural incorporation) strongly affects their mobility and sequestration. In the environment a of deep geological nuclear waste repositories, reducing conditions prevail and the radionuclides are present in their low oxidation states. In particular trivalent actinides like Am(III), Cm(III) and Pu(III) contribute highly to the radiotoxicity of a HLW disposal. This work focuses on the interaction of radionuclides with the mineral calcite $CaCO_3$.

Calcite is an omnipresent crystalline mineral phase in many soil and marine formations. It plays an important role in the retention of toxic and radiotoxic elements.
Geological clay formations (Bure, Boom clay, Opalinus) containing a high percentage of calcite (up to 40 %) are intensively discussed as a host rock formation for a nuclear waste repository. Moreover, many waste repository designs include cement-based components of which calcite is a major secondary alteration product formed over geological timescales. Besides its importance for the potential retention of radionuclides as a retention capacity, calcite is also a crystalline model phase of particular spectroscopic interest in investigating the formation of solid solutions by substitution of Ca^{2+} by a higher charged cation as there is only one cation site in calcite's crystallographic structure.
Because of their electronic 4f configuration (ionic radius, charge), the trivalent lanthanides are considered as non radioactive chemical analogues of 5f trivalent actinides (Am(III), Cm(III), Pu(III)).

The optical properties of 4f-elements, in particular of Eu^{3+} have proven to be very efficient as a luminescent probe to investigate the local structure, hydration state and

substitution mechanisms in hydrated and non-hydrated crystalline systems, glasses, and solution. Many spectroscopic studies have been performed on different systems (e.g. single crystals, microcrystalline samples, and inorganic salts) to observe the influence of different crystal fields on the europium fluorescence emission, to identify the symmetry of the main crystallographic sites, and to determine the energy of the electronic sublevels/transitions induced by these different crystal fields for crystal field calculations [1-6].

The present work, spectroscopic properties of the trivalent lanthanide Eu^{3+} as local fluorescing probe are used, to investigate the nature of sites induced by the interaction of trivalent actinides ions with the crystalline mineral phase calcite, with special focus on the structural incorporation and charge compensation mechanisms. In this work as site is considered a Eu(III) ion in a given chemical environment/crystal field in calcite.

It is presumed that the structural incorporation of trivalent actinides and lanthanides into calcite occurs on a calcite lattice site by the substitution of a Ca^{2+}. The size of the sixfold coordinated trivalent actinides (Cm^{3+}: 97 pm, Am^{3+}: 98 pm) and lanthanides (Eu^{3+}: 95 pm, Nd^{3+}: 98 pm) is close to that of Ca^{2+} (100 pm) [7]. Calcite has a trigonal space group (D_{3d}). In the calcite structure, Ca^{2+} occupies a regular octahedron with a six-fold coordination to oxygen of six adjacent CO_3^{2-} groups. The symmetry of the centrosymmetric Ca^{2+} site is C_{3i}. An important question for any heterovalent substitution is the charge compensation mechanism in the near field of the substituting cation, to maintain electrical neutrality.

Several studies have dealt with the interaction of trivalent lanthanides resp. actinides with calcite. Empirical partition coefficients for REE have been determined from sorption and coprecipitation experiments [8-11]. Extended X-ray absorption fine structure (EXAFS) studies of REE coprecipitated with calcite provided structural information (coordination number, bond distances) [12, 13]. Synthetic calcite crystals containing a lanthanide (Eu(III)) [6] or an actinide (Cm(III), Am(III)) have been studied by TRLFS to characterize the

structural incorporation mechanism [14, 15]. Curti et al. [16] used a thermodynamic "inverse" modeling approach to model the Eu/calcite solid solution-aqueous solution (SSAS) system based on different experimental data.

Based on macroscopic sorption experiments as well as spectroscopic studies mentioned above various substitution mechanisms have been discussed but no unambiguous conclusion has been drawn. Zhong and Mucci [10] suggest that Na^+, because of its quite similar ionic size and charge, might serve to balance the excess charge generated by the incorporation of trivalent REE in calcite. A substitution scheme with the end-members $CaCO_3$-$Eu_{2x}(CO_3)_3$, where x represents a Ca^{2+} vacancy in the calcite lattice has been proposed by Lakshtanov and Stipp [9]. To explain the data obtained by EXAFS, Withers et al. [13] suggested mechanisms like bidentate linkage of one carbonate group, or retention of an OH^-/H_2O from the hydration shell of REE. Curti et al. [16] proposed the formation of a ternary solid solution. At low pH, Ca^{2+} is substituted by H^+ and Eu^{3+} At higher pH, EuO(OH) is incorporated into the calcite lattice. In this study, we focused in particular on this substitution mechanism: $2Ca^{2+} \leftrightarrow Na^+ + An^{3+}/Ln^{3+}$.

As mentioned above, in this work a study of the optical properties of Eu^{3+} was carried out to investigate the nature of the different sites (different chemical environments or crystal fields) induced by the substitution of Ca^{2+} by Eu^{3+} in the calcite lattice and the potential influence of sodium (Na^+) as charge compensating cation. For this reason site selective time resolved laser fluorescence spectroscopy was performed on Eu(III) doted calcite samples synthesized in the presence of Na^+ and samples synthesized in the presence of K^+. Since K^+ has a larger ionic radius (138 pm in the sixfold coordination) than Na^+ (102 pm) and Ca^{2+} (100 pm), it is presumed that the incorporation of K^+ or the vacancy site induced because K^+ is not incorporated, will modify the crystal field around Eu(III) ion [7].

2. EU(III) OPTICAL PROPERTIES

Most luminescence spectra recorded for Eu(III) complexes are emission spectra of the $^5D_0 \rightarrow {}^7F_J$ (J = 0-6) transitions obtained when exciting the $^7F_0 \rightarrow {}^5L_6$ transition. The f-f transitions of Eu^{3+} consist mainly of magnetic dipole (MD) and induced electric dipole (ED) transitions. The most intensive transitions are $^5D_0 \rightarrow {}^7F_{1,2,4}$. The intensity of the MD transition $^5D_0 \rightarrow {}^7F_1$ is independent of the chemical environment of Eu(III), whereas the intensity of the ED transition $^5D_0 \rightarrow {}^7F_2$, referred to as hypersensitive, strongly depends on the local crystal field and local symmetry of the ion [17-22]. For europium containing systems, the time resolved laser fluorescence analysis of the $^5D_0 \rightarrow {}^7F_J$ fluorescence transitions yields structural and chemical information (chemical bonding and local site symmetry, hydration state). Fluorescence measurements at low temperature increase the efficiency of the fluorescence intensity, as the fluorescence increases with decreasing temperature. Additionally cryogenic conditions allow a better spectral resolution of the magnitude of the crystal-field splitting of the ^7F_J than measurements at room temperature.

The ground state $^7F_0$ is not degenerated, the same applies to the $^5D_0$ state. The number of components observed in $^5D_0 \rightarrow {}^7F_0$ region is necessarily related (as far they can be observed, weak or no F_0 transition indicates high site symmetry) to the number of chemically different (non-equivalent) sites occupied by Eu^{3+}.

The analysis of the lifted degeneracy of the $^5D_0 \rightarrow {}^7F_J$ transitions (obtained after selectively exciting the $^5D_0 \rightarrow {}^7F_0$ transitions) in terms of the group theory provides information on the symmetry of the sites occupied by Eu^{3+} in the investigated system. The maximum splitting of the F_J levels for a given site is 2J+1. In highly symmetric sites, the ED transitions $^5D_0 \rightarrow {}^7F_0$ and $^5D_0 \rightarrow {}^7F_2$ transitions are forbidden or weak.

The higher the splitting magnitude of the $^5D_0 \rightarrow {}^7F_{1,2,3,4}$ transitions of one Eu(III) site, the lower the symmetry of the site.

Furthermore the Eu(III) fluorescence decay rate allows determining the hydration state of Eu(III) in a given site. If no other fluorescence quenching ligands, except OH-oscillators of bonded water molecules are present in the inner coordination sphere of Eu^{3+}, the rate of radiationless de-excitation is directly proportional to the number of H_2O/OH^- ligands in the inner coordination sphere of the Eu(III) ion. According to the linear relationship developed by Horrocks and Sudnick [23], the number of associated hydration waters for Eu(III) is given by the following equation.

$$n(H_2O)=1.07k_{obs}-0.62$$

$n(H_2O)$: number of coordinated water molecules, k_{obs}: observed decay rate (reciprocal lifetime) of the excited state (ms^{-1}).

3. EXPERIMENTAL DETAILS

Eu^{3+} doted calcite samples

The investigated Eu-doped calcite crystals were synthesized by using a Mixed Flow Reactor (MFR). MFRs are particularly useful because they allow crystal growth under constant and controlled conditions with defined hydrodynamic conditions, saturation state, pH, ionic strength and temperature (25 ± 0.2 °C). In a stirred MFR, the concentrations of the precipitating and co-precipitating components are expected to be constant during the experiment and a homogeneous precipitate should be obtained. Co-precipitation was conducted over extended periods of time (up to three weeks). The MFR was fed by three independent solutions, which were introduced separately by a peristaltic pump (0.150 ml/min) from reservoir bottles. The input solutions were pumped from the reservoir bottles to the reactor at a constant rate so that the concentrations of the precipitating and co-precipitating components reach steady-state and remain constant. The reactor has an internal volume of 45 ml. Input solutions entered and left the reactor through a 0.45 μm pore size hydrofoil Teflon

membrane. Grained natural calcite was used as seed material for calcite precipitation. The specific surface area of the seed calcite measured by the N_2BET method was found to be 2.7 and 0.75 $m^2 \cdot g^{-1}$. In case of seeded co-precipitation, it is assumed that growth occurs only on the crystallites. The following input solutions (ionic strength I=0.01) saturated with respect to calcite were used for Eu(III) co-precipitation experiments: 1) 2 mM $CaClO_4$, 2) an appropriate mixture of 1.8 mM $NaHCO_3$ and 0.15 mM Na_2CO_3 resp. $KHCO_3$ and K_2CO_3, and 3) an Eu^{3+} solution. Concentration of calcium, sodium resp. potassium and europium were measured by ICP-MS.

The steady-state pH of the reacting solution was measured once a day and remained constant during the experiments. The steady-state calcite precipitation rate R has been determined as:

$$R \cdot (\mu mol \cdot m^{-2} \min^{-1}) = -\frac{F}{S \nu_i W_{seed}} \Delta C_i$$

ΔC_i: concentration difference between input and reacting solution of the element i; F: solution addition rate ($L \cdot min^{-1}$); S: specific reactive surface area ($m^2 \cdot g^{-1}$); W_{seed}: mass of calcite seeds (g); ν_i: molar fraction of element i in the calcite overgrowth.

To investigate the charge compensating influence of sodium on the incorporation of Eu^{3+} in the calcite structure, different samples were synthesized and investigated by time resolved laser fluorescence spectroscopy (TRLFS). Two samples Eu:calcite I and III were synthesized in the presence of Na^+ by using $NaHCO_3$ and Na_2CO_3. Another sample, Eu:calcite II was synthesized in the presence of K^+ ($KHCO_3$ and K_2CO_3).

All samples have been synthesized at similar pH (7.9 - 8.1) and similar temperature (25°C). The surface area of the seed calcite used for Eu:calcite I and II was about 0.4 m^2 whereas the surface of the seed calcite used for Eu:calcite II was about 0.075 m^2 (Tab. 1).

Tab. 1 Composition of the investigated europium doted calcite samples

Sample designation	Eu(III) content	Cation

Eu:calcite I	1020 µg.g-1	Na+
Eu:calcite II	646 µg.g-1	K+
Eu:calcite III	210 µg.g-1	Na+

Fluorescence measurements

TRLFS measurements were performed using a pulsed Xe:Cl (excimer) pumped dye laser system (frequency 20Hz). The dye QUI with an emission maximum at λ = 380 nm, was used for the UV excitation of the $^5L_6$ level to obtain the $^5D_0 \rightarrow {}^7F_{0,1,2}$ transitions of Eu^{3+}. The dye coumarin153 with emission maximum at λ = 520 nm was used for the direct excitation of the Eu(III) $^7F_0 \rightarrow {}^5D_0$ transition. For the detection of the fluorescence emission, an optical multi-channel system consisting of a polychromator with a 300, 600 and 1200 lines/mm grating and an ICCD camera were used.

The time resolved detection was controlled via a PG200 delay generator. The fluorescence lifetime was measured by varying the delay time between laser pulse and camera gating with time intervals of 20 to 100 µs.

For the low temperature spectroscopy the Eu:calcite powders were transferred in a self-constructed copper cell with a sapphire window sealed with a teflon disk and a total cell volume of 200 µL. The cooling system (Cryodyne Cryocooler Model 22C, compressor 8200, CTI-Cryogenics, USA) uses helium as the refrigerant. It consists of a continuous closed-cycle refrigeration, which allows cooling a copper sample holder at the cold head down to approximately 17 K in a two-stage decompression step. The cold head with the sample holder is surrounded by a vacuum chamber with four quartz windows. The pressure at low temperatures is in the range 10^{-4}–10^{-5} mbar. A microcontroller-based auto tuning temperature controller (Model 330-1X, Lake Shore, USA) with a silicon dioxide temperature sensor is used for temperature controlling. By use of the heater, temperatures between 17 K and 370 K can be adjusted. For sample excitation, the laser beam is focused on the copper cell in the

vacuum chamber. The fluorescence signal is collected via glass fiber and directed into the monochromator.

4. RESULTS

Time resolved laser fluorescence spectroscopy

All three samples Eu:calcite I, II and III were investigated by TRLFS at room temperature (RT) T~300 K and at low temperature T ~ 17 K.

At RT, the Eu^{3+} fluorescence emission spectrum of the $^5D_0 \rightarrow {}^7F_{0,1,2}$ transition when exciting the $^5L_6$ level were recorded in the region [18180-13515 cm^{-1}] and the time dependent fluorescence decay behavior was characterized (by the time dependent variation of the Eu^{3+} fluorescence intensity). The excitation profile of the $^5D_0 \rightarrow {}^7F_0$ region and the corresponding different site-dependent Eu(III) fluorescence emission spectra of the $^5D_0 \rightarrow {}^7F_{0,1,2}$ transitions were recorded.

To obtain a higher resolution fluorescence measurements at low temperature T~17 K were performed. The excitation profile of the $^5D_0 \rightarrow {}^7F_0$ transitions, the corresponding different site-dependent Eu(III) fluorescence emission spectra were recorded and the hydration state of Eu(III) occupying the given sites characterized.

Fluorescence emissions from $^5D_0 \rightarrow {}^7F_{0,1,2}$ transitions at 300 K

Fig. 1 shows the emission spectrum of Eu:calcite I at different delay times. For Eu:calcite I the intensity of the F_2 level is rather high due to the "hypersensitive effect". A slight splitting into at least two sublevels can be observed for the F_1 transition whereas a minimum of three sublevels is observed for the hypersensitive transition $^5D_0 \rightarrow {}^7F_2$ which is an indication for a strong ligand field. An exact characterization and quantification of the F_J sublevels is not possible at RT (since at RT the population of the F_J sublevels is comparable to thermal

population kT). One broadened $^5D_0 \rightarrow {}^7F_0$ transition appears in the emission spectra of Eu(III) in Eu:calcite I (Fig. 1), indicating the presence of a Eu(III) site with lower symmetry since this transition is forbidden for high symmetric crystallographic sites. The same observations were made for the fluorescence emission spectra of Eu(III) in Eu:calcite II and III.

Fluorescence decay

Fig. 2 shows the emission decay profiles of Eu:calcite I, II and III. The time resolved fluorescence decay of the $^5D_0 \rightarrow {}^7F_{0,1,2}$ transitions follow a bi-exponential decay behavior for all three samples, which indicates the presence of at least two Eu(III) species with different hydration shell in the calcite structure.

The hypersensitivity of the $^5D_0 \rightarrow {}^7F_2$ transition, expressed by the time dependent variation of the intensity ratio of the $^5D_0 \rightarrow {}^7F_2$ und $^5D_0 \rightarrow {}^7F_1$ transitions, can be used to characterize in a first approximation the complexation state of Eu(III). None of the three samples shows a constant F_2/F_1 intensity ratio with increasing delay time, which confirms the existence of at least two different Eu(III) species. Tab. 2 shows the variation of the F_2/F_1 intensity ratio at different delay times for Eu:calcite I.

Tab. 2. Intensity F_2/F_1 ratio at different delay times for Eu:calcite I

Sample	**delay time /µs**	1	501	1001	3001	5001	7001	9001
Eu:calcite I	**F_2/F_1**	1.49	1.41	1.32	1.16	1.08	1.01	0.93

In Fig. 1 the Eu(III) fluorescence emission spectra of Eu:calcite I at different delay times are shown. At short delay time, the fluorescence emission spectrum exhibits an intense F_1 and F_2 transition. At longer delay times when the emission of the shorter fluorescing Eu(III) species

has vanished, the spectrum is characterized by a relative decrease of the F_2 transition compared to the emission spectrum at shorter delays.

For the three Eu:calcite samples I, II, and III the decay behavior could be fitted with two different lifetimes. The lifetimes and the corresponding numbers of H_2O molecules in the first coordination sphere of Eu^{3+} are summarized in the Tab. 3.

The result of a detailed examination of the $^5D_0 \rightarrow {}^7F_0$ transition in the emission spectrum of Eu:calcite I at different delay times is shown in Fig. 3. With increasing delays, the main line shifts towards lower energy and the shoulder around 17309 cm^{-1} disappears.

The fluorescence emission spectra as well as the fluorescence decay clearly indicate that in calcite exist at least two differently hydrated Eu^{3+} species occupying different sites.

Tab. 3. Fluorescence emission lifetimes of Eu:calcite I, II and III

Sample	**bi-exponential decay lifetimes**	**inner sphere H_2O: n(H_2O)**
Eu:calcite I	798 ± 47 µs	0.72 ± 0.5
	3760 ± 200 µs	-0.34 ± 0.5
Eu:calcite II	1043 ± 81 µs	0.41 ± 0.5
	3572 ± 150µs	-0.32 ± 0.5
Eu:calcite III	1084 ± 65 µs	0.37 ± 0.5
	3723 ± 200 µs	-0.33 ± 0.5

Selective excitation: excitation spectra of the $^5D_0 \rightarrow {}^7F_0$ transition(s) at 300 K of Eu:calcite I

Since the $^5D_0 \rightarrow {}^7F_0$ transition is non degenerate, the excitation spectra of the $^5D_0 \rightarrow {}^7F_0$ transition allows determining the number of different sites occupied by Eu(III) in calcite.

Fig. 3a shows the excitation spectra of the $^5D_0 \rightarrow {}^7F_0$ transition of Eu:calcite I at 300 K and at different delay times. Two maxima are observed in the excitation spectra at 17310 cm^{-1} and

17269 cm^{-1}, indicating the emission from Eu(III) occupying two different sites in calcite: site 1 (17310 cm^{-1}) and site 2 (17269 cm^{-1}). The F_0 transitions of site 1 and site 2 are quite broad, in particular the F_0 transitions of site 2 shows a FWHM (full-width at half maximum) of ~13.5 cm^{-1}, which might indicate a distribution of discrete sites.

By changing the delay time, the ratio of the intensity of the two $^5D_0 \rightarrow {}^7F_0$ transitions changes. This shows that Eu(III) in the two sites has different fluorescence lifetime indicating two Eu(III) species with different hydration spheres. The shorter lifetime can be attributed to Eu(III) ions occupying site 1 and the longer lifetime to Eu(III) ions occupying site 2. The exact values of the lifetimes of these two sites were not determined. This observation is in a good agreement with the bi-exponential fluorescence decay behavior of Eu:calcite I by excitation of the $^7F_0 \rightarrow {}^5L_6$ transition at 25380 cm^{-1} (394 nm).The emission spectra of Eu(III) occupying site 1 and site 2 were obtained by exciting selectively each of the $^5D_0 \rightarrow {}^7F_0$ transitions.

Fig. 4 shows $^5D_0 \rightarrow {}^7F_{0,1,2}$ emission spectra of Eu(III) in site 1 (excited at 17310 cm^{-1}) and in site 2 (excited at 17269 cm^{-1}). The emission spectra of Eu(III) in these two sites show notably different features. The emission spectrum of site 1 exhibits a total splitting of the $^7F_1$ transition (3 sublevels) which is usually found for Eu(III) occupying low symmetry sites, whereas for the so-called hypersensitive $^7F_2$ level three components are observed. In the emission spectrum of site 2, a slight splitting of the $^7F_1$ level into two components and a splitting of the $^7F_2$ level into three sublevels can be distinguished.

Even though two maxima can clearly be distinguished, these F_0 transition remain rather broad. In order to get a better spectral resolution of the magnitude of the crystal-field splitting of the ^7F_J levels, so that the number of components of each sublevel can be determined more accurately, the three europium samples Eu:calcite I, II and III were investigated at low temperature.

Excitation spectra of the $^5D_0 \rightarrow {}^7F_0$ transition(s) at T < 20 K

To improve the discrimination between the spectra of the various kind of observed Eu(III) sites, the excitation spectra of the $^5D_0 \rightarrow {}^7F_0$ transition(s) and the corresponding site-dependent Eu(III) emission spectra of $^5D_0 \rightarrow {}^7F_{0,1,2}$ transitions were measured at low temperature (< 20 K). Fig. 5 shows the excitation spectra of the $^5D_0 \rightarrow {}^7F_0$ region of Eu:calcite I, II, and III. Three lines were observed at 17296, 17289 and 17253 cm^{-1} in all three Eu:calcite samples and identified as $^5D_0 \rightarrow {}^7F_0$ transitions, which are related to Eu(III) ions occupying three different sites. The $^5D_0 \rightarrow {}^7F_0$ line observed at 17253 cm^{-1} related to site C is quite large (~12 cm^{-1} FWHM) compared to the lines at 17286 (~1.3 cm^{-1} FWHM) and 17296 cm^{-1} (~1.5 cm^{-1} FWHM) related to the sites B and A. For Eu:calcite I and II, the F_0 transition of site A dominates the excitation spectrum, whereas for Eu:calcite III the excitation spectrum is dominated by the F_0 transition of site C. The relatively slight shifts to lower energy of the three identified F_0 transitions (nephelauxetic effect) indicate an increasing complexation strength as the energy of the F_0 transition decreases [24]. The ranges of the $^5D_0 \rightarrow {}^7F_0$ transition energies differ by 7 cm^{-1} and 43 cm^{-1} out of 17286 cm^{-1}.

Tab. 4. Excitation energy of the three Eu^{3+} sites (A, B, and C) in calcite

Site	Excitation energy cm^{-1}
A	17296
B	17289
C	17253

The emission spectra of these sites were obtained by exciting resonantly each of these levels (17296, 17289 and 17253 cm^{-1}). Fig. 6 shows the site selective emission spectra of Eu(III) ion at the sites labeled as A, B, and C in each of the Eu:calcite samples. The noticeably different

patterns observed when comparing the fluorescence emission of the sites A, B and C indicate very distinct chemical environments for Eu(III) in calcite.

The fluorescence emission spectra from $^5D_0 \rightarrow {}^7F_{0,1,2}$ transitions by excitation of the $^5D_0 \rightarrow {}^7F_0$ related to the sites A are identical in the three europium doted calcite samples. The emission spectrum of site A exhibits a total splitting of the $^7F_1$ transition (3 sublevels), whereas for the hypersensitive $^7F_2$ level three components can be observed (Fig. 6). The high splitting magnitude of the F_1 transition is typical for Eu(III) in a low symmetry site.

The fluorescence emission spectra from $^5D_0 \rightarrow {}^7F_{0,1,2}$ transitions by excitation of the $^5D_0 \rightarrow {}^7F_0$ related to the sites B are also identical in the three europium doted calcite sample. The emission spectrum of site B exhibits a total splitting of the $^7F_1$ transition (3 sublevels) as well of the hypersensitive $^7F_2$ level (five sublevels) (Fig. 6). These emission spectra correlate also with Eu(III) occupying a site with low symmetry.

Of particular interest are the emission spectra of site C (Fig. 7). The emission spectra of site C are identical in Eu:calcite I and III (both samples synthesized in presence of Na^+ ions) whereas the emission spectra of site C in Eu:calcite II (synthesized in presence of K^+ ions) is different.

The emission spectrum of site C in Eu:calcite I and III exhibits a twofold splitting of the $^7F_1$ transition and a threefold splitting of hypersensitive $^7F_2$ level (Fig. 6). The magnitude of the splitting of the F_1 and F_2 transitions correlate with a trigonal site symmetry. However, the relatively intense emission from the F_2 levels indicates that this site is not centrosymmetric (F_2 transition is forbidden for centrosymmetric sites) contrary to the C_{3i} site of Ca^{2+} in calcite.

The emission spectrum of site C in Eu:calcite II exhibits higher magnitude of the splitting than in the europium calcite samples synthesized in presence of Na^+. A threefold splitting of the $^7F_1$ transition and a fivefold splitting of the hypersensitive $^7F_2$ level characterize the fluorescence emission spectrum of this site (Fig. 7), indicating that the degeneracy of both

transitions has been completely removed. The total splitting of the F_1 and F_2 transitions is a clear indication for low symmetry site which indicates that the coordination geometry of site C is strongly disrupted in Eu:calcite II compared to the coordination geometry of site C in Eu:calcite I and III.

In the excitation spectrum of Eu:calcite I small peaks symbolized by (*) in Fig. 5 can be observed when exciting into the higher energy range (17310 – 17340 cm^{-1}). The emission spectra produced show more than 2J+1 sublevels for the F_J transitions. This forbidden feature is due to the simultaneous excitation of the Eu^{3+} ions in the different sites.

Fluorescence decay

The luminescent decays were measured for the $^5D_0 \rightarrow {}^7F_{0,1,2}$ emitting levels of Eu^{3+} occupying sites A, B and C in Eu:calcite I, II and III by exciting the $^5D_0 \rightarrow {}^7F_0$ transition related to each site. Fig. 8 shows the decay profiles of the sites A, B and C in Eu:calcite I,II and III. The time resolved decay of the $^5D_0 \rightarrow {}^7F_{0,1,2}$ transitions follows for each of the three sites a mono-exponential decay behavior. This is again a clear indication that Eu(III) is occupying three different sites in calcite. Tab. 5. summarizes the lifetimes of the three different Eu(III) sites.

Tab. 5. Fluorescence emission lifetimes of site A, B and C in Eu:calcite I, II and III

Sample	Site A	Site B	Site C
Eu:calcite I	460 ± 80 µs	4082 ± 350 µs	3603 ± 245 µs
Eu:calcite II	406 ± 80 µs	3616 ± 450 µs	2676 ± 157 µs
Eu:calcite III	384 ± 100 µs	3638 ± 420 µs	3661 ± 220 µs

Decay is fast for Eu(III) in site A, whereas the fluorescence lifetimes for the sites B and C are long. The average lifetime of 416 μs for Eu(III) in site A corresponds to an Eu(III) ion with 1-2 H_2O molecule in its inner coordination sphere, the long lifetime observed for Eu(III) in site B and C, correlates with the total loss of the hydration sphere for Eu(III) in both of the sites. The fluorescence lifetime of Eu(III) related to site C in Eu:calcite II is shorter than in the two other samples (Tab. 5), however, still large enough to indicate the complete loss of the hydration shell.

5. DISCUSSION AND CONCLUSION

Based on the information provided by the site selective time resolved laser fluorescence analysis, different sites in the three europium doted calcite samples were characterized.

At room temperature under selective excitation of the $^5D_0 \rightarrow {}^7F_0$ transition and the detection of the site dependent Eu(III) fluorescence emission spectra at different delay times, two differently hydrated Eu(III) ions occupying two different sites 1 and 2 could be characterized in the Eu:calcite I sample (at low temperature three sites A, B and C are found). Site 1 has been attributed to surface incorporated Eu^{3+} with one H_2O molecule in the inner coordination sphere, because of its fluorescence lifetime, the higher energy of the F_0 band (weaker complex than site 2) and the total splitting of the F_1 and F_2 transitions. Site 2's F_0 transition is shifted to lower energy, the F_1 and F_2 transitions are split less, together with a long fluorescence lifetime this coincides with Eu^{3+} incorporated into the calcite lattice. These results are in a good agreement with the TRLFS investigation at RT of Cm(III)/calcite suspension [14] and of Am(III) doted calcite synthesized under identical conditions as the samples investigated here [15]. However, the excitation spectra, emission spectra as well as the fluorescence lifetimes observed at RT provide only averaged information on the sites

induced by the interaction of Eu^{3+} with calcite. No significant spectroscopic differences have been observed between the different samples Eu:calcite I, II and III.

Spectroscopic measurements of the three europium doted samples at low temperature allowed to discriminate three unequivocal sites (sites A, B, and C) occupied by Eu(III) in calcite.

In the samples Eu:calcite I and II site A is the dominating site, which can be easily explained by the experimental conditions. Indeed for the growth of Eu:calcite I and II the surface area of calcite seed crystals used is about five times larger than the one used for Eu:calcite III, leading to more surface incorporated Eu(III) species. Additionally, the samples Eu:calcite I an II exhibit a much higher Eu^{3+} content than Eu:calcite III.

Site A can be observed without ambiguity in the three Eu:calcite samples. The position of the F_0 transition, the magnitude of the splitting of F_1 and F_2 transitions as well as the short fluorescence lifetime correlates with a Eu(III) ion incorporated at the calcite surface with 1-2 H_2O molecules in the first coordination sphere. A similar site has been observed by Piriou et al. [6]. However, the emission spectrum of Eu(III) at this site seems not to correlate with the one observed in the present study.

Site B has also been observed without ambiguity in all three Eu:calcite samples. The position of the F_0 transition, the total splitting of F_1 and F_2 transitions as well as the long fluorescence lifetime permitted to attribute these features to an Eu(III) species without H_2O molecules in the inner coordination sphere incorporated in the calcite structure. The emission spectrum of Eu(III) in this site is typical for a low symmetry site. Further information on the coordination chemistry of this site can not be deduced. This site was not observed in the study performed by Piriou et al. The spectroscopic features do not coincide with Eu^{3+} occupying a C_{3i} site.

The position of the F_0 transition and fluorescence lifetime measured for site C are in favor of Eu^{3+} incorporated into the calcite lattice. The energy of the F_0 transition of site C is the same

in the three samples indicating it is the same site in each sample. However the emission spectra of this site exhibits different features in Eu:calcite I and Eu:calcite II leading to the assumption that the exchange of Na^+ by K^+ has an impact on the substitution of Ca^{2+} by Eu^{3+}. In Eu:calcite I and II the energy of sublevels observed for the F_1 and F_2 transitions correlate with the number of sublevels generated by a trigonal site symmetry. If Eu^{3+} substitutes perfectly for Ca^{2+} in the centrosymmetric C_{3i} site of calcite, two levels are expected for the MD transition $F_0 \rightarrow F_1$, whereas the ED transition $F_0 \rightarrow F_2$ is forbidden. However, the substitution of Ca^{2+} by Eu^{3+} (different charge and cation size) creates local strains that seem to lower the symmetry of the site. The charge compensation by Na^+, or the substitution of divalent Ca^{2+} by trivalent Eu^{3+} itself, gives rise to a distortion of the site symmetry allowing stronger interaction with F_2 transitions.

The total splitting of the F_1 and F_2 transition in the emission spectrum of site C in Eu:calcite II (synthesized in presence of K^+ ions), indicates a strong distortion of this site compared to site C in Eu:calcite I and III (synthesized in presence of Na^+). Indeed, the magnitude of splitting is typical of Eu(III) occupying a low symmetry site in calcite. Two explanations are possible. The incorporation of the larger K^+ (138 pm) in the neighborhood of Eu^{3+} instead of smaller Na^+ (102 pm) would lower the symmetry of the site considerably. A similar effect would be induced by a vacancy site in the neighborhood of Eu^{3+} since K^+ is too large for the Ca^{2+} site. Both mechanisms proof the charge-compensating role of Na^+ during the incorporation of Eu^{3+} into calcite. Additionally, the lifetime of Eu(III) in site C is considerably shortened (2676 μs) in Eu:calcite II compared to Eu:calcite I and II (~3600 μs) which might be explained by a lowering of the site symmetry. The characterization at low temperature of different Eu(III) sites in calcite are in good agreement with the low temperature TRLFS measurements performed on homogenous doted Am(III) calcite [15]. This site selective time resolved laser

fluorescence spectroscopic study presents the first results of the coupled substitution mechanism in the presence of Na^+: $An/LnNa(CO_3)_2$ - $CaCO_3$: $2Ca^{2+} \leftrightarrow Na^+ + An^{3+}/Ln^{3+}$.

The spectroscopic method (site selective time resolved laser fluorescence spectroscopy) applied for the investigation of the interaction of Eu^{3+} with calcite allowed the discrimination and molecular level characterization of three discrete Eu(III) sites.

Acknowledgments

This work was co-financed by the Helmholtz Gemeinschaft Deutscher Forschungszentren (HGF) by supporting the Helmholtz-Hochschul-Nachwuchsgruppe "Aufklärung geochemischer Reaktionsmechanismen an der Wasser/Mineralphasen Grenzfläche".

List of figures

Fig. 7. Emission spectra of the $^5D_0 \rightarrow {}^7F_{0,1,2}$ transitions of site C at T < 20 K in Eu:calcite II and III. Excitation at 17253 cm^{-1}.

Fig. 8. Fluorescence decay profiles of the $^5D_0 \rightarrow {}^7F_{0,1,2}$ transitions for site A, B and C when exciting the $^5D_0 \rightarrow {}^7F_0$ transition of site A, B and C at 17296 cm^{-1}, 17289 cm^{-1} and 17253 cm^{-1}.

Figures

Fig. 1

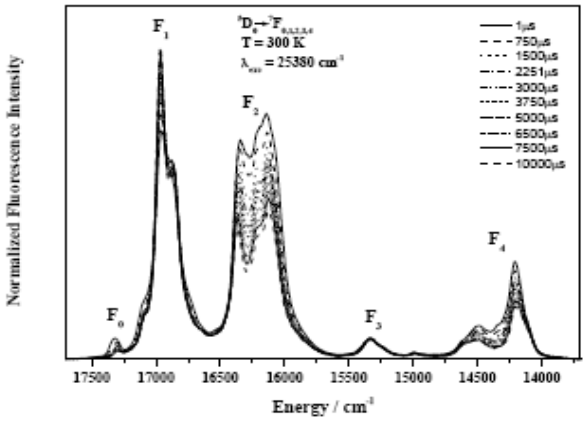

Fig. 2

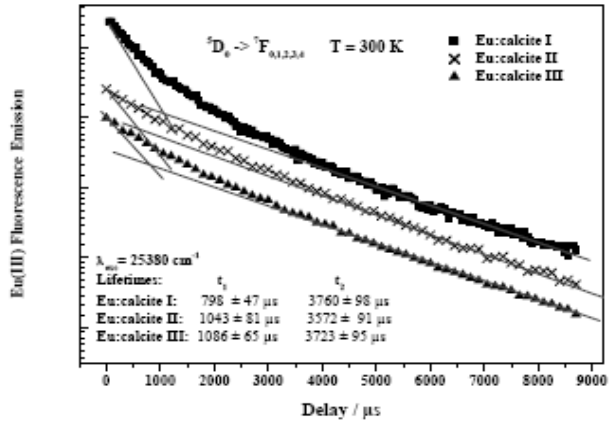

Fig. 3

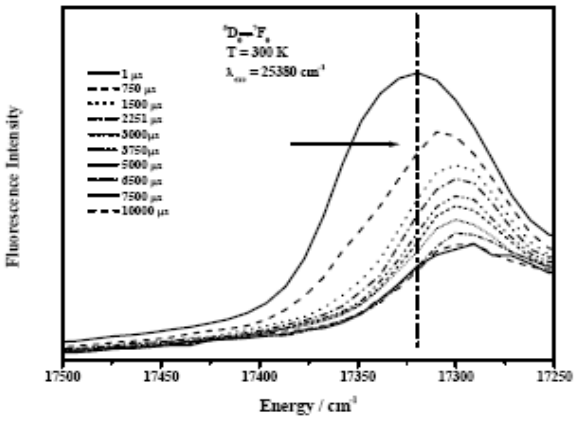
$^5D_0 \rightarrow ^7F_0$
T = 300 K
λ_{exc} = 25380 cm^{-1}
1 µs
750 µs
1500 µs
2251 µs
3000µs
3750µs
5000 µs
6500 µs
7500 µs
10000 µs
Fluorescence Intensity
17500
17450
17400
17350
17300
17250
Energy / cm^{-1}

Fig. 3a

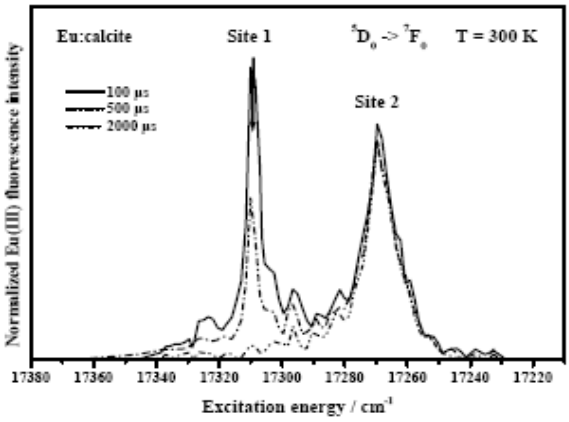
Eu:calcite
Site 1
$^5D_0 \rightarrow ^7F_0$
T = 300 K
Site 2
100 µs
500 µs
2000 µs
Normalized Eu(III) fluorescence intensity
17380
17360
17340
17320
17300
17280
17260
17240
17220
Excitation energy / cm^{-1}

Fig. 4

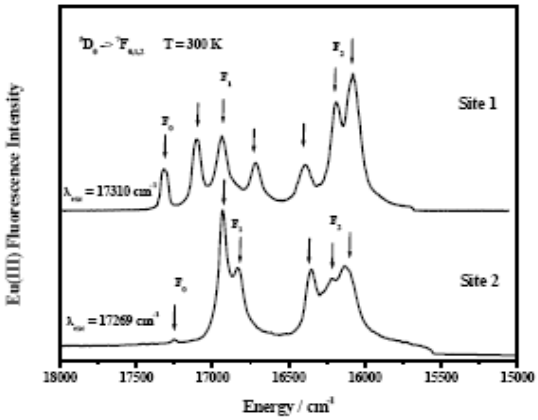
Eu(III) Fluorescence Intensity
Site 1
Site 2
18000
17500
17000
16500
16000
15500
15000
Energy / cm-1

Fig. 5

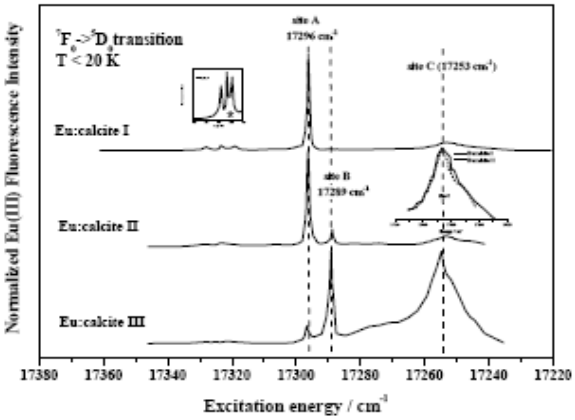
Normalized Eu(III) Fluorescence Intensity
Eu:calcite I
Eu:calcite II
Eu:calcite III
17380
17360
17340
17320
17300
17280
17260
17240
17220
Excitation energy / cm-1

Fig. 6

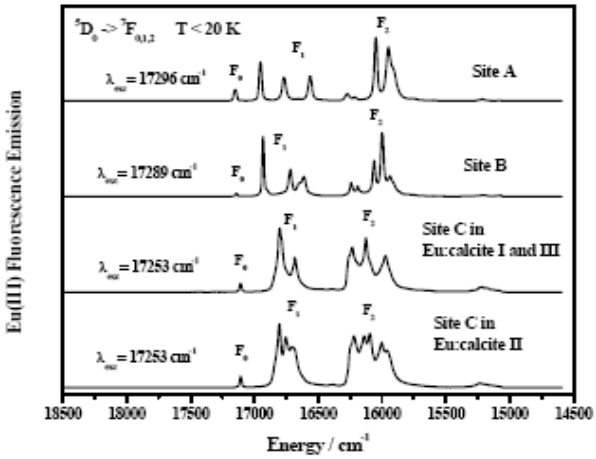
$^5D_0$ -> $^7F_{0,1,2}$ T < 20 K
λ_{exc} = 17296 cm^{-1}
λ_{exc} = 17289 cm^{-1}
λ_{exc} = 17253 cm^{-1}
λ_{exc} = 17253 cm^{-1}
F_0
F_1
F_2
Site A
Site B
Site C in Eu:calcite I and III
Site C in Eu:calcite II
Eu(III) Fluorescence Emission
18500 18000 17500 17000 16500 16000 15500 15000 14500
Energy / cm^{-1}

Fig. 7

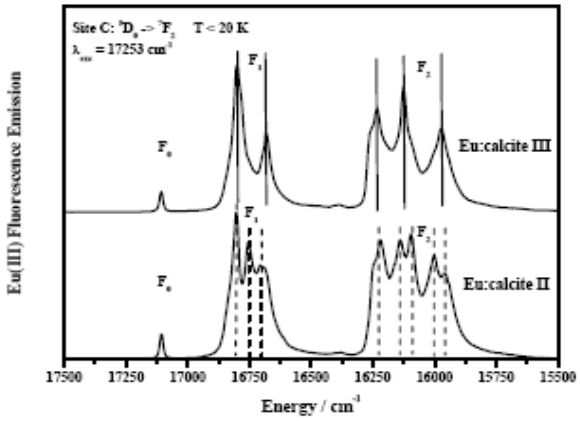
Site C: $^5D_0$ -> $^7F_2$ T < 20 K
λ_{exc} = 17253 cm^{-1}
F_0
F_1
F_2
Eu:calcite III
Eu:calcite II
Eu(III) Fluorescence Emission
17500 17250 17000 16750 16500 16250 16000 15750 15500
Energy / cm^{-1}

Fig. 8

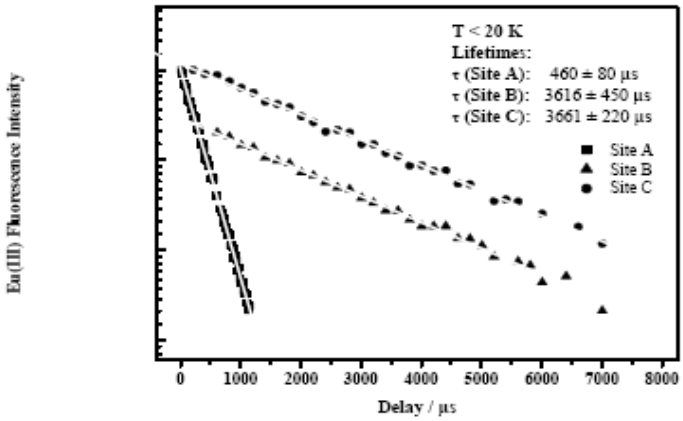
T < 20 K
Lifetimes:
τ (Site A): 460 ± 80 µs
τ (Site B): 3616 ± 450 µs
τ (Site C): 3661 ± 220 µs
Site A
Site B
Site C
Eu(III) Fluorescence Intensity
0
1000
2000
3000
4000
5000
6000
7000
8000
Delay / µs

Bibliography

1. Lavin, V., U.R. Rodriguez-Mendoza, I.R. Martin, and V.D. Rodriguez, Optical spectroscopy analysis of the Eu3+ ions local structure on calcium diborate glasses. Journal of Non-Crystalline solids, 2003. 319: p. 200-216.

2. Lavin, V., P. Babu, C.K. Jayasankar, I.R. Martin, and V.D. Rodriguez, On the local structure of 3+ ions in oxyfluoride glasses. Comparison with fluoride and oxide glasses. Journal of Chemical Physics, 2001. 115(23): p. 10935-10944.

3. Capobianco, J.A., P.P. Proulx, N. Raspa, D.J. Simkin, and D. Krashkevich, Site selective spectroscopy and crystal field analysis of Eu3+ doped in lanthanum-calcium-zirconium-silicon borate. Journal of Chemical Physics, 1989. 90(6): p. 2856-2864.

4. Eilers, H. and B.M. Tissue, Laser spectroscopy of nanocrystalline Eu2O3 and Eu3+:Y2O3. Chemical Physics Letters, 1996. 251: p. 74-78.

5. Binnemans, K. and C. Görller-Walrand, Crystalfield analysis of EuCl3-6H2O. Journal of Alloys and Compounds, 1997. 250: p. 326-331.

6. Piriou, B., M. Fedoroff, J. Jeanjean, and L. Bercis, Characterization of the sorption of europium(III) on calcite by site-selective and time-resolved luminescence spectroscopy. Journal of Colloid and Interface Science, 1997. 194(2): p. 440-447.

7. Shannon, R.D., Revised effective ionic radii and systematic studies of interatomic distances in halides and chalcogenides. Acta Crystallographica section A, 1976. 32: p. 751-167.

8. Terakado, Y. and A. Masuda, The Coprecipitation of Rare-Earth Elements with Calcite and Aragonite. Chemical Geology, 1988. 69(1-2): p. 103-110.

9. Lakshtanov, L.Z. and S.L.S. Stipp, Experimental study of Europium(III) coprecipitation with calcite. Geochimica Et Cosmochimica Acta, 2004. 68(4): p. 819-827.

10. Zhong, S.J. and A. Mucci, Partitioning of Rare-Earth Elements (Rees) between Calcite and Seawater Solutions at 25-Degrees-C and 1 Atm, and High Dissolved Ree Concentrations. Geochimica Et Cosmochimica Acta, 1995. 59(3): p. 443-453.

11. Zavarin, M., S.K. Roberts, N. Hakem, A.M. Sawvel, and K.A. B., Eu(III), Sm(III), Np(V), Pu(V), and Pu(IV) sorption to calcite. Radiochimica Acta, 2005. 93(2): p. 93-102.

12. Elzinga, E.J., R.J. Reeder, S.H. Withers, R.E. Peale, R.A. Mason, K.M. Beck, and W.P. Hess, EXAFS study of rare-earth element coordination in calcite. Geochimica Et Cosmochimica Acta, 2002. 66(16): p. 2875-2885.

13. Withers, S.H., R.E. Peale, A.F. Schulte, G. Braunstein, K.M. Beck, W.P. Hess, and R.J. Reeder, Broad distribution of crystal-field environments for Nd^{3+} in calcite. Physics and Chemistry of Minerals, 2003. 30(7): p. 440-448.

14. Stumpf, T. and T. Fanghänel, A time-resolved laser fluorescence spectroscopy (TRLFS) study of the interaction of trivalent actinides (Cm(Ill)) with calcite. Journal of Colloid and Interface Science, 2002. 249(1): p. 119-122.

15 Stumpf, T., M. Marques Fernandes, C. Walther, K. Dardenne, D. Bosbach, and T. Fanghanel, Structural characterization of Am incorporated into calcite: A TRLFS and EXAFS study. Journal of Colloid and Interface Science, 2006. 302(1): p. 240-245.

16. Curti, E., D.A. Kulik, and J. Tits, Solid solutions of trace Eu(III) in calcite: Thermodynamic evaluation of experimental data over a wide range of pH and pCO2. Geochimica Et Cosmochimica Acta, 2005. 69(7): p. 1721-1737.

17. Carnall, W.T., The absorption and fluorescence spectra of rare earth ions in solution, in Handbook on the Physics and Chemistry of rare earth, K.A. Gschneider and L. Eyring, Editors. 1979, North Holland publishing company. p. 171-206.

18. Görller-Walrand, C. and K. Binnemans, Rationalization of crystal-field parametrization, in Handbook on the Physics and Chemistry of rare earth, K.A. Gschneider and L. Eyring, Editors. 1996, Elsevier Science. p. 122-268.

19. Carnall, W.T., G.L. Goodman, K. Rajnak, and R.S. Rana, A systematic analysis of the spectra of the lanthanides doped into single crystal LaF3, R.A. 88-8, Editor. 1988, Argonne National Laboratory.

20. Judd, B.R., Optical Absorption Intensities of Rare Earth Ions. Physical Review, 1962. 127: p. 750.

21. Bünzli, J.C.G. and G.R. Choppin, Lanthanides Probes in Life, Chemical and Earth Sciences.Theory and Practice. Elsevier Science Publischer, 1989.

22. Jorgensen Klixbüll, C. and B.R. Judd, Hypersensitive pseudoquadropole transitions in Lanthanides. 1964.

23. Horrocks, W. DeW.; Sudnick, D. R., Lanthanide Ion Probes of Structure in Biology. Laser Induced Luminescence Decay Constants Provide a Direct Measure of the Number of Metal-Coordinated Water Molecules. J. Am. Chem. Soc., 1979, 101, p. 334-340.

24. Albin, M. and W.D. Horrocks, Europium (III) luminescence excitation spectroscopy. Qunatitative correlation between the total charge on the ligands and the 7F0-5D0 transition frequency in europium(III) complexes. Inorganic Chemistry, 1985. 24: p. 895-900.

Environ. Sci. Technol. **2007**, *41*, 3186–3191

Incorporation of Eu(III) into Hydrotalcite: A TRLFS and EXAFS Study

T. STUMPF,*,†,‡ H. CURTIUS,§ C. WALTHER,† K. DARDENNE,† K. UFER,§ AND T. FANGHÄNEL‡,∥

Forschungszentrum Karlsruhe GmbH, Institut für Nukleare Entsorgung, P.O. Box 3640, D-76021 Karlsruhe, Germany, Ruprecht-Karls-Universität Heidelberg, Physikalisch-Chemisches Institut, Im Neuenheimer Feld 253, 69120 Heidelberg, Germany, Forschungszentrum Jülich GmbH, Institut für Sicherheitsforschung und Reaktorsicherheit, 52425 Jülich, Germany, and European Commission, Joint Research Center, Institute for Transuranium Elements, P.O. Box 2340, 76125 Karlsruhe, Germany

The behavior of radionuclides in the environment (geo-, hydro-, and biosphere) is determined by interface reactions like adsorption, ion exchange, and incorporation processes. Presently, operational gross parameters for the distribution between solution and minerals are available. For predictive modeling of the radionuclide mobility in such systems, however, individual reactions and processes need to be localized, characterized, and quantified. A prerequisite for localization and clarification of the concerned processes is the use of modern advanced analytical and speciation methods, especially spectroscopy. In this study, Eu(III) was chosen as an analogue for trivalent actinides to identify the different species that occur by the Ln(III)/hydrotalcite interaction. Therefore, Eu(III) doped Mg–Al–Cl–hydrotalcite was synthesized and investigated by TRLFS, EXAFS, and XRD measurements. Two different Eu/hydrotalcite species were obtained. The minor part of the lanthanide is found to be inner-sphere sorbed onto the mineral surface, while the dominating Eu/hydrotalcite species consists of Eu(III) that is incorporated into the hydrotalcite lattice. Both Eu/hydrotalcite species have been characterized by their fluorescence emission spectra and lifetimes. Structural parameters of the incorporated Eu(III) species determined by EXAFS indicate a coordination number of 6.6 ± 1.3 and distances of 2.41 ± 0.02 Å for the first Eu–OH shell.

Introduction

The behavior of actinides in the environment is to a large extent governed by reactions like adsorption, ion exchange, and incorporation processes. Especially, the incorporation of actinides into secondary phases and the formation of solid solutions play a key role in the retardation process. In literature, the interaction of radionuclides with mineral surfaces is often described by operational distribution coefficients. These distribution coefficients (K_d values) are macroscopic parameters that are valid only for the mineral and solute composition of a given system. Their application is rather limited. For this purpose, the interaction mechanisms and the formation process of solid solutions need to be understood on a molecular level. A substantial contribution can be achieved by the application of spectroscopic methods.

Different leaching experiments with material test reactor fuel elements (*1*) in highly concentrated salt brines at 90 °C showed that the radionuclides were rapidly mobilized but then trapped by the corrosion products (*2*). It was found that one important secondary corrosion product is a Mg–Al–Cl layered double hydroxide (LDH), also referred to as a hydrotalcite-like compound (HTlc) (*3*).

Hydrotalcite-like compounds can be structurally characterized as brucite-like layers in which some divalent cations have been substituted by trivalent ions to form positively charged sheets (*4*). The cationic charge created in the layers is compensated by the presence of hydrated anions in the interlayer. The main features of HTlc structures and of HTlc properties are determined by the nature of the brucite-like sheet, by the type of stacking of the brucite-like sheets, by the amount of water, and by the position and type of anions in the interlayer.

In this paper, the synthesized secondary phase Mg–Al–Eu–Cl–hydrotalcite was investigated by time-resolved laser fluorescence spectroscopy (TRLFS) and X-ray absorption spectroscopy (XAS). Europium was chosen as a nonradioactive analogue for trivalent actinides because its high fluorescence yield enables speciation studies in the submicromol concentration range (*5*, *6*). In previous TRLFS studies of Eu(III) sorption onto γ-alumina (*7*), silica (*8*), clay minerals (*9*), and calcite (*10*), different surface sorbed and incorporated europium species have been identified.

The positions of the main Eu(III) fluorescence emission bands ($^5D_0 \rightarrow {}^7F_{1-4}$ transitions) are almost independent of the chemical environment of the metal ion. Only the intensity of the $^5D_0 \rightarrow {}^7F_2$ transition changes significantly when Eu(III) is complexed. This is a consequence of the so-called hypersensitive effect, which is described elsewhere (*11–13*). Additional information can be derived by observation from the $^5D_0 \rightarrow {}^7F_0$ transition (*14*, *15*). The ground state $^7F_0$ is nondegenerate. This simplifies the interpretation of Eu(III) spectra to a great extent because only one transition is expected for each Eu species. TRLFS enables us also to study the hydration status of the Eu species. The rate of the fluorescence decay depends on radiative and nonradiative processes. Nonradiative decay is due mainly to energy transfer from the excited state to ligand vibrations (e.g., OH vibration of coordinated H_2O molecules). The experimental lifetime for the Eu^{3+} aquo ion is 110 ± 5 μs in water (*5–10*). A linear correlation is observed between the decay rate and the number of H_2O molecules in the first coordination sphere of Eu(III), where a lifetime of 110 μs corresponds to 9 and 1725 μs corresponds to zero H_2O molecules (*16*). Hence, TRLFS with Eu(III) allows us to distinguish between surface sorption and incorporation into the lattice of a given mineral. Additional information about atomic distances and coordination numbers of incorporated lanthanide or actinide ions can be derived by XAS spectroscopy (*17*, *18*). As shown in the present paper, the combination of the two complementary spectroscopic methods XAS and TRLFS allows us to characterize and quantify Eu(III)/hydrotalcite incorporation species.

* Corresponding author phone: 0049 (0)7247-82 6023; fax: 0049 (0)7247-82 3927; e-mail: Thorsten.Stumpf@ine.fzk.de.
† Institut für Nukleare Entsorgung.
‡ Ruprecht-Karls-Universität Heidelberg.
§ Institut für Sicherheitsforschung und Reaktorsicherheit.
∥ European Commission.

10.1021/es0624873 CCC: $37.00 © 2007 American Chemical Society
Published on Web 03/31/2007

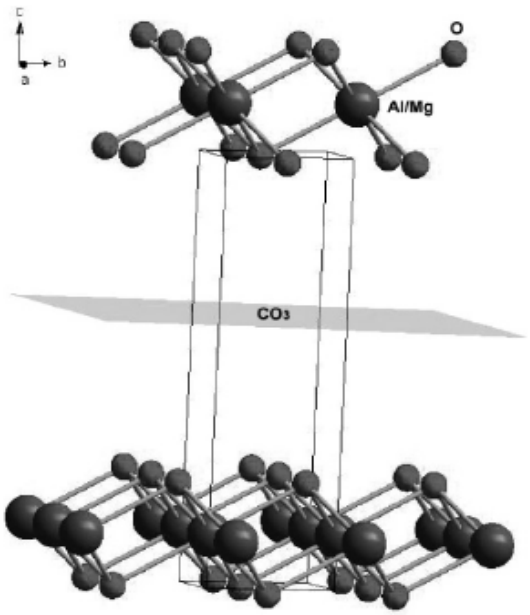

FIGURE 1. Perspective view of the hydrotalcite structure. Al/Mg is represented as big balls, O is the smaller balls, and CO_3 is located in the gray plane.

Experimental Procedures

Deionized water was boiled and stored under an argon atmosphere before use. Chemicals were purchased from Merck and Aldrich and used without further treatment. All experiments were performed under an argon atmosphere.

Two Eu(III) doped hydrotalcite samples with different lanthanide concentrations were synthesized. For the preparation of Mg–Al–Eu–Cl–LDH, a three-necked glass flask was filled with 250 mL of water, and the pH was adjusted to 10 using NaOH. A mixed aqueous solution (250 mL) of $MgCl_2 \cdot 6H_2O$ (0.3 M), $AlCl_3 \cdot 6H_2O$ (0.09 M), and $EuCl_3 \cdot 6H_2O$ (0.01 M) for Eu/hydrotalcite **1** and of $MgCl_2 \cdot 6H_2O$ (0.15 M), $AlCl_3 \cdot 6H_2O$ (0.04 M), and $EuCl_3 \cdot 6H_2O$ (0.01 M) for Eu/hydrotalcite **2** was added over a period of 3 h, while the pH was kept at 10 and the temperature was maintained at 70 °C. After complete addition, the temperature was raised to 90 °C, and the solution was stirred for 24 h. After cooling to room temperature, the precipitate formed was filtered and then dialyzed at 60 °C. A dialysis hose was filled with the substance and placed in a 2 L vessel containing deionized water. The water was exchanged until it was almost chloride-free (chloride measurements were performed with the cuvette test LCK 311, DR. LANGE). The precipitate was filtered, dried in a desiccator, and characterized by photometry, XRD, DTA-TGA, FTIR, and ICP-MS. For the DTA-TGA, XRD, and FTIR measurements, dry samples were milled to powder. For photometric and ICP-MS measurements, the solid samples were dissolved in 2 M HNO_3. The XAFS sample was pressed in dried form into a polyethylene pellet of 13 mm diameter.

TABLE 1. Metric Parameters[a] of Hydrotalcite Used as Model[b] as Compared to Normal Structure[c]

back-scatterer	*N*	*R* (Å) hydrotalcite	*R* (Å) model
O (from OH)	6	2.03	2.40
Al	6	3.06	3.36
O (from OH)	6	3.67	3.95
C	2	4.00	4.20
O	6	4.19	4.41

[a] *R* = distances and *N* = coordination numbers. [b] Eu(III) as center of the cluster. [c] Mg/Al as center; issued from a structure refinement based on ref *23*.

From these results, the formula of Eu/hydrotalcite **1** could be derived as $[Mg_3Al_{0.94}Eu_{0.099}(OH)_8]Cl_{0.94}(CO_3)_{0.03} \cdot 5.04H_2O$, whereas the formula of Eu/hydrotalcite **2** was calculated to be $[Mg_3Al_{0.84}Eu_{0.22}(OH)_8]Cl_{0.88}(CO_3)_{0.06} \cdot 2.46H_2O$. The specific surface area of Eu/hydrotalcite **1** was 72 m^2/g, while the cationic exchange capacity was 83 mmol/100 g. In the case of Eu/hydrotalcite **2**, the measured BET surface area was 54 m^2/g, and the cationic exchange capacity was 76 mmol/100 g. The treatment of the Mg–Al–Eu–Cl–hydrotalcites with ammonium carbonate solution as described by Duff et al. (*19*) did not result in any change of the Mg–Al–Eu molar ratios, indicating that the Eu in both cases was mainly incorporated into the hydrotalcite lattice.

TRLFS measurements were performed using a pulsed excimer pumped dye laser system. Details are given elsewhere

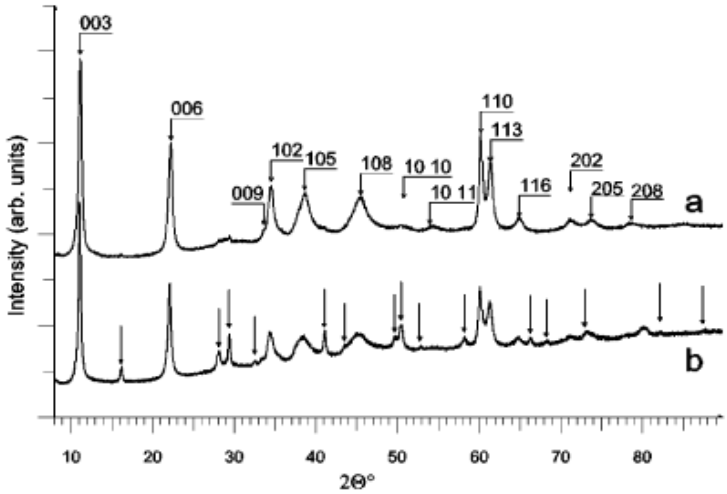

FIGURE 2. XRD pattern of Eu/hydrotalcite 1 (a) and 2 (b). Pattern a indexed for a $R\bar{3}m$ unit cell. $Eu(OH)_3$ peaks in pattern b are marked with an arrow.

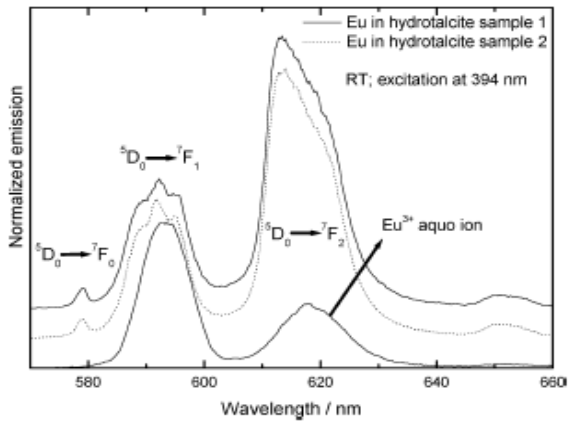

FIGURE 3. Emission spectrum of the Eu^{3+} aquo ion together with the Eu(III) spectra of the solid samples Eu/hydrotalcite 1 and 2 by exciting at 394.0 nm.

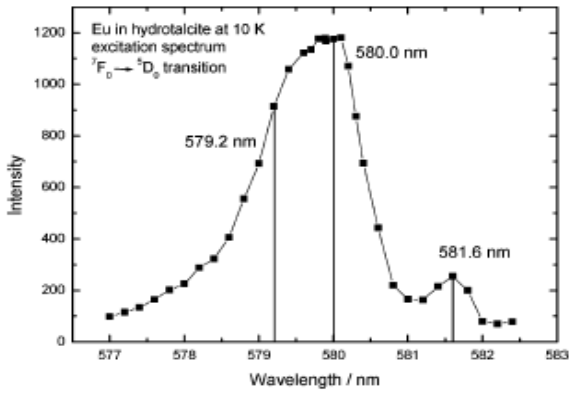

FIGURE 4. Eu(III) excitation spectrum of Eu/hydrotalcite 1, measured at 10 K.

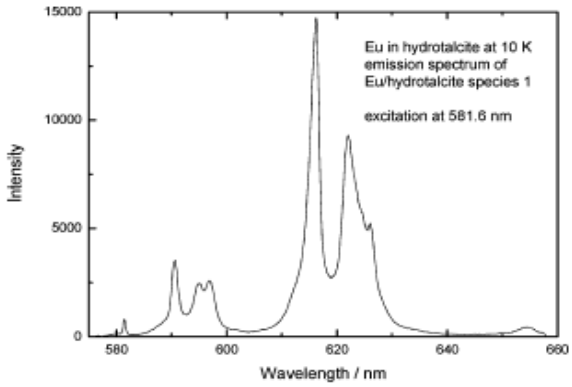

FIGURE 5. Fluorescence emission spectrum of Eu(III)/hydrotalcite species 1; excitation at 581.6 nm.

(*18*, *20*, *21*). An ICCD camera and a polychromator with 300: 600:1200 lines/mm grating were used in this system. The fluorescence emission spectra of Eu(III) were recorded within a constant time window of 1 ms, exciting at 394.0, 578.2, 580.0, and 581.6 nm. The Eu(III) emission decay was recorded within a constant time window of 10 ms, and the delay time between laser pulse and camera gating was scanned with time intervals of 25 and 50 μs, respectively.

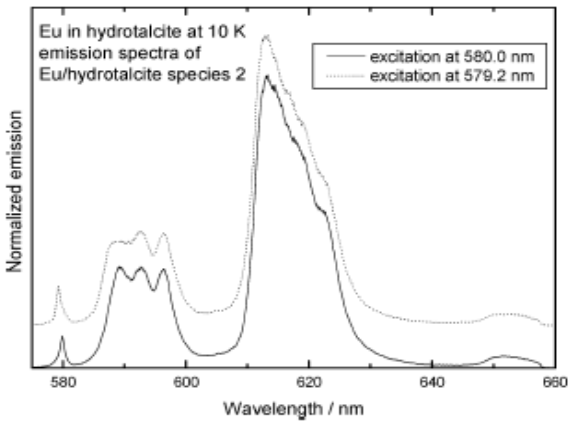

FIGURE 6. Fluorescence emission spectrum of Eu(III)/hydrotalcite species 2; excitation at 580.0 and 579.2 nm.

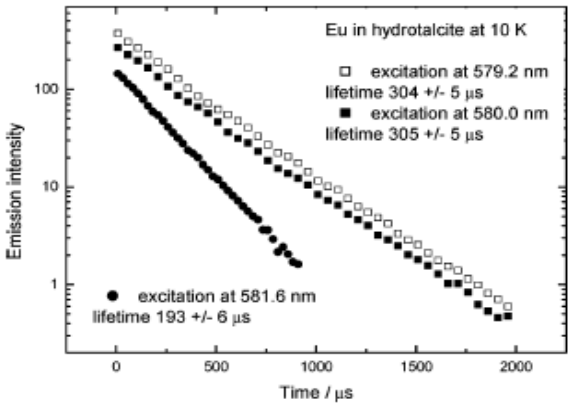

FIGURE 7. Time dependence of Eu(III) fluorescence emission decay by selective excitation of Eu(III)/hydrotalcite species 1 and 2.

Eu L_{III} X-ray absorption fine structure (XAFS) spectra were recorded at the INE beamline (ANKA, Karlsruhe, Germany). N_2 filled ionization chambers at ambient pressure were used. Spectra were energy calibrated to the first inflection point in the XANES of a Fe foil (7.112 keV) measured simultaneously. The Eu(III) doped hydrotalcite XAFS was recorded at room temperature in fluorescence mode using a Canberra LEGe five-element solid state detector. Si <111> crystals were used in the monochromator, operating in fixed-exit mode. The incident intensity was held constant by means of a piezo-driven feedback system to the second crystal. The parallel alignment of the crystal faces was detuned to ~70% of the maximum beam intensity.

The fluorescence spectrum was corrected for self-absorption using the FLUO software (D. Haskel, unpublished results), which is one of the UWXAFS suite of programs (*22*). EXAFS fits were performed with feffit (*22*) using phase and amplitude data calculated for single scattering paths. Eu incorporation in the hydrotalcite structure is shown in Figure 1 (*23*), and the different shells expected are listed in Table 1. The cell parameters were increased to account for the larger size of the Eu cation (+0.40 Å) as compared to Mg and Al (Table 1). Fits were carried out in the *R*-space (1−3.5 Å) using the (1.5−12.2 $Å^{-1}$) *k*-range, which yielded a maximum resolution δR of 0.15 Å.

The XRD data were collected with a Bruker D8 Advance diffractometer. The diffractometer with Bragg−Brentano geometry was equipped with a Cu tube, an automatic

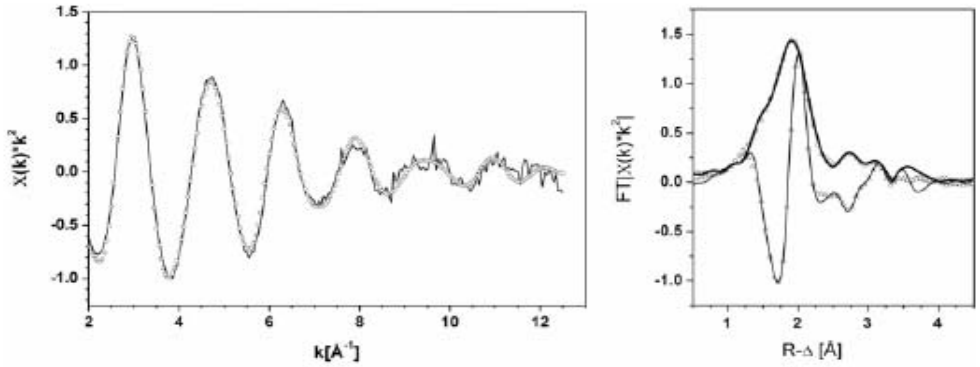

FIGURE 8. (Left) k^2-weighted Eu(III) L_{III}-edge EXAFS of the Eu(III)/hydrotalcite 1 sample (solid line) and its fit result (open circles) and (right) corresponding FT magnitude (thick solid line) and fit result (open symbols).

TABLE 2. Metric Parameters[a] from Least-Squares Analysis of FT Data[b]

sample	back-scatterer	R (Å) (±0.02 Å)	N (±20%)	σ^2 (Å^2) × 10^{-3}	ΔE_0 (eV)	goodness of fit (%)
Eu doped hydrotalcite	O from OH	2.41	6.6	9.0	3.0	0.8
	Al	3.20	0.7	1.0	5.8	
	Al	3.41	1.5	6.6		

[a] R = distances, N = coordination numbers within 20% error, σ^2 = EXAFS Debye–Waller factors, and ΔE_0 = relative energy shifts held as global parameters for like atoms. [b] S_0^2 was held constant at 1.0.

divergence slit (6 mm sample length in this work), and a position sensitive detector (Vantec) with an active length of 3°. The patterns were recorded from 8 to 90° 2Θ with a step width of 0.007° 2Θ and a total measuring time of 5 h.

Results and Discussion

XRD Measurements. In Figure 2, the X-ray diffraction patterns of Eu/hydrotalcite **1** (pattern a) and Eu/hydrotalcite **2** (pattern b) are shown. The maxima of pattern a can be indexed as the reflections of a Cl^- exchanged hydrotalcite with space group $R\bar{3}m$. However, the {*hkl*} dependent broadening of the reflections suggests that these hydrotalcites contain defective stacking sequences of different polytypes (*24*). Besides the hydrotalcite reflections, pattern b shows additional reflections. These reflections match the peak positions of $Eu(OH)_3$ (JCPDF card no. 01-083-2305). Hence, we conclude that in both cases, Eu(III) doped hydrotalcite is synthesized, but the higher Eu(III) concentration of Eu/hydrotalcite **2** leads to the formation of the additional pure Eu(III) phase $Eu(OH)_3$.

TRLFS Measurements at Room Temperature. In Figure 3, the emission spectrum of the Eu^{3+} aquo ion together with the spectra of Eu(III) in the solid samples of Eu/hydrotalcite **1** and **2** by exciting at 394.0 nm are shown. Whereas compared to sample **1**, Eu/hydrotalcite **2** contained twice the concentration of Eu(III). In comparison to the spectrum of Eu^{3+}-(aq), the signal of the $^5D_0 \rightarrow {}^7F_2$ transition of Eu in hydrotalcite is very pronounced as a result of the hypersensitive effect, which was mentioned before. The spectra of hydrotalcite **1** and **2** are very similar, indicating that in both samples, the same europium species are present. This assumption is validated by the measured emission lifetimes of hydrotalcite **1** and **2**. The observed decay of the fluorescence emission of Eu(III) in both solid samples is identical within the experimental errors. A monoexponential fit describes the emission decay satisfactorily, indicating that only one dominating Eu(III) hydration sphere in the Eu/hydrotalcite system exists. A lifetime of 285 ± 10 μs was detected. The increase in lifetime to a value of 285 ± 10 μs in both Eu hydrotalcite samples in comparison to 110 μs measured for Eu^{3+} (aq) indicates the exclusion of water molecules from the first coordination shell of Eu(III). According to the method developed by Horrocks and Sudnick (*16*), the number of water molecules in the first coordination shell decreases from 9 to 3 ± 1. Taking the similarities of the emission spectra and fluorescence emission lifetimes of Eu/hydrotalcite **1** and **2** into account, we suggest that both doped hydrotalcites show an identical spectroscopic behavior. Therefore, further experiments were carried out by using only one sample: Eu/hydrotalcite **1**.

TRLFS Measurements at 10 K. At low temperature, the Eu(III) spectra of solid samples exhibit additional structures that are not present at room temperature. Especially, the narrowing of the excitation and emission bands allows us to distinguish between different Eu(III) species. The excitation spectrum of Eu/hydrotalcite **1** measured at 10 K is shown in Figure 4. Eu(III) is excited to the $^5D_0$ level instead of excitation to the $^5L_6$ level (excitation wavelength 394.0 nm), as is the case for the previous section. Two peaks are observed. The dominating one has its peak maximum at 580.0 nm, whereas the second signal shows a peak maximum at 581.6 nm. Because of the fact that the ground state $^7F_0$ is nondegenerate and therefore each $^5D_0 \rightarrow {}^7F_0$ transition belongs to exactly one Eu species, we conclude that two different Eu(III)/hydrotalcite species exist. Excitation at 581.6 nm leads to the emission spectrum shown in Figure 5. The $^5D_0 \rightarrow {}^7F_1$ and $^5D_0 \rightarrow {}^7F_2$ emission bands are each split three-fold. Because of the selection rules for Eu(III) F_J transitions, such a strong splitting indicates a low site symmetry around the europium atom (*14*). The obtained emission decay of this Eu/hydrotalcite species **1** (selective excitation at 581.6 nm) is monoexponential, and the lifetime is found to be 193 ± 6 μs, which corresponds to 4.9 ± 0.5 water molecules in the first Eu(III) coordination shell. A value of ~5 water molecules in the first coordination sphere is usually found for actinide and lanthanide inner-sphere surface complexes. Taking the emission spectrum and the emission lifetime into account, we suggest that Eu/hydrotalcite species **1** is an inner-sphere surface sorbed Eu(III). The intensity of the fluorescence signal of this species indicates that Eu/hydrotalcite species **1** is present only as a minor component.

In comparison to the signal of Eu/hydrotalcite species **1**, the signal of species **2** is more blue-shifted, indicating a stronger Eu(III) complexation. This dominating peak is relatively broad. To rule out that peaks of different species are covered by this signal, emission spectra and emission lifetimes were measured at two excitation wavelengths, 579.2 and 580.0 nm, respectively. Figure 6 shows the emission spectra of the $^5D_0 \rightarrow {}^7F_0$ transition by excitation at 579.2 and 580.0 nm. The fluorescence spectra are very similar, indicating that the same Eu/hydrotalcite species is obtained and that no inhomogeneous line broadening is present. Furthermore, the $^5D_0 \rightarrow {}^7F_1$ and $^5D_0 \rightarrow {}^7F_2$ emission bands are not as much split as was found for Eu/hydrotalcite species **1**. This is a clear indication for a higher site symmetry around the central europium atom in the case of Eu/hydrotalcite species **2**. The emission decay behavior, shown in Figure 7, is for both excitation wavelengths (579.2 and 580.0 nm) identical and monoexponential. A lifetime of $305 \pm 5\ \mu s$ is obtained, which corresponds to 2.9 ± 0.5 water molecules in the first coordination sphere of the lanthanide ion. Taking into account that each water molecule consists of two O−H quenchers, 2.9 ± 0.5 water molecules correspond to 6 ± 1 hydroxyl groups. Hence, we suggest that Eu/hydrotalcite species **2** consists of an Eu(III) ion that is incorporated into the hydrotalcite lattice (approximately by replacing an Al(III)) and is surrounded by six hydroxyl groups.

Structural information about surface sorbed and incorporated Eu(III) species such as bond lengths and coordination numbers cannot be derived from TRLFS measurements. Therefore, an EXAFS study of the Eu(III)/hydrotalcite sample was carried out.

EXAFS Measurements. The k^2-weighted fluorescence Eu L_{III}-edge EXAFS spectrum and corresponding Fourier transformed spectrum (FT) of the Eu/hydrotalcite solid sample is shown in Figure 8. One peak in the FT dominates, which can be attributed to an Eu−O coordination shell. The whole spectrum is well reproduced using three shells in the FT range (1−3.5 Å; shown in Figure 8). The fit results are given in Table 2. The first coordination shell has six to seven O atoms at 2.41 Å with a Debye−Waller factor of 9.0×10^{-3} Å^2. This is slightly more than the expected N (Table 1) but still within the 20% error. The Eu−O distance is slightly shorter than for the aquo ion (2.43 Å, ref *25*). The Al coordination sphere is split into two components, unlike in the hydrotalcite structure, and the total coordination number is reduced by half. Taking into account the results of the TRLFS, we know that two species are present in the studied sample. The main species is identified as an incorporated Eu species, and the minor one is a sorbed Eu species. On the basis of the hydrotalcite structure and previous experiments (*26*) with Eu sorption/incorporation on/into mineral phases, we note that the shorter Eu−Al distance of 3.20 Å matches with a bidentate bound Eu on the hydrotalcite surface. This may indicate that we have a sorbed species or reveal an important local disorder around Eu in the hydrotalcite structure, a disorder not observable in XRD. The longer Eu−Al distance of 3.41 Å is attributed to Eu incorporated into the hydrotalcite. Attempts to add an O shell (from OH) around 4 Å does not improve the fit and yields non-physical parameters. The reduced Al coordination number as compared to the expected value as well as the missing associated O shell (from OH) indicates either disorder in the Eu near-neighbor structure or that Eu having a larger radius does not replace Al/Mg exactly at their lattice position. No Eu−Eu interactions can be evidenced, ruling out the presence of $Eu(OH)_3$ within the EXAFS detection limit.

In summary, Eu(III) TRLFS and EXAFS measurements of a lanthanide doped hydrotalcite show that europium is incorporated into the bulk structure of the mineral. The incorporated species revealed by the TRLFS study induces distortion in the hydrotalcite lattice as suggested by the high Debye−Waller factor and the partial mismatch with the ideal structure.

Acknowledgments

We gratefully acknowledge the assistance of Boris Brendebach during the EXAFS measurements. Thanks to Reinhardt Klenze and Dirk Bosbach for fruitful discussions. This work was co-financed by the Helmholtz Gemeinschaft Deutscher Forschungszentren (HGF) by supporting the Helmholtz-Hochschul-Nachwuchsgruppe "Aufklärung Geochemischer Reaktionsmechanismen an der Wasser/Mineralphasen Grenzfläche".

Literature Cited

(1) Brodda, B.; Fachinger, J. J. Corrosion behavior of spent MTR fuel elements in a drowned salt mine repository. *Mater. Res. Soc. Symp. Proc.* **1995**, *353*, 593−600.

(2) Brücher, H.; Curtius, H; Fachinger, J. *Research and Development for Back-End Options for Irradiated Research Reactor Fuel in Germany*, Transactions of the 5th Topical Meeting on Research Reactor Fuel Management, Aachen, Germany, April 1−3, 2001; ENS RRFM.

(3) Mazeina, L.; Curtius, H.; Fachinger, J.; Odoj, R. Characterization of secondary products of uranium−aluminum material test reactor fuel element corrosion in repository relevant brine. *J. Nucl. Mater.* **2003**, *323*, 1−7.

(4) Miyata, S. The synthesis of hydrotalcite-like compounds and their structures and physicochemical properties. *Clays Clay Miner.* **1975**, *31*, 369−375.

(5) Dobbs, J. C.; Susetyo, W.; Knight, F. E.; Castles, M. A.; Carreira, L. A.; Azarraga, L. V. Characterization of metal binding sites in fulvic acids by lanthanide ion probe spectroscopy. *Anal. Chem.* **1989**, *61*, 483−488.

(6) Richardson, F. S. Terbium(III) and europium(III) ions as luminescent probes and stains for biomolecular systems. *Chem. Rev.* **1982**, *82*, 541−552.

(7) Rabung, T.; Stumpf, T.; Geckeis, H.; Klenze, R.; Kim, J. I. Sorption of Am(III) and Eu(III) onto γ-alumina: Experimental results and modeling. *Radiochim. Acta* **2000**, *88*, 711−716.

(8) Takahashi, Y.; Kimura, T.; Kato, Y.; Minai, Y.; Tominaga, T. Characterization of Eu(III) species sorbed on silica and montmorillonite by laser-induced fluorescence spectroscopy. *Radiochim. Acta* **1998**, *82*, 227−232.

(9) Stumpf, T.; Bauer, A.; Coppin, F.; Fanghänel, T.; Kim, J. I. Inner-sphere, outer-sphere, and ternary surface complexes: A TRLFS study of the sorption process of Eu(III) onto smectite and kaolinite. *Radiochim. Acta* **2002**, *90*, 345−349.

(10) Piriou, B.; Fedoroff, M.; Jeanjean, J.; Bercis, L. Characterization of the sorption of europium(III) on calcite by site-selective and time-resolved luminescence spectroscopy. *J. Colloid Interface Sci.* **1997**, *194*, 440−447.

(11) Carnall, W. T.; Goodman, G. L.; Rajnak, K.; Rana, R. S. *A Systematic Analysis of the Spectra of the Lanthanides Doped into Single Crystal LaF_3*; Report ANL-88-8, Argonne National Laboratory: Argonne, IL, 1988.

(12) Carnall, W. T. The Absorption and Fluorescence Spectra of Rare Earth Ions in Solution. In *Handbook on the Physics and Chemistry of Rare Earth*; Gschneider, K. A., Eyring, L., Eds.; Elsevier: Amsterdam, 1976.

(13) Jörgensen, C. K.; Judd, B. R. Hypersensitive pseudo-quadrupole transitions in lanthanides. *Mol. Phys.* **1964**, *8*, 281−290.

(14) See, for example, Görller-Walrand, C.; Binnemans, K. Rationalization of Crystal-Field Parameterization. In *Handbook on the Physics and Chemistry of Rare Earth*; Gschneider, K. A., Eyring, L., Eds.; Elsevier: Amsterdam, 1996.

(15) Hubert, S.; Thouvenot, P.; Edelstein, N. Spectroscopic studies and crystal-field analyses of Am^{3+} and Eu^{3+} in the cubic symmetry site of ThO_2. *Phys. Rev. B* **1993**, *48*, 5751−5760.

(16) Horrocks, W. DeW.; Sudnick, D. R. Lanthanide ion probes of structure in biology. Laser induced luminescence decay constants provide a direct measure of the number of metal-coordinated water molecules. *J. Am. Chem. Soc.* **1979**, *101*, 334−340.

(17) Stumpf, S.; Stumpf, T.; Dardenne, K.; Hennig, C.; Foerstendorf, H.; Klenze, R.; Fanghänel, T. Sorption of Am(III) onto six-line ferrihydrite and its alteration products: Investigations by EXAFS. *Environ. Sci. Technol.* **2006**, *40*, 3522−3528.

(18) Stumpf, T.; Marques Fernandes, M.; Walther, C.; Dardenne, K.; Fanghänel, T. Structural characterization of Am incorporated into calcite: A TRLFS and EXAFS study. *J. Colloid Interface Sci.* **2006**, *302*, 240−245.
(19) Duff, C. M.; Coughlin, J. U.; Hunter, D. G. Uranium coprecipitation with iron oxide minerals. *Geochim. Cosmochim. Acta* **2002**, *66*, 3533−3547.
(20) Stumpf, T.; Tits, J.; Walther, C.; Wieland, E.; Fanghänel, T. Uptake of trivalent actinides (Cm(III)) by hardened cement paste: A time-resolved laser fluorescence spectroscopy (TRLFS) study. *J. Colloid Interface Sci.* **2004**, *276*, 118−124.
(21) Stumpf, S.; Stumpf, T.; Walther, C.; Bosbach, D.; Fanghänel, T. Sorption of Cm(III) onto different feldspar surfaces: A TRLFS study. *Radiochim. Acta* **2006**, *94*, 243−248.
(22) Newville, M.; Livins, P.; Yacoby, Y.; Rehr, J. J.; Stern, E. A. Near-edge X-ray absorption fine structure of Pb: A comparison of theory and experiment. *Phys. Rev. B* **1993**, *47*, 14126−14131.
(23) Bellotto, M.; Rebours, B.; Clause, O.; Lynch, J.; Bazin, D.; Elkaim, E. A. Reexamination of hydrotalcite crystal chemistry. *J. Phys. Chem.* **1996**, *100* (20), 8527−8534.
(24) Drits, V. A.; Bookin, A. S. Crystal Structure and X-ray Identification of Layered Double Hydroxides. In *Layered Double Hydroxides: Present and Future*; Rives, V., Ed.; Nova Science: New York, 2001.
(25) Allen, P. G.; Bucher, J. J.; Shuh, D. K.; Edelstein, N. M.; Craig, I. Coordination chemistry of trivalent lanthanide and actinide ions in dilute and concentrated chloride solutions. *Inorg. Chem.* **2000**, *39*, 595−601.
(26) Dardenne, K.; Bosbach, D.; Denecke, M. A.; Brendebach, B. *EXAFS Investigation of the* $NaLn(MoO_4)_2$−$Ca_2(MoO_4)_2$ *Solid Solution Series Local Structure*, Proceedings of the 4th Workshop on Speciation, Techniques, and Facilities for Radioactive Materials at Synchrotron Light Sources (Actinide-XAS-2006), Karlsruhe, September 18−20, 2006.

Received for review October 17, 2006. Revised manuscript received February 23, 2007. Accepted February 28, 2007.

ES0624873

5. Fazit

In der vorliegenden Arbeit wurde die Wechselwirkung von dreiwertigen Actiniden und Lanthaniden mit diversen Wasser/Mineralphasen Grenzflächen systematisch untersucht. Eine besonderes Intensive Anwendung fand dabei die zeitaufgelöste Laserfluoreszenzspektroskopie sowohl unter Einsatz von Eu(III) als auch von Cm(III). Als ergänzende, komplementäre und Strukturinformationen liefernde Methode wurde bei einigen Systemen die Rötenabsorptionsspektroskopie genutzt. Die Kombination der Methoden bot die Möglichkeit ein Prozessverständnis der Sorptions- und Inkorporationsvorgänge an der Mineralphasenoberfläche auf molekularer Ebene zu entwickeln.

Trotz der Vielfalt der untersuchten Systeme konnte gezeigt werden, dass die Wechselwirkungen von Lanthaniden und dreiwertigen Actiniden mit der Wasser/Mineralphasen Grenzfläche im Wesentlichen zu drei unterschiedlichen M(III)/Mineral Spezies führt.

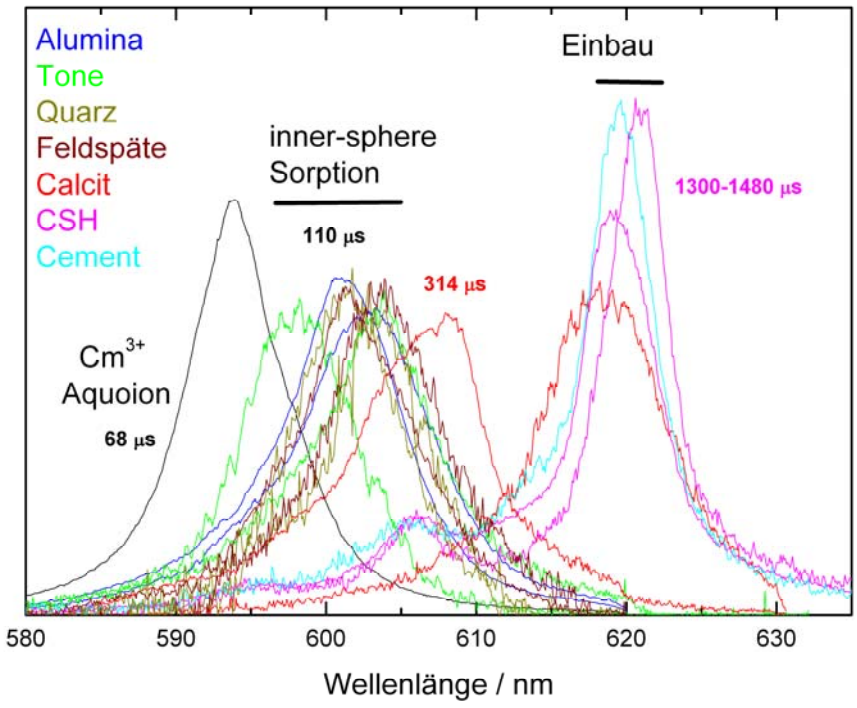

Abbildung 13 Emissionsspektren verschiedener Cm(III) Spezies mit den zugehörigen Fluoreszenzemissionslebensdauern

Bei Mineralen mit Permanentladung (in dieser Arbeit wurde exemplarisch das Tonmineral Smectit untersucht) dominieren bei niedrigen pH Werten (< 5) outer-

sphere Komplexe. Bei dieser Form der Actinidanbindung an die Oberfläche behält das Eu^{3+}/Am^{3+}/Cm^{3+} Ion seine komplette Hydrathülle von 9 Wassermolekülen. Folglich ist im Falle der Cm(III) TRLFS ein Peakmaximum bei 593.8 nm zufinden; die Emissionslebensdauer beträgt, wie für das Cm(III) Aquoion üblich, 68 +/-3 µs (Abbildung 13 bzw. 14).

Die zweite Form der Wechselwirkung von dreiwertigen Actiniden und Lanthaniden mit der Wasser/Mineralphasen Grenzfläche besteht in der Bildung von inner-sphere Komplexen. Diese pH Wert abhängige Oberflächenreaktion führt im Fall der TRLFS mit Cm(III) zu einer Rotverschiebung der Emission im Vergleich zum Spektrum des Aquoions. Mineralabhängig finden sich die Peakmaxima zwischen 598 nm und 604 nm (Abbildung 13). Diese Form der Curium Sorption lässt sich bei Feldspäten (Albit, Orthoklas), Tonmineralen (Kaolinit, Smectit), γ-Al_2O_3, sowie bei Quarz (Stumpf et al. In Vorbereitung) nachweisen. Bei jedem dieser untersuchten Systeme treten pH abhängig zwei Cm/Mineral inner-sphere Komplexe auf, die sich jeweils um ~4 nm in der Lage des Peakmaximums unterscheiden. Wie EXAFS Messungen zur Sorption von Am(III) an Tonmineralen belegen, handelt es sich bei dem bei höheren pH Werten auftretenden zweiten inner-sphere Komplex um die Hydrolysespezies der ersten Sorptionsspezies. Alle angeführten inner-sphere Komplexe zeigen eine Cm(III) Fluoreszenzemissionslebensdauer von 110 +/- 10 µs. Dies deutet auf den Verlust der halben Hydrathülle des Actinids bei der Anbindung an die Mineraloberfläche hin (Abbildung 14).

Die dritte Art der Wechselwirkung von M(III) mit einer Wasser/Mineralphasen Grenzfläche, die mit Hilfe der TRLFS nachgewiesen werden konnte, ist der kristallchemische Einbau des Actinids. In Gegenwart der Ca^{2+}-haltigen Phasen Calcit und CSH zeigt das Cm(III) Fluoreszenzspektrum mit der Zeit eine sehr starke Rotverschiebung. Die Peakmaxima liegen zwischen 618 nm und 621 nm. Die gemessenen, sehr langen Cm(III) Emissionslebensdauern dieser Spezies von über 1.3 ms belegen, dass das Actinidion seine Hydrathülle komplett verloren hat und in die Struktur des Gastminerals eingebunden wurde. Emissionsspektren bei tiefen Temperaturen (< 15 K) von gezielt Cm dotierten Calcitkristallen zeigen diverse Peakaufspaltungen, die ebenfalls ein eindeutiger Hinweis auf den Einbau des Actinids in die Calcitstruktur darstellen. Die „Site-selektive“ zeitaufgelöste Laserfluoreszenzspektroskopie an mit Eu(III) dotierten Calciten bei tiefen Temperaturen lieferte zusätzliche Informationen zu den Punktsymmetrien der

eingebauten Fremdionenzentren und zum Mechanismus des Einbaus insbesondere im Hinblick auf die Ladungskompensation beim Ersatz eines zweiwertigen Calciumions durch ein dreiwertiges f-Element.

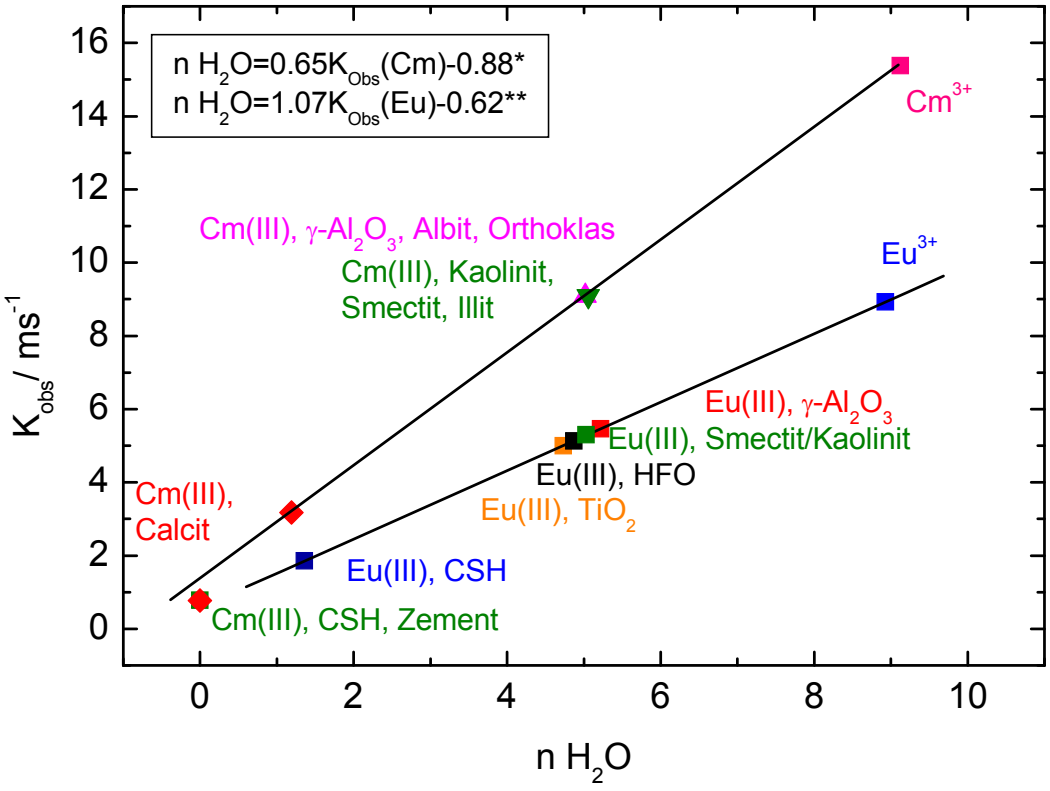

Abbildung 14 Korrelation zwischen gemessenen Quenchraten und der Zahl der Wassermoleküle in der ersten Cm(III) Koordinationssphäre verschiedener Cm(III) Spezies (*Cm: Kimura et al. 1994; **Eu: Horrocks et al. 1979)

Eine Ausnahme hinsichtlich der Einordnung in outer-sphere, inner-sphere oder Einbau Spezies stellt Cm/Calcit Spezies 1 dar (Abbildung 13). Aufgrund der schnellen Kinetik bei der Entstehung, dem nicht Aufspalten des Emissionssignals bei Tieftemperaturmessungen sowie der Möglichkeit das Emissionssignal dieser Cm Spezies durch mit $CaCO_3$ "Überwachsenlassen" deutlich zu reduzieren, ist eine Sorptionsspezies anzunehmen. Die Fluoreszenzemissionslebensdauer allerdings ist mit 314 µs deutlich länger, als dies für eine Sorptionsspezies zu erwarten wäre (Abbildung 14). Ein Wert von 314 µs entsprich einem Verlust von sieben bis acht Wassermolekülen in der ersten Hydrathülle des Actinidions. Auch die

Rotverschiebung hin zu 607.5 nm ist deutlich stärker ausgeprägt als im Fall der inner-sphere Komplexierung durch andere Mineraloberflächen wie z.B. Kaolinit oder Albit. Allerdings weder die Werte von > 618 nm, die bei der Peakverschiebung nach Einbau des Curiums in eine Mineralphase gefunden werden, noch die extrem langen Lebensdauern von über 1.3 ms, die für Einbauspezies üblich sind, werden für Cm/Calcit Spezies 1 gemessen. Somit nimmt dieser Komplex eine Sonderstellung zwischen Sorption und Einbau ein. Ein Vorschlag für die Struktur einer solchen "Zwitterspezies" ist ein Actinidion, dass in die erste Lage einer Calcitkristalloberfläche eingebunden ist und bereits von einem weiteren Carbonat aus der Lösung komplexiert wird. Ein solcher Komplex kann als Zwischenprodukt auf dem Weg zur Bildung einer "solid solution" angesehen werden.

Die im Rahmen dieser Arbeit zusammengefassten Ergebnisse zur Wechselwirkung von dreiwertigen Actiniden und Lanthaniden mit der Wasser/Mineralphasen Grenzfläche liefern einen Beitrag zur Identifizierung und Quantifizierung der für die Mobilisierung oder Rückhaltung von Actiniden verantwortlichen Reaktionen im Nah- und Fernfeld eines nuklearen Endlagers. Das erhaltene Prozessverständnis kann als belastbare Grundlage dienen, die Migration der Radionuklide über lange Zeiträume zu extrapolieren. Die in dieser Arbeit vorgestellten Grundlagenuntersuchungen auf molekularer Ebene sind somit ein weiterer Baustein im Konzept eines geochemisch geführten Sicherheitsnachweises.

6. Literatur

Aas, W., Steinle, E., Fanghänel, Th., Kim, J. I., Radiochim. Acta 84, 85 (1999).

Allard, T., Ildefonse, P., Beaucaire, C., Calas, G., Chem. Geol. 158, 81 (1999).

Allen, P. G., Bucher, J. J., Shuh, D. K., Edelstein, N. M., Reich, T., Inorg. Chem. 36, 4682 (1997).

Allen, P. G., Bucher, J. J., Shuh, D. K., Edelstein, N. M., Craig, I., Inorg. Chem. 39, 595 (2000).

Altermatt, D., Brown, I. D., Acta Cryst. B41, 240 (1985).

Ankudinov, A. L., Ravel, B., Rehr, J. J., Conradson, S. D., Phys. Rev. B 58, 7565 (1998).

Arakawa, T., Akamine, M., Sensors and Actuators B 91, 252 (2003).

Atkins, M., Glasser, F. P., Kindness, A., Cem. Concr. Res. 22, 241 (1992).

Bargar, J. R., Towle, S. N., Brown, G. E., Parks, G. A., J. Colloid Interface Sci. 185, 473 (1997).

Bargar, J. R., Reitmeyer, R., Davis, J. A., Environ. Sci. Technol. 33, 2481 (1999).

Bargar, J. R., Reitmeyer, R., Geochim. Cosmochim. Acta 64, 2737 (2000).

Bauer, A., Berger, G., Applied Geochemistry 13, 905 (1998)

Baumgarten, E., Kirchhausen-Düsing, U., J. Colloid Interface Sci. 194, 1 (1997).

Bayens, B., Bradbury, M. H., J. Contam. Hydrol. 27, 199 (1997)

Beeby, A., Clarkson, I., Dickins, R., Faulkner, S., Parker, D., Royle, L., de Sousa, A., Williams, J., Woods, M., J. Chem. Soc., Perkin Trans. 2, 493 (1999).

Beitz, J. V., Bowers, D. L., Doxtader, M. M., Maroni, V. A., Reed, D. T., Radiochim. Acta 44-45, 87 (1988).

Beitz, J. V., Hessler, J. P., Nucl. Techn. 51, 169 (1980).

Beitz, J. V., Radiochim. Acta 52/53, 35 (1991).

Berner, U., A Thermodynamic Description of the Evolution of Pore Water Chemistry and Uranium Speciation during the Degradation of Cement, Paul Scherrer Institut (1990).

Bernkopf, M. F., Kim, J. I., Hydrolysereaktionen und Karbonatkomplexierung von dreiwertigem Americium in natürlichen aquatischen Systemen, Report RCM 02884, Inst. für Radiochemie, Techn. Univ. München (1984).

Blum, A. E., Stillings, L. L., Feldspar dissolution kinetics in: Reviews in Mineralogy, Vol. 31, Chemical Weathering Rates of Silicate Minerals, Ed. A. F. White, S. L. Brantley, Mineralogical Society of America (1995).

Bonen, D., Sarkar, S. L., Advances in Cement and Concrete, Grutzeck, W. M., Sarkar, S. L., Eds., American Society of Civil Engineers: New York (1994).

Bradbury, M. H., Baeyens, B., J. Contam. Hydrol. 27, 223 (1997).

Bradbury, M. H., Baeyens, B., Geochim. Cosmochim. Acta 63, 325 (1999).

Brown, I. D., Altermat, D., Acta Cryst. B41, 244 (1985).

Brunauer, S., Emmett, P. H., Teller, F., J. Am. Chem. Soc. 60, 309 (1938).

Bünzli, J. C. G., Choppin, G. R., Lanthanides Probes in Life, Chemical and Earth Sciences. Theory and Practice. Elsevier Science Publisher, North Holland, Amsterdam (1989).

Carnall, W. T., Crosswhite, H. M., Optical Spectra and Electronic Structure of Actinide Ions in Compounds and Solutions. Report ANL, 84 (1995).

Carnall, W. T., Goodman, G. L., Rajnak, K., Rana, R. S., A systematic analysis of the spectra of the lanthanides doped into single crystal LaF_3. Report ANL-88-8, Argonne National Laboratory, Argonne (1988).

Carnall, W. T., The absorption and fluorescence spectra of rare earth ions in solution. Handbook on the Physics and Chemistry of Rare Earth, North Holland Publishing, Amsterdam (1976).

Carnall, W. T., Crosswhite, H. M., J. Chem. Phys. 63 (1975).

Carnall, W. T., Report ANL-89-39; Argonne National Laboratory, Argonne (1989).

Carnall, W.T.; Rajnak, K., J. Chem. Phys. 63 (1975).

Chou, L., Wollast, R., A. J. Sci. 285, 963 (1985).

Chou, L., Wollast, R., Geochimica et Cosmochimica Acta 48, 2205 (1984).

Chung, K. H., Klenze, R., Park, K. K., Paviet-Hartmann, P., Kim, J. I., Radiochim. Acta 82, 215 (1998).

Cocke, D. L., Mollah, M. Y. A., The Chemistry and Leaching Mechanism of Hazardous Substances in Cementitious Solidification/Stabilization Systems, Lewis Publishers (1993).

Combes, J. M., Chrisholm-Brause, C. J., Brown Jr., G. E., Parks, G. A., Conradson, S. D., Eller, P. G., Triay, I. R., Hobart, D. E., Meijer, A., Environ. Sci. Technol. 26, 376 (1992).

Cong, X., Kirkpatrick, R., J. Cem. Concr. Res. 23, 1065 (1993).

Cornell, R. M., Schwertmann, U., The Iron Oxides: Structure, Properties, Reactions, Occurrence and Uses, VCH Verlagsgesellschaft, Weinheim (1996).

Cotton, F. A., Wilkinson, G., Advanced Inorganic Chemistry, Interscience Publishers: New York (1972).

Csoban, K., Joo, P., Colloids Surf. 151, 97 (1999).

Curti, E., Appl. Geochem. 14, 433 (1999).

Dardenne, K., Schäfer, T., Denecke, M. A., Rothe, J., Kim, J. I., Radiochim. Acta 89, 469 (2001).

Dardenne, K., Denecke, M. A., Schäfer, Th., Advanced Photon Source Activity Report 2002, ANL-03/21 (2003).

Dardenne, K., Schäfer, T., Lindqvist-Reis, P., Denecke, M. A., Plaschke, M., Rothe, J., Kim, J. I., Environ. Sci. Technol. 36, 5092 (2002).

Dario, M., Ledin, A., Chem. Spec. Bioavail. 9/1, 3 (1997).

Davis, J. A., Fuller, C. C., Cook, A. D., Geochim. Cosmochim. Acta 51, 1477 (1992).

Degueldre, C., Ulrich, H. J., Silby, H., Radiochim. Acta 65, 173 (1994).

Denecke, M. A., Marquardt, C. M., Rothe, J., Dardenne, K., Jensen, M. P., J. Nuclear Science Technology 3(Suppl.), 410 (2002).

Denecke, M. A., Rothe, J., Dardenne, K., Lindqvist-Reis, P., Phys. Chem. Chem. Phys. 5, 939 (2003).

Denecke, M. A., Dardenne, K., Marquardt, C., Talanta 65, 1008 (2005).

Dobbs, J. C., Susetyo, W., Knight, F. E., Castles, M. A., Carreira, L. A., Azarraga, L. V., Anal. Chem. 61, 483 (1989).

Döhring, L., Görlich, W., Rüttener, S., Schwerzmann, R., Herstellung von Homogenen Zementsteinen mit hoher Hydraulischer Permeabilität, Nagra (1994).

Dromgoole, E. L., Walter, L. M., Chem. Geol. 81, 311 (1990).

Dzombak, D. A., Morel, F. M. M., Surface Complexation Modeling, Hydrous Ferric Oxide, Wiley, New York (1990).

Eggleton, R. A., Fitzpatrick, R., Clays Clay Min. 36, 111 (1988).

Elzinga, E. J., Reeder, R. J., Withers, S. H., Peale, R. E., Mason, R. A., Beck, K. M., Hess, W. P., Geochim. Cosmochim. Acta. 66, 2875 (2002).

Fanghänel, Th., Kim, J. I., J. Alloys Comp. 271-273, 728 (1998).

Fanghänel, Th., Kim, J. I., Klenze, R., Kato, J., J. Alloys Comp. 225, 308 (1995).

Fanghänel, Th., Kim, J. I., Paviet, P., Klenze, R., Hauser, W., Radiochim. Acta 66/67, 81 (1994).

Fanghänel, Th., Weger, H. T., Könnecke, T., Neck, V., Paviet-Hartmann, P., Steinle, E., Kim, J. I., Radiochim. Acta 82, 47 (1998).

Fanghänel, Th., Weger, H. T., Schubert, G., Kim, J. I., Radiochim. Acta 82, 55 (1998).

Fanghänel, Th., Kim, J. I., J. Alloys Compd. 271–273, 728 (1998).

Fanghänel, Th., Könnecke, Th., Weger, H., Paviet-Hartmann, P., Neck, V., Kim, J. I., J. Solution Chem. 4, 447 (1999).

Farley, K. J., Dzombak, D. A., Morel, F. M. M., J. Colloid Interface Sci. 106, 226 (1985).

Faucon, P., Delaye, J. M., Virlet, J., J. Solid State Chem. 127 (1996).

Ford, R. G., Bertsch, P. M., Farley, K. J., Environ. Sci. Technol. 31, 2028 (1997).

Fung, P. C., Bird, G. W., Mc Intyre, N. S., Sanipelli, G. G., Nuclear technology 51, 188 (1980).

Fuller, C. C., Bargar, J. R., Davis, J. A., Piana, M. J., Environ. Sci. Technol. 36, 158 (2002).

Fuller, C. C., Bargar, J. R., Davis, J. A., Environ. Sci. Technol. **37**, 4642 (2003).

Geckeis, H., Klenze, R., Kim, J. I., Radiochim Acta 87, 13 (1999).

George, G. N., Pickering, I. J., EXAFSPAK: A suite of computer programs for analysis of X-ray absorption spectra. Stanford Synchrotron Radiation Laboratory, Stanford (1995).

Girvin, D. C., Gassman, P. L., Bolton, H., Soil Sci. Soc. Am. J. 57, 47 (1993).

Glasser, F. P., Chemistry and Microstructure of Solidified Waste Forms, Spence, R. D., Ed., Lewis Publishers: Boca Raton, FL (1993).

Görller-Walrand, C., Binnemans, K., Rationalization of Crystal-Field Parameters. Handbook on the Physics and Chemistry of Rare Earths, 121–244, North Holland Publishing, Amsterdam, , Editors: Gschneider, K. A., Eyring, L. (1996).

Gougar, M. L. D., Scheetz, B. E., Roy, D. M., Waste Management 1996, 16, 295 (1996).

Grützeck, M., Benesi, A., Fanning, M., J. Am. Ceram. Soc. 72, 665 (1989).

Haas, Y., Stein, G., J. Chem. Phys. 75, 3668 (1971).

Hamid, S. A., Z. Kristallogr. 154, 189 (1981).

Hayes, K. F., Redden, G., Ela, W., Leckie, J. O., J. Colloid Interface Sci. 142, 448 (1991).

Heller, A., J. Am. Chem. Soc. 88, 2058 (1966).

Hellmann, R., Penisson, J. M., Hervig, R. L., Thomassin, J. H., Abrioux, M. F., Phys. Chem. Minerals 30, 192 (2003).

Hennig, C., Reich, T., Dahn, R., Scheidegger, A. M., Radiochim. Acta 90, 653 (2002).

Hohl, H., Stumm, W., J. Colloid Interface Sci. 55, 281 (1976).

Holdren, G. R., Berner, R. A., Geochimica et Cosmochimica Acta 43, 1161 (1979).

Horrocks, W. DeW., Sudnick, D. R., J. Am. Chem. Soc. 101, 334 (1979).

Horst, J., Höll, W. H., J. Colloid Interface Sci. 195, 250 (1997).

Huang, C.-P., Stumm, W., J. Colloid Interface Sci. 43, 409 (1973).

Hummel, W., Berner, U., Curti, E., Pearson, F. J., Thoenen, T., Nagra/PSI Chemical Thermodynamic Data Base 01/01, Nagra: Wettingen, Switzerland (2002).

Hyun, S. P., Cho, Y. H., Kim, S. J., Hahn, P. S., J. Colloid Interface Sci. 222, 254 (2000).

Janney, D. E., Cowley, J. M., Buseck, P. R., American Mineralogist 86, 327 (2001).

Janney, D. E., Cowley, J. M., Buseck, P. R., Clays Clay Min. 48/1, 111 (2000).

Jörgensen, C. K., Judd, B. R., Mol. Phys. 8, 281 (1964).

Judd, B. R., Phys. Rev. 127, 750 (1962).

Karthikeyan, K. G., Elliott, H. A., Cannon, F. S., Environ. Sci. Technol. 31, 2721 (1997).

Katz, L. E., Hayes, K. F., J. Colloid Interface Sci. 170, 477 (1995).

Kim, J. I., Klenze, R., Wimmer, H., Eur. J. Solid State Inorg. Chem. 28, 347 (1991).

Kimura, T., Choppin, G. R., J. Alloys Comp. 213/214, 313 (1994).

Kirkpatrick, R. J., Brown, G. E., Xu, N., Cong, X,. Adv. Cem. Res. 9, 31 (1997).

Kitamori, T., Yokose, K., Suzuki, K., Sawada, T. and Goshi, Y., Japanese J. Appl. Phys. 27, L983 (1988).

Klenze, R., Kim, J. I., Wimmer, H., Radiochim. Acta 52/53, 97 (1991).

Koningsberger, D. E., Prins, R., X-Ray Absorption: Principles, Applications, Techniques for EXAFS, SEXAFS and XANES, Wiley Interscience, New York (1988).

Könnecke, Th., Fanghänel, Th., Kim, J. I., Radiochim. Acta 76, 131 (1997).

Kosmulski, M., J. Colloid Interface Sci. 192, 215 (1997).

Kropp, J. L., Windsor, M. W., J. Chem. Phys. 39, 769 (1965).

Kummert, R., Stumm, W., J. Colloid Interface Sci. 75, 373 (1980).

Lakowicz, J. R., in Principles of Fluorescence Spectroscopy, Plenum Press, New York/London (1983).

Lewis, D. G., Schwertmann, U., Clays and Clay Min. 27/3, 195 (1979).

Lis, S., J. Alloys Compounds, 341, 45 (2002).

Marques Fernandes, M., Stumpf, T., Rabung, T., Bosbach, D., Fanghänel, Th., Geochim. Cosmochim. Acta, eingereicht (2007).

Marques Fernandes , M., Schmidt, M., Stumpf, T., Walther, C., Bosbach, D., Fanghänel, Th., Geochim. Cosmochim. Acta, eingereicht (2007).

Martínez, C. E., Sauvé, S., Jacobson, A., Mc Bride, M. B., Environ. Sci. Technol. 33, 2016 (1999).

Matz, W., Schell, N., Bernhard, G., Prokert, F., Reich, T., Claußner, J., Oehme, W., Schlenk, R., Dienel, S. , Funke, H., Eichhorn, F., Betzl, M., Pröhl, D., Strauch, U., Hüttig, G., Krug, H., Neumann, W., Brendler, V., Reichel, P., Denecke, M. A., Nitsche, H., J. Synchrotron Rad. 6, 1076 (1999).

Mazeina, L., Curtius, H., Fachinger, J., Odoj, R., J. Nucl. Mat. 323, 1 (2003).

McMaster, W. H., Kerr Del Grande, Mallett, J. H., Hubbell, J. H., Compilation of X Ray Cross Sections, Report UCRL-50174, Section II, Revision I Lawrence Livermore National Laboratory (1969).

Meier, L., Kahr, G., Clays Clay Miner. 47, 386 (1999).

Moll, H., Reich, T., Szabó, Z., Radiochim. Acta 88, 411 (2000).

Moll, H., Stumpf, Th., Merroun, M., Roßberg, A., Selenska-Pobell, S., Bernhard, G., Environ. Sci. Technol. 38, 1455 (2004).

Moulin, V., Tits, J., Moulin, C., Decambox, P., Mauchien, P., De Ruty, O., Radiochimica Acta 58/59, 121 (1992).

Mucci, A., Morse, J. W., Geochim. Cosmochim. Acta 47, 217 (1983).

Musić, S., Šarić, A., Nomura, K., Popović, S., Models in Chemistry 136/4, 457 (1999).

Natoli, C. R., EXAFS and Near Edge Structure 27 in Chemical Physics, Bianconi, A., Incoccia, L., Stipcich, S., Springer Verlag, Berlin (1984).

Neck, V., Fanghänel, Th., Kim, J. I., Aquatische Chemie und thermodynamische Modellierung von trivalenten Actiniden, Wissenschaftliche Berichte, FZKA 6110, Forschungszentrum Karlsruhe (1998).

Newville, M., Livins, P., Yacoby, Y., Rehr, J. J., Stern, E. A., Phys. Rev. B47, 14126 (1993).

Nordèn, M., Ephraim, J. H., Allard, B., Radiochim. Acta 65, 265 (1994).

Ofelt, G. S., J. Chem. Phys. 37 (1962).

Östhols, E., Manceau, A., Farges, F., Charlet, L., J. Colloid Interface Sci. 194, 10 (1997).

Paviet, P., Fanghänel, Th., Klenze, R., Kim, J. I., Radiochim. Acta 74, 99 (1996).

Piriou, B., Fedoroff, M., Jean, J., Bercis, L., J. Colloid Interface Sci. 194, 440 (1997).

Pointeau, I., Piriou, B., Fedoroff, M., Barthes, M.-G., Marmier, N., Fromage, F., J. Colloid Interface Sci. 236, 252 (2001).

Rabung, T., Stumpf, T., Geckeis, H., Klenze, R., Radiochim. Acta 88, 711 (2000).

Rabung, T., Geckeis, H., Kim, J. I., Beck, H. P., J. Colloid Interface Sci. 208, 153 (1998).

Rabung, T., Der Einfluss von Huminsäure auf die Sorption von Eu(III) auf Hämatit, Dissertation, Anorganische und Analytische Chemie und Radiochemie, Universität des Saarlandes (1998).

Reeder, R. J., Nugent, M., Lamble, G. M., Tait, C. D., Morris, D. E., Environ. Sci. Technol 34, 638 (2000).

Reich, T., Moll, H., Denecke, M. A., Geipel, G., Bernhard, G., Nitsche, H., Radiochim. Acta 74, 219 (1996).

Reich, T., Moll, H., Arnold, T., Denecke, M. A., Hennig, C., Geipel, G., Bernhard, G., Nitsche, H., Allan, P. G., Bucher, J. J., Edelstein, N. M., Shuh, D. K., Journal of spectroscopy & related phenomena 96, 237 (1998).

Ressler, T., J. Physique IV 7, 269 (1997).

Richardson, F. S., Chem. Rev. 82, 541 (1982).

Rizkalla, E. N., Choppin, G. R., Handbook on the Physics and Chemistry of Rare-Earths, Gschneider, K. A., Eyring, L., Choppin, G. R., Lander, G. H. Eds., Elsevier North-Holland, Amsterdam (1994).

Rothe, J., Denecke, M. A., Neck, V., Mueller, R., Kim, J. I., Inorg. Chem. 41, 249 (2002).

Scheinost, A. C., Abend, S., Pandya, K. I., Sparks, D. L., Environ. Sci. Technol 35, 1090 (2001).

Scherbaum, F. J., Knopp, R., Kim, J. I., Appl. Phys. B 63, 299 (1996).

Schmidt, M., Stumpf, T., Marques Fernandes , M., Walther, Fanghänel, Th., Geochim. Cosmochim. Acta, eingereicht (2006).

Schwertmann, U., Cornell, R. M., Iron Oxides in the Laboratory (Preparation and Characterization). VCH-Verlag, Weinheim (1991).

Schwertmann, U., Friedl, J., Stanjek, H., Schulze, D. G., Clays and Clay Min. 48/2, 159-172 (2000).

Shannon, R. D., Prewitt, C. T., Acta. Cryst. B 25, 925 (1969).

Sherman, D. M., Waite, T. D., American Mineralogist 70, 1262 (1985).

Sposito, G., Geochemical Processes at Mineral Surfaces, Davis, J. A., Hayes, K. F. Eds., ACS Symposium Series 323, pp. 217-230, Am. Chem. Soc. Washington, DC (1986).

Stadler, S., Kim, J. I., Radiochim. Acta 44/45, 39 (1988).

Stein, G., Würzberg, E., J. Chem. Phys. 62, 208 (1975).

Stillings, L. L., Brantley, S. L., Geochim. Cosmochim. Acta 59, 1483-1496 (1995).

Stipp, S. L., Hochella Jr., M. F., Parks, G. A., Leckie, J. O., Geochim. Cosmochim. Acta 56, 1941 (1992).

Strawn, D. G., Sparks, D. L., J. Colloid Interface Sci. 216, 257 (1999).

Stumpf, S., Stumpf, T., Walther, C., Bosbach, D., Fanghänel, Th., Radiochim. Acta 94, 243 (2006).

Stumpf, S., Stumpf, T., Dardenne, K., Hennig, C., Förstendorf, Klenze, R., Fanghänel, Th., Environ. Sci. Technol. 40, 3522 (2006).

Stumpf, T., Bauer, A., Coppin, F., Kim, J. I., Environ. Sci. Technol. 35, 3691 (2001).

Stumpf, T., Rabung, T., Klenze, R., Geckeis, H., J. Colloid Interface Sci. 238, 219 (2001).

Stumpf, T., Fanghänel, Th., J. Coll. Int. Sci. 249, 119 (2002).

Stumpf, T., Bauer, A., Coppin, F., Fanghänel, Th., Kim, J. I., Radiochim. Acta 90, 345 (2002).

Stumpf, T., Fanghänel, Th., Grenthe, I., J. Chem. Soc., Dalton Trans. 3799 (2002).

Stumpf, T., Tits, J., Walther, C., Wieland, E., Fanghänel, Th., J. Colloid Interface Sci. 276, 118 (2004).

Stumpf, T., Hennig, C., Bauer, A., Denecke, M. A., Fanghänel, Th., Radiochim. Acta 92, 1 (2004).

Stumpf, T., Marques Fernandes, M., Walther, C., Dardenne, K., Fanghänel, Th., J. Colloid Interface Sci. 302, 240 (2006).

Stumpf, T., Curtius, H., Walther, C., Dardenne, K., Ufer, K., Fanghänel, T., Environ. Sci. Technol. 41, 3186 (2007).

Takahashi, Y., Kimura, T., Kato, Y., Minai, Y., Tominaga, T., Radiochim. Acta 82, 227 (1998).

Taubald, H., Bauer, A., Schäfer, T., Geckeis, H., Satir, M., Kim, J. I., Clay Minerals 35, 515 (2000).

Tits, J., Jakob, A., Wieland, E., Spieler, P., J. Contamin. Hydr. 61, 45 (2003).

Tits, J., Stumpf, Th., Rabung, T., Wieland, E., Fanghänel, Th., Environ. Sci. Technol. 37, 3568 (2003).

Waite, T. D., Davis, J. A., Payne, T. E., Waychunas, G. A., Xu, N., Geochim. Cosmochim. Acta 58(24), 5465 (1994).

Walther, C., Bitea, C., Hauser, W., Kim, J. I., Scherbaum F. J., Nucl. Instr. Meth. B, 195, 374 (2002).

Walther, C., Coll. Surf. A, 217, 81 (2003).

Walter, M., Arnold, T., Reich, T., Bernhard, G., Environ. Sci. Technol. 37, 2898 (2003).

Waychunas, G. A., Fuller, C. C., Davis, J. A., Geochim. Cosmochim. Acta, 66/7, 1119 (2002).

Westall, J. C., Morel, F. M. M., FITEQL: A General Algorithm for the Determination of

Metal-Ligand Complex Stability Constants from Experimental Data, Technical Note 18, Ralph M. Parsons Laboratory, Department of Civil Engineering, Massachusetts Institute of Technology, Cambridge, Mass (1977).

White, A. F., Brantley, S. L., Chemical Weathering Rates of Silicate Minerals, Rev. Mineral. 31, Mineral. Soc. of Am., Washington, D.C. (1995).

Wimmer, H., Kim, J. I., Klenze, R., Radiochimica Acta 58 / 59, 165 (1992).

Wimmer, H., Klenze, R., Kim, J. I., Radiochim. Acta 56, 79 (1992).

Withers, S. H., Peale, R. E., Schulte, A. F., Braunstein, G., Beck, K. M., Hess, W. P., Reeder, R., J. Phys. Chem. Minerals, 30, 448 (2003).

Yaita, T., Tachimori, S., Edelstein, N. M., Bucher, J. J., Rao, L., Shuh, D. K., Allen, P. G., J. Synchrotron Rad. 8, 663 (2001).

Young, J. F., J. Am. Ceram. Soc. 71, C118 (1988).